Oscillatory mechanisms for controlling information flow in neural circuits

Thomas Akam

Dissertation submitted for the degree of

Doctor of Philosophy

of the

University College London

Department of Clinical and Experimental Epilepsy
University College London

Declaration

I, Thomas Akam, confirm that the work presented in this thesis is my own. Where information has been derived from other sources, I confirm that this has been indicated in the thesis.

5th May 2011

Abstract

Mammalian brains generate complex, dynamic structures of oscillatory activity, in which distributed regions transiently engage in coherent oscillation, often at specific stages in behavioural or cognitive tasks. Much is now known about the dynamics underlying local circuit synchronisation and the phenomenology of where and when such activity occurs. While oscillations have been implicated in many high level processes, for most such phenomena we cannot say with confidence precisely what they are doing at an algorithmic or implementational level. This thesis presents work towards understanding the dynamics and possible function of large scale oscillatory network activity. We first address the question of how coherent oscillatory activity emerges between local networks by measuring phase response curves of an oscillating network *in vitro*. The network phase response curves provide mechanistic insight into inter-region synchronisation of local network oscillators. Highly simplified firing models are shown to reproduce the experimental data with remarkable accuracy. We then focus on one hypothesised computational function of network oscillations; flexibly controlling the gain of signal flow between anatomically connected networks. We investigate coding strategies and algorithmic operations that support flexible control of signal flow by oscillations, and their implementation by network dynamics. We identify two readout algorithms which selectively recover population rate coded signal with specific oscillatory modulations while ignoring other distracting inputs. By designing a spiking network model that implements one of these mechanisms, we demonstrate oscillatory control of signal flow in convergent pathways. We then investigate constraints on the structures of oscillatory activity that can be used to accurately and selectively control signal flow. Our results suggest that for inputs to be accurately distinguished from one another their oscillatory modulations must be close to orthogonal. This has implications for interpreting *in vivo* oscillatory activity, and may be an organising principle for the spatio-temporal structure of brain oscillations.

Table of Contents

List of Figures

Preface

Acknowledgements

Foremost, I would like to thank Dimitri Kullmann for his invaluable supervision, support and encouragement throughout the PhD process. I have learnt from him a huge amount about the details of neurobiology and a broader range of skills and lessons; from the fine distinction between a piste and a cliff, to an inspirational example of how to go about being a scientist. I have greatly appreciated the balanced supervision which both gave me the freedom to follow my interests and the guidance, advice and direction needed to turn them into scientific output.

I am grateful to all the members of the Experimental Epilepsy group who have taught me techniques and helped me with experiments, particularly to Iris Oren who provided so much instruction in the early stages of my PhD. I am indebted to Emily Ferenczi for her work gathering data on the slice rephasing experiments, a project which sometimes felt like squeezing blood from a stone. Her persistence and hard work made a large contribution to the eventual data set, while her enthusiasm and positive attitude made working with her a great pleasure.

I am grateful to Peter Latham for supervision on the theoretical components of the project, particularly for invaluable advice on both the technical details and presentation of the work in Chapter 4, which I believe contributed greatly to its publication. I am grateful to all the staff of the 2008 Advanced Course in Computational Neuroscience for providing one of the most stimulating and educational months of my life, and particularly to Jeff Beck, Alex Lerchner and David Hansel for discussions which provided useful ideas for subsequent work.

I would like to thank Jon Driver, Markus Bauer and Sabine Joseph for their collaboration on psychophysical experiments and stimulating discussions about visual attention.

I am very grateful to my examiners Neil Burgess and Máté Lengyel for their robust questioning and stimulating discussions during the viva and feedback provided on an earlier version of the manuscript.

I could not have done the PhD without the friends who have made my time in London so enjoyable, supported me through the tough bits, and tolerated and sometimes encouraged the occasional late night neuroscience discussion. Finally, I would like to thank my wonderful parents for the years of love and support and for teaching me so much of what I know. This thesis is dedicated to them.

Contributions and Collaborations

Emily Ferenczi gathered approximately half of the experimental data used in Chapter 3, all analysis was performed by Thomas Akam. A collaborative project is underway working with Jon Driver's attention group looking the effect of gamma frequency flicker on visual perception, but results from this work have not been included in the thesis.

Publications

The word described in Chapter 4 was published in Neuron (Akam and Kullmann, 2010). A paper based on the work in Chapter 3 has been submitted to Nature Neuroscience and additional experiments are currently being planned to address reviewer's comments in preparation for second round submission. A manuscript based on Chapter 5 is under preparation. *C*hapter 6 will be developed into a manuscript with additional spiking network model data in collaboration with Alex Lerchner.

Chapter 1: Introduction

1.1 Introducing the question

Oscillatory phenomena occur ubiquitously in the brain, manifesting experimentally as periodic modulation of spike trains and aggregate measures of neural activity. Such activity occurs in diverse brain regions and behavioural states and spans several orders of magnitude in frequency. Task dependent changes in patterns of oscillatory activity suggest possible roles in computation and cognition and have attracted intense interest from experimental and computational neuroscientists. Despite extensive experimental characterisation, modelling and speculation, the role played by most oscillatory phenomena remains unclear and in many cases little direct evidence exists to prove functional significance.

This thesis focuses on the hypothesis that network oscillations play a role in flexibly controlling the flow of signal through the fixed anatomical connectivity of the brain. Specifically, we are interested in how oscillatory and resonant network dynamics can be used to selectively control the gain of interactions between networks; and whether these mechanisms are in fact employed by the brain. This question defines the scope of our work so our first priority is to attempt to convince the reader that it is interesting and worthwhile.

The behavioural flexibility of higher animals is perhaps the most compelling argument for the existence of mechanisms for rapid and flexible remapping of the brain's connection structure. Though some behaviours appear to be hard-wired mappings from sensory stimuli to motor responses, much behaviour is characterised by sensitivity to context. The significance of a given sensory event to an animal may vary dramatically in different situations, ranging from complete irrelevance to requiring immediate approach, avoidance or a more subtle motor response. It is likely that such context-dependent behaviour requires flexibility throughout the complex web of processing linking sensory inputs to motor outputs. The current salience of different components of the sensory input may determine the extent to which they are allocated high level representational and memory capacity through attentional mechanisms. The mapping of these high level representations onto motor plans or cognitive actions may in turn depend flexibly on current context.

There are of course many ways in which flexible mapping between inputs and outputs could be implemented in a network. Given the non-linearity of neural systems, an input-output transformation could be radically changed in the absence of any change in connectivity by the

addition of a contextual input signal to some of the neurons in the network. However, the connectivity structure of a network plays such a fundamental role in shaping activity that modifications to it are clearly a potentially powerful mechanism for implementing functional flexibility. Synaptic plasticity mechanisms play a fundamental role in modifying connectivity on a range of time-scales from sub-second changes due to short term plasticity, through to potentially lifelong changes due to long term and structural plasticity. These direct modifications of the efficacy of individual synapses certainly play important roles in behavioural flexibility on a range of time-scales. We are interested in whether these are supplemented by mechanisms which achieve rapid and selective modification of the strength of functional interactions by using oscillatory dynamics rather than directly modifying synaptic strengths.

How could oscillations affect the strength of functional interactions? The basic concept is that oscillatory dynamics induce periodic modulation of the output of a network and that the response of regions receiving the output is sensitive to this modulation. Depending on the dynamics of the receiving region, the modulation might increase the spikes elicited in response to the input, have little effect, or even in principle decrease the response. Selective control of interaction strength could be achieved by changing dynamics in a sending region to modify the frequency, amplitude or phase of the modulation, or by changing the filtering properties of a receiving region to affect its sensitivity to these characteristics. Susceptibility for synaptic plasticity may also be modulated as a function of oscillation phase, such that changes in structure of oscillatory activity could control which inputs drive plasticity in target structures.

Where may such mechanisms exist in the mammalian brain? In the next chapter we review the experimental evidence implicating changes in structures of oscillatory network activity in brain function during behaviour. Here we briefly highlight the brain regions and oscillatory activity patterns we think are most plausibly implicated in controlling the strength of functional interactions. The theta oscillation in hippocampus and connected structures is perhaps the most compelling. The activity of hippocampal pyramidal cells is strongly modulated as a function of oscillation phase. The structure of the oscillation is in turn strongly modulated during behaviour, both in the phase of spiking of individual hippocampal pyramidal cells relative to the local oscillation, and the coupling of extra hippocampal regions with hippocampal theta. The mechanistic consequences of these changes remain incompletely understood, but the former may plausibly play a role in controlling the gain of plasticity between neuronal assemblies in the hippocampus, while the latter may control information flow into and out of the structure. The functional importance of this oscillation is underlined by the behavioural consequences of its disruption by pharmacological agents. Another candidate activity pattern is beta oscillations in regions associated with motor planning and

execution, including motor, premotor and parietal cortex, and connected structures including the basal ganglia and cerebellum. These oscillations deeply modulate neuronal spiking of at least a subset of cells, and both local circuit and inter-region synchronisation are highly task dependent, consistent with a role in flexibly controlling signal flow. Changes in structures of oscillatory activity during tasks requiring selective attention are also interesting in this context. Visual attention produces modest but significant effects on local circuit gamma band synchronisation in several visual areas, and striking effects on the inter-region coherence of such oscillations. Correlation between gamma synchronisation and behavioural performance supports the functional significance of these effects, though one caveat is an absence of evidence indicating that spike probability is deeply modulated by gamma oscillation phase in the regions with pronounced attentional effects. Alpha frequency oscillations in thalamo-cortical circuits are also strongly affected by attentional state, typically exhibiting desynchronisation in cortical regions representing the attended area enhanced synchronisation in non-attended areas. While this could suggest they reflect idling or an inactive state of cortical circuits, a variety of cognitive tasks enhance alpha band oscillations suggesting a more active role in reconfiguring neural circuits to different task demands.

Though much is now known about structures of oscillatory activity *in vivo* and their modulation during behaviour, the great majority of experimental evidence implicating oscillations in controlling signal flow remains correlational. Evaluating whether the observed activity is consistent with this function is complicated by the lack of quantitative proposals for how these mechanisms may function. A principle aim of the work in this thesis is to develop such models. We now briefly explain why we believe that focusing on this basic operation of controlling the gain of signal flow using oscillations may help evaluate the proposed roles of network oscillations in a wide range of high level cognitive functions.

1.2 Gain control and multiplexing as basic components of high-level functions of oscillations

Network oscillations have been proposed to play roles in many different high level processes including visual scene segmentation, representation of navigational path sequences, selective attention and working memory, multi-sensory integration, and the storage, recall and consolidation of long term memories. In these different proposals oscillatory modulations convey diverse information about the status of signals. For example they may indicate attentional salience, whether a set of place cells represents a past or future location, or whether multiple sensory attributes have common or distinct causes. However, in all cases this meta-information is only meaningful if target networks can treat the signals differently on the basis of their oscillatory

modulations. Responding to inputs with different gains is the most basic way in which a target network may distinguish these signals. Of course the differential treatment may be much more complex than simply applying different linear gains to different components of the signal. However, selective gain control may be an important component of more complex operations used to select specific subsets of combined signals for further processing steps.

The advantage of focussing on this low level operation of selective gain control is that important features of the problem may become apparent which are not obvious when thinking about high level computations directly. A major theme which emerged in the current work, that we believe has received insufficient attention in the oscillations literature to date, is that of multiplexing population codes. Multiplexing is the process of combining multiple signals into a single stream for transmission through a communication channel, in such a way that the combined signal can be separated by a receiver to recover the individual components. Multiplexing is used ubiquitously in man-made communication systems to enable multiple signals to share expensive or limited resources such as optic fibres or radio bandwidth. This is often achieved by separation of signals into distinct frequency bands (frequency division multiplexing) or time slots (time division multiplexing). We will see in Chapters 4 and 5 that both these schemes can be applied to multiplexing neural codes.

Multiplexing necessarily plays a fundamental role in any scheme where network oscillations are used to implement changes in the gain for signal transmission that are **selective** for either a subset of the regions that a population of neurons projects to, or for a subset of the inputs received by a network (Figure 1.1). This is because both cases require that a single communication channel carries two separable signals, the component whose gain is to be varied, and the component whose gain is to remain unchanged. In the former case the communication channel is a divergent pathway in which a single population of neurons projects to multiple target networks. A simple example is a network in which neurons make both recurrent local connections and long range projections to other regions. The hippocampus provides an example of this arrangement where CA3 pyramidal cell axons form local recurrent connections en route to the CA1 region. It is easy to imagine situations where it may be useful to independently control the gain of signals sent to different target networks in a divergent pathway. For example if a computation performed by the local circuit takes time to execute it may be desirable to suppress output until the answer is ready. This could be achieved without oscillations by having distinct populations of neurons mediating the two connections. However, this additional circuitry could potentially be avoided if, for example, the local computations are performed in an asynchronous state, with a burst of oscillation used to transmit the output to the distal network. This is multiplexing, as the same anatomical pathway carries two

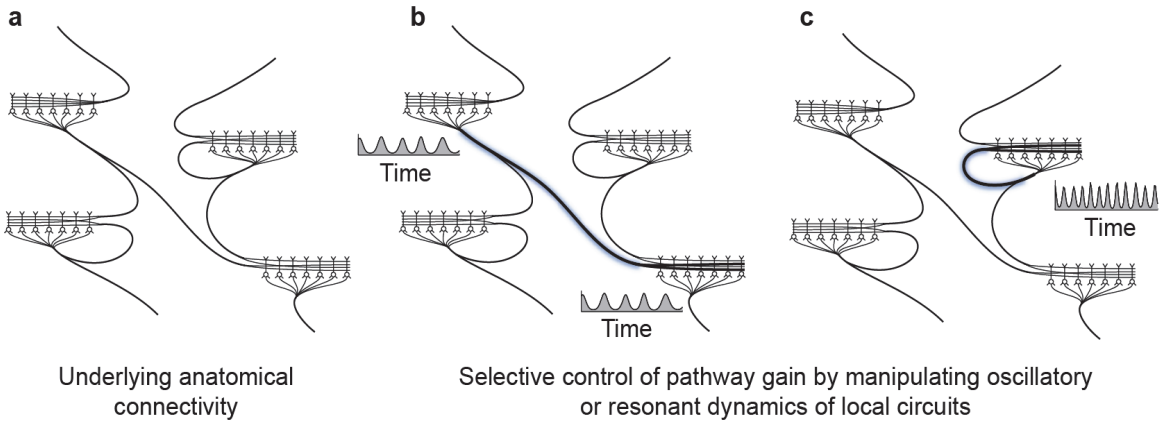

Figure 1.1 **Selective gain control in convergent and divergent pathways. a)** Long range connections between local circuits including convergent and divergent pathways. **b)** The gain of the highlighted pathway cannot be selectively controlled either by changing the gain in the receiving region or the firing rate in the sending region, as both manipulations will also affect other pathways. Multiplexing population codes using network oscillations in principle allows selective gain control for subsets of network inputs in convergent pathways, and of projection targets in divergent pathways. Selective enhancement of the gain between two regions might be achieved by coherent oscillation **(b)**, or the gain of local connections might be selectively varied relative to long range connection by a change in local circuit oscillatory dynamics **(c).**

distinct signals to the two targets. The first component is carried by the firing rate as in a traditional population code and must be ignored by the distal target network. The second component must in some way be encoded into the oscillatory modulation of the firing rate such that it can be read out independently of the first component by a network with appropriate filtering properties.

Multiplexing is also necessary if oscillations are to be used to selectively control the gain for a subset of inputs to a network in a convergent pathway. Convergent pathways are common in sensory processing where low level regions representing different attributes, such as local orientations in retinotopic space, converge to higher level regions which have larger receptive fields for more complex attributes (Jones 1970, Cavada 1989). These anatomical motifs are therefore of interest in hypotheses concerning the role of oscillations in selective attention, feature binding, and multi-sensory integration. If oscillations are used in a convergent pathway to distinguish multiple components of a combined input, this is an example of multiplexing where the shared communication channel is the input space of the receiving region. If the receiving region needs to

treat these components differently, for example by responding to them with different gains, their modulations must be organised such that there is a de-multiplexing operation that can separate them.

We emphasise the role of multiplexing because it focuses attention on the informational aspects of this problem rather than the dynamical aspects that have been the principal focus of previous work on the topic. This prompts the questions of what neural codes and structures of oscillatory activity can enable multiple signals to occupy a single channel, what operations can be used to separate the combined signal, and how accurately the individual components can be recovered. Our approach to addressing these questions is to consider a feed forward convergent pathway in which signals from a number of input networks converge to a single receiving network. We identify ways in which the receiving network can selectively read out the signal encoded by a single input network while ignoring the others, on the basis of differences in their oscillatory modulations. In Chapter 4 we show that evaluating spatial patterns of firing rate oscillation amplitude can selectively readout signals oscillating in specific frequency bands, and design a biophysical model that implements such a mechanism. We argue in Chapter 5 that efficiently multiplexing population codes imposes previously unrecognised constraints on the structure of oscillatory modulations of component signals, due to the requirement that individual components of the signal are orthogonal under the de-multiplexing operation that separates them. Orthogonality ensures that when one of the signal components varies this does not affect the readout of the other components.

While we believe this informational perspective can provide novel insights into how oscillations may enable flexible control of signal flow, any such operations must be implemented by the dynamics of biological networks. Understanding these dynamics plays two critical roles in evaluating the hypothesis. The first is to explain the dynamics underlying the task dependent changes in local circuit synchronisation and inter-region coherence that are used to argue for the hypothesis. The second is to understand how network dynamics can implement the mathematical operations which permit flexible control of signal flow by oscillations. Our work makes two contributions in these directions. Chapter 3 presents experimental and modelling work which aims to understand the emergence of coherent oscillatory activity between regions. We use an *in vitro* model system to measure the phase response of an oscillating network to stimulation of input pathways and the local circuit. The shape of the measured phase response curves provides insight into how local networks can couple through excitatory long-range connections. Close correspondence between the experimental data and a simple neural mass model suggests that such models may provide a powerful tool for understanding the dynamics of changes in inter-region coherence. In Chapter 4 we look at how biologically plausible networks can generate activity that

supports multiplexing of population codes, and at how resonant dynamics in feed-forward interneuron layers can perform the filtering needed to de-multiplex combined activity patterns in convergent pathways.

In reducing the problem to the simplest form that we felt preserved access to these issues, we have necessarily discarded many important aspects of real brain networks when constructing our conceptual and computational models. One such simplification is that our model networks do not do any computations with the information they represent, but instead passively transmit signals from one layer the next, albeit with selective changes in gain for different pathways. We leave for further work the important issue of how easily the mechanisms we outline can be integrated into networks implementing real computations. A related simplification is that we consider only changes in gain that consist of completely turning on or off pathways, rather than the graduated reweighting of different inputs and outputs that more likely characterises modulation of real brain networks. In the discussion Chapter 7 we discuss how this limitation could be relaxed in extensions to the models and the likely consequences of this for our conclusions.

Chapter 2: Literature Review

2.1 What are network oscillations?

Network oscillations are dynamical states where the spiking activity of populations of neurons exhibits periodic synchronisation. Though this simple definition describes the feature common to all network oscillations, it obscures a large amount of heterogeneity in the network states that have been described as oscillations in the literature. A wide variety of experimental data are interpreted as evidence of oscillations, ranging from signals with clearly visible periodicity, to changes in broad frequency bands of spectral measures which show no clear peak. Theoretical work on network dynamics suggests that even in randomly connected networks there is a range of different dynamical mechanisms which can lead to oscillatory synchronisation. Before we turn to task-dependent changes in oscillatory activity within and across regions, we review what is known about local circuit activity during oscillations, and their underlying dynamical mechanism.

We will first briefly outline the signals and analysis methods that are used to identify oscillatory activity in local networks, indicating their respective strengths and weaknesses. We do this because our view of networks *in vivo* is restricted to that provided by the small window of experimentally measured signals. Though the size of this window is growing rapidly (Stevenson and Kording, 2011), we still see only a tiny fraction of the total activity whose state we wish to infer. Understanding how the presence of oscillatory activity is identified is important for interpreting task-dependent changes in these signals.

2.2 Detecting oscillations in experimental signals

The most direct measure of neural activity is spikes trains, which may be either single or multi-unit activity recorded at one or more sites simultaneously. *In vivo* spike trains in cortex are highly irregular (Softky and Koch, 1993; Baddeley et al., 1997) with high coefficients of variation of spike counts and inter-spike intervals. Such irregularity in no way precludes the possibility of periodic modulation of the probability of spiking or of a strong oscillation at the population level. Indeed, irregular spiking of single units is frequently observed concurrently with evidence of periodic activity (Bragin et al., 1995; Fries et al., 2001; Logothetis et al., 2001; Hasenstaub et al., 2005). However, as we discuss below, the irregularity of unit activity *in vivo* does constrain the types of dynamical states that may underlie observed periodic signals.

Various analysis methods are used to detect periodic modulation of spiking activity. For single spike trains the presence of periodic modulation produces multiple regularly spaced peaks in the autocorrelation function and a peak at a particular frequency of the power spectrum (Perkel et al., 1967a; Eckhorn et al., 1988; Gray and Singer, 1989; Fries et al., 1997; Friedman-Hill et al., 2000). A possible confound can occur in using these measures due to bursting dynamics of single neurons, which can produce peaked spectra in the absence of network oscillations (Bair et al., 1994). This confound can be avoided by analysis methods which combine signals from two electrodes (Perkel et al., 1967b; Jarvis and Mitra, 2011). The cross-correlation function or cross spectra of pairs of spike trains were widely used to evaluate population oscillations (Eckhorn et al., 1988; Gray et al., 1989; Wehr and Laurent, 1996). Spurious central peaks can occur in cross-correlograms due to correlations in response latency or variations in excitability on a slow timescale (Brody, 1999), however these do not produce the multiple regularly spaced peaks indicative of a network oscillation.

Recently, raw cross spectra have been largely supplanted by coherence measures in evaluating the frequency content of activity correlations (Fries et al., 2008; Gregoriou et al., 2009; Jutras et al., 2009; Ray and Maunsell, 2010). Coherence is a spectral measure generated by normalizing the cross-spectrum of two signals by the autospectrum of each individual signal. In neuroscience applications the coherence is usually calculated between two simultaneously recorded local field potentials (LFPs), two spike trains (spike-spike coherence), or a spike train and an LFP (spike-field coherence). The normalisation has several advantages. It produces a signal with a defined range of zero to one, with zero indicating no correlation between the signals at that frequency and one indicating that they are identical up to a constant shift in time. The normalisation also makes coherence invariant to linear filtering or one or both signals. This is desirable for signals such as the LFP which, as we discuss below, may be related to physiological activity of interest by considerable filtering. The normalisation also prevents the possibility of spurious peaks in the cross spectra that can occur due to limited data if one or both signals are strongly periodic but the two are uncorrelated.

Oscillatory network activity produces peaks in coherence spectra, but it is not straightforward to estimate the strength of the oscillatory modulation of network firing rates from the height of the peaks. This is because the average firing rate of spike trains, and the size of time bins at which they are discretized, affect the value of the coherence (Zeitler et al., 2006; Lepage et al., 2011). This can be understood qualitatively by considering two Poisson processes with identical periodic modulations of their firing rates. Though the firing rates are identical, the spike trains will be distinct due to the stochastic timing of individual spikes, so the coherence between the signals will

be less than one. In the presence of common periodic firing rate modulation we expect a peak in the coherence spectrum, but how high will this peak be for a given modulation depth? This depends on spike rate because, if the spike trains are represented as counts in time bins of a given width, the two spike trains will become more similar as their average spike rate increases (up to a multiplicative factor if they have different average rates). We illustrate these effects quantitatively in Chapter 6 for a multiplicative modulation model of activity we use in Chapter 5. This means that while coherence is a powerful tool for detecting the presence of correlated fluctuations in spiking activity in a particular frequency band, it impossible to interpret their strength if we are not also given their average spike rate. It is sometimes incorrectly stated that coherence is invariant to changes in rate (Fries et al., 2001; Gregoriou et al., 2009) and frustratingly, average firing rates are rarely reported with coherence measurements. The dependence on firing rate could cause task-dependent changes in coherence in the absence of any change in network synchronisation. Recent studies are beginning to counteract this possibility by discarding spikes to normalise rates across conditions (Gregoriou et al., 2009), or testing statistically if variance changes are correlated with rate changes (Pesaran et al., 2008).

Intracellular recordings provide very direct information about network state by allowing approximate measurements of excitatory and inhibitory currents received by a cell, or through information about sub-threshold membrane potential trajectories. Performing such recordings in behaving animals is formidably difficult and hence their application to task-dependent changes in oscillatory activity has been limited. In the study of oscillations, they have principally been applied to *in vitro* oscillation models (e.g Oren et al., 2006) where they have provided considerable insight into mechanisms of oscillations. Intracellular recordings *in vivo* have been used to study oscillatory activity in the hippocampus in the anaesthetised (Ylinen et al., 1995; Atallah and Scanziani, 2009), and awake state (Harvey et al., 2009).

If spike rates are low it can be hard to resolve periodic modulation of spiking probability against stochastic variability in spike activity. Aggregate measures of activity such as the local field potential (LFP) can help overcome these difficulties, at the cost of a less direct relationship between the measured signal and the activity of interest. The local field potential is the low frequency (<200 Hz) components of signals recorded in the extracellular space. The signal is generated principally by synaptic input to cells within ~250 um of the recording electrode (Katzner et al., 2009; Xing et al., 2009; Ray and Maunsell, 2010). It is thought that the contribution from individual synaptic currents sum approximately linearly to generate the LFP (Nicholson and Freeman, 1975; Holt and Koch, 1999; Pettersen et al., 2008), but that the contribution of individual synaptic currents may be strongly low-pass filtered. Such filtering can occur due to the location of synapses on the dendritic

tree and their position relative to the recording electrode (Lindén et al., 2010a). Non-resistive properties of the extracellular medium may also contribute to low-pass filtering the spectrum of the LFP relative to intracellular voltage fluctuations (Bedard et al., 2006, 2006; Bédard and Destexhe, 2009; Bédard et al., 2010a). Local field potentials *in vivo* characteristically have a 1/f power spectrum (Buzsaki and Draguhn, 2004; Bedard et al., 2006), with peaks at particular frequencies present in some structure and states (e.g Gray and Singer, 1989; Pesaran et al., 2002; Henrie and Shapley, 2005; Chalk et al., 2010). The presence of peaks indicates some degree of periodic modulation of the network activity but the complex relationship between activity and the LFP makes it hard to quantify the strength of synchronisation indicated by a given spectrum.

The linear component of filtering between neural activity and the LFP does not contribute to coherence spectra due to normalisation by the auto spectra of the signals of interest. For this reason spike-field coherence spectra can show large peaks at frequencies where little evidence of synchronisation is evident in the LFP power spectra (Fries et al., 2008). Spike-field coherence is more sensitive to correlated modulations of the firing rate in local circuits than spike-spike measures (Zeitler et al., 2006). This is due to the large number of neurons that contribute to the LFP which reduces fluctuations due to stochastic spiking and increases the size of the coherence for a given modulation strength. These features make spike-field coherence spectra highly sensitive measure of oscillatory synchronisation, particularly when combined with multi-taper methods for optimal spectral smoothing (Zeitler et al., 2006; Fries et al., 2008; Jarvis and Mitra, 2011). This has made spike-field coherence a popular analysis for evaluating task dependent changes in oscillatory synchronisation both within (Fries et al., 1997, 2008; Chalk et al., 2010; Ray and Maunsell, 2010) and between (Pesaran et al., 2008; Gregoriou et al., 2009; Benchenane et al., 2010) regions. As with spike-spike coherence, spike-field coherence depends on firing rates, which makes it hard to interpret the strength of synchronisation (Zeitler et al., 2006). The sensitivity of spike-field coherence is something of a two-edged sword as it can produce dramatically peaked spectra when oscillatory modulations are weak (see Chapter 6).

In human cognitive neuroscience, the most widely used measures for studying oscillatory activity are electroencephalography (EEG) and magnetoencephalography (MEG). These non-invasive methods measure respectively electrical potentials on the scalp or magnetic fields just above (Darvas et al., 2004). Contemporary equipment offers massively parallel recording of over 100 channels spaced over the head which provides the ability to investigate large scale activity patterns in behaving humans (Siegel et al., 2008; Hipp et al., 2011). Modern analysis methods attempt to recover the sources that generate the recorded signal by inverting a forward model linking sources to sensor data (Van Veen et al., 1997; Gross et al., 2001). However, even with large numbers of

channels and advanced analysis methods, spatial resolution is limited to between several millimetres and centimetres such that many tens of thousands of neurons contribute to the signal from a given spatial region. EEG and MEG signals characteristically have a 1/f power spectrum, similar to the LFP, with peaks at specific frequencies in some states and regions (Freeman et al., 2000). The mechanisms described above, which filter the contribution of activity to the LFP, also filter EEG and MEG signals. Fluctuations that are coherent over large spatial distances contribute strong to these signals due to spatial averaging. Involvement of oscillatory activity in tasks is usually inferred from changes in the power in particular frequency bands in specific spatial locations, or from frequency specific changes in the coherence between regions (Siegel et al., 2008; Hipp et al., 2011). These indirect measures provide little quantitative information about the strength of oscillatory modulation underlying the observed changes.

2.3 In vivo network dynamics and mechanisms of oscillation

In this section we review what is known about the dynamical state of local networks *in vivo* during both asynchronous and oscillatory activity. This is a necessary prerequisite to understanding task-dependent changes in oscillatory activity and has important implications for the representation of information by neural codes, which we address in more detail in the subsequent section.

Much of the modelling and theoretical work aiming to understand the basic dynamical states available to neural networks has been carried out in networks with random or all-to-all connectivity. While real networks have much more complex connectivity structures, these simple networks show a rich range of dynamics which provide considerable insight into network states *in vivo* (Van Vreeswijk and Sompolinsky, 1996, 1998; Brunel and Hakim, 1999; Brunel, 2000; Brunel and Wang, 2003). There are two dimensions along which states of these networks can be usefully categorised for our purposes. Firstly, the spiking of individual neurons may be regular or irregular. This can be quantified by the Fano factor, which is the variance of spike counts in a given interval divided by the mean, or by the distribution of inter-spike intervals. For a Poisson process the Fano factor is one while for a neuron spiking regularly the Fano factor is much less than 1. Secondly, the activity can be oscillatory or asynchronous, which refers to whether the global activity is periodically modulated.

2.3.1 Irregular activity and the balanced state

The irregularity of the spike activity of cortical neurons *in vivo* (Softky and Koch, 1993; Baddeley et al., 1997) has prompted intense debate because it is seemingly incompatible with the integration of a large number of uncorrelated excitatory postsynaptic potentials (EPSPs) (Softky and Koch,

1993). Two basic mechanisms have been proposed to account for this discrepancy which, as we discuss in the subsequent section, have profoundly different implications for the nature of the neural code. One possibility is than rather than integrating input, neurons act as coincidence detectors and spike in response to synchronous activity in presynaptic afferents (Softky and Koch, 1993; Stevens and Zador, 1998; Izhikevich, 2006; Abeles, 2009). This could occur due to spike initiation by a limited number of EPSPs in small compartments of active dendrites (Softky, 1994; Häusser et al., 2000), or due to highly synchronous presynaptic activity (Stevens and Zador, 1998), perhaps enhanced by spike threshold adaptation to slow depolarisation (Azouz and Gray, 2000).

An alternative mechanism for generating irregularity is a balance between excitatory and inhibitory currents (Shadlen and Newsome, 1994, 1998; Tsodyks and Sejnowski, 1995; Amit and Brunel, 1997). This creates irregular activity because, although fluctuations of both currents are small relative to their average values, they are large relative to the net current. A key development in the study of cortical network dynamics was the realisation that generating this balance does not require fine tuning of network parameters, but instead occurs dynamically over wide parameter ranges for sparsely connected networks of excitatory and inhibitory neurons (Van Vreeswijk and Sompolinsky, 1996, 1998; Brunel, 2000; Latham et al., 2000). In these balanced networks, individual neurons operate in a fluctuation driven regime in which the net current they receive is smaller than the rheobase, with spikes elicited by fluctuations in the input. This explanation for the irregularity of cortical activity is consistent with intracellular recordings of cortical cells in activated asynchronous network states both *in vitro* (Shu et al., 2003) and *in vivo* (Paré et al., 1998; Steriade et al., 2001; Haider et al., 2006), which reveal balanced excitatory and inhibitory conductances, which in turn are large relative to the leak conductance (reviewed in Destexhe et al., 2003). The conductances produce an average membrane potential that is significantly depolarised relative to the resting potential, with large membrane potential fluctuations and irregular spiking. Balanced states have various possible computational advantages including responding to changes in input on time-scales much faster than the membrane time constant (Tsodyks and Sejnowski, 1995; Van Vreeswijk and Sompolinsky, 1998), allowing graduated responses over wide ranges of input firing rates (Shadlen and Newsome, 1998; Hô and Destexhe, 2000), and permitting equalisation of responsiveness to synapses across the dendritic tree (Rudolph and Destexhe, 2003). An important feature of balanced states is that the micro-structure of activity is chaotic (Van Vreeswijk and Sompolinsky, 1996; Banerjee et al., 2008; London et al., 2010). A small perturbation such as the addition of a single extra spike will grow rapidly and completely change spike timing in the subsequent network activity. While the micro-structure of activity (the precise sequence of spikes across neurons) is chaotic, macroscopic features of the activity such as average firing rate will rapidly return to their steady state values after perturbations. This has important implications for coding as aspects of the

activity that are chaotic are poorly suited to representing information due to their susceptibility to noise.

2.3.2 Oscillating states with regular and irregular unit activity

Oscillating network states can be divided into two categories based on the irregularity of spiking of individual neurons. In low noise conditions with heterogeneous firing rates, oscillations can occur through 'spike to spike' synchrony, in which individual neurons fire regularly at the frequency of the network oscillation (Van Vreeswijk et al., 1994; Wang and Buzsaki, 1996; Smeal et al., 2010), or at integer divisions of this frequency in cluster states (Golomb and Rinzel, 1994). These oscillations occur in population of cells that are depolarised with similar currents, such that they fire at similar frequencies, each neuron acting like a clock ticking with approximately the same period. Depending on the properties of the individual neurons and their synaptic interactions, coupling between the cells may bring them into synchrony to produce a network oscillation. A critical factor determining whether the network will synchronise is the phase response curve of the neurons to their synaptic interaction (Van Vreeswijk et al., 1994; Ermentrout, 1996; Rinzel and Ermentrout, 1998; Smeal et al., 2010), which is influenced both by the synaptic and intrinsic membrane properties.

An alternative mechanism of synchronisation can occur in networks where noise or heterogeneity of firing rates is too large to permit spike to spike synchrony. In these sparsely synchronised states, individual neurons fire irregularly at rates that may be very different from the oscillation frequency, but the spiking probability across the network is periodically modulated, generating a population oscillation (Brunel and Hakim, 1999, 2008; Brunel, 2000). The simplest case in which this can happen is in a reciprocally connected network of inhibitory cells receiving strong external excitatory input. If the inhibitory coupling is weak, the firing rate of the interneuron population will adjust such that the self inhibition balances some of the excitatory drive, leaving a small inward current that maintains firing rates. However, if the recurrent inhibitory coupling is strong and delayed, for example due to axonal conduction delay and synaptic rise time, this asynchronous state can be unstable. The steady state firing rate becomes unstable because a fluctuation in the population activity will only start to correct itself after a latency due to the delays; this produces an overshoot past the stable state and hence a fluctuation in the opposite direction, which in turn leads to an overshoot in the direction of the original fluctuation, and so on to produce an oscillation. This instability due to inhibitory - inhibitory coupling can also occur in mixed networks of excitatory and inhibitory cells. Sparsely synchronised oscillations in excitatory inhibitory networks can also occur due to the excitatory-inhibitory loop rather than inhibitory - inhibitory coupling (Brunel, 2000).

Which of these dynamical mechanisms underlies *in vivo* oscillatory activity? As studies of *in vivo* oscillatory activity do not generally provide population level statistics on the irregularity of individual unit activity, we are forced to rely on evidence provided by example spike trains. Irregular spiking has been observed during cortical (Donoghue et al., 1998; Fries et al., 2001; Hasenstaub et al., 2005), striatal (Popescu et al., 2009) and hippocampal (Bragin et al., 1995; Tukker et al., 2007), gamma frequency (30 – 80 Hz) oscillations, cortical (Witham et al., 2007; Reimer and Hatsopoulos, 2010) and striatal (Courtemanche et al., 2003) beta (15-30 Hz) oscillations, and hippocampal (Klausberger et al., 2003) and cortical (Benchenane et al., 2010) theta (4- 10 Hz) oscillations. We are not aware of any clear evidence, in the mammalian brain *in vivo,* of oscillatory activity in which individual neurons spike regularly on each cycle of the oscillation*,* though such activity has been reported in some *in vitro* oscillation models (Traub et al., 1996; Whittington et al., 1997a; Kopell et al., 2000). In some parameter regimes networks can transition smoothly as the noise level varies, between 'spike to spike' synchrony and sparsely synchronised oscillation via increasingly irregular cluster states (Brunel and Hansel, 2006). While we certainly cannot rule out the possibility that states close to 'spike to spike' synchrony may occur *in vivo,* the available evidence suggests that the majority of oscillatory activity is best understood as sparsely synchronised dynamics. Where computational models are used in this thesis, they are constructed on this assumption. From a coding perspective, a key advantage of sparsely synchronised oscillatory activity is that firing rates of individual neurons can vary independently of the population rate, in principle allowing rate coding to coexist with oscillatory coding schemes.

Though we have discussed asynchronous and oscillating networks as two discrete states, this dichotomy is only accurate in the idealised situation of infinitely large spiking networks, which have been considered analytically by network dynamics theorists (Brunel, 2000; Brunel and Wang, 2003), or in noise free firing rate models (Wilson and Cowan, 1972). In finite size networks, the instantaneous activity necessarily fluctuates due to the discrete nature of spikes. Individual neurons receive a fluctuating input that is heterogeneous across the population because of the fine structure of the connectivity, which effectively acts as an internal noise source. In networks where there is either external noise or this effective internal noise, the transition between asynchronous activity and strong oscillation occurs through a continuum of states in which the network activity gradually becomes more periodic as the bifurcation parameter is varied (illustrated in detail in Chapter 6).

The significance of this for evaluating *in vivo* network oscillations is that evidence of statistically significant oscillatory synchronisation does not necessarily imply strong oscillation, but could instead be shallow ripples on activity which is much closer to asynchronous than strongly oscillating. As we show in chapters 4 and 5, the strength of oscillatory synchronisation has a major

impact on the efficacy with which the oscillations can be exploited for selective gain control, with weak oscillations leading to very poor signal to noise ratios. Accurately quantifying the strength of oscillations in a given system is therefore important in evaluating their functional significance, though this is a challenging problem given the potential inhomogeneity and non-stationarity of such activity. In some systems, most notably the hippocampal theta oscillation, there is clear evidence of strong oscillation from studies showing deep modulation of spike probability as a function of the local LFP phase. Where such evidence is lacking, it is important to consider the dynamical possibility of statistically significant but none the less shallow oscillatory activity, when interpreting *in vivo* data.

2.4 The neural code

In order to study how oscillations may control the flow of signals between networks we must address how information is represented in neural activity. It is meaningless to discuss controlling the gain of a neural signal if we do not know which aspects of the activity are signal and which are noise. This is a fundamental question in neuroscience and remains unresolved (Rieke et al., 1999; deCharms and Zador, 2000; Dayan and Abbott, 2001). We briefly outline the debate and then explain the choices we have made in our work with regards to this question. The principal question is whether information is represented primarily by the firing rate of neurons, or whether precise timing relationships between spikes carries information (Shadlen and Newsome, 1994; Singer, 1999). These questions have been explored most intensively in sensory systems where the response to known stimuli can be accurately quantified over repeated presentations. Neurons in primary sensory cortices characteristically show highly variable responses across repeated presentations of the same stimulus (Tolhurst et al., 1983; Richmond et al., 1987; Victor and Purpura, 1996). Averaging the spiking activity over many trials to produce a peri-stimulus time histogram (PSTH) reveals changes in firing rate which are correlated with stimulus attributes, and hence carry information about the stimulus (Perkel et al., 1967a; Bair and Koch, 1996; Reich et al., 1997; Kayser et al., 2010). The dependency of firing rate on the stimulus is frequently represented as a tuning curve, indicating the average firing rate as a function of one or more stimulus features such as the orientation of a visual stimulus (Henry et al., 1974; Georgopoulos et al., 1982; Dayan and Abbott, 2001). Variations in firing rate are known to encode many different types of information in a multitude of brain areas including sensory information from primary sensory cortex (Hubel and Wiesel, 1962) to high level parietal areas (Albright, 1984; Pesaran et al., 2006), motor related signals (Georgopoulos et al., 1982), spatial information (O'Keefe, 1976; O'Keefe and Burgess, 1996), and a wide range of signals related to the subjective value of potential actions and states in a

range of regions implicated in decision making (Schultz et al., 1997; Platt and Glimcher, 1999; Shadlen and Newsome, 2001; Samejima et al., 2005). At first glance rate codes appear to suffer from the disadvantage that activity must be observed over considerable time in order to accurately estimate the firing rate. While this is true for single neurons, the problem is overcome if signals are carried by populations, as the average firing rate may be accurately estimated over very short times if the number of neurons is large (Shadlen and Newsome, 1998). Theoretical studies have demonstrated how populations of rate coding neurons can implement sophisticated computations such as coordinate transforms (Deneve et al., 2001), and operations such as short term memory storage (Amit and Brunel, 1997; Roudi and Latham, 2007). Population rate codes have been extended to the representation and manipulation of probability distributions (Ma et al., 2006) including optimal Bayesian inference in decision making (Beck et al., 2008).

While firing rates clearly play a role in encoding information, many researchers have argued that they are only part of the story and other aspects of the spiking activity may be equally or more important. Both precise timing of spikes and correlations between spike trains of different neurons have been argued to play roles in representing information (Abeles, 1991; König et al., 1996; Rieke et al., 1999; Averbeck et al., 2006). There is no doubt that in some sensory systems the timing of spikes on a scale of milliseconds is important. Examples include the auditory system (Heil and Irvine, 1997; Wehr and Zador, 2003; Elhilali et al., 2004; Kayser et al., 2010) and whisker system (Panzeri and Schultz, 2001; Arabzadeh et al., 2006). In both these systems, fine grained temporal structure in the stimuli themselves caries salient information for the animal and the precise spike timing in early parts of these sensory systems reflect this. Spike timing precisely locked to stimuli extends to the primary sensory cortices in these systems, which could appear incompatible with evidence suggesting that the cortex operates in a balanced state in which precise spike times are chaotic. This seeming dynamical inconsistency is resolved if these precisely timed cortical spikes reflect rapidly varying feed-forward input to the cortex driving variations in firing rate, rather than internally generated precise timing relationships. Indeed, analysis of coding in primary auditory cortex indicates that while rate fluctuations must be analysed on a time-scale of milliseconds to extract maximum information about stimuli, correlations between neurons do not contribute significantly (Kayser et al., 2010).

A radical departure from rate coding is proposed by researchers who argue that precisely timed correlations between spikes of different neurons are a fundamental part of the cortical neural code. Initial proposals suggested information propagation by synchronous volleys of spikes across pools of neurons, in network structures known as synfire chains (Abeles, 1991, 2009; Bienenstock, 1995; Diesmann et al., 1999). In such networks the simultaneous arrival of spikes from a presynaptic pool

triggers a subsequent volley of spikes in the next pool. These ideas have since been extended to synfire braids (Bienenstock, 1995) and polychronisation (Izhikevich, 2006) which incorporate differences in conduction delays between neurons. In these proposals it is still the synchronous arrival of spikes, at neurons operating as coincidence detectors, which triggers a postsynaptic spike, but the presynaptic spikes may occur at different times due to differences in conduction delays. In these schemes spatio-temporal sequences of precisely timed but asynchronous spikes, termed polychronous groups, trigger further such groups in their downstream targets. Izhikevich (2005) demonstrated that spike timing dependent plasticity in initially unstructured networks with delays can give rise to such group activation patterns. The importance of precisely timed spike sequences for information representation in these proposals places them at odds with evidence that the micro-structure of activity in balanced networks is chaotic (Van Vreeswijk and Sompolinsky, 1998; Banerjee et al., 2008; London et al., 2010). It is possible to embed synfire chains in balanced networks (Aviel et al., 2003; Mehring et al., 2003), but the conflicting requirements of stable pulse propagation and asynchronous activity require very large networks and carefully tuned parameters. If synfire chains or polychronizing networks were embedded in cortex, they would require rapid, large amplitude depolarising events which can overcome noisy subthreshold voltage fluctuations to drive precisely timed spikes. *In vivo* recordings suggest that such events occur very infrequently, in cortical networks *in vivo* (London et al., 2010).

To summarise, there is abundant evidence for the importance of firing rates in representing information, and the computational power of such schemes. There are apparent inconsistencies between *in vivo* network dynamics in cortex and the requirements of precise spike timing codes, and indeed evidence for such coding is sparse apart from rapidly varying firing rates in early sensory cortices (but see (Riehle et al., 1997). We therefore take the position that in studying the control of signal flow by network oscillations, it is reasonable to focus our energies on how periodic modulations due to network oscillations may supplement and extend rate coding schemes.

2.5 State dependent changes in oscillatory network activity

We now review experimental evidence showing changes in oscillatory network activity that occur in response to changes in sensory stimuli, internal states or behaviours. These experimental data provide circumstantial evidence for the functional significance of network oscillations. In some cases additional support for functional relevance is provided by correlation of trial-to-trial fluctuations in oscillatory activity with perceptual or behavioural differences between trials. Further evidence is provided in studies where decoding approaches suggest that oscillations participate in information representation. This literature is vast and we do not attempt to review it exhaustively.

We focus on three areas where task dependent modulations of oscillatory activity have been well documented in the chain of processing linking sensory input to motor outputs. These are sensory processing and selective attention, hippocampal dependent behaviours; and movement planning and execution.

2.5.1 Oscillations in sensory processing

In reviewing oscillations in sensory processing we focus primarily on mammalian visual cortex as this is the best characterised sensory system and shows both stimulus dependent oscillatory activity and modulation of oscillations by task demands during attentional processing. We first outline the well characterised oscillations in gamma (30-80 Hz), alpha (8-14 Hz) and slow (<1 Hz) frequency bands that occur in different states of the visual system. We then evaluate evidence for richer and more complex oscillatory patterning of activity during sensory processing in visual and auditory cortex. Finally we review how structures of oscillatory activity are modulated by attentional tasks requiring selective processing of sensory inputs.

Stimulus dependent gamma frequency oscillations were discovered in anaesthetised cat V1 by Gray and Singer (Gray and Singer, 1989; Gray et al., 1989). Neurons in V1 respond to contrast between bright and dark regions of visual space and are tuned to particular orientations and spatial frequencies (Hubel and Wiesel, 1962; Carandini et al., 2005). Gray and Singer (1989) demonstrated that when regions of V1 are stimulated with bars of light, the LFP shows increased power around 40 Hz, with clear evidence of oscillatory activity in spike autocorrelograms and spike field phase locking. The degree of synchronisation depends on the orientation of the bar, with strongest synchronisation for orientations which drive the highest firing rates. These oscillations can be generated by the cortex in the absence of periodic input from the lateral geniculate nucleus, though earlier stages of the visual system can generate oscillations in the high gamma band (60 – 120 Hz which can propagate to cortex (Castelo-Branco et al., 1998). Oscillatory synchronisation with very similar properties to that observed in cat V1 has also been reported in macaque V1 though with a higher frequency of ~ 60 Hz (Friedman-Hill et al., 2000). In addition to the dependence on orientation, the strength of oscillatory synchronisation in macaque V1 increases smoothly with stimulus contrast (Henrie and Shapley, 2005; Ray and Maunsell, 2010) and activity at low contrast does not show significant gamma frequency modulation. The frequency of the induced gamma rhythm also depends on stimulus parameters including size (Gieselmann and Thiele, 2008), contrast (Ray and Maunsell, 2010) and drift velocity (Friedman-Hill et al., 2000). Presentation of natural movies selectively enhanced power around 60 Hz in anaesthetised macaques, with fluctuations in gamma power correlated with firing rate fluctuations (Belitski et al., 2008).

The dependence of synchronisation strength on both contrast and orientation correlates closely with the dependence of firing rate on these variables. The dynamics of excitatory-inhibitory recurrent networks provides a plausible mechanistic explanation for this correlation (Mazzoni et al., 2008). For a wide range of network parameters, such networks exhibit a transition between an asynchronous balanced state and a state characterised by sparsely synchronised oscillatory dynamics as the strength of external input is increased (Brunel, 2000). It is therefore plausible that stimuli that produce strong feed-forward excitation of V1 drive the network into oscillation simply because of the increased excitatory input.

Though gamma oscillations in primary visual cortex have been studied extensively, it remains unclear what their computational function is, and indeed whether they are functionally important. An influential but controversial view holds that they play a role in relating different features of the visual scene represented by different local networks (Milner, 1974; Von Der Malsburg, 1981; Eckhorn et al., 1988; Singer, 1999; Uhlhaas et al., 2009). This 'binding by synchrony' hypothesis proposes that oscillatory synchronisation between regions signifies that the individual features represented by local circuits are part of a single object or concept. For example, a visual scene consists of a great many local features such as oriented edges generated by discrete objects in the external world. Binding by synchrony proposes that local circuits representing parts of a single object will selectively synchronise with each other, while local circuits representing parts of different objects will not. The hypothesis received initial experimental support with the observation of selective synchronisation between two regions of cat V1 when simultaneously excited by a single moving bar of light, which did not occur when stimulated by two bars of light moving in opposite directions (Gray et al., 1989). These experiments prompted a wave of subsequent studies on stimulus dependent inter-region synchronisation in a variety of sensory regions and species (reviewed in Gray, 1999; Singer, 1999; Uhlhaas et al., 2009). Though some studies have shown increased inter-region synchronisation for stimuli which satisfy Gestalt criteria for perceptual grouping, several studies that directly tested the relationship between synchronisation and perceptual grouping failed to find evidence for the hypothesis (Lamme and Spekreijse, 1998; Thiele and Stoner, 2003; Roelfsema et al., 2004; Dong et al., 2008; Lima et al., 2010). Additionally, the strong dependence of oscillation frequency on local contrast was shown to greatly reduce coherence across stimuli with spatially varying contrast (Ray and Maunsell, 2010).

Though current evidence suggests that gamma oscillations in the early visual system are unlikely to play a role in feature binding, there is abundant evidence that they are stimulus dependent and under some conditions very strong (Gray and Singer, 1989; Friedman-Hill et al., 2000). It is therefore plausible that they affect functional interactions among networks and play a role in computation.

Recent accounts of V1 function have proposed that it implements low level operations such as divisive gain control (Carandini et al., 1997, 2005), which reduce correlations between representations of features such as the orientation and contrast of local image patches, which occur as a result of the statistics of natural scenes (Schwartz and Simoncelli, 2001). Such operations may serve to increase coding efficiency or implement generative models of low level image statistics for use in inference (Schwartz et al., 2007). If oscillatory dynamics at gamma frequencies do play a role in computation in V1, it is more likely that it is in such low level operations rather than in representing high level features such as binding. This would be consistent with the strong dependence of gamma oscillation frequency and strength on low level stimulus features (Gray and Singer, 1989; Friedman-Hill et al., 2000; Henrie and Shapley, 2005; Gieselmann and Thiele, 2008; Ray and Maunsell, 2010).

In the absence of visual stimulation, visual cortex exhibits prominent alpha frequency (10-15 Hz) oscillatory activity (Berger, 1929; Pfurtscheller and Lopes da Silva, 1999; Fries et al., 2008). The alpha oscillation observed in visual cortex is thought to be primarily generated in the lateral geniculate nucleus (LGN) of the thalamus (Hughes and Crunelli, 2005; Lorincz et al., 2009). Because alpha oscillations occur most prominently with the eyes shut and are reduced by visual stimulation, they were initially thought to reflect idling (Adrian and Matthews, 1934) of cortical regions. However, recent reports indicate that visual cortex alpha oscillations occur in behaving animals (Lorincz et al., 2009; Mo et al., 2011), and in humans, where they have been shown to modulate cortical excitability (Scheeringa et al., 2011) and perception (VanRullen et al., 2006; Busch et al., 2009; Mathewson et al., 2009) (Van Rullen 2006, Busch 2009, Mathewson et al 2009). Cortical alpha oscillations are enhanced by certain cognitive tasks (reviewed in Klimesch et al., 2007; Palva and Palva, 2007), particularly those involving short term memory (Klimesch et al., 1999; Jensen et al., 2002). These data suggest that thalamo-cortical alpha oscillations do not simply reflect the idle cortical state but in fact are actively and selectively modulated across cortex in response to task demands. The precise function of this modulation remains unclear but has been proposed to play a role in top-down inhibition of activity (Klimesch, 1996; Pfurtscheller, 2003; Klimesch et al., 2007), and in coordination of activity across cortical regions (Klimesch, 1996).

Another well characterised oscillatory activity pattern observed in visual cortex is the slow (<1 Hz) sleep oscillation (Steriade et al., 1993). This occurs during slow wave sleep and under some anaesthetics and is a transition between a quiescent network state (down state) in which membrane potentials are near resting and no spiking occurs, and an active network state, similar to asynchronous activity observed in awake animals in which membrane potentials are maintained near spike threshold by balanced excitatory and inhibitory currents (Haider et al., 2006; Destexhe et

al., 2007; Crunelli and Hughes, 2010). Transitions between these states are thought to be mediated by slow adaptation processes in cortex including synaptic depression (Contreras et al., 1996), activity dependent potassium conductances (Sanchez-Vives and McCormick, 2000), and $GABA_b$ receptor activation (Mann et al., 2009), potentially interacting with intrinsically oscillating thalamic cells (Crunelli and Hughes, 2010).

The above studies suggest that while the early visual system generates several distinct oscillations in different states, the temporal dynamics of the states themselves are fairly straightforward, with a single characteristic frequency of oscillatory or resonant network dynamics. However, several recent studies have argued for more complex oscillatory patterning of activity during early visual and auditory processing. Recent studies in primary visual (Montemurro et al., 2008) cortex of anaesthetised macaques and primary auditory (Kayser et al., 2009) cortex of awake macaques, argue that information is encoded by spike phase relative to low frequency oscillations (<10 Hz). In these studies, naturalistic stimuli (either movies or natural sounds) were played to macaques, while spikes and field were recorded from primary visual or auditory cortex. Repeated presentations of the stimuli allowed the probability distribution of responses to be estimated. The authors used these probability distributions to estimate the mutual information between which section of the stimulus was being played and different measures of the elicited spikes and field. The authors compared information carried by the spike activity alone, with information carried by spike activity labelled with the phase at which each spike occurred relative to different frequency bands of the LFP, extracted by bandpass filtering the raw LFP signal. In both studies the authors report that the phase of low frequency LFP fluctuations is consistent across repeated presentations of the stimulus and that spike phase relative to low frequency LFP fluctuation carried additional information which was not available from the spike activity alone. The additional information was maximal for the lowest LFP frequency band evaluated (1-4 Hz) and decreased monotonically with frequency. The authors proposed that low frequency oscillations were entrained by the stimulus and provide a temporal framework against which timing codes operate. They suggest that multiplexing sensory information into rate, phase and timing codes enhances the total information carried by sensory responses and increases robustness or signal to noise ratio (Kayser et al., 2009; Panzeri et al., 2010).

If this interpretation is correct, these studies provide evidence of sophisticated involvement of low frequency oscillatory dynamics in encoding stimuli in primary sensory cortices. This is somewhat surprising as although low frequency (<4 Hz) oscillatory activity occurs in sleep and some anaesthetised states, there is not strong evidence for oscillatory dynamics at these frequencies in visual cortex of awake animals or anaesthetised animals during stimulation with static stimuli. In these conditions the spectrum of the LFP is ~1/f, with peaks at gamma frequency at high contrast

and at alpha frequency in the absence of stimuli (Henrie and Shapley, 2005; Fries et al., 2008; Ray and Maunsell, 2010). Although there is a lot of power in the LFP at low frequencies, the absence of a peak in the spectrum suggests this does not arise from oscillatory dynamics, but rather reflects broadband activity fluctuations.

A recent study by Lakatos et al (2005) did report delta (1-4 Hz), theta and gamma oscillations occurring simultaneously in spontaneous activity of primary auditory cortex, in a hierarchy in which the phase of lower frequency oscillations modulates the amplitude of the higher frequency oscillations (a phenomenon known as nesting). However, aspects of this study make the results difficult to interpret. Firstly, the modulation of multi-unit activity by the phase of each of these oscillations was extremely shallow (~5% peak to trough). Shallow spike-field phase modulations and weak nested 'oscillations' can occur artifactually for even homogeneous Poisson models of network activity with no oscillatory dynamics (T. Akam, unpublished observations). Secondly the LFP did not show the characteristic 1/f spectra which has been reported in a study of spontaneous activity in awake human auditory cortex (Nir et al., 2008).

There are several mechanisms by which the LFP phase could have provided information that was not present in the simultaneously recorded spikes in the absence of oscillatory dynamics. Firstly, the LFP samples the activity of a greatly larger number of neurons than those whose spiking activity is recorded. Even if these neurons shared the same stimulus tuning as the recorded spikes, the LFP responses may be more consistent than the spikes and hence carry additional information. Additionally, if the stimulus tuning of the neurons contributing to the LFP is different from that of the spikes, the LFP phase and spikes may carry complementary information in the absence of any oscillation. A second reason why the LFP and spikes may have carried different information in this analysis comes not from different neurons contributing to the two signals, but rather from contributions of activity occurring at different times. The LFP phase was calculated by band pass filtering the raw LFP around the chosen frequency and then using a Hilbert transform to evaluate the phase at the time of each spike. The instantaneous phase of a band-pass filtered signal necessarily reflects activity over a time window around the timepoint a which phase is evaluated. Though the precise duration of this time window will depend on the filtering, it is reasonable to assume that at least one period of the frequency of interest will contribute. For the 1-4 Hz LFP fluctuations whose phase was found to be most informative, this corresponds to ~ 500 ms of LFP. By contrast, the time windows used to evaluate the information carried by spiking activity were 4 or 8 ms in the Montemurro et al. (2008) study and varied between 8 and 48 ms in the Kayser et al. (2009) study. Given this difference in the timescales sampled by the two measures, it is perhaps unsurprising that the spiking activity and LFP phase carried distinct information. This interpretation

is consistent with the observed monotonic decrease in phase-coded information with frequency, whereas phase coding with respect to a genuine oscillation would be expected to peak at the oscillation frequency. We therefore remain unconvinced that the above studies provide strong evidence for phase of firing coding in these systems.

These studies exemplify an ambiguity which crops up again and again in the oscillations literature: whether observed phenomena reflect oscillatory dynamics or broadband fluctuations. This issue is particularly acute in studies of task dependent modulation of oscillatory activity in which activity is generally less well characterised than for basic stimulus driven activity in V1, and where indirect measures of activity such as EEG or MEG are often used. Our approach is to focus on studies where clear peaks in spectral measures of activity provide strong evidence for oscillatory dynamics.

2.5.2 Attentional modulation of oscillations in sensory processing

The term attention encompasses a diverse range of phenomena related to selective processing of sensory stimuli. Organisms need mechanisms for flexibly selecting sub-sets of their sensory input for two basic reasons. The first is due to the nature of the control problem that the brain has evolved to solve: that of mapping sensory inputs onto adaptive behavioural outputs. In any given environment and incentive state (such as hunger or thirst), some sensory cues have important behavioural implications while other do not. Across different environments and incentive states, both the set of sensory cues that are relevant to controlling behaviour, and the appropriate responses to a given cue, may change. Normative solutions to even simple reinforcement learning problems therefore require that organisms selectively use those sensory cues that are informative about the probable value of different courses of action in a given state, while ignoring those that are irrelevant (Mackintosh, 1975; Dayan et al., 2000; Yu and Dayan, 2005).

In principle, sensory processing and decision making could be implemented in entirely separate systems with selection occuring only at the point of calculating decision variables such as state or action values. In practice, it appears that task demands progressively shape sensory representations from primary sensory corticies (Motter, 1993; Luck et al., 1997) through to high level representations, such as those in parietal cortex which utilise sensory information (Shadlen and Newsome, 2001) in calculating decision variables (Platt and Glimcher, 1999).

Resource constraints provide a different motivation for selection earlier in the sensory hierarchy, which has long informed thinking about attention (Broadbent, 1958; Treisman, 1969; Duncan, 1980; Desimone and Duncan, 1995). Such theories posit that the brain is not able to completely process all stimuli simultaneously due to limited representational or computational capacity, and so selectively processes a subset of stimuli in greater depth than others. The selection of stimuli for

processing by a constrained resource should clearly depend on their behavioural relevance. Therefore, although there is a clear conceptual distinction between selective processing for normative decision making and that due to resource constraints, in practice mechanisms addressing each are likely to be closely intertwined. Heterogeneous behavioural results in different tasks, and an absence of physiological evidence for a single bottleneck, suggest that a variety of different selectional processes underlie disparate attentional phenomena at different levels between early sensory processing and action execution (Wolfe, 1998; Driver, 2001; Zelinsky, 2005).

The proposal that oscillations play a role in selective attention (Crick and Koch, 1990; Niebur et al., 1993) preceded experimental evidence and grew out of theories that both attention and oscillations were involved in binding features represented in different networks. Though evidence for binding by synchrony in the early visual system now appears questionable, experimental studies have revealed a wide range of phenomena in which selective attention modulates oscillatory activity.

Much of the work on oscillations in attentive processing has used classical visual spatial attention tasks originally used to study the effects of attention on the firing rate of visual cortical neurons (Moran and Desimone, 1985; Desimone and Duncan, 1995; McAdams and Maunsell, 1999). In such tasks subjects maintain fixation on a central point while multiple stimuli are presented in their peripheral vision. A pre-stimulus cue informs the subject which of the stimuli will be behaviourally relevant. The subject performs a discrimination task on the target stimulus such as detecting a change in its orientation, while ignoring distracting stimuli. Attentional effects in such paradigms have been most intensively studied in V4 (Moran and Desimone, 1985; McAdams and Maunsell, 1999; Reynolds et al., 1999, 2000). When the two stimuli fall within the receptive field of a single V4 neuron, changing which of the stimuli is attended has a dramatic effect on neuronal responses. If the two stimuli elicit different firing rate responses when presented individually, the response to simultaneous presentation of both in the absence of selective attention generally results in an intermediate response. Selective attention to one or other of the stimuli modifies the response to the presentation of the pair towards the response elicited by the attended stimulus presented in isolation (Reynolds et al., 1999). Where only a single stimulus is in the receptive field of a V4 neuron, selctive attention has an approximately multiplicative effect on orientation tuning curves (McAdams and Maunsell, 1999). Smaller though still significant attentional effects on firing rates are observed earlier in the visual system in V1 and V2 (Motter, 1993; Luck et al., 1997).

Recording of spike and LFPs in macaque cortex during spatially selective attention tasks have demonstrated modulation of both gamma and alpha oscillations. Gamma frequency synchronisation during stimulus presentation in V4 is increased in the region representing the attended stimuli (Fries et al., 2001, 2008; Taylor et al., 2005; Gregoriou et al., 2009), while alpha oscillations in the pre-

stimulus period are suppressed (Fries et al., 2008). The speed of detection of a change in an attended stimulus was shown to correlated with the strength of gamma band synchronisation in regions of V4 representing that stimulus both before and after the change (Womelsdorf et al., 2006). Trial to trial variation in gamma synchronisation was more strongly correlated with behaviour than variations in firing rate, and was predictive of behavioural performance earlier in the trial than rate changes. Behavioural performance was also shown to correlate strongly with V4 gamma synchronisation on a spatial attention task in which macaques attended to one of two simultaneously presented stimuli whose shape varied smoothly, and had to respond whenever the attended stimuli took on a specific target shape (Taylor et al., 2005).

The increase in local circuit gamma synchronisation in V4 is accompanied by a strong narrow-band increase in coherence at gamma frequencies between regions of frontal eye field (FEF) and V4 representing the attended stimulus (Gregoriou et al., 2009). The FEF is strongly implicated in top-down attentional modulation of visual cortex (Moore and Armstrong, 2003; Ekstrom et al., 2008) and the relative timing of changes in firing rates and gamma power in the two regions suggests that an initial increase in firing rates in FEF may initiate the inter-region oscillatory activity. Gamma frequency synchronisation in V4 is also strongly enhanced by feature selective attention when the colour or shape of an object in the receptive field matched that of a target object during visual search (Bichot et al., 2005). The narrowband increases in power in these studies clearly point to an oscillatory rather than broadband phenomenon, but the depth of oscillatory modulation is hard to evaluate as the studies primarily use coherence measures which do not directly map onto a given strength of oscillatory modulation (see Chapter 6).

Studies using EEG or MEG have observed attentional modulations in humans that are consistent with the modulation of oscillatory activity reported from intracortical recordings from macaques. To overcome spatial resolution limitations, studies present widely spaced visual stimuli, generally in opposite hemifields of visual space such that visual evoked activity is induced in opposite hemispheres of the brain. Subjects are cued to make a discrimination about one or other of the stimuli and the effect of attention is evaluated by comparing signals evoked on the sides ipsilateral and contralateral to the attended stimulus. Such studies have consistently reported enhanced stimulus induced gamma power over the hemisphere representing the attended stimulus and suppressed gamma power in the hemisphere representing the non-attended hemisphere (Gruber et al., 1999; Vidal et al., 2006; Jensen et al., 2007; Siegel et al., 2008). Selective attention also increases alpha band power in networks representing non-attended regions of space while suppressing alpha activity in the attended regions (Worden et al., 2000; Sauseng et al., 2005; Thut et al., 2006; Rihs et al., 2007).

The spatial resolution of EEG and MEG is improving due to increased numbers of channels and analysis methods to reconstruct the spatial distribution of sources from the sensor data (Van Veen et al., 1997; Gross et al., 2001). This is allowing identification of frequency specific changes in coherence between signals originating in local regions of cortex. Using these methods, Siegel et al. (2008) identified attentional enhancement of gamma frequency coherence between FEF and visual cortex, consistent with the macacque data (Gregoriou et al., 2009), and between parietal and visual cortex.

Attentional studies in other sensory modalities have reported similar modulations of oscillatory activity to those observed in the visual system, though the paucity of intracortical recordings gives a more limited picture of the effects of attention. MEG studies of spatially selective attention to somatosensory stimuli have reported increased gamma power (Bauer et al., 2006), and decreased alpha and beta power (Bauer et al., 2006; Jones et al., 2010; van Ede et al., 2011) in regions of somatosensory cortex representing the attended stimuli. In the auditory modality, selective attention to sounds presented in one or other ear was shown to enhance a narrowband peak at ~40 Hz in the EEG response evoked by sound presentation, suggesting increased cortical gamma band synchronisation (Tiitinen et al., 1993, 1997; Debener et al., 2003). Though effects of attention on alpha power in auditory cortex have not been reported, working memory for auditory stimuli was recently shown to enhance MEG alpha power over temporal and frontal regions during stimulus retention (Leiberg et al., 2006; Van Dijk et al., 2010).

Though many studies have shown increased gamma and reduced alpha frequency oscillatory activity in regions of cortex representing attended sensory stimuli, recent results indicate that attentional effects on oscillations in cortex are not homogeneous. Unlike in V4, spatially selective attention was shown to decrease gamma frequency synchronisation in V1 (Chalk et al., 2010). Another recent study investigated attentional effects on alpha frequency oscillation in a high level visual region, the inferotemporal cortex (IT) (Mo et al., 2011). Visual and auditory stimuli were simultaneously presented to macaques in a block design in which the animals alternately attended to each modality. The LFP power spectra in IT showed a clear peak in the alpha band. Unexpectedly, alpha power was higher in blocks were the animal attended to the visual stimulus, and both stimulus evoked multi-unit activity and LFP gamma power were higher during periods of strong alpha. These results build on a previous study which found that while alpha power in V2 and V4 negatively correlated with performance on a visual discrimination task, alpha power in IT was positively correlated (Bollimunta et al., 2008). Interestingly, the laminar distribution of alpha current generators was different for IT compared with V2 and V4, with alpha currents generated in deep layers of V2 and V4 and superficial layers of IT.

Though less extensively documented than attentional modulations of gamma and alpha frequency oscillations, several studies have reported changes in the beta (15-30 Hz band). A study in humans exploited a phenomenon known as attentional blink to investigate MEG correlates of attentional processing (Gross et al., 2004). Attentional blink is a phenomenon in which for a period of several hundred milliseconds after the presentation of a target stimulus, the probability of detecting a subsequent target is reduced. Subjects were required to detect a target letter in rapid stream of letters sequentially flashed on a screen. MEG was used to identify a distributed fronto-parieto-temporal network of cortical regions which selectively responded to presentation of the target stimuli. The authors compared trials in which two rapidly presented targets were successfully detected with trials on which attentional blink obscured the second target. Beta frequency synchronisation between regions in the target associated network was significantly enhanced prior to successful detection of the second target. In a more traditional spatial attention task, spatial attention was also shown to selectively enhance beta band coherence of activity between parietal cortex and visual area MT using intracortical recordings in the macaque (Saalmann et al., 2007). Enhanced beta frequency synchronisation has been reported in cat visual cortex and thalamus when attention was directed to visual rather than auditory stimuli (Wróbel et al., 2007).

To summarise, selective attention imposed by task requirements causes changes in both the strength of local circuit oscillatory synchronisation and in large scale patterns of synchronisation between brain regions. Though enhancement of gamma oscillations and suppression of alpha oscillations are common, different attentional requirements produce heterogeneous changes in different regions of cortex. In several studies local circuit or inter-region oscillatory synchronisation has been shown to correlate with behavioural performance. The functional significance of these changes remains poorly understood. Attentional modulation of alpha oscillation power in many studies is broadly consistent with the hypothesis that alpha oscillations are a mechanism for suppressing activity in cortical regions where it is not needed or would interfere with task performance. However, the suppression of activity in a cortical region does not in principle necessitate oscillatory activity, and indeed increased synchronisation of activity would be expected to increase the impact on downstream regions. Additionally, recent reports of increased alpha power with attention in some cortical areas (Mo et al., 2011) are inconsistent with the alpha inhibition hypothesis.

Many accounts of the role of oscillatory activity in attention focus on the hypothesis that the oscillations effectively remap the connection structure between networks to implement the required selective stimulus processing (Niebur et al., 1993; Varela et al., 2001; Schnitzler and Gross, 2005; Womelsdorf and Fries, 2007). We discuss in detail in a dedicated later section of this review, mechanistic proposals that have been advanced for how changes in structures of oscillatory activity

may control the gain of interactions between neurons. As many such proposals invoke changes in local circuit or inter-region synchronisation as mechanisms for gain modulation, they are broadly consistent with observations of these phenomena in attentional processing.

We note here a broader conceptual difficultly in evaluating whether observed modulations of oscillatory activity by attention are consistent with this functional role. There is currently only a partial picture of what computations are implemented at different levels of sensory processing and a very limited description at a computational level (Marr and Poggio, 1976) of what attentional mechanisms are doing in different brain regions. Therefore we cannot with any great confidence provide a quantitative picture of what changes in connection structure we expect to see during attentional processing. Classical conceptual accounts consider attention as a process of selectively routing information through a convergent hierarchy, in which multiple low level regions compete for representation in each higher level region (Anderson and Essen, 1987; Olshausen et al., 1993; Desimone and Duncan, 1995). This would suggest that the gain of feed-forward connections from attended regions should be increased while that from non-attended regions should be decreased. There is some experimental support for this picture in the visual system (Desimone, 1998; Reynolds et al., 1999), and it provided some motivation for the convergent pathway models considered in Chapters 4 and 5. However, it does not really address the basic question of what computations each level is performing, as low level representations of simple local features are transformed through the sensory hierarchy to extract those attributes of the sensory scene that are currently relevant to the organism. Contemporary theoretical accounts of behavioural data on simple spatial attention tasks, which treat them as a problem of Bayesian inference over spatially confounded inputs (Yu et al., 2009; Dayan and Solomon, 2010), suggest considerably more complex computations than selectively routing a subset of inputs through a convergent pathway. This is not to say that changing the gain of pathways, potentially by oscillatory mechanisms, does not play a key role in implementing attentional computations. Rather, it is to highlight that we only have a limited understanding at this point of what changes in gain we expect to see in a given attentional task, which poses a challenge for interpreting attentional modulations of oscillatory activity.

2.5.3 Theta oscillations in hippocampal dependent behaviours

The hippocampi play a key role in spatial navigation and episodic memory and are implicated in many other behaviours. They are of interest to us primarily because of the theta oscillation: a 4 -10 Hz oscillation which is most prominent in the hippocampal formation where it supports a rich structure of phase and rate coding. It is increasingly becoming clear that the theta oscillation also patterns activity in other cortical and sub cortical structures, and that the strength of coupling of different structures to hippocampal theta is strongly modulated in a task dependent manner. We first

briefly review the theta oscillation in the hippocampal formation and then focus on task dependent modulations of inter-region theta activity.

2.5.4 The hippocampal theta oscillation

Though a number of different sub-cortical structures have been implicated in generating the theta oscillation (reviewed in Buzsáki, 2002), it has recently been demonstrated that the intact hippocampus *in vitro* is capable of generating a robust theta oscillation (Goutagny et al., 2009). In rodents *in vivo*, the theta oscillation is prominent in the LFP recorded from all sub-fields of the hippocampus during movement, REM sleep, and various other behaviours (Vanderwolf, 1969). The theta oscillation is thought take the form of a travelling wave along the long axis of the hippocampus (Lubenov and Siapas, 2009). The spiking probabilities of both pyramidal cells and interneurons are strongly modulated as a function of the phase of ongoing theta oscillations in both anaesthetised and awake animals. Different interneuron populations fire most strongly at different phases of the locally recorded LFP theta phase in both anaesthetised (Klausberger et al., 2003) and awake (Czurko et al., 2011) animals.

The spiking of pyramidal cells shows a complex structure of activity in behaving animals, in which both the average firing rate, and phase of firing with respect to the local LFP oscillation, appear to play a role in encoding information. Coding in the hippocampus has been most extensively studied in the context of spatial navigation. The firing rate of many pyramidal cells is strongly modulated by the spatial position of the animal in its environment (O'Keefe and Dostrovsky, 1971; O'Keefe, 1976; Muller, 1996). The code is sparse, with only a fraction of cells active in any one environment and a tiny fraction of cells active at any one time. Those cells that are active in a given environment fire selectively at particular locations in space, usually showing one or a small number of place fields. The phase of firing of individual cells relative to the local theta rhythm varies systematically as animals move through the place field of a cell, firing late in the theta cycle when the animal first enters the place field and moving to progressively earlier phases as the animal traverses the place field (O'Keefe and Recce, 1993; Skaggs et al., 1996; Huxter et al., 2003, 2008). A consequence of this phase precession is that on each theta cycle active place cells fire sequentially, ordered by the sequence of their place field locations on the animal's trajectory (Skaggs et al., 1996; Huxter et al., 2008). This compression of sequences of sequentially visited locations into each theta cycle may play an important role in storing trajectories through spike timing dependent plasticity (Sato and Yamaguchi, 2003). Phase precession of hippocampal pyramidal cells has also been reported in non-spatial behaviours such a wheel running, and during REM sleep (Harris et al., 2002). The phase of firing and average firing rate appear to be at least partially dissociated suggesting they are able to independently participate in coding (Huxter et al., 2003). Phase precession extends to

entorhinal cortex grid cells during navigation (Hafting et al., 2008), and to other brain regions as described below.

A variety of models have been proposed to explain phase precession, although the subject remains contentious. Phase precession can occur due to interaction between periodic inhibition at theta frequency and periodic (Harris et al., 2002) or unmodulated (Mehta et al., 2002) excitation whose strength varies on a slower time-scale. These mechanisms do not permit spike phase to be fully dissociated from firing rate, though spike-frequency adaptation (Harris et al., 2002) or synaptic regulation by cannabinoids (Losonczy et al., 2010) have been proposed to explain the observed dissociation of rate and phase as the animal leaves the place field. Greater independence between rate and phase is achieved by models in which phase precession occurs as a result of interference between oscillators with slightly different frequencies (Lengyel et al., 2003; O'Keefe and Burgess, 2005; Burgess et al., 2007). These could be network oscillators or dendrites with sub threshold oscillatory dynamics (Burgess et al., 2007), though it has been argued that phase locking between coupled oscillating dendrites precludes this possibility (Remme et al., 2010). The role played by the richly structured interneuron activity in generating phase coding remains unclear, though phase precession in hippocampal interneurons has been reported (Maurer et al., 2006; Geisler et al., 2007). Propagation of activity through directional connections on each cycle of an oscillation has also been proposed as a mechanism to generate phase ordered sequences of spiking (Tsodyks et al., 1996).

2.5.5 Task dependent extra-hippocampal theta oscillations

In recent years a number of studies have identified theta frequency oscillations in brain areas outside the hippocampal formation which are strongly modulated by behavioural tasks. In some cases these have been shown to be part of a large scale oscillatory activity pattern also involving the hippocampal formation while in others the relationship to hippocampal theta oscillations remains unclear.

Cortico – hippocampal theta oscillations have principally been studied in rodents, where simultaneous recording in the two structures are routine. Phase locking of a fraction of units in the prefrontal cortex (PFC) to simultaneous recorded LFP theta oscillations in CA1 was first reported by Siapas et al. (2005), and has since been explored in a number of behavioural tasks (Hyman et al., 2005; Jones and Wilson, 2005b; Adhikari et al., 2010; Benchenane et al., 2010). The strength of oscillatory coupling between PFC and hippocampus appears to be selectively increased during decision making in maze based tasks. Jones and Wilson (2005) observed stronger phase locking of PFC units to hippocampal theta in sections of a maze task that required a choice of which direction to turn based on the animals starting position on that trial. This stronger phase locking resulted in increased cross correlations between PFC and CA1 units, and was accompanied by increased LFP

theta coherence between PFC and hippocampus. The strength of PFC neuron phase locking to hippocampal theta was correlated with behavioural performance, with stronger phase locking during the decision on trials in which the animal made the correct choice. Detailed analysis of the phase relationship between PFC neurons and hippocampal theta revealed phase precession, which was most robust during the decision making section of the task (Jones and Wilson, 2005a). Benchenane et al. (2010) also reported increased PFC – CA1 coherence and PFC theta phase locking at the choice point in a T-maze task, which emerged progressively as the decision rule was learnt by the animal. Again, choice performance was significantly correlated with the strength of PFC – hippocampus theta coherence. Interestingly, the increased PFC – hippocampal theta coupling during decision making did not appear to result from changes in hippocampal theta amplitude (Jones and Wilson, 2005b; Benchenane et al., 2010), or from increased firing rate of hippocampal units (Jones and Wilson, 2005b). These results provide a tantalising suggestion that specialised mechanisms exist which enable prefrontal cortex to selectively couple to hippocampal theta oscillations, and that engaging these mechanisms plays a functional role in decision making in these tasks.

Transient, task-dependent bursts of cortical theta frequency oscillation have been identified in humans and monkeys, which may be related to the hippocampal – cortical coupling observed in the rodent studies. Using sub-dural electrode arrays on the cortical surface of pre-operative epileptic patients, Kahana et al. (1999) observed transient bursts of high amplitude theta frequency activity in a wide range of cortical areas as subject navigated through a virtual reality maze. Cortical theta episodes were more common once the subjects had learnt the route through the maze, consistent with the increased hippocampal – cortical theta coupling observed by Benchenane et al. (2010) as rats acquired the decision rule in a T-maze. Subsequent studies also using sub-dural electrodes revealed that similar theta frequency bursts in cortical areas occurred during non-spatial working memory tasks in humans (Raghavachari et al., 2001). At a number of recording sites the theta oscillation started abruptly at the beginning of each trial, continued throughout, and then decreased to baseline following the end of the trail. Similar enhancement of LFP theta power during the delay period of a visual working memory task has also been observed in intra-cortical recording in macaque V4 (Lee et al., 2005). A majority of simultaneously recorded units showed significant modulation of spike probability with theta phase. The stimulus selectivity of spike activity of individual neurons varied as a function of theta phase, with ratios of firing rates between preferred and non-preferred stimuli around the phase at which the neurons spiked most strongly. The function of this activity is somewhat mysterious as V4 does not show the sustained elevated firing rates observed during the delay period in prefrontal cortex (Fuster and Alexander, 1971; Goldman-

Rakic, 1995), which are thought to play a key role in maintaining the memory through attractor dynamics (Amit and Brunel, 1997).

Whether these transient bursts of cortical theta activity observed in monkeys and humans reflect coherent cortico – hippocampal oscillations remains unclear. Less is known about theta oscillations in primate hippocampus than in the rat, though data from depth electrodes in epileptic patients and from source reconstruction methods using EEG or MEG, are starting to provide a window into human hippocampal activity (reviewed in Kahana, 2006). Theta frequency oscillations are less prominent in the primate hippocampus than in rodents but have been observed in both waking (Meador et al., 1991; Tesche and Karhu, 2000; Cantero et al., 2003; Ekstrom et al., 2005) and sleeping (Cantero et al 2003) states. Both spatial navigation (Ekstrom et al., 2005) and working memory tasks (Tesche and Karhu, 2000) have been shown to increase human hippocampal theta power, and successful memory formation is correlated with tighter hippocampal spike-LFP phase locking in the theta band (Rutishauser et al., 2010). These results may indicate that the cortical theta bursts observed in spatial navigation and memory tasks are part of a wider cortico – hippocampal theta oscillation. However, analysis of spatial patterns of coherence between local theta oscillations in human cortex measured with sub-dural EEG revealed that distal sites are often incoherent (Raghavachari et al., 2006). These results suggest that independent generators of theta frequency oscillations exist in primate cortex, but they certainly do not rule out the possibility that these sometimes couple with hippocampal theta. Additionally, it is currently not known whether theta activity in the primate hippocampus is a single coherent oscillation or is spatially patterned.

The available evidence suggests large scale structures of theta frequency oscillatory activity in cortico-hippocampal circuits which are dynamically modulated by behavioural and cognitive demands. We now briefly review evidence that this structure extends to a range of sub – cortical regions beyond the hippocampus.

The amygdala is a subcortical structure which plays important roles in decision making and behavioural control, particularly in the context of aversive learning (LeDoux, 2000). Interactions between the hippocampus and amygdala are thought to be important in fear conditioning, in which an animal learns that a particular sensory stimulus (the conditioned stimulus) predicts an aversive outcome such as a foot shock. Seidenbecher et al (2003) compared LFPs simultaneously recorded in hippocampal CA1 and lateral amygdala (LA) of mice between fear conditioned and control animals. Fear conditioned animals showed higher baseline theta power in CA1 than control, but the most striking differences were observed in response to the conditioned stimulus (CS+). When the CS+ was presented to fear conditioned animals, periodic activity in the theta band occurred in the amygdala LFP, which was coherent with that simultaneously recorded in CA1. These coherent LA-

CA1 oscillations were at a lower frequency than the theta that occurred in CA1 during exploration. The CS+ did not evoke any change in amygdala LFP in control animals. Freezing, a behavioural measure of fear, correlated with the strength of LA-CA1 oscillations. Theta frequency oscillations in amydala-hippocampal networks in response to aversive cues have been reported in several other studies (Pape et al., 2005; Narayanan et al., 2007) and in other species (Paré and Collins, 2000). A recent study suggests that amygdala – hippocampal theta synchronisation may be part of a larger oscillatory activity pattern involved in responses to fearful situations. Adhikari et al (2010) observed increased hippocampal – prefrontal cortex theta coupling in anxiogenic environments such as open arenas, in which theta power in PFC correlated with behavioural measures of anxiety.

The striatum is a component of the basal ganglia, that receives most of the cortical and hippocampal input to this system, and plays an important role in behavioural control and decision making (Knutson et al., 2008). The striatum receives an extensive projection from the hippocampus, particularly in the ventral subregions (Groenewegen et al., 1987). Coherent theta frequency rhythmicity between hippocampus and striatum has been reported in a number of studies and shows strong modulations with behaviour (Tabuchi et al., 2000; DeCoteau et al., 2007; van der Meer and Redish, 2011). DeCocteau et al (2007) recorded LFPs simultaneously from dorsomedial striatum (DMS) and the CA1 subfield of the dorsal hippocampus, as rats learnt to perform a conditional T-maze task in which two different tones indicated whether a turn to the left or right are would be rewarded. Theta power in DMS and CA1 were differentially modulated throughout each trial. In rats that successfully learnt the task, strong theta frequency coherence emerged between the two regions, starting shortly before the tone, and lasting till after the turn. Rats that did not successfully learn the task did not show this coherence peak during the decision, though baseline coherence between the two regions was the same as in successful learners.

Recently, phase precession of cells in the ventral striatum relative to hippocampal theta has been reported on a T-maze task (van der Meer and Redish, 2011). Phase precession was most prominent in ramp cells, whose activity slowly ramps up as the animal approaches a reward site, before dropping rapidly after the reward is obtained. Interestingly, the phase precession in ramp cells was slower than that in CA1 place cells, taking far more theta cycles to vary through a given angle of theta phase. Additionally, the range of phases spanned by the phase precession of striatal cells was the opposite half of the theta cycle to that spanned by CA1 place cells.

These results on hippocampal – striatal theta oscillations parallel many of the findings from simultaneous hippocampal – prefrontal recordings. Both show a selective increase in inter-region coherence at the decision point in maze tasks (Jones and Wilson, 2005b; DeCoteau et al., 2007; Benchenane et al., 2010) and all three regions show clear evidence of phase precession relative to

hippocampal theta (Jones and Wilson, 2005a; van der Meer and Redish, 2011). The prefrontal cortex projects directly to the dorsal striatum (McGeorge and Faull, 1989) so the three regions form a richly interconected structure. These results suggest these three anatomically connected regions selectively participate in a complex large-scale pattern of theta frequency oscillatory activity during decision making. How this recently discovered activity contributes to the computations underlying behavioural control remains unclear. To understand on a computational level why this burst of large-scale oscillatory activity occurs around the decision point, we need to understand how the computations occurring in this system differ between the period of elevated theta activity and other sections of the trial. On an implementational level we do not know what causes the task dependent modulation of oscillatory activity. However, these fascinating activity patterns are certainly consistent with the broad hypothesis that changing structures of oscillatory activity vary the effective connection structure of these networks to produce the required computational functions in different task epochs.

2.5.6 Oscillations in motor planning and execution

We now briefly review task dependent oscillatory activity in regions implicated in movement planning and execution. Oscillations in the beta and low gamma frequency range (15-50 Hz) are prominent in primate motor and premotor areas during behavioural tasks (Murthy and Fetz, 1992; Sanes and Donoghue, 1993; MacKay, 1997; Donoghue et al., 1998; Pesaran et al., 2008). The activity is characterised by short bursts of oscillation lasting from a few cycles to several seconds, which is often coherent across distances of several millimetres. The oscillations are clearly task associated as they occur preferentially in task periods compared with quiet sitting (Donoghue et al., 1998), and are more prominent in demanding tasks that require fine motor control (Murthy and Fetz, 1992). Beta frequency oscillations appear to be more strongly associated with movement planning than execution, as in tasks where the animal must wait for a go cue before starting movement, they occur strongly in the delay period but are greatly reduced during the movement (Sanes and Donoghue, 1993; Donoghue et al., 1998; Pesaran et al., 2008). Neuronal activity is modulated as a function of the phase of LFP oscillations, in some cases very strongly (Donoghue et al., 1998; Baker et al., 1999; Pesaran et al., 2008). Parallel recording from distributed sites suggest that beta oscillations in motor and premotor regions may exhibit travelling wave like spatial propagation (Rubino et al., 2006), reminiscent of that observed in hippocampal theta (Lubenov and Siapas, 2009).

Beta oscillations in motor and premotor cortex are part of a larger structure of task dependent beta frequency oscillatory activity that occurs during motor planning in primates. The cerebellum shows beta oscillation episodes during movement tasks (Courtemanche et al., 2002), which synchronise

with those in primary motor and somatosensory corticies in a task dependent manner (Courtemanche and Lamarre, 2005). As in the motor cortex, cerebellar beta oscillations are strongest during movement planning and reduced during movement execution. Beta oscillations have also been reported in the macaque striatum during a visuomotor task (Courtemanche et al., 2003), though their relation with cortical beta oscillations remains unclear.

Coherent beta oscillations have been observed between premotor cortex (PMd) and the parietal reach region, (PRR), a cortical region involved in representing reach locations (Pesaran et al., 2008). This study is of particular interest as it used carefully controlled behavioural tasks which revealed strong modulation of the oscillatory activity both during each trial and across trial types with different cognitive demands. Monkeys performed a visually guided reach task in which an array of reach targets appeared on a screen and after a delay period the monkey reached to touch the targets. In free choice trials the monkey chose in which sequence to reach for three identical targets, with equal probability of each being rewarded. In instructed choice trials the monkey had to reach for three different targets in a particular sequence to obtain reward, and in centre out trial, only a single reach target was presented. At search array onset a burst of strong oscillatory activity at ~ 15 Hz occurred coherently between PMd and PRR, which lasted for ~ 300 ms before disappearing. This activity was stronger on free choice trials than on instructed choice, and was much weaker on center out trials. Although this burst of oscillatory activity occurred simultaneously with a large increase in firing rates in both regions, firing rate changes were largest for centre out trials, indicating a dissociation between firing rate and the oscillatory activity. Decoding approaches indicated that neurons that participated in this oscillatory activity carried distinct information from those that did not.

Though we have only briefly touched on this subject, the reviewed literature indicates a pattern of strongly oscillatory activity in the beta frequency range which spans many different brain regions and is dynamically modulated on a rapid timescale during motor tasks. While the function of this fascinating activity remains poorly understood, the data is consistent with the existence of mechanisms that actively manipulate oscillatory network dynamics to control network function.

2.6 Oscillations as a gain control mechanism

Having reviewed task dependent modulations in a range of neural systems, we now turn explicitly to the hypothesis that one function of such activity is to control the gain of interactions between neural populations. Based on experiments measuring the cortical response to stimulation of the optic nerve, Bishop (1932) concluded, 'there is some level at which a rhythmic variation in

irritability takes place, apparently spontaneously'. Since this initial report of oscillatory modulation of the gain of nervous tissue, considerable interest has focussed on periodic modulation of excitability due to oscillatory network dynamics, and the possible functional role it may play in controlling the gain of interactions between neurons (Crick and Koch, 1990; Niebur et al., 1993; Salinas and Sejnowski, 2001a; Varela et al., 2001; Fries, 2005; Sejnowski and Paulsen, 2006).

We focus here on computational and conceptual proposals for how network oscillations may control the effective gain for anatomical pathways. These proposals address broadly the same computational problems as the models that we describe in Chapters 4 and 5. Therefore, where relevant we highlight similarities and differences from the mechanisms we have investigated, and how our work builds on these previous studies.

The first computational study to address this question was a model by Niebur et al (1993) aiming to reproduce experimental results on the effects of attention on activity in V4, evoked when two stimuli were simultaneously presented within the receptive field of a neuron (Moran and Desimone, 1985). In that study (see above p. 36), a preferred stimulus which elicited high spike rates when presented individually, and a non-preferred stimulus which elicited low spike rates, were presented simultaneously. Directing attention to one or other stimuli when they were presented simultaneously drove the firing rate of the V4 neuron close to that evoked by the attended stimulus presented in isolation. Based on proposals by Crick and Koch (1990), Niebur and colleagues hypothesised that the effect of attention might be mediated by selective oscillatory modulation in the gamma band of neuronal responses in regions of V1 representing the attended stimulus.

The response of V1 neurons was modelled as a Poisson process whose average firing rate was determined by the stimulus in its receptive field, while the focus of attention on that region was indicated by a sinusoidal modulation of the firing rates around their average value. To detect this periodic modulation of firing rates, the study postulated the existence of inhibitory interneurons with strong bandpass filtering properties, implemented as an integrate and fire model with resonant sub-threshold voltage dynamics combined with an adaptive spike threshold. These dynamics ensured that the interneurons would not spike in response to slowly varying depolarising inputs but would spike readily when driven by inputs modulated at 40 Hz. When an attended stimulus was present, the periodically modulated spiking in V1 drove activity in V4 interneurons, which, as a result of the network structure, provided feed-forward inhibition to V4 principal cells with preferred stimuli different from the attended stimulus.

While in the light of subsequent findings (e.g Chalk et al. 2010), the model cannot be taken as a realistic description of the experimental phenomenon, several aspects are interesting in the context

of controlling signal flow with oscillations. The study is an early quantitative exploration in a neuroscience context of how periodic modulation of a subset of signals in a convergent pathway could be exploited to process them differentially. Although it is not directly discussed by the authors in these terms, the study suggests that networks with appropriate filtering properties can selectively read out spatial patterns of firing rates with specific oscillatory modulations. In this case the spatial patterns are very simple; activity in one of two groups of V1 neurons with different preferred stimuli. We extend these ideas in Chapter 5 to show how multiplicative modulation can multiplex and de-multiplex firing rate population codes to selectively propagate signals through convergent pathways. In the Nieber model, it is the V4 interneurons that perform the readout, selectively responding to oscillating but not asynchronous inputs. However, their postulated neuronal dynamics have an implausible adaptive threshold, such that arbitrarily strong depolarising inputs will not drive spikes if they are slowly varying. We show in Chapter 4 that biologically plausible networks can be designed which produce a graded response to oscillating inputs at a specific frequency but ignore simultaneously presented asynchronous input, by using feed-forward inhibition with a network-level resonance phenomenon.

Subsequent computational studies have looked at different aspects of how changes in the synchronisation state of networks can affect their response to external inputs. Tiesinga et al (2004), investigated the response of a Hodgkin Huxley neuron receiving asynchronous excitatory input and periodically modulated inhibitory input, as a function of the strength and frequency of modulation of the inhibition. They demonstrate that increasing the synchronisation of the inhibition can increase the firing rate of the neuron, and that for some parameter ranges this increase is an approximately multiplicative change in the F-I curve. The increase in firing rate with inhibitory synchrony occurs because of periodic disinhibition of the neuron, increasing its spike probability for a given excitatory input level. A similar effect was reported in network simulations where periodic modulation of inhibition generated by the network dynamics increased the responsiveness of principal cells to excitatory inputs (Borgers et al., 2008). In a complementary study Tiesinga and Sejnowski (2004) demonstrated that the strength of oscillatory synchronisation of a recurrently connected inhibitory network could be modulated on a rapid time-scale without modifying its average rate by changing the spatial distribution of excitatory input.

In networks where excitatory neurons mutually inhibit each other through an E-I loop, changes in the synchronisation state can change the extent to which winner-takes all dynamics ensure that only the most strongly driven cells fire. Transition from an asynchronous state to a spike to spike oscillation in which cells spike once each cycle, can allow strongly driven cells to more effectively inhibit weakly driven cells, as on each cycle the strongly excited cells spike approximately

simultaneously and strongly inhibit the entire network before the more weakly driven cells have a chance to spike (Borgers et al., 2005). It is unclear whether these effects extend to sparsely synchronised oscillations that are likely more relevant in cortical networks. Though these studies are examples of how changes in oscillatory synchronisation in a local network can change its responses to inputs, they are conceptually further from our work than the Niebur study as they consider only asynchronous excitatory inputs and hence do not address how inputs with different modulation may be differentially processed.

The discovery of phase coding in the hippocampus has motivated studies of how patterns of activity occurring at different phases of an oscillation can be selectively read out by neural networks. Jensen (2001) proposed a simple mechanism for readout of specific components of a phase coded input by a single layer of integrate and fire neurons. Phase selectivity was generated by an externally imposed sinusoidal input current coherent with the phase coded input. Neurons only spiked in response to the phase coded input when this coincided with the depolarising phase of the sinusoidal current, such that by varying the phase of this current different phases of the input could be read out. Conceptually this model is similar to that considered in chapter 5 as the sinusoidal current effectively modulates the gain of the output neurons coherent with the input to generate a selective readout mechanism. The proposed gain modulation mechanism will clearly only work effectively over a rather narrow dynamic range of input firing rates and noise levels, as it exploits the strong nonlinearity of the neuronal input-output relationship around the spike threshold. Further work is required to quantify such limitations and identify how the robustness can be improved.

Recent work (Nadasdy, 2009, 2010) explored how coincidences between the timing of input spikes and the peaks of a travelling wave of sub-threshold oscillations could be used to generate a phase code which multiplexed a spatially extended representation into a single channel. This multiplexed representation could be converted back into a spatial representation by interference with a second travelling wave of sub-threshold oscillations. However, the highly structured oscillatory activity was externally imposed rather than dynamically generated, the system was noise-free, and the spatial input and output representations were latency coded. Therefore, while a demonstration of the multiplexing potential of spatially structured oscillations, it is unclear to what extent the model is compatible with the dynamics and noise levels of real networks, and with the extensive evidence for rate coding *in vivo*.

The 'communication through coherence' (CTC) hypothesis (Fries, 2005) has generated renewed interest in the idea that oscillations control signal flow between networks. This proposes that the strength of effective connectivity between two networks can be selectively enhanced when they engage in coherent oscillatory activity. Review articles had previously emphasised the role

oscillations may play in setting up flexible structures of signal flow between networks (Salinas and Sejnowski, 2001a; Varela et al., 2001) , but the CTC hypothesis made specific mechanistic proposals that have proved highly influential. Selective communication in CTC is proposed to occur through interaction between periodic modulation of the spike output of networks, and periodic modulation of their responsiveness to their inputs. Fries envisions that 'oscillations of a neuronal group rhythmically open and close the group's windows for communication'. Coherence between oscillations in two networks ensures that spikes from one network arrive during these windows of heightened excitability in the other network, and therefore that their effectiveness in driving activity is enhanced relative to other inputs.

As with the work of Neibur et al (1993), the CTC hypothesis emphasises the possibility that spatially overlapping inputs can be treated differentially by a receiving network on the basis of their oscillatory modulations. A major focus of the work in this thesis, particularly in Chapter 5, is investigating how accurately individual components of a combined input can be selectively read out by a receiving network, as a function of how different their modulations are. Our results suggest that in order for inputs to be accurately separable, it is important that their modulations are close to orthogonal. This questions Fries proposal that incoherent oscillations functionally decouple anatomically connected networks. However, where oscillations are appropriately structured, our results demonstrate the power of gain modulation coherent with a target input to accurately read out select components of a combined input.

A experimental study by Womelsdorf et al. (2007) aimed to test the CTC hypothesis by looking at the covariance of gamma oscillation amplitude in pairs of local cortical networks, as a function of their relative phase. They found that the distribution of phases was non-random, such that there was a preferred relative phase which occurred most frequently. The correlation of gamma oscillation amplitudes in the two networks varied as a function of their instantaneous relative phase, with higher correlation when their relative phase was around the preferred value. The authors argue that this is evidence for CTC as it suggests that bringing oscillations in the two regions into a particular phase alignment increases coupling strength between the networks and hence increases gamma amplitude covariance. However, an alternative explanation is that an increase in the coupling strength between the networks, due for example to increased firing rate in their projection neurons, both drives the networks towards a particular relative phase and increases the covariation of their amplitudes. The phase response dynamics that we measure for gamma oscillating networks in Chapter 3 is consistent with this alternative account. We therefore do not believe the Womelsdorf et al study provides conclusive evidence for CTC.

Several computational studies have aimed to model CTC at the network or neuronal level. A popular approach has been to evaluate the response of a population of neurons receiving two excitatory Poisson inputs with different oscillatory modulations, with either an externally imposted periodic inhibitory input (Mishra et al., 2006; Masuda, 2009) or a feed-forward interneuron population (Zeitler et al., 2008). Changing the relative phase of excitatory and inhibitory inputs was shown to change the output firing rate (Mishra et al., 2006). Where two excitatory inputs were coherent with each other but at different phases, changing the phase of inhibition relative to the excitatory inputs could vary the relative gain for each (Mishra et al., 2006; Masuda, 2009). Where two inputs influenced output activity both through direct excitation and feed-forward inhibition, with one predominantly exciting and the other predominantly inhibiting the output, increasing the strength of gamma frequency modulation of either input gave it more influence over output firing rates (Zeitler et al., 2008). In excitatory-inhibitory loop networks with winner-takes-all type dynamics due to mutual inhibition between excitatory cells, periodically modulated inputs were shown to be more effective at driving activity and suppressing cells driven by asynchronous inputs.

2.7 Conclusions of literature review

In this literature review we have aimed to outline the *in vivo* data which informs the hypothesis underlying this thesis, and provide a rationale for the approach we have taken in our work and the assumptions that it is based on.

We have really only scratched the surface of the vast literature on oscillatory neural phenomena. Nonetheless we hope to have demonstrated that clearly oscillatory activity patterns occur in a great range of brain regions and behaviours, that these structures of activity are often strongly modulated in diverse and interesting ways by changes in cognitive or behavioural states, and that trial to trial fluctuations in oscillatory activity in many cases correlate with behavioural performance.

These results are certainly consistent with the hypothesis that oscillatory or resonant aspects of network dynamics are actively modulated to change network function in response to differing computational requirements in different situations. Though currently available data do not amount to conclusive proof that oscillatory mechanisms are used to control the flow of neural signals, this hypothesis has attracted widespread interest and we believe the data are sufficiently suggestive to justify investigations into how such mechanisms may function.

We have reviewed evidence that motivated us to take two related decisions in the design of our computational models. The first was to focus on sparsely synchronised oscillatory dynamics in which individual neurons spike irregularly. The second was to focus on how oscillatory dynamics

can extend coding strategies that use spatial patterns of firing rates, rather than precise sequences of spike times, for the representation of information. We do not claim that precise spike timing codes or spike to spike oscillatory dynamics play no role in brain function, but have aimed to provide evidence that the codes and dynamics we focus on are relevant to understanding at least some of the activity observed in neural systems.

Chapter 3: Dynamical mechanisms of inter-region phase coherence

3.1 Introduction

Inter-region coherence of oscillatory network activity has been intensively studied with a focus on state, stimulus and task dependent modulation of coherence. Changes in coherence between local networks have been suggested to serve computational functions such as directing signal flow between regions, modulating synaptic plasticity or binding features of sensory representations. This chapter focuses on the basic question of how coherence arises between local networks. We briefly review prior experimental and computational approaches to this problem and then outline the contribution of the work described in this chapter.

Mechanisms of inter-region gamma coherence were first investigated in a series of studies using an *in vitro* paradigm in which local oscillatory activity was induced simultaneously in two regions of CA1 using tetanic stimulation. This induces transient gamma frequency oscillatory activity through activation of metabotropic glutamate receptors (Whittington et al., 1995). During this activity at least some pyramidal cells and interneurons spike once each cycle, indicating network dynamics in the 'spike to spike' synchrony regime (Kopell et al., 2000). For strong stimulation intensities, the induced oscillation can exhibit a transition to a beta rhythm in which pyramidal cells spike at half the frequency of interneurons (Whittington et al., 1997b; Kopell et al., 2000). When two local regions of CA1 are simultaneously stimulated, the resulting oscillations can synchronise with close to zero phase lag for both the gamma and beta rhythms (Traub et al., 1996; Whittington et al., 1997a; Kopell et al., 2000). Computational studies suggest that interneuron spike doublets played a critical role in synchronising local networks in these experiments (Traub et al., 1996; Whittington et al., 1997b; Kopell et al., 2000). A doublet consists of the interneuron spiking twice on a single cycle of the oscillation, with the second spike driven in large part by synaptic input from the distal oscillating network. This second spike allows the distal input to modify the timing of the next cycle of the local oscillation and hence bring the two local oscillations into synchrony.

Alhough these influential studies provided a detailed picture of mechanisms of inter-region synchronisation in this model system, their applicability to *in vivo* oscillatory coherence phenomena is questionable. The concern is that the 'spike to spike' synchrony regime in these models is incompatible with *in vivo* observations of irregular firing of individual units during periodic

network activity. These data suggest that *in vivo* gamma oscillations are sparsely synchronised, with activity characterised by irregular spiking of individual neurons but periodic modulation of network firing rates (see literature review). In the sparsely synchronised state it is not meaningful to talk about spike doublets as a critical component of the synchronisation mechanism, as on any given cycle a particular neuron may spike once, several times, or not at all.

In vivo studies suggest that transient enhancement of inter-region coherence often occurs concurrently with increases in local circuit spike rates (Pesaran et al., 2008; Gregoriou et al., 2009). A plausible qualitative explanation for the large increase in inter-region coherence in such studies is that increased firing rates in the neurons making up the inter-region connections increase the coupling between the regions, and this stronger coupling synchronises their oscillatory fluctuations. A quantitative understanding of inter-region oscillatory coherence requires a mathematical framework that can predict large scale activity patterns as a function of the local dynamics and inter-region connectivity. A crucial decision in constructing such a model is selecting the appropriate level of detail. At one extreme, the Blue Brain project (Markram, 2006) aims to model large scale brain activity at a microscopic level of detail, using supercomputers to simulate large populations of multi-compartmental neuron models. While these simulations could in principle inform how the micro-structure of circuits affects large scale activity, the complexity of the models is a formidable obstacle to understanding the emergent dynamics. At the opposite end of the complexity scale are neural mass models, which describe the aggregate activity of local populations as analogue firing rates. These models dispense with a vast amount of detail and hence can only address a limited range of questions. However, their simplicity can provide great insight into aspects of the dynamics they are capable of reproducing. Pioneering work by Wilson and Cowan (1972) proposed equations to describe the evolution of population firing rates in a system consisting of local excitatory and inhibitory neural populations interacting through synaptic connections. Depending on its parameters, the model either converges to a steady state or to an oscillatory limit cycle. If the oscillating state captures the relevant dynamics of real local networks, the model's simplicity makes it a powerful tool for understanding inter-region coherence. Large scale dynamics can be modelled either as interacting discrete local populations (König and Schillen, 1991; Campbell and DeLiang Wang, 1996) or as neural field models in which space is represented as a continuous variable (Coombes, 2010).

A large body of work has been dedicated to understanding how the dynamics of individual oscillators determine their synchronisation properties when coupled together. Much of this was motivated by a desire to understand the emergence of synchrony among individual neurons in low noise regimes, but the mathematical framework is very general and has been applied to systems as

diverse as circadian, cardiac and respiratory oscillators. This identified the phase response curve (PRC) of an oscillator as a critical determinant of synchronisation in coupled systems (Ermentrout, 1996; Rinzel and Ermentrout, 1998; Winfree A., 2000; Izhikevich, 2007; Smeal et al., 2010). The PRC measures the change in phase produced by an input pulse as a function of the phase at which the pulse is delivered. A key feature of the PRC of a system is whether it has the same sign for all phases (for example input advances the phase irrespective of the phase of stimulation), or has a region in which the input advances the phase and a region in which it delays it (henceforth described as a biphasic PRC). If an external input can only advance the phase of the oscillator, the oscillator can only entrain to periodic inputs with a higher frequency that the unperturbed oscillation frequency. If the phase response curve is biphasic, the oscillator can entrain to inputs over a range of frequencies spanning the unperturbed frequency. Biphasic PRCs strongly promote synchronisation of systems of coupled neuronal oscillators (Hansel et al., 1995; Abouzeid and Ermentrout, 2009; Smeal et al., 2010) and the relative phase of sychronisation is determined by the unperturbed frequencies of oscillators and the location of the regions of phase advance and delay in their PRCs. The phase response behaviour of local oscillating networks is therefore a key measurement for linking the local dynamics to large scale coherence.

The principal goal of the work in this chapter was to experimentally measure the PRCs of a sparsely synchronised oscillating network to determine if they are indeed biphasic. We used the well characterised model system of carbachol induced oscillations in CA3 *in vitro*. Carbachol induces oscillations by activating muscarinic acetylcholine receptors (Fisahn et al., 1998), which depolarise pyramidal cells by blocking a potassium conductance (Benson et al., 1988). Carbachol also heterogeneously excites different interneuron subtypes (Kawaguchi, 1997), modulates the strength of synaptic transmission (Scanziani et al., 1995), and supresses the slow calcium mediated after-hyperpolarisation (Cole and Nicoll, 1984). The overall effect on the network is highly excitatory, raising pyramidal cell firing rates to 2-3 Hz and interneuron firing rates up to ~ 20 Hz (about 0.6 times the oscillation frequency) depending on the interneuron subtype (Hajos et al., 2004; Mann et al., 2005). Individual neurons spike irregularly but the firing probability of both pyramidal cells and interneurons is strongly modulated with the phase of the network oscillation, with a small phase lag between pyramidal cells and interneurons consistent with *in vivo* data (Csicsvari et al., 2003). Fast excitatory and inhibitory synaptic transmission are required for the oscillations (Fisahn et al., 1998; Mann et al., 2005), but principally in the pyramidal cell layer as selective blockade in strata radiatum or lacunosum-moleculare does not abolish the activity. Taken together these data indicate sparsely synchronised dynamics mediated by an excitatory – inhibitory synaptic feedback loop involving perisomatic interneurons. Current source density analysis revealed alternating sink source pairs in stratum pyramidale and stratum radiatum (Mann et al., 2005), consistent with those

observed *in vivo* (Csicsvari et al., 2003). The oscillation frequency is strongly temperature dependent (Fisahn et al., 1998; Mann et al., 2005), but at 34º is approximately 40 Hz, indicating a gamma band oscillation at physiological temperatures. Carbachol induced oscillations in CA3 are therefore an attractive model system for studying mechanisms of gamma-band oscillatory coherence in the hippocampal formation, and more generally the response dynamics of sparsely synchronised network oscillations. However, spike-field phase locking *in vitro* is substantially stronger than that observed on average *in vivo* (Csicsvari et al., 2003; Hajos et al., 2004; Tukker et al., 2007). This may in part reflect spatial inhomogeneity of *in vivo* oscillations, which will dilute the contribution of participating neurons to the LFP, and non-stationary, which will reduce average phase locking relative to periods of strong oscillation. Such structure is poorly constrained by current data so it is not clear whether the *in vitro* oscillation is within the range of synchronisation strengths spanned by *in vivo* activity.

We characterised the phase response curve of the oscillating CA3 network as a function of stimulus strength for stimulation of the external mossy fibre input and recurrent collaterals. This revealed richly structured rephasing behaviour in which biphasic PRCs at low stimulation intensities gave way to complete resetting by strong stimuli. The measured rephasing behaviour was reproduced with remarkable accuracy by a model based on the Wilson-Cowan equations. Systematic differences between the effects of mossy fibre and local circuit stimulation could be explained by different coupling of these pathways to excitatory and inhibitory populations.

3.2 Materials and methods

3.2.1 Slice Preparation

Experiments were conducted in accordance with the United Kingdom Animals (Scientific Procedures) Act (1986). Sprague Dawley rats (postnatal day 17 – 21) were deeply anaesthetised with sodium pentobarbital and decapitated. The brain was removed and placed in ice cold cutting solution containing the following; (in mM): 252 sucrose, 2.5 KCl, 26 $NaHCO_3$, 0.5 $CaCl_2$, 5 $MgCl_2$, 1.25 NaH_2PO_4, and 10 glucose). All solutions were bubbled with 95% oxygen, 5% CO_2 for at least half an hour before use. Horizontal slices (400 - 450μm) were cut and extra-hippocampal areas were trimmed. Slices were left to recover for 1hr in an interface chamber with ACSF containing the following (in mM) 126 NaCl, 3 KCl, 1.25 NaH_2PO_4, 2 $MgSO_4$, 2 $CaCl_2$, 24 $NaHCO_3$, 10 glucose.

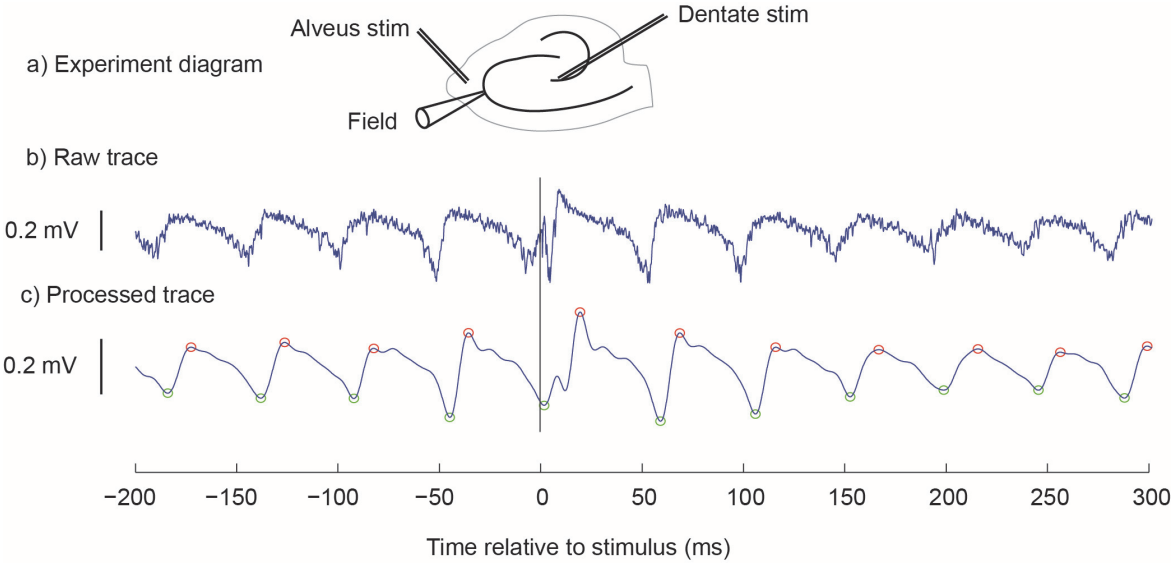

Figure 3.1 **Experiment setup and trace pre-processing. a)** Schematic indicating positions of recording and stimulating electrodes. **b)** Raw local field potential (LFP) trace recorded around stimulation event. **c)** Filtered LFP trace with location of peaks and troughs found by algorithm marked with red and green circles respectively.

3.2.2 Recording

Some recordings were performed in interface conditions and some in submerged conditions. For submerged recordings slices were superfused with ACSF at high flow rates (10 – 15 ml/min) using a harp and recording chamber designed to generate rapid laminar flow over the slice to maximise the oxygenation of the tissue. Temperature was maintained at 28-30ºC. Oscillations were induced in the slice using bath application of 20μM carbachol. Field potentials were recorded from the CA3 pyramidal layer using a patch pipette filled with ACSF (Fig 3.1a). Afferent pathways were stimulated using a bipolar electrode situated in the dentate granule cell layer to stimulate mossy fibers or CA3 alveus to stimulate the local circuit. After carbachol was washed in, oscillations developed over 5-10 minutes. Once oscillatory activity was established, stimuli were delivered in blocks of 60-100 stimuli at a given intensity. Stimuli were delivered every 1.5 or 2.5 seconds which produced stimuli randomly spaced in phase due to the variability in the period of the oscillatory activity. At the end of the block the stimulus intensity was changed and another block of stimuli was started. The experiment was halted when the oscillation stopped or became very irregular. Traces were recorded using a Multiclamp 700B amplifier (Molecular Devices) and digitized at 5 kHz (PCI-6221, National Instruments) with the amplifier low pass filter cut-off frequency set to 2 kHz.

3.3 Analysis

3.3.1 Trace preprocessing

Each trace consisted of a 1 second recording of LFP centred on the stimulus. Raw LFP traces were first processed to remove the stimulation artefact. Stimulus artefact duration was estimated by eye from the average of all traces for that section (artefact duration was usually ~1ms and never longer than 4ms). The stimulus artefact was cut out of each trace and replaced with linearly interpolated values.

Traces were then digitally low-pass filtered with a 6^{th} order Butterworth filter with cut-off frequency of four times the oscillation frequency F_{est} for that block. F_{est} was evaluated as the peak of the averaged Fourier power spectrum for the pre stimulus sections of all traces in the block. The filter frequency was determined with reference to the oscillation frequency rather than as an absolute value to make the change in waveform associated with filtering as consistent as possible across oscillations with different frequencies. Figure 3.1 shows an example of a raw trace and the resulting trace after filtering. Filtering inevitably changes the shape of the waveform due to a frequency dependent reduction in amplitude and phase shifts of components of the signal. The phase shift can be eliminated by filtering in the forward and reverse directions to produce a filter with zero phase shift at all frequencies. Although such filtering better preserves the shape of the oscillation waveform we did not use it for our analysis because reverse filtering caused the effect of stimulation to distort the pre-stimulus waveform. This changed the estimate of the phase at which the stimulus was delivered in a stimulus strength dependent fashion, and at high stimulus strengths caused artificial bunching of the estimated phases at which the stimulus was delivered. We therefore filtered only in the forward direction.

To evaluate the phase shift caused by filtering we calculated the cycle averaged unfiltered LFP by resampling all pre stimulus cycles to a uniform length of 200 samples. The average unfiltered LFP across all oscillations is shown in figure 3.8.

3.3.2 Identification of peaks and troughs

The timing of troughs of the local field potential was used to evaluate the phase shift due to stimulation. Evaluating phase shifts using a Hilbert transform of the band pass filtered LFP was also considered (Freeman, 2007), however this method performed poorly, probably because higher harmonics contained substantial phase information due to the saw tooth like LFP waveform.

Troughs were used rather than peaks as they were sharper (Figure 3.1b,c), and have a straightforward physiological interpretation as they correspond to the phase of maximum firing of

the pyramidal cells (Hajos). Troughs of the filtered LFP were found by an algorithm that stepped forward through the trace from trough to trough. Such an algorithm needs to avoid spuriously identifying local minima which can occur between troughs in even the low pass filtered trace but also be resistant to missing troughs completely. For each trace an estimate of the period P_{est} of the oscillation was calculated as the reciprocal of the oscillation frequency F_{est}. This estimate was used to determine where the algorithm looked for a trough relative to the previously found trough. The algorithm searched for each trough using the following steps:

1. Define a window from 0.6 to1.4 P_{est} after the previously identified trough.
2. Find position of minimum (most negative) value of the trace in the window.
3. If the minimum is more than 0.2 P_{est} from both the start and end of the window, accept minimum as genuine trough and return to step 1 to find the next trough.
4. If the minimum is within 0.2 P_{est} of the start or end of the window, move window 0.2 P_{est} earlier or later respectively and return to step 2.
5. If trough found is the previous trough, reinitialise search with window from 0.8-1.6 P_{est} after previous trough and only allow forward movement of the window.

Peaks were identified as the maxima of the trace between successive troughs.

The design of the algorithm started from the principle of looking for a trough in the region of trace where it is expected given the previous trough time and oscillation frequency (steps 1 & 2). Steps 3 – 5 were introduced when it was observed that troughs found near the edge of the window were sometimes local minima close to the true trough. Parameters of the algorithm were chosen by hand after experimentation with a range of values. For traces where there was a clear oscillation in the LFP this algorithm robustly found the positions of the troughs and peaks. Figure 3.1.c shows an example of the peaks and troughs identified by the algorithm.

3.3.3 Selection of data for analysis

The strength of oscillatory activity elicited by washing on carbachol varied both across slices and over time, with some slices not showing any clear oscillation and others only intermittent or irregular oscillatory activity. If the network was not oscillating it was not meaningful to measure the phase response. Additionally, if the oscillation was very irregular the variability in period length from cycle to cycle obscured the phase perturbation due to the stimulus. We therefore needed a procedure to select for analysis only those blocks of stimuli where there had been a regular oscillation. This selection was done on the basis of the coefficient of variation (CV, standard deviation divided by mean) of the period of the oscillation. Blocks were rejected for further

analysis if the CV of cycle duration in the pre-stimulus section was greater than 0.15. Period duration was evaluated as the time between successive troughs of the LFP oscillation identified using the algorithm outlined below. This block selection process accepted 60 stimulus intensity blocks from 30 separate slices out of a total of 218 stimulus intensity blocks from 63 experiments in which carbachol elicited oscillations. Even in slices where the oscillation was mostly strong and regular there was variation in the amplitude from cycle to cycle and the oscillation would in some cases occasionally collapse for a short period before re-establishing itself. To avoid including traces where stimuli were delivered without ongoing oscillation, we rejected traces where the peak to trough amplitude of the cycle preceding stimulation was less than half the average amplitude for that section.

3.3.4 Plotting phase response curve

The mean (P_{mean}) and standard deviation of the unperturbed period duration were evaluated for all periods in the sections of traces preceding the stimulus. For each trace the phase at which stimulation was delivered was estimated from the time of stimulation T_{stim} relative to the time of the previous trough $T_{tr:-1}$ as $S = (T_{stim} - T_{tr:-1})/P_{mean}$. We call S the old phase to distinguish it from the oscillation phase after perturbation by the stimulus which we describe as the new phase and define below. Consistent with previous work on rephasing of biological oscillators we describe phase as a variable that varies between zero and one.

The effect of stimulation on the oscillation phase was evaluated by looking at the timing of troughs following the stimulus as a function of the phase of stimulation. These data were either plotted directly as trough times or converted into phase shifts to produce phase response curves.

A phase response curve (PRC) shows the change in phase produced by the stimulation as a function of the phase of stimulation. Just as the phase of the oscillation at the time of stimulation can be defined relative to troughs preceding the stimulus, it can also be defined relative to troughs occurring after the stimulus as $S = (T_{stim} - T_{tr})/P_{mean}$ modulo 1. If the stimulus affects the phase of the oscillation, the new phase will differ systematically from that defined by the trough preceding the stimulus. The phase shift is given by $\Delta S = S_{new} - S_{old}$. To evaluate S_{new} for the calculation of PRCs we used those troughs that occurred within $0.5\,P_{mean}$ of the expected unperturbed position of the second trough after the stimulus. For a given trace, if the final trough before stimulation occurred at time $T_{tr:-1}$, the expected unperturbed position of the second trough after stimulation is $T'_{tr:2} = T_{tr:-1} + 2\,P_{mean}$.

3.3.5 Combining data from multiple experiments

To combine data across experiments all trough times were first expressed in cycles rather than milliseconds by dividing them by the mean unperturbed period duration for that block.

The effect of stimulation on the oscillation varied depending on the stimulus strength. To combine data across experiments in a way that did not obscure this strength dependence, a measure of stimulation strength was needed that could be compared across recordings in different slices. The electrical stimulation intensity was not a suitable measure as the precise location of the stimulus electrode can greatly affect the number of fibers recruited and hence the physiological stimulation strength. The size of the stimulus artefact or response (EPSP and population spike) was also not suitable as it is strongly affected by recording electrode.

We used a measure based on the effect of the stimulus on the oscillation: the circular variance of the distribution of new phases after stimulation. We first explain how this measure was calculated and then why it works as a measure of stimulation strength.

To evaluate the circular variance we included all troughs that occurred in the time interval between P_{mean} and 2 P_{mean}after the stimulus for all traces in the block. Each trough gives a measure of the new phase: $S_{new} = (T_{stim} - T_{tr})/P_{mean}$ modulo 1. These new phases S_{new} form a circular distribution with circular variance:

$$var(S_{new}) = 1 - \left|\frac{1}{N}\sum e^{i2\pi S_{new}}\right|$$

The circular variance takes values between 0 and 1 with a value of 1 indicating that the new phases are evenly distributed and a value of 0 indicating that the new phase is identical for every trace.

For very weak stimuli, the phase was essentially unchanged by the stimulation so the new phases were evenly distributed and their circular variance was close to 1. For very strong stimuli, the oscillation was completely reset by the stimulus such that the new phase after stimulation was independent of the phase before stimulation and very similar for all traces. This produced a highly peaked distribution with a circular variance close to 0. The circular variance of the new phase distribution was therefore tightly negatively correlated with stimulus strength. We divided blocks into 4 stimulus strength categories on the basis of this circular variance measure with the category ranges 0-0.25, 0.25-0.5, 0.5-0.75, 0.75-1.

We evaluated how accurately this measure ordered blocks by stimulus intensity using data from experiments where we had usable blocks (period CV<0.15) recorded at multiple stimulus intensities. For every pair of blocks whose relative stimulus strengths were known, we evaluated whether the new-phase variance measure correctly ordered the pair. Of the 76 such pair-wise comparisons, 89% were correctly ordered. For the incorrectly ordered pairs the average absolute difference in the new-phase circular variance was small (0.12) and in only 4 pairs (5% of the total) did the block with a weaker stimulus intensity end up in a stronger strength category.

There is a degree of circularity in using a measure based on the effect of stimulation in individual blocks in grouping blocks for the population level analysis of the effect of stimulation. However, specifying a given value for the circular variance of the new phase distribution still allows a very wide range of structures for the two-dimensional circular distribution of new phase as a function of old phase. The measure is completely insensitive to the distribution of points in the old phase axis such that even for a fixed marginal distribution on the new phase axis a very wide range of two-dimensional distributions is possible. Additionally, specifying the circular variance of the new-phase marginal distribution only partially constrains this marginal distribution. This is because both the circular mean and higher order moments apart from the variance are unconstrained.

To plot data from multiple experiments (Figure. 3.5, 3.6, 3.10c-f) we show both the timing of individual troughs and the circular mean and variance of the distribution of troughs on each cycle for each of ten groups of traces divided by stimulation phase. The circular mean is defined:

$$\bar{S} = \frac{1}{2\pi}\arg\left(\sum e^{i2\pi S}\right)$$

The circular variance Var was indicated by error bars of length ± 0.5 Var such that the total length of the error-bar was Var. This is the natural choice for circular variance error-bar length as it ensures that for uniformly distributed data the error-bars from two points separated by one cycle will just touch each other.

In figure 3.8 we show 95% confidence intervals on phase response curves due to alveus and dentate stimulation. The confidence intervals were calculated according to Fisher and Lewis (1983).

3.3.6 Wilson-Cowan Model

The time evolution of the activity levels of the excitatory (E) and inhibitory (I) populations were described by the following equations.

$$\tau_e \frac{dE}{dt} = -E + \Phi(g_{ee}E + g_{ei}I + S_e(t) + a_e) + N_e(t)$$

$$\tau_i \frac{dI}{dt} = -I + \Phi(g_{ie}E + g_{ii}I + S_i(t) + a_i) + N_i(t)$$

Where:

Sigmoidal activation function $\Phi(a) = \frac{1}{1+e^{-a}}$

Noise $N(t)$ = Gaussian distributed white noise with mean of 0 and standard deviation σ

Stimulus $S(t)$; parameterized by stimulation intensity S_0 and stimulation angle ɵ which determines the relative strength of input to the excitatory and inhibitory populations.

$$S_e(t) = S_i(t) = 0 \qquad \text{for } t < t_{stim}$$

$$S_e(t) = S_0 \cos(ɵ)\, e^{-(t-t_{stim})/\tau_{stim}} \qquad \text{for } t > t_{stim}$$

$$S_i(t) = S_0 \sin(ɵ)\, e^{-(t-t_{stim})/\tau_{stim}} \qquad \text{for } t > t_{stim}$$

Network parameters common to all simulations:

$$g_{ee} = 10,\ g_{ei} = -10,\quad g_{ie} = 12,\quad g_{ii} = -10,$$
$$\tau_e = 3,\quad \tau_i = 8,\ \tau_{stim} = 6,\quad a_e = -2,\ a_i = -3.5$$

Parameters g_{ab} are synaptic coupling strengths with the first subscript indicating the postsynaptic population and the second subscript the presynaptic population. Parameters a_e and a_i control the tonic activity of each population in the absence of synaptic input. Though the values are negative they in fact represent a low level of tonic activation. This is because we used a form of the sigmoidal activation function which saturates at negative values of the input.

Stimulus parameters and noise level were varied across simulations:

Figure. 3.10b: σ = 0.13, ɵ = 85, S_0 = 1, 1.5, 4, 10 in panels left to right (weak to strong) .

Figure. 3.10d: σ =0.2-0.5, ɵ =80, S_0 = 0.4, 1.6, 3, 12 in panels left to right, respectively.

Figure. 3.10f: σ =0.4-0.6, ɵ =60, S_0 = 0.5, 2.2, 4.1, 8 in panels left to right, respectively.

Figure. 3.9c: σ = 0, ɵ = 85, S_0 = 1

Figure. 3.9d: σ = 0, ɵ = 85, S_0 = 10

Figure. 3.9e: σ = 0, ɵ = 60, S_0 = 2.2

Figure. 3.9f: σ = 0, ɵ = 60, S_0 = 8

For each rephasing simulation, 100 instances of the model were simulated with initial conditions equally spaced in phase around the limit cycle of the unperturbed oscillation. The stimulus was delivered at t_{stim}= 180 ms and total simulation duration was 400 ms. Numerical integration was performed using the exponential Euler method with a timestep of 0.01 ms. For population plots 6 separate simulations contributed to each panel with pseudo-randomly distributed noise level and stimulation intensity. Noise levels were drawn from a uniform distribution with the range specified above. Stimulation intensities were normally distributed with a mean for each panel specified above and a standard deviation equal to 0.1 times the mean.

To allow comparison of model and experiment we exploited the fact that during carbachol induced gamma oscillations in CA3, troughs of the unfiltered LFP occur at the time of maximum spiking of the pyramidal cells (Hajos et al., 2004). We therefore used the time of maximum excitatory population activity on each cycle as the phase reference point used for plotting and equated this conceptually with the troughs of the unfiltered LFP in the experimental data. Filtering of the experimental data introduced a mean delay of 0.16 cycles between troughs of the unfiltered LFP and troughs of the filtered LFP used for rephasing plots (Figures. 3.8). To compensate for this in the simulated rephasing plots we therefore plotted 'trough' positions that were delayed by 0.16 times the average unperturbed cycle duration after the peak of excitatory population activity on each cycle.

Isochrons (see results section 3.4.6) were calculated by reverse integration from initial conditions spaced along a line normal to the limit cycle of length 0.001. The timestep for reverse integration was 0.001 ms. All simulations were performed in MATLAB (Mathsworks).

3.4 Results

3.4.1 Local field potentials over stimulation

Figure 3.2 shows the local field potential recorded in the CA3 pyramidal layer before and after weak (3.2.a) and strong (3.2.b) recurrent collateral stimulation in the same slice, during carbachol induced oscillation. Each figure shows traces from ~ 60 individual stimulation events, binned into 5 groups by the phase at which stimulation occurred. The individual traces and average LFP signal are plotted for each group. Strong stimulation completely reset the ongoing oscillation such that the phase after stimulation varied very little with the phase before stimulation. The rapid negative deflection shortly after stimulation is consistent with a population spike recorded in the pyramidal cell layer. For the weaker stimulation, the phase of the oscillation after stimulation was perturbed by the stimulus but not completely reset, such that the new phase was strongly dependent on the old phase. Resolving the structure of these weaker phase shifts requires alternative ways of plotting the data described below. The phase at which the weaker stimulation occurred affected the amplitude of the oscillation: the amplitude was smaller immediately following the stimulus for traces where the stimulus was delivered approximately half way through a trough – trough oscillation cycle.

3.4.2 Rephasing evaluated by LFP trough times

To better resolve the effect of stimulation on the phase of the oscillation we plot the timing of troughs of the LFP oscillation as a function of the phase at which the stimuli were delivered (Figure 3.3.1-3.a, 3.4.1-3.a). Troughs for each trace are plotted with time running vertically upwards. The position of the trace on the X axis is determined by the phase at which stimulation occurred. The solid diagonal lines indicate the expected position of the troughs if the stimulus had no effect on phase. Data points deviate from these lines due to both systematic perturbation by the stimulus and random variability in the period of the oscillation, which smears the distribution in time. Blocks from the same slice with different stimulus strengths are arranged horizontally on separate axis with stimulus strength increasing from left to right.

We also plot the data as phase response curves which show the displacement of troughs from their expected unperturbed position as a function of the phase of stimulation (Figure 3.3.1-3.b, 3.4.1.3.b). Figure 3.3 shows rephasing by stimulation of local axon collaterals in the alveus while figure 3.4 shows rephasing by stimulation in the dentate gyrus to recruit mossy fibres. Each figure shows data from 3 experiments in which usable data were recorded at a range of stimulation strengths. The examples chosen were those that had highly regular oscillations as indicated by the coefficient of variation of the period duration (period CV<0.15). Population data aggregated across multiple experiments is shown in figures 3.5 and 3.6 for alveus and dentate gyrus stimulation respectively.

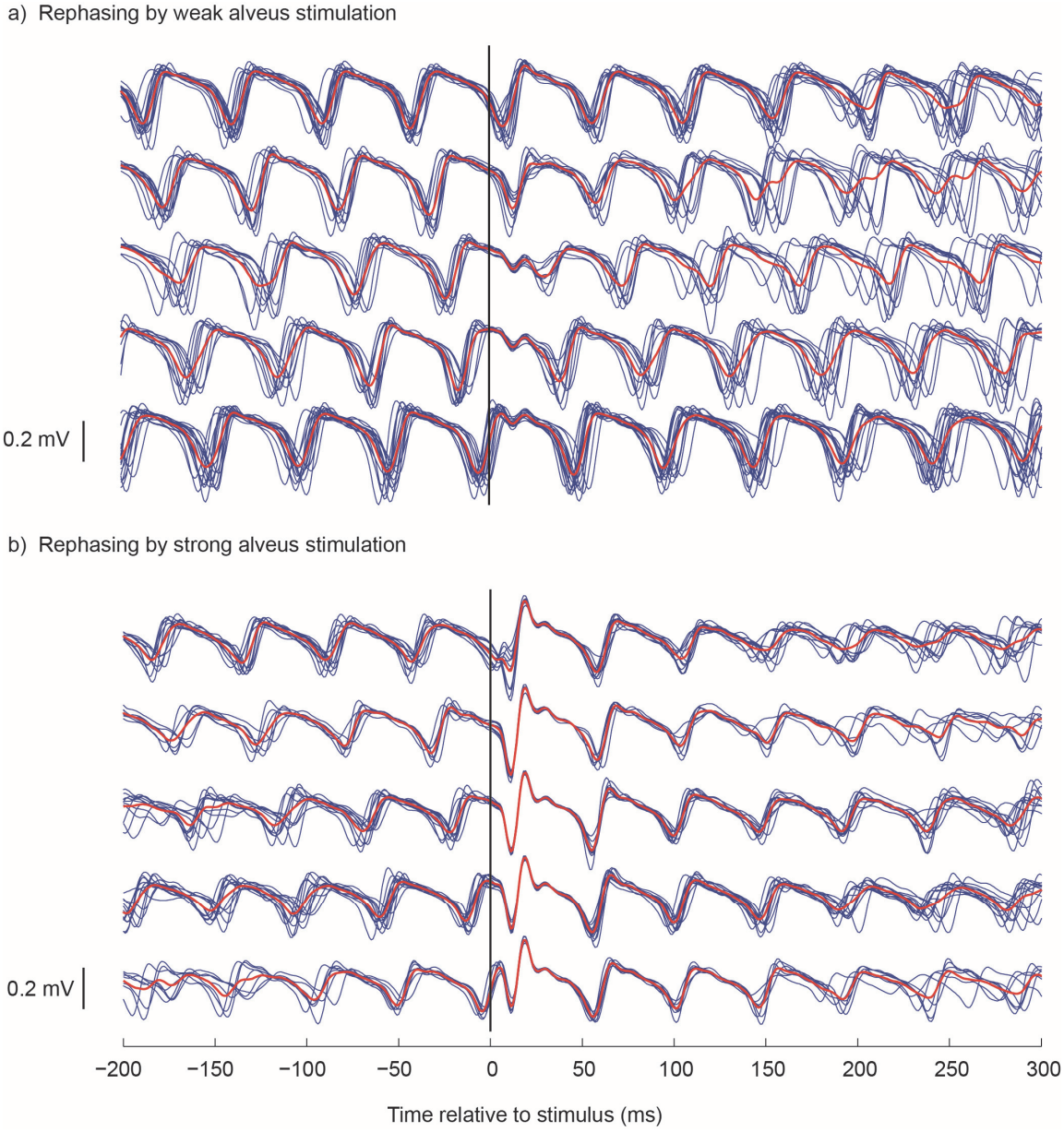

Figure 3.2 **Local field potential traces during rephasing.** Filtered local field potential (LFP) traces in one experiment, aligned by time of alveus stimulation (blue), with the average superimposed (red), sorted into 5 groups by phase of stimulation. **a)** weak stimuli; **b)** strong stimuli.

Fig 3.3 Alveus stimulation rephasing examples.

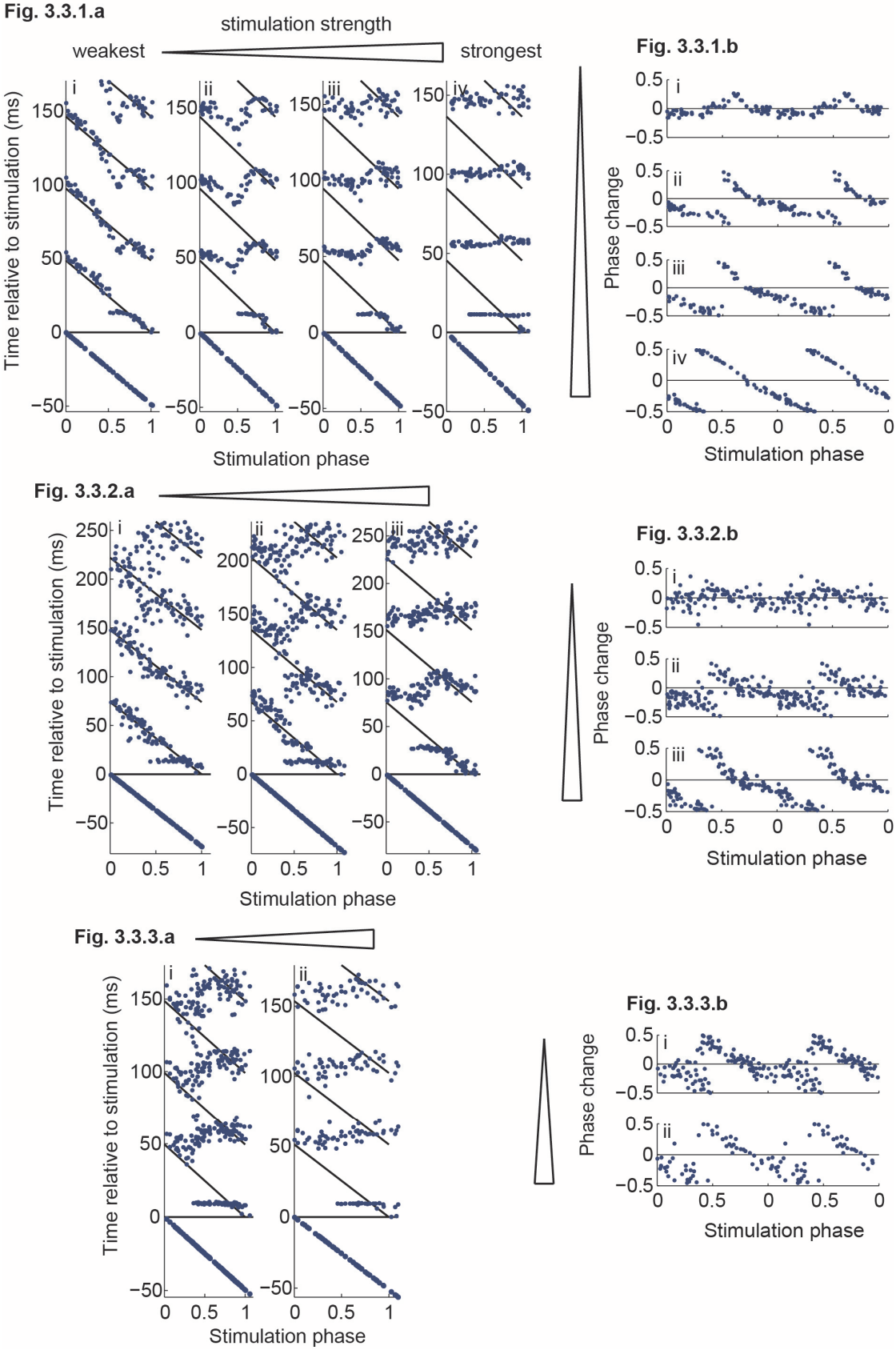

Fig 3.4 Dentate gyrus stimulation rephasing examples.

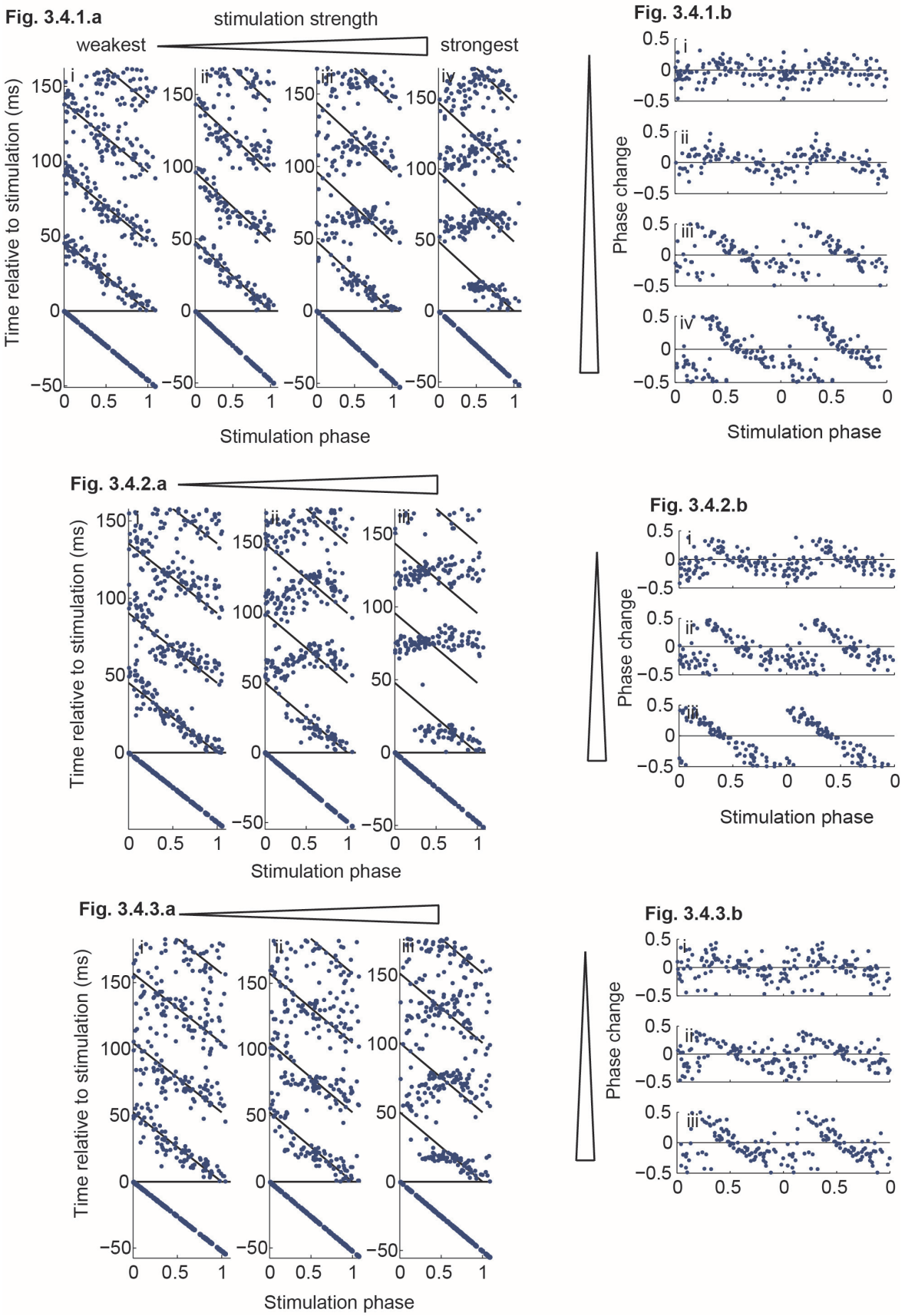

Fig 3.5 Alveus stimulation poplulation data.

Fig. 3.5.a

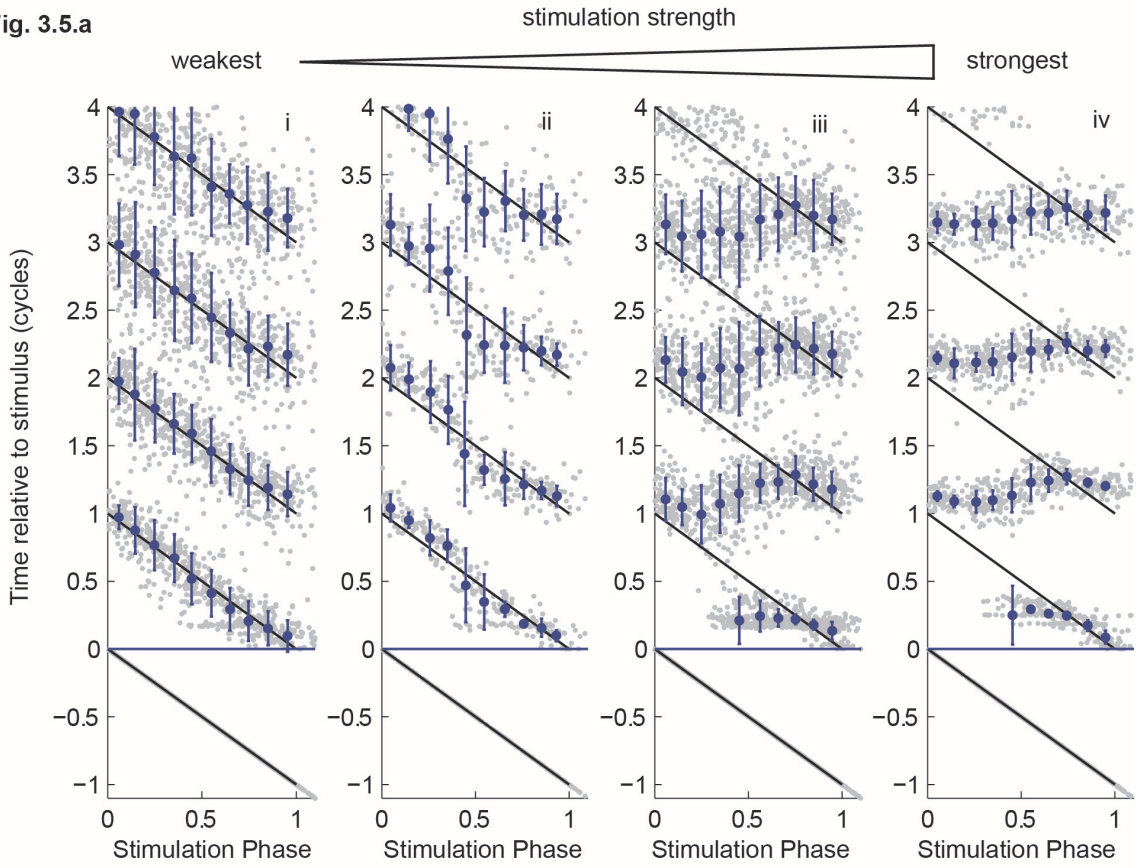

Fig. 3.5.b

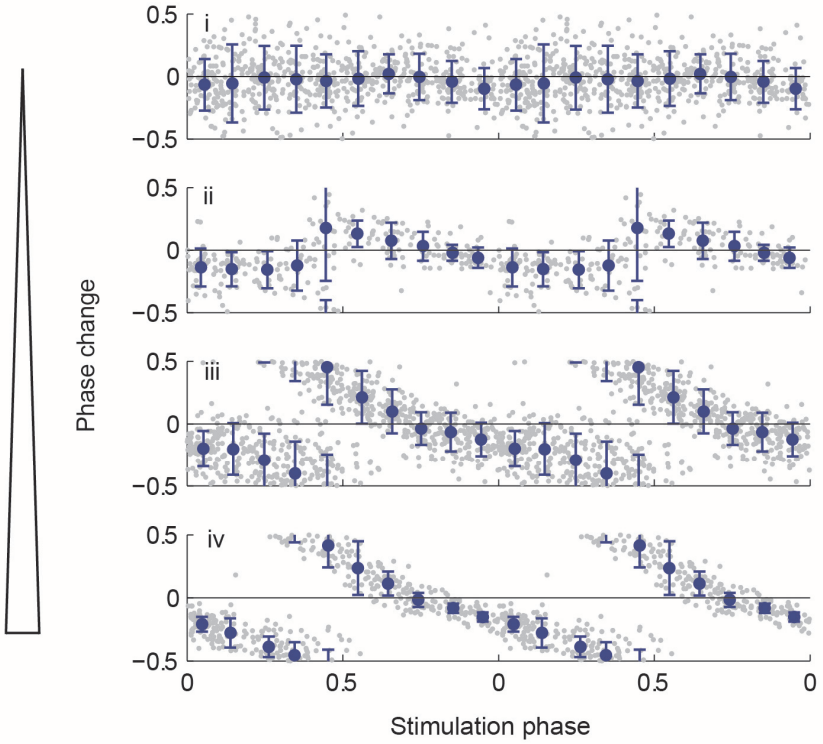

Fig 3.6 Dentate granule cell layer stimulation population data.

Fig. 3.6.a

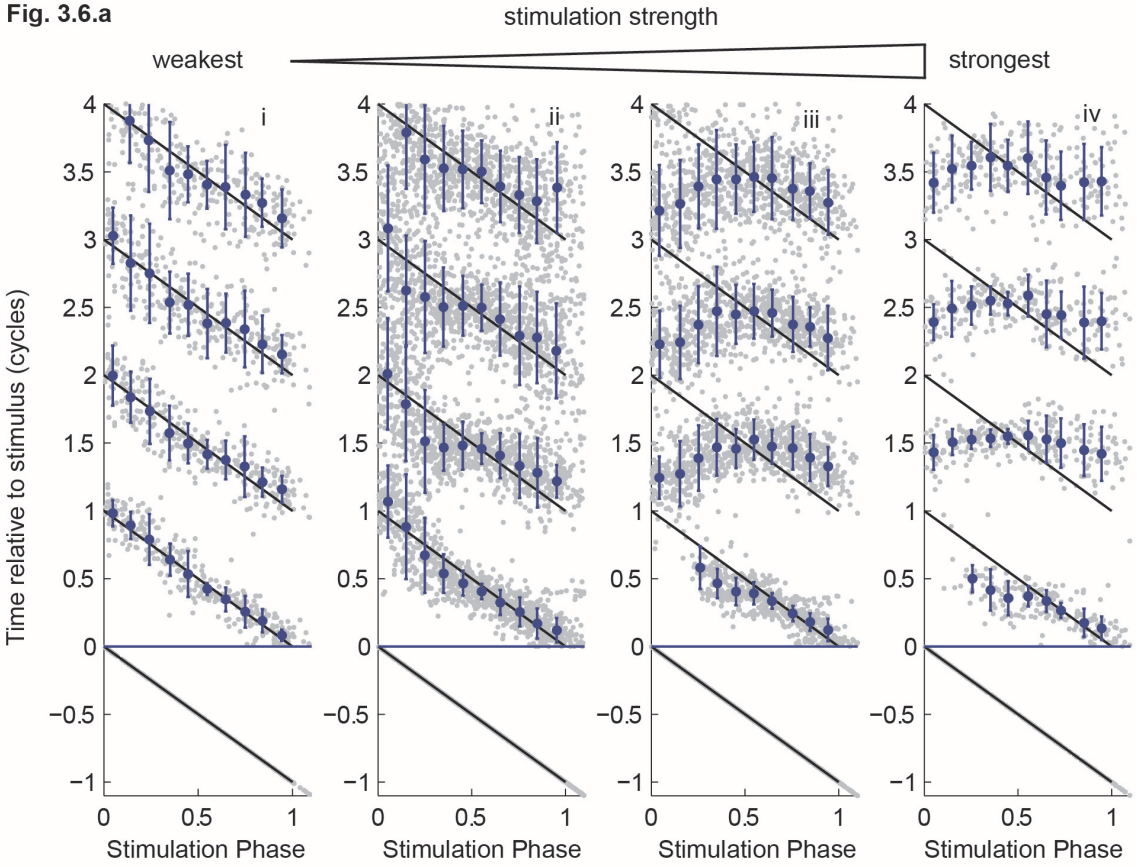

Fig. 3.6.b

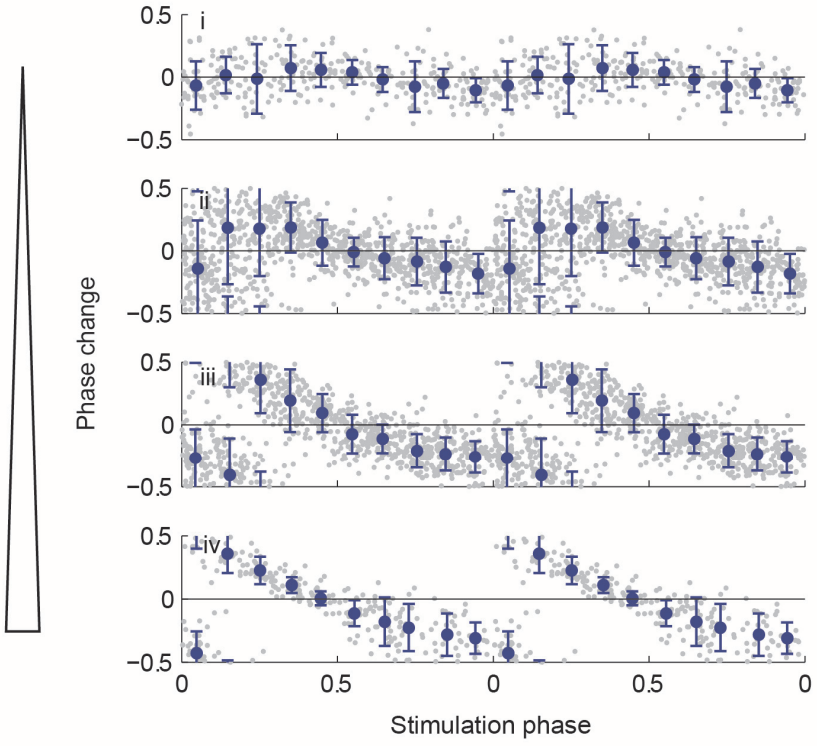

Preceding Pages:

Figure 3.3 **Alveus Stimulation rephasing examples. 3.3a)** Effects of stimuli of different strengths shown on the timing of oscillation troughs on successive cycles. Each sub-figure (e.g. 3.3.1) shows data from a different slice. Each sub panel (e.g. 3.3.1.i) shows data from a single stimulation intensity. Blue dots show timing of troughs of the filtered LFP trace. Diagonal lines indicate the expected positions of troughs in the absence of stimulation, calculated from time of the final trough before the stimulus and the mean unperturbed cycle period. **1.3b)** Same data as in 3.3a but re-plotted as phase response curves showing the change in phase as a function of phase of stimulation.

Figure 3.4 **Dentate Stimulation rephasing examples.** Plotted as in figure 3.3.

Figure 3.5 **Alveus stimulation population data.** Population rephasing data. Grey dots indicate times of troughs in individual traces, plotted as in Fig. 3.3 but combining data across experiments. Blue symbols indicate the circular mean trough position for data binned by phase of stimulation (error bars: circular variance).

Figure 3.6 **Dentate stimulation population data**. Plotted as in figure 3.5.

The overall structure of the rephasing behaviour as a function of stimulation phase and strength was similar for both dentate gyrus (DG) and alveus stimulation, but there were systematic differences in the detailed shape of the phase response between the two stimulus types. Some aspects of the rephasing behaviour of oscillators are unavoidable and hence uninformative about the system dynamics. Specifically, in the limit of very weak stimulation the effect on phase will be imperceptible and the PRC will be flat. Likewise, complete resetting by very strong stimuli, such that phase after stimulation is the same irrespective of the phase before, is common to many different oscillator types (Winfree A., 2000). It is therefore the response to stimuli of intermediate intensity (e.g Figures 3.5ii-iii, 3.6ii-iii) that provides insight into the system dynamics.

Weak stimulation of both DG and alveus produced biphasic phase response curves with a region in which the oscillation was delayed by the stimulus and a region in which it was advanced (Figures 3.3.1.a.i, 3.4.1a.ii, 3.4.2.a.i, 3.5.1.a.ii and 3.6.1.aii and their corresponding phase response curves). As the stimulation strength was increased a discontinuity emerged in the PRC such that the oscillation was re-set to a narrow range of phases irrespective of the phase of stimulation. In this strong stimulation regime the phase after stimulation had an approximately sinusoidal dependence on the phase of stimulation (Figures 3.5iii, 3.6iii). Further increase in the stimulation strength caused the range of new phases to narrow until the phase after stimulation was largely independent

of the phase before (Figures 3.3.1a.iv, 3.3.2a.iii, 3.3.3a.ii, 3.4.1a.iv, 3.4.2a.iii, 3.5.1.a.iv and 3.6.1.a.iv).

3.4.3 Weak and strong rephasing are topologically different

This type of transition between biphasic continuous PRCs at weak stimulation intensities and discontinuous PRCs at strong intensities has been observed before in biological oscillators and has an interesting geometrical feature identified by Winfree (2000). As both the old phase and the new phase are circular variables the space in which one can be plotted against the other is toroidal. This is illustrated in figure 3.7 with old phase going horizontally round the ring of the torus and new phase going vertically passing through the hole. In weak rephasing, as the old phase is varied through one cycle, the new phase also varies through one cycle, such that the phase response curve passes once through the hole of the torus (the curve's "winding number" is 1). For strong rephasing, as the old phase varies through one cycle, the new phase hardly varies and the PRC does not pass through the hole of the torus (its winding number is 0). These two types of rephasing are topologically different so it is not possible to smoothly deform the weak stimulation PRC into the strong stimulation PRC. Something other than smooth deformation must occur as stimulus strength is increased and this is indeed what we observed.

As the stimulation strength was increased from weak intensities, the PRC took on a sawtooth shape, such that there was a shallow transition from phase advance to delay with increasing phase of stimulation followed by a rapid transition back into the region of phase advance (3.3.2.b.ii, 3.3.3.b.i, 3.4.2.b.i, 3.4.3.b.ii, population data 3.5.1.b.ii, 3.6.1.b.ii). In this region of rapid transition the variability of the new phase became large such that troughs from one cycle began to join up with troughs from the next to form a close to uniform distribution of new phases (3.3.2.a.i, 3.3.3.a.i, 3.4.2.a.i, population data 3.5.1.a.ii, 3.6.1.a.ii). With further increase of stimulation strength the variability of new phase in this region of the PRC decreased once again, but now the new phase no longer varied through a whole cycle over a cycle of the old phase.

This type of transition, in which an intermediate strength stimulus at a particular phase produces a highly variable new phase, is typical of perturbing an attracting cycle oscillator (Winfree A., 2000). The oscillating Wilson-Cowan model is just such a system and as we show for this model later in the chapter how the dynamics reproduce the experimentally measured rephasing.

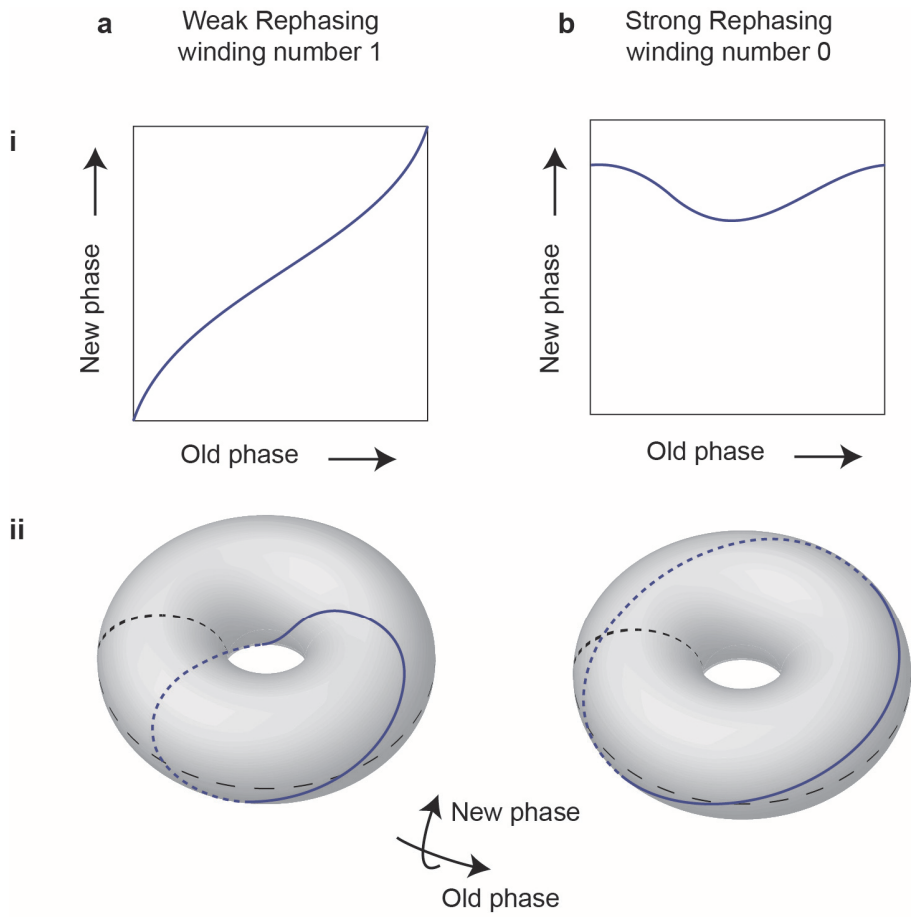

Figure 3.7 **Weak and strong rephasing are topologically different.** Diagram illustrating weak (a) and strong (b) rephasing showing new phase as a function of old phase on regular (i) and toroidal (ii) axis.

3.4.4 Differences between the phase response to dentate and alveus stimulation

Features of the rephasing behaviour described above occurred for both dentate gyrus and recurrent collateral stimulation, however clear differences in the effect of the two stimulus types can be resolved in the population data. For weak stimuli, although both stimulus types produced biphasic PRCs, the regions of phase advance and delay were located at different phases (Figure 3.8). For recurrent collateral stimulation, stimuli delivered in the phase range between 0.45 – 0.75 advanced the oscillation while those delivered in the range 0.85 – 0.35 delayed the oscillation (Figure. 3.5.b.ii). For dentate stimulation, phase advance occurred for stimuli delivered in the range 0.15 – 0.45 while phase delay occurred in the range 0.55 – 0.05 (Figure. 3.6.b.ii). A fraction of this phase shift is accounted for by the conduction delay between the dentate granule cell layer. We estimated this conduction delay from the timing of population spikes elicited by stimulation of the quiesent

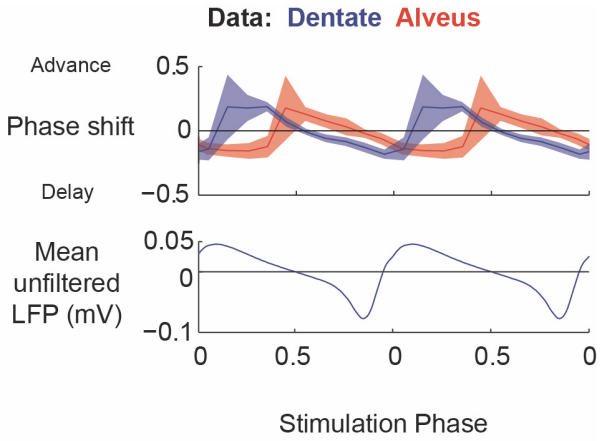

Figure 3.8 **Comparison of dentate and alveus stimulation phase response curves.** Population average phase response curves for weak dentate and alveus stimulation with circular 95% confidence interval. The cycle averaged unfiltered LFP is shown for reference

slice before carbachol was washed in. Population spikes occurred at 6.5 ± 0.7 and 2.6 ± 0.6 ms after stimulation for DG and recurrent stimulation respectively. This 3.9 ms difference corresponds to a phase shift of 0.073 at the mean oscillation frequency of 18.6 ± 0.4 Hz. This implies that conduction delay only accounts for approximately 25% of the measured difference in the PRCs due to the two stimulus types.

Differences in the effect of the two stimulus types were also observed at strong stimulation intensities. Although moderately strong stimuli reset the oscillations to a narrow range of phases, there was still some variability in the new phase as a function of old phase (Figure. 3.6.a.iii, 3.4.a.iii). For both stimulus types the new phase was an approximately sinusoidal function of the old phase but the sinusoid was translated in both new and old phase for dentate relative to alveus stimulation. For the strongest stimulation intensities, the troughs occur approximately 0.3 cycles later relative to the stimulus for dentate when compared with after alveus stimulation.

3.4.5 Rephasing the Wilson-Cowan model

To try to understand the structure of the rephasing behaviour we investigated whether perturbing an oscillating Wilson-Cowan model could reproduce the experimental data (Figure 3.9). Although the model is simple, there is a small set of free parameters that need to be chosen. These are the strength of synaptic coupling between the populations, their external input, and the time constants for each population. Additionally, to reproduce the irregularity of experimentally measured network oscillations we added noise in the form of normally distributed random fluctuations in the rate of

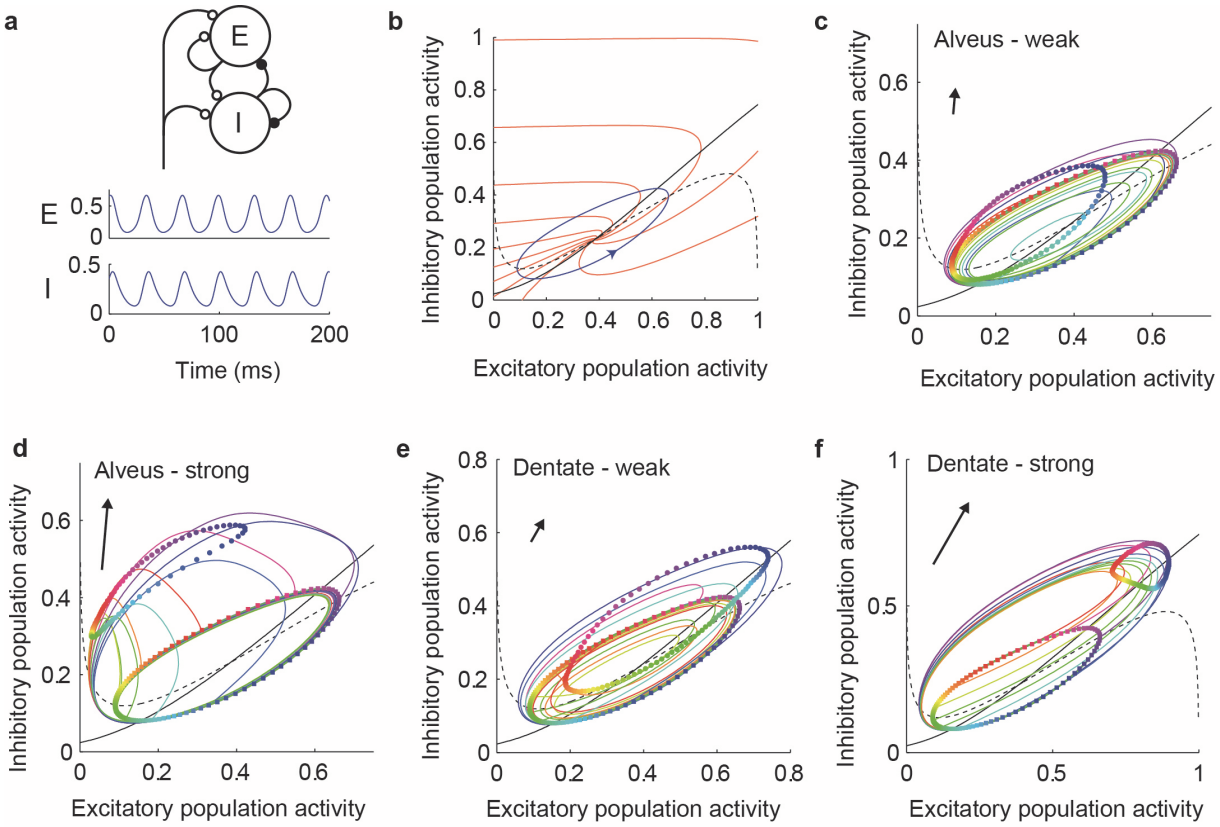

Figure 3.9 **Model connectivity and phase plane diagrams. a)** Wilson-Cowan model connectivity diagram, with (below) activity of excitatory (E) and inhibitory (I) populations. **b)** Phase plane diagram showing the limit cycle (blue), nullclines (black; dashed: excitatory; solid: inhibitory), and isochrons (red). **C-f**, Rephasing phase plane diagrams. Coloured squares show position at time of stimulation for 100 simulations equally spaced in phase. Correspondingly coloured circles show the state 6 ms after the stimulus. Coloured lines show trajectories of 10 of these simulations from the time of stimulation until their return to the limit cycle. Arrows indicate the direction (ratio of inhibitory to excitatory stimuli) and strength of the input pulse.

change of the activity variables. Perturbation due to stimulation was represented as an exponentially decaying transient increase in the external input.

Parameter choice was constrained by the requirement that the model be in an oscillating state. A necessary and sufficient condition for this is that the dynamics have a single unstable fixed point (Wilson & Cowen 1972). This requires that the excitatory nullcline is kinked such that it has a region of positive gradient, and that the inhibitory nullcline intersects it from underneath in this region (Figure 1.9b) (Rinzel and Ermentrout, 1998; Latham et al., 2000).

The shape of the nullclines is entirely determined by the synaptic coupling strengths between the populations and their external input. The coupling and input parameters we used produced a fixed point that corresponds to a balanced state in which both excitatory and inhibitory populations receive strong local excitatory and inhibitory inputs, which approximately balance to produce a much smaller net input. The above constraints on nullcline shape are necessary for a single unstable fixed point but are not sufficient. The stability of the fixed point is further determined by the ratio of the excitatory to inhibitory time constants. As the ratio τ_e/τ_i is decreased, the fixed point loses stability through a supercritical Hopf bifurcation, giving way to an unstable fixed point surrounded by an infinitesimally small limit cycle (see Chapter 6). As the ratio is further decreased, the limit cycle grows and the oscillation amplitude increases. Any dynamical system that loses stability through a supercritical Hopf bifurcation (including all oscillating Wilson-Cowan models) will have biphasic PRCs, and these will be sinusoidal in the limit of small amplitude limit cycles (Ermentrout and Kopell, 1984; Ermentrout, 1996). Large amplitude limit cycles can cause large absolute values of net inputs (excitatory minus inhibitory) to the populations. This can start to saturate the models input-output nonlinearity, reducing the sensitivity to input pulses, and hence affecting the shape of PRCs.

Within the constraints outlined above we chose parameters by hand to best reproduce the unperturbed oscillatory activity and measured rephasing behaviour. In its unperturbed state the model reproduced several features of slice gamma oscillations (Figure 3.9a). Activity of both excitatory and inhibitory populations oscillated approximately in phase with a small lag between the peak firing of excitatory and inhibitory populations (Hajos et al., 2004). The oscillation was non-sinusoidal with low activity for most of the cycle and a sharp peak around the phase of maximum activity. Both populations received strong excitatory and inhibitory input from the local circuit which approximately balanced to produce a smaller net input (Oren et al., 2006; Atallah and Scanziani, 2009).

Figure 3.10a,b compares experimental and model rephasing for a slice where oscillations were extremely regular and hence the rephasing data were very clean. Across the range of stimulation intensities and phases the model very closely reproduced the experimental data. To produce model data for comparison with the experimental population data, we ran repeated rephasing simulations at a range of stimulation intensities and noise levels and then aggregated the resulting individual data sets using the same analysis as that used for the experimental data. The model could accurately reproduce the experimental data for stimulation of both the dentate gyrus and CA3 alveus (Figure 3.10c-f). Remarkably, the only modification needed to reproduce the systematic differences

Fig 3.10 Comparison of experimental and model rephasing.

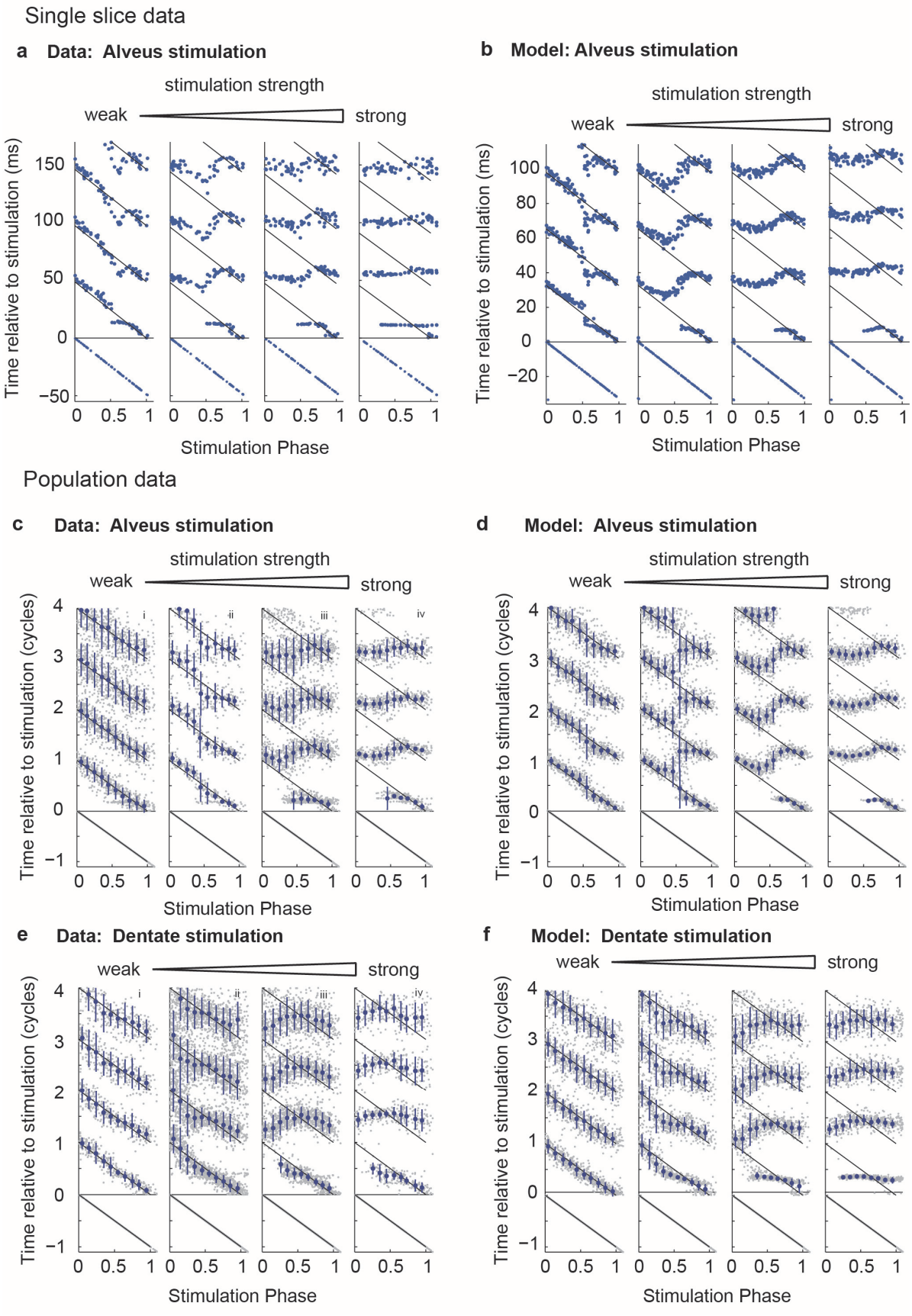

Figure 3.10 (Preceding page) **Comparison of experimental and model rephasing. a)** Experimental rephasing data from single slice (as shown in 1.3.1a). **b)** simulated single slice data. **c,e)** Population rephasing data as in figures 1.5, 1.6. **d,e)** simulated population data.

between the two stimulation types was a change in the relative strength of the input pulse to the excitatory and inhibitory populations. Stimulation of CA3 alveus was best reproduced by a pulse of input that strongly excited the inhibitory population with ~6 fold weaker excitation of the excitatory population. Dentate stimulation, on the other hand, was best reproduced by an excitatory input pulse that targeted the inhibitory population ~1.7 fold more strongly than the excitatory population.

3.4.6 Understanding the rephasing structure through phase plane trajectories and isochrons

We can gain insight into why the rephasing behaviour has its particular structure by considering the trajectories in the phase plane that the system moves through as a result of the stimulus (Figure 3.9c-f). During rephasing, the transient input pulse perturbs the system away from the limit cycle and it then relaxes back, eventually returning to the limit cycle with a phase which is in general different from that which it would have had in the absence of perturbation. To understand the effect of the stimulus on the resulting phase it is therefore useful to know what phase of oscillation will result if the system is started from initial conditions away from the limit cycle. As all trajectories (except those starting at the fixed point) eventually return to the limit cycle, for any point a_0 in the phase plane there is a point b_0 on the limit cycle for which $a(t) \rightarrow b(t)$ as $t \rightarrow \infty$. We can therefore define the phase of the trajectory a(t) as the same as that of the periodic trajectory b(t). Phases for points off the limit cycle are often referred to as the latent phase (Winfree A., 2000). A useful way of visualising the latent phase is to plot lines on the phase plane which pass through all points with the same latent phase. These lines are called isochrons and are shown for the model in figure 3.9b. The isochrons radiate outward from the unstable fixed point, pass through the limit cycle and continue out to the edge of the phase plane.

The effect of a transient stimulus on the oscillation phase is determined by the direction it pushes the system relative to the local isochrons. An impulse which pushes the system perpendicular to the isochrons in the direction of increased (decreased) latent phase will advance (delay) the oscillation, while a perturbation that pushes the system parallel to the isochrons will have little effect on the phase. For example, alveus stimulation was represented in the model as an excitatory input that strongly targeted the inhibitory population and much more weakly targeted the inhibitory population. This corresponds to an impulse vector in the phase plane at an angle of 85˚ (measured

counter-clockwise from a horizontal rightward vector, figure 3.9c,d). Shortly before the peak excitatory firing rate in the unperturbed limit cycle, the isochrons cross the cycle approximately horizontally with increasing latent phase in the upward direction. This predicts that the simulated alveus input will advance the oscillation when it occurs during this phase and this is indeed what is observed. The impulse vector for the dentate stimulation was further from the vertical at an angle of 60˚ which predicts correctly that the region of phase advance will occur at an earlier phase in the cycle.

In addition to predicting the regions of phase advance and delay, the structure of the isochrons explains why there is a particular combination of stimulus strength and phase which results in highly variable new phase. For a given stimulus a particular combination of intensity and phase will push the system to the unstable fixed point in the centre of the limit cycle where all the isochrons meet. This point is a phase singularity, it does not have a phase as in the absence of noise a system with initial conditions at the fixed point will stay there indefinitely and never join the limit cycle. However, points spanning the full range of latent phase can be reached by moving an infinitesimally small distance from the fixed point. The phase of oscillation obtained when the system eventually returns to the limit cycle is therefore extremely sensitive to noise when the initial conditions are near the fixed point.

Experimentally, the stimulus intensity that could produce extremely variable new phase was in the transition region between weak rephasing, (where the PRC is continuous and the winding number of new phase with respect to old phase is one), and strong rephasing, (where the PRC is discontinuous and the winding number is zero). We can understand this transition by considering the effect of stimulation on an ensemble of networks with initial conditions evenly spaced in phase round the limit cycle at t = 0. If we plot the position of all the different networks in the phase plane at any point in time, they form a closed loop (Figures 3.9c-f). Before stimulation this loop lies on the limit cycle (coloured squares). After stimulus onset, each network moves on its own trajectory and the loop moves and distorts before eventually returning to the limit cycle. The determinant of whether the perturbation is in the strong or weak regime is whether the loop moves sufficiently during stimulation that it no longer encircles the fixed point. As all the isochrons converge at the fixed point, any loop that encloses it crosses isochrons of all latent phases and hence when the system relaxes back to the limit cycle the distribution of new phases will span the full cycle (Figure 3.9c,e). For strong stimulation the loop is displaced so much that it no longer encircles the fixed point and only intersects with a subset of the isochrons (Figure 3.9d,f). When it relaxes back to the limit cycle the distribution of new phases will only subtend a range of phases indicated by this subset of isochrons and hence will not span the whole cycle. The transition between these regions

occurs for the stimulation intensity which is just strong enough that the loop touches the fixed point at the end of stimulation. In a noise-free regime this would lead to the oscillation permanently ceasing for the network which ended up exactly on the fixed point but in the case of noise this leads to the region of highly variable new phase as described above.

3.4.7 Wilson-Cowan model does not reproduce rapid transients due to stimulation

Finally, although the model accurately reproduces the rephasing behaviour when measured as the timing of activity peaks/LFP troughs, there is a seeming inconsistency between the LFP trajectories immediately following stimulation and the state space trajectories in the model. Specifically, the LFP traces after strong alveus stimulation show what appears to be a pyramidal cell population spike occurring shortly after the stimulus (Figure 3.2b). The latency (3.3 ms in unfiltered trace) is similar to population spikes elicited during calibration in the absence of oscillation. These appeared to be due to synaptic input, and not back-propagation, as they were preceded by the beginning of an EPSP (data not shown). However, alveus stimulation was best modelled by an input that almost exclusively targeted the inhibitory cells and did not strongly excite the pyramidal population. For many stimulation phases the trajectories in the model do not have a prominent spike of pyramidal cell activity.

This seeming inconsistency is resolved by considering what the model is and is not expected to reproduce. In order to reduce the dynamic state variable to two numbers a great deal of simplification necessarily has to take place. One important part of this is how the previous history of spiking is translated into the instantaneous drive to the neurons. A more complete model would need to integrate over the previous history of spiking with some coupling kernels that represented filtering by axonal delays, synapses and dendrites. In deriving their equations Wilson and Cowan (1972) replaced these integrals over past history with time-averaged quantities, such that the equations are best thought of as representing the evolution of the firing rates averaged over some time period. We therefore do not expect the model to reproduce very fast transients in the activity that occur directly following stimulation. It is remarkable that the rephasing behaviour, which is by definition a temporal phenomenon, is reproduced so accurately despite this very crude handling of the detailed time evolution of the system.

3.5 Discussion

The work presented in this chapter makes three principal findings. Firstly we have characterised the phase response of carbachol induced network oscillations in CA3, revealing biphasic continuous PRCs for weak stimulation intensities giving way to discontinuous PRCs and complete resetting at

strong intensities. Secondly, we have demonstrated that the Wilson-Cowan equations are able to reproduce the measured rephasing behaviour with remarkable accuracy. Thirdly, we found that regions of advance and delay in the PRC were located in different regions for dentate compared with alveus stimulation, and that this could be explained in the model by differences in the relative strength of input to excitatory and inhibitory populations. These data are of interest both for understanding the emergence of synchronisation between networks and for the information they provide about the local oscillating network.

Synchronisation is a process in which reciprocal interactions between coupled oscillators bring their phases into a consistent relationship. The effect on the phase of an oscillator of perturbation by external inputs is clearly relevant to understanding this process, and substantial theoretical effort has gone into linking phase response properties of individual oscillators to their collective behaviour when coupled together (reviewed in Izhikevich, 2007; Smeal et al., 2010). For individual neurons coupled by excitatory synapses, PRC shape is a critical determinant of synchronisation properties, with biphasic PRCs strongly promoting synchronisation (Hansel et al., 1995). However, there are important differences between oscillating neurons and sparsely synchronised networks which may affect the conclusions that can be drawn about the relationship between PRC shape and synchronisation properties. Therefore, while we think it highly likely that the data presented here are relevant to understanding coherence between networks, care is required in extrapolating to network oscillators results linking neuronal PRCs with their synchronisation properties.

One key difference is that for most commonly considered neuronal models, the PRC is zero at the time of the spike as currents due to the spiking dynamics overwhelm the effect of the stimulus. This substantially restricts the range of possible PRC shapes and relaxing this constraint may remove the straightforward link between biphasic PRCs and synchronisation through excitatory connections. For an example of this consider the effect of translating an oscillators PRC vertically, such that $\mathrm{PRC}(\theta) \rightarrow \mathrm{PRC}(\theta) + \alpha$, where α is small relative to the period of the oscillation. If this change is applied to both PRCs of a pair of weakly coupled oscillators, it will not affect their phase interaction (the slow change in relative phase as a function of phase difference) and hence will not affect the stability of the synchronised state, even if it transforms a biphasic PRC into an entirely positive PRC. Numerical simulations confirm that this intuition is indeed correct for a pair of pulse coupled oscillators with sinusoidal PRCs (data not shown).

How then can we link network PRCs to their synchronisation properties? The theory of weakly coupled oscillators (reviewed in Izhikevich, 2007) provides a powerful framework for understanding synchronisation in systems where coupling is sufficiently weak that oscillators are never perturbed far from their limit cycles. This permits two key simplifications of the problem.

Firstly, the potentially high dimensional state space of each oscillator can be reduced to one dimensional phase variable. Secondly, the effect on phase of perturbations of different amplitudes A can be expressed as a linear scaling of a single *infinitesimal PRC*, such that $\mathrm{PRC}(A, \theta) = A\,\mathrm{PRC}(\theta)$. The phase interaction between oscillators depends both on this iPRC, which specifies the sensitivity to input as a function of phase, and also on the oscillators outputs as a function of phase. For a neuronal oscillator this output is a spike at phase zero convolved with a synaptic kernel. For a network oscillator this output is a varying firing rate as a function of phase rather than a single spike. Incorporating such continuous interaction is straightforward in the weak coupling framework, so analytical study of the behaviour of weakly coupled neural mass models is one possible approach to linking network PRCs to large scale coherence.

One consideration in applying this approach to our data is that we have not measured infinitesimal PRCs, and indeed we cannot resolve the effect of very small perturbations on the oscillation phase due to the irregularity in cycle duration. It could be argued that the infinitesimal network PRC is likely to be qualitatively similar to the PRCs obtained for the weakest stimuli we were able to resolve. However the irregularity of network oscillations both *in vitro* and *in vivo* more fundamentally challenges the applicability of the framework, as it suggests that activity does not remain close to a limit cycle at all times and hence reduction to a phase model may be inappropriate.

Analytically studying synchronisation of strongly and continuously coupled oscillators is challenging, and as far, as we are aware, model independent results linking PRC shapes to synchronisation have not been reported (Izhikevich, 2007). Empirically, numerical simulations of coupled pairs or chains of the Wilson-Cowan models used in this chapter indicate that they readily synchronise with each other where there intrinsic frequencies are not too disparate (T. Akam, data not shown). This ability to synchronise is consistent with an *in vitro* study using voltage sensitive dye imaging and multi-electrode arrays which demonstrated that oscillations induced by carbachol in CA3 are coherent across distances of several millimetres (Mann et al., 2005).

A further consideration is that it may be more appropriate to treat large scale networks as continuous in space rather than as discreet local networks, a modelling framework known as neural fields. The rich dynamics of such models are an active area of current research, which offers a promising approach to linking the phase response properties of local circuits to patterns of oscillatory activity in spatially extended networks. Current developments in this field are beyond the scope of the current work but readers are directed to the following recent reviews (Deco et al., 2008; Coombes, 2010).

The relevance of our data to understanding coherence phenomena in other brain regions (and indeed in the hippocampus) depends on the extent to which oscillation in CA3 *in vitro* are similar dynamically to that of the *in vivo* oscillatory activity. As discussed in the literature review and chapter introduction, carbachol induced oscillations in CA3 are a good model system for sparsely synchronised oscillations in excitatory-inhibitory networks. *In vivo* data overwhelmingly indicates that gamma oscillations in cortex are of this type although the modulation strength in the *in vitro* model is probably considerably higher than average values in *in vivo*. One question which is essentially unresolved (both *in vitro* and *in vivo*) is whether the instability that produces gamma oscillations is due to inhibitory to inhibitory coupling, or due to the excitatory to inhibitory loop. Oscillations in the Wilson-Cowan model only occur due to the excitatory-inhibitory loop (inhibitory-inhibitory oscillations only occur in rate models with delays), so our data are consistent with this mechanism. As both types of instabilities occur through the same bifurcation type we expect them to have broadly similar rephasing behaviour. Biphasic network PRCs have been identified in a computational study of inhibitory only oscillations (Battaglia et al., 2007).

Gap junctions have also been implicated in oscillogenisis, both in hippocampal theta and gamma oscillations (LeBeau et al., 2003; Bennett and Zukin, 2004; Bissiere et al., 2011). Though gap junctions are in principle sufficient to generate spike to spike synchronisation in the absence of chemical synapses, they are not sufficient to generate sparsely synchronised activity as they do not provide the delayed negative feedback critical to this mode of activity. However, they may greatly increase the susceptibility of networks to such synchronisation by propagating the effect of chemical synapses between neurons, and are necessary for some oscillations that appear to be sparsely synchronised such as carbachol gamma in CA3 (LeBeau et al., 2003). The neural mass model framework used in this chapter to understand network phase response properties is appropriate where gap junctions facilitate sparsely synchronised oscillations, but is not applicable to networks in spike to spike oscillations states, either due to gap junctions or chemical synapses.

Our results question the interpretation of a study by Atallah and Scanziani (2009) which investigated cycle to cycle variation in the frequency of gamma oscillations in the CA3 *in vitro* and *in vivo*. They observed that the amplitude of each gamma cycle correlated positively with the duration of the next cycle and that large amplitude cycles produced larger and longer lasting hyperpolarisations of pyramidal cells. They conclude that inhibition plays a key role in controlling instantaneous frequency with recruitment of more inhibition leading to longer cycles. Correlation between cycle amplitude and subsequent period is consistent with our model, however our results indicate that stimulating inhibitory cells can either delay or advance the oscillation depending on the phase at which the stimulation occurs.

The model indicates that the location of regions of advance and delay in the PRC of network oscillators can be shifted by changing the relative coupling of the input to excitatory and inhibitory populations. The phase at which an oscillator will entrain to periodic inputs, and the relative phase at which coupled oscillators will synchronize, is determined by the location of these regions in the PRC. This indicates that the phase relationship between oscillating networks could be controlled by changing the relative strength of inter-network connections onto local excitatory and inhibitory populations. Control of the relative phase of network oscillations is potentially useful computationally, both for creating phase-coded signals, and for reading them out by controlling the phase of oscillatory gain modulation relative to the input. As we show in Chapter 5 this is an efficient way of using oscillations to controlling the gain of interactions between populations.

The correspondence between model and experiment can be used to make inferences about the input to the local network produced by stimulation of each pathway. An interesting feature implied by the model is the relative strength of input to excitatory and inhibitory populations. To produce rephasing consistent with the experimental data, alveus stimulation was represented in the model as strongly exciting the inhibitory cells but minimally exciting the pyramidal cells. At first glance this seems inconsistent with the known anatomy and the model connectivity. Alveus stimulation recruits pyramidal cell axons and these provide a strong recurrent input to pyramidal cells in the slice. The model synaptic strengths indicate that a pulse of activity in the excitatory population will result in excitatory input to both populations of about equal strength. However, alveus stimulation will also directly recruit activity in local circuit interneurons. The synaptic weights in the model are such that if the stimulus caused an equal sized transient increase in the activity of excitatory and inhibitory populations, the excitatory population would receive a net input of zero while the inhibitory input would receive a net excitatory input. The representation of alveus stimulation is therefore consistent with the model connectivity.

The effect of mossy fibre input has been studied intensively in the quiescent slice (Mori et al., 2004) but our measurements provide additional information about its effect on the active CA3 network. Our data suggest that at the population level, mossy fibres excite inhibitory cells in CA3 more strongly than the pyramidal cells. This is consistent with anatomical data showing that granule cells innervate more inhibitory than excitatory cells (Acsady et al., 1998; Henze et al., 2002), and with *in vivo* physiological data showing that increased granule cell activity decreases the overall excitability of CA3 (Bragin et al., 1995; Penttonen et al., 1998). Of course, this population level measure says nothing about the spatial distribution of input across each population. Given the sparse population activity in both CA3 and dentate gyrus *in vivo*, it is highly likely that physiological patterns of activity in the dentate gyrus produce highly heterogeneous drive to CA3 pyramidal cells with a

small fraction of cells strongly excited and others excited much more weakly or even inhibited by feed-forward inhibition.

As we fitted the model by hand we cannot provide confidence intervals on the values of network parameters. An alternative approach would have been to use mathematical methods which can fit parameters of non-linear models to partially observed systems. One method is to use the unscented Kalman filter (Wan and Van Der Merwe, 2000) in a Bayesian framework (Sitz et al., 2002; Quach et al., 2007) to provide parameter estimates and confidence intervals. This is beyond the scope of the work presented in this chapter but would be an interesting extension which would allow more accurate quantitative statements about the network state.

Chapter 4: Oscillations and filtering networks support flexible routing of information

4.1 Introduction

This chapter presents a biophysical model which implements the operation at the heart of this thesis; the use of network oscillations to selectively control of the gain of anatomically defined pathways. There are two sets of ideas developed in this work. Firstly, we identify a simple mathematical operation that can selectively read out individual components of a combined input based on their oscillatory modulation. This is our first encounter with multiplexing and demultiplexing population codes, which as we argue in the introduction and discussion, is likely to be a critical component of many functional roles performed by oscillations. Secondly, we investigate how these operations can be implemented by biologically plausible network dynamics. We begin by briefly summarizing the motivation for addressing this problem and previous work on the topic.

Different behavioural tasks require distinct patterns of functional interaction between brain regions. For example, when you read a book in a noisy train carriage, information from your visual stream is processed by language regions while auditory input is ignored. Then, if a conversation catches your attention, you can effortlessly switch focus, processing linguistic content from the auditory input that you were ignoring a moment before. A more concrete experimental example is provided by visual attention experiments in which participants perform a perceptual discrimination task about a stimulus in one part of their visual field while ignoring simultaneously presented distracting stimuli (see literature review). These tasks require selective processing of information from the regions of the early visual system representing the task-relevant stimulus. While important in attentional processing (Berman and Colby, 2009), signal routing is likely necessary for other cognitive tasks involving distributed brain systems (Anderson et al., 2004).

Proposals for how this routing is achieved can be broadly divided into two groups; those in which asynchronous rate-coded signals are routed by dedicated switching circuits (Anderson and Essen, 1987; Vogels and Abbott, 2009), and those in which changes in patterns of synchronized network activity play a key role in regulating signal flow (Crick and Koch, 1990; Salinas and Sejnowski, 2001a; Fries, 2005). The ability to selectively and accurately route a target signal to a receiving population in the presence of multiple distracting inputs was recently demonstrated using a 'detailed balance' non-oscillatory gating mechanism (Vogels et al., 2009). Comparable capability has not so

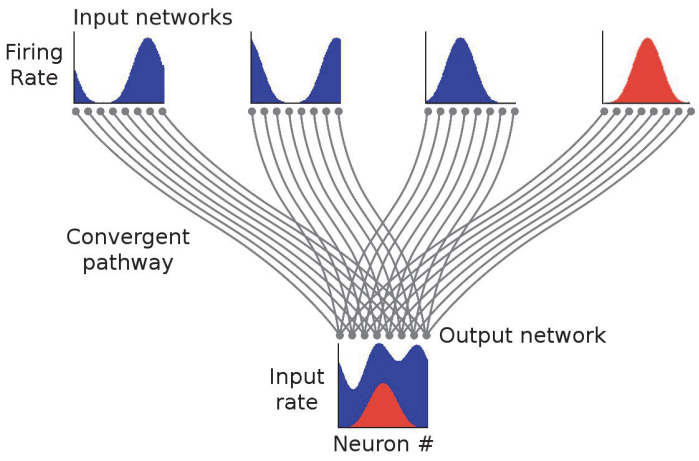

Figure 4.1 **Population-coded information and oscillations.** Input networks represent independent variables as population codes with bell-shaped firing rate tuning curves with respect to stimulus orientation. If one input network switches from an asynchronous (blue) to an oscillating state (red), how much more information is available to the output network about the variable it encodes?

far been demonstrated using oscillatory mechanisms. Furthermore, it remains unclear how synchrony changes in population codes can mediate signal gating, what operations downstream regions must perform on their inputs to achieve gating, and how these operations can be implemented by neural network dynamics.

We have addressed these questions using a feed-forward model in which independent stimuli are represented as population codes in separate networks of spiking neurons. These populations converge to form the input to a single output network (Figure 4.1). When activity in all input networks is asynchronous, little information is available to the output network about the stimulus represented in any one of them because each contributes a small fraction of the total spike input. However, we show that when one of the input networks is switched from an asynchronous to an oscillatory state, accurate information about the stimulus represented by this network becomes available to the output network. This is because in the oscillating network, the spatial pattern of firing rates is reproduced in the spatial pattern of firing rate oscillation amplitude, thus providing a parallel channel for information transmission that is minimally affected by asynchronous distracting inputs. We further show that the filtering necessary to read out such information can be achieved by a simple and biologically plausible network of excitatory and inhibitory neurons exploiting a novel network-level resonance phenomenon. The resulting signal gating mechanism allows accurate and selective propagation of a target signal in the presence of multiple distracting inputs.

Switching among inputs can be achieved within a few cycles. Finally, we show that, when multiple input networks are oscillating in different frequency bands, filtering at the appropriate frequency can be used to pull out individual signals from the combined input, a form of frequency-division multiplexing for neural codes.

4.2 Materials and methods

In this section we provide technical details of the simulations and analysis used in this chapter. Written descriptions and diagrams of the networks are provided in the results section in parallel with data from simulations. We feel this arrangement makes it more straightforward for the reader to link data and results to the network structures that generated them.

Simulations were performed using the software NEST (Gewaltig and Diesmann, 2007) except those for figures 4.12 and 4.14 which were performed in BRIAN (Goodman and Brette, 2009). A 0.1 ms time-step was used for numerical integration. All data analysis and plotting were carried out in python using the Ipython, Numpy, Scipy and Matplotlib libraries.

4.2.1 Neurons

All neurons were described as exponential integrate-and-fire models (Fourcaud-Trocme et al., 2003), and synapses were conductance-based with alpha function time-courses. The membrane potential of the exponential integrate-and-fire neuron obeys the equation:

$$C\frac{dV}{dt} = g_l(V - E_l) + g_l\,\Delta_T\,e^{(\frac{V-V_T}{\Delta_T})} - g_e(t)(V - E_e) - g_i(t)(V - E_i) + I_e$$

When the membrane potential reaches the spike cut-off of 0 mV it is reset to -65 mV.

The following parameters were the same across all neuron populations: Membrane capacitance C = 100 pF, leak conductance g_l = 10 nS, leak reversal potential E_l = -60 mV, spike threshold V_T = -50 ± 2 mV, slope factor Δ_T = 2 mV, excitatory synaptic reversal potential E_e = 0 mV, inhibitory reversal potential E_i = -80 mV.

Synaptic time-courses, synaptic conductances and tonic current were different across populations: Sender network principal cells: Excitatory alpha function τ = 4 ms, Inhibitory τ = 3 ms, tonic current I_e = 30 ± 20 pA. Sender network interneurons: Excitatory τ = 4 ms, Inhibitory τ = 3.5 ms, tonic current I_e = 30 ± 80 pA. Receiver network principal cells: Excitatory τ = 4 ms, Inhibitory τ = 4 ms, tonic current I_e = 30 ± 20 pA. Receiver network Interneurons: Excitatory τ = 4 ms, Inhibitory τ = 8 ms, tonic current I_e = 30 ± 20 pA.

Heterogeneity was introduced in the populations by randomly varying the spike threshold and tonic current across individual cells according to a normal distribution. These parameters are quoted as mean ± standard deviation.

4.2.2 Sender/distractor network

The sender/distractor networks consisted of 8000 excitatory and 2000 inhibitory neurons with random internal connectivity. Each principal cell in the network received synaptic input from a randomly selected 400 principal cells and 200 interneurons. Each interneuron received synaptic input from a randomly selected 400 principal cells and 100 interneurons. Each pyramidal cells received external Poisson spike input with a rate R_{ex} given by:

$$R_{ex} = 400 + 140 \cos\ (2\ (\theta_{stim} - \theta_{pref}))\ Hz$$

Where θ_{stim} was the current stimulus orientation and θ_{pref} was the neurons preferred orientation. Each interneuron received external Poisson input with a constant rate of 400 Hz. In the asynchronous state, alpha function peak conductivities (in nS) between external inputs (X), interneurons (I) and pyramidal cells (E) were: E-E = 0.1, E-I = 0.2, I-E= 0.6, I-I = -1.5, X-E = 1, X-I = 0.8. To switch the network into the oscillating state, the synapses from excitatory to inhibitory and from external to inhibitory were modified to E-I = 0.3, X-I = 0.4.

4.2.3 Sender/distractor network variants

For Figure 4.9, the sender network was modified by changing synaptic weights and time-courses to produce two variants, one of which oscillated at ~16 Hz and one of which oscillated at ~100 Hz.

16 Hz Beta frequency synaptic parameters:

Principal cells: Excitatory alpha function τ = 12 ms, Inhibitory τ = 15 ms,

Interneurons: Excitatory τ = 12 ms, Inhibitory τ = 15 ms,

Alpha function peak conductances (in nS): E-E = 0.05, E-I = 0.08, I-E= 0.1, I-I = -0.2, X-E = 0.47, X-I = 0.5.

100 Hz High gamma frequency synaptic parameters:

Principal cells: Excitatory alpha function τ = 4 ms, Inhibitory τ= 3.5 ms,

Interneurons: Excitatory τ = 4 ms, Inhibitory τ = 2 ms,

Alpha function peak conductivities (in nS): E-E = 0.1, E-I = 0.2, I-E= 0.6, I-I = -2.5, X-E = 1.55, X-I = 0.8.

For Supplementary Figure 4.8, three variant networks were created with parameter values between those used for the asynchronous distractor network and for the oscillating sender network. These spanned the transition from asynchronous to sparsely synchronized dynamics. The only parameters changed were the synaptic strengths from the external input to the inhibitory interneurons and from the principal cells to the interneurons. In order of increasingly oscillatory dynamics, the modified alpha function peak conductances (in nS) in the three variants were:

Variant one: X-I = 0.6, E-I = 0.24, Variant two: X-I = 0.5, E-I = 0.26, Variant three: X-I = 0.45, E-I = 0.28

4.2.4 Receiver network

The receiver network connectivity consisted of 8000 input afferents, 2000 principal cells and 2000 interneurons. The input afferents each had a preferred orientation, which varied smoothly across the population from 0 to 180°. Orientation tuning of interneuron and principal cell activity was inherited entirely from their connectivity to the input afferents; however in describing the connectivity pattern it is useful to think of each pyramidal cell and interneuron as having a predefined orientation preference that again varied across the population from 0 to 180°. For each connection type (for example interneuron to principal cell), the average connection weight between a presynaptic cell and a postsynaptic target was defined as a Gaussian function of the separation of their orientation preferences. The Gaussian function was specified for each connection type by a width in orientation space and an average total number of afferents of that type received by each cell. The width of the connection pattern is the expected standard deviation of orientation preferences of the afferents received by a cell. For the connections between input afferents (X), principal cells (E) and interneurons (I), these connection widths were: X-I = 13.5°, X-E = 13.5°, I-I = 13.5°, I-E = 17°. The average number of afferents received by a postsynaptic cell for each connection type were: X-I = 100, X-E = 600, I-I = 200, I-E = 200. Specific connections onto each cell were generated stochastically with the number of connections between a presynaptic and postsynaptic pair drawn from a Poisson distribution with a mean determined by the spatial Gaussian distributions described above. The peak conductance (in nS) of the alpha function synaptic time-course for each connection type were: X-I = 0.3, X-E = 0.1, I-I = 0.1, I-E = 0.75.

4.2.5 Filter network variants

Alternative implementations of the filtering network were created for Figure 4.12. For simplicity we did not implement a spatially mapped version of these networks in which different cells had different orientation preferences; instead there was a single population of 800 input afferents whose firing rate was homogeneous. These projected to a population of 400 interneurons and 400 principal cells. The interneuron population was recurrently connected and made connections onto

the principal cells. The connection probability between cells in each pathway (X-E, X-I, I-E, I-I) was such that the average number inputs received by cells of each type was the same as in the original filtering network. Except where stated otherwise below, neuronal and synaptic parameters were the same as in the original filter network.

In the first variant filter network (Figure 4.12.3), interneurons had a spike after-hyperpolarization current modeled as an alpha function conductance with τ = 10 ms, conductance 18 nS and reversal potential -80 mV. Interneurons in this network were recurrently connected with gap junctions with a conductance of 0.04 nS and a connection probability of 0.5. The tonic current received by interneurons was 50 ± 20 pA, and the alpha function τ of I-I synapses was 3 mS.

The second filter network variant had two interneuron populations, a feed-forward (FF) population and an interneuron-selective (IS) population (green and purple respectively in network diagram Figure 4.12). For both populations, neuronal parameters and connections from the input afferents were the same as for the interneurons in the original filtering network. To describe the inhibitory connectivity we state for each pathway the alpha function τ, peak conductance and average number of synapses of each type received by a postsynaptic cell. FF-FF: τ = 3 ms, peak conductance = 0.1 nS, N synapses = 200. FF-Principal cell: τ = 4 ms, peak conductance = 0.75 nS, N synapses = 200. IS-IS: τ = 8 ms, peak conductance = 0.1 nS, N synapses = 200. IS-FF: τ = 8 ms, peak conductance = 0.1 nS, N synapses = 200.

For comparison, we also implemented a pathway with no feed forward inhibition (Figure 4.12.1). Each principal cell received on average 600 synaptic connections from input afferents with alpha function τ = 4 ms, peak conductance = 0.018 nS.

For Figure 4.13.2-3 we added an additional population of feedback interneurons to the filtering network. These had the same intrinsic properties as the normal interneurons in the filtering network except for the tonic current, which was 120 ± 20 pA. Each feedback interneuron received 100 excitatory synapses from randomly selected filter network principal cells with alpha function conductance τ = 4 ms, peak conductance = 0.6 nS, reversal potential 0 mV. Each feedback interneuron received 100 recurrent inhibitory synapses from randomly selected feedback interneurons with alpha function conductance τ = 3 ms, peak conductance = 1.5 nS, reversal potential -80 mV. Each filter network principal cell received 100 inhibitory synapses from randomly selected feedback interneurons with alpha function conductance τ = 4 ms, peak conductance = 0.6 nS, reversal potential -80. The tonic current received by filter network principal cells was increaced to 120 ± 20 pA.

For Figure 4.13.4-6, we added a feedback connection from the filter network principal cells to the feed-forward interneurons. Each interneuron recieved 100 excitatory synapses from randomly selected filter network principal cells with alpha function conductance τ = 4 ms, reversal potential 0 mv. In Figure 2.13.4,5, the peak alpha function conductance was 0.075 nS while in Figure 4.13.6it was 0.15 nS.

For Figure 4.14.1 we implemented a filtering network with the pass band tuned to 10 Hz. The filter network was identical to those used in 4.12.3 except for synaptic timescales and strengths which were as follows. Peak conductances: X-I 0.3 nS, X-E 0.1 nS, I-E 0.8 nS, I-I 0.1 nS. Alpha function τ's: X-I 8 ms, X-E 8 ms, I-E 15 ms, I-I 30 ms.

4.2.6 Simulations and analysis

For each network configuration we performed 200 simulations of 1 second of network activity The initial 100 ms of all simulations were discarded to prevent start-up transients contaminating the data.

To quantify the 0 Hz and gamma amplitude, and the decoded estimation accuracy, simulations were divided into non-overlapping 50 ms sections. In all convergent pathway conditions, the orientations of the target and distractor stimuli were randomly drawn from uniform distributions. The spatial pattern of 0 Hz amplitude (average firing rate) and 41 Hz gamma amplitude for each section was analyzed by dividing the neurons into 20 sub-populations and pooling the activity in each group to produce a firing rate signal (all population firing rates were discretized with a 1ms time bin). The Fourier transform of these 20 firing rate signals was analyzed using a 50 ms Hanning window to reduce spectral leakage. The amplitude of the Fourier transforms was measured at 0 Hz to give the population average firing rate and at the 41 Hz oscillation frequency.

4.2.7 Decoding

The 50 ms sections were divided into a training set and a test set. The spatial pattern of average firing rates and gamma amplitude across 20 sub-populations was calculated for each 50 ms section as described above. The training set was used to produce a template of the average firing rate (or gamma amplitude) R as a function of the orientation offset θ between the populations preferred orientation and the stimulus orientation. The template used was a least squares fit of a Von Mises distribution to the average spatial pattern of firing rates (or gamma amplitudes) over the training set:

Template function: $R(\theta) = Ae^{k\cos(2\theta)}$

This template function was then used to decode an estimate of the stimulus orientation for each section in the test set by finding the orientation estimate θ_{est} that minimized the least squared error between the measured firing rates (or gamma amplitudes) and the template function. We report the

standard deviation of these estimates over the test set, the lower bound on the Fisher information given by the reciprocal of the variance and the circular correlation coefficient (Fisher and Lee, 1983) between the uniformly distributed target stimuli and their decoded estimates.

We are grateful to the thesis examiners for pointing out that in fact estimate standard deviation and variance are not the correct metrics to use here as they neglect the estimator bias. Root mean squared error should instead have been used. To quantify how much this affected the results, we evaluated the root mean squared error (E_{RMS}), mean error ($\bar{E}$), and estimate standard deviation (σ), for one condition with highly accurate and one condition with highly inaccurate decoding (respectively; decoding from target input only and from combined input with asynchronous target and distractors). The ratio $\frac{\bar{E}}{\sigma}$ was respectively 0.024 and 0.018 in these two conditions, and the ratio $\frac{E_{RMS}-\sigma}{E_{RMS}}$ was respectively 0.00029 and 0.00016. This confirms that with the size of training and tests sets used, the bias was very small relative to standard deviation and hence using estimate standard deviation instead of root mean squared error will have negligibly affected our results.

4.3 Results

We start with a model consisting of four input networks, each of which represents a separate population-coded stimulus. These converge to form the input to a single output network. The task required of the model is to act as a switch, selecting the signal encoded in any one input network (the 'sender' network), to be routed to the output network, while ignoring the signals encoded in the other input networks ('distractors').

4.3.1 Input Networks

Each input network was represented by 8000 excitatory principal cells and 2000 inhibitory interneurons, described as exponential integrate-and-fire models, mutually and reciprocally interconnected with conductance-based synapses and random connectivity. Spiking activity was induced through tonic depolarization, supplemented by a spatially patterned external Poisson spike input, used to impart stimulus tuning to the neurons as described below.

Input networks were independently switched from asynchronous to oscillatory dynamics by increasing the strength of local excitatory synapses onto interneurons, while reducing the strength of external synaptic drive to the interneurons to maintain the average firing rate of both populations (average firing rates in the asynchronous state: principal cells 4.98 Hz, interneurons 13.64 Hz; in the oscillating state: principal cells 5.34 Hz, interneurons 14.62 Hz).

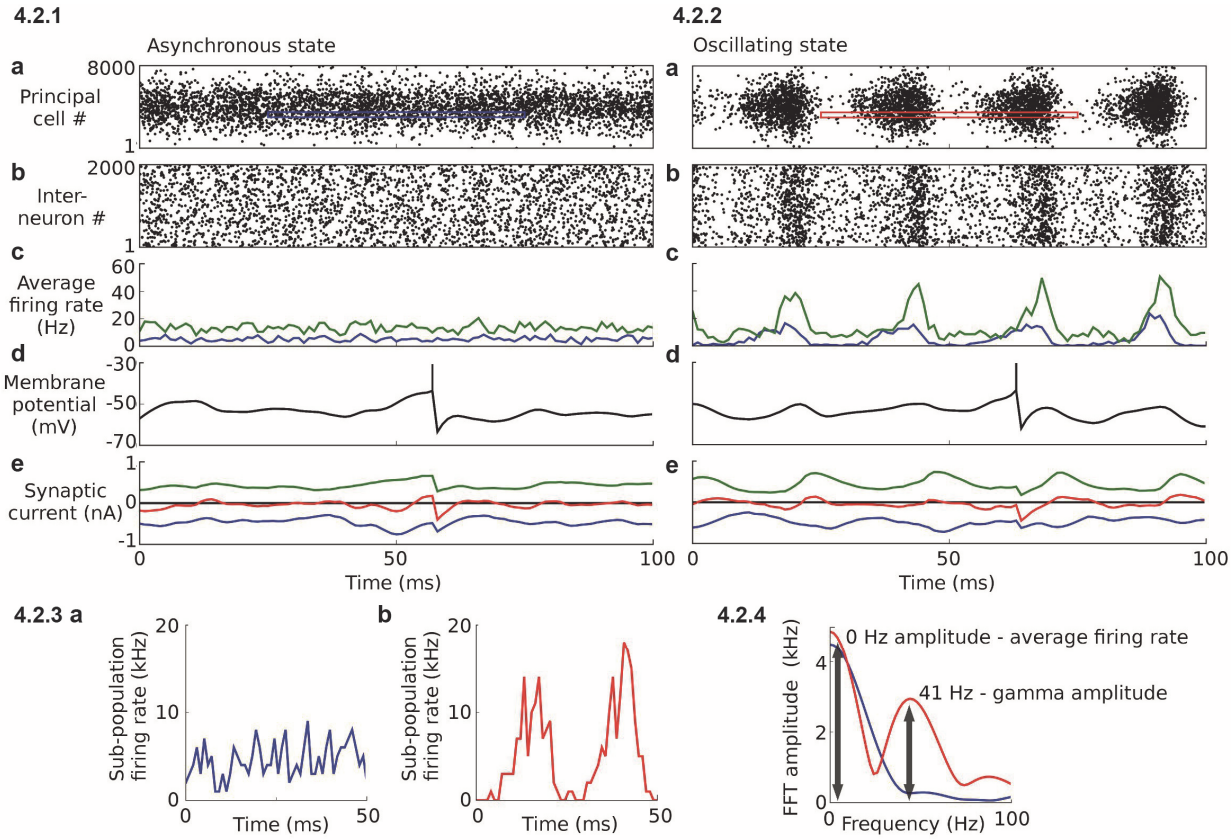

Figure 4.2 **Sender network activity.** (**a,b**) Spike raster showing 100 ms of activity in the sender network in the asynchronous (**4.2.1**) and oscillating (**4.2.2**) state. Panels show: (**a**) principal cell spike raster, (**b**) interneuron spike raster, (**c**) average firing rate for the principal cells (blue) and interneurons (green), (**d**) membrane potential of sample principal cell, (**e**) synaptic currents in sample principal cell (excitatory - blue, inhibitory - green, net current - red). (**4.2.3**) Aggregate firing rate of a sub-population of 400 principal cells over a 50 ms window in the asynchronous (**a**) and oscillatory (**b**) states. Activity was sampled from the areas indicated by colored outlines in the spike rasters (**a**). (**4.2.4**) Fourier transforms of the sub-population firing rates shown in (**4.2.3**). Arrows illustrate the 0 Hz (average firing rate) and 41 Hz (gamma amplitude) measurements used in later analysis.

This switch could equally be achieved by changing other parameters such as synaptic time-courses (Buehlmann and Deco, 2008), external noise (Brunel and Hansel, 2006), or by periodic external input. The precise method does not qualitatively affect the rest of this study.

In the asynchronous state (Figure 4.2.1), network activity generated large excitatory and inhibitory synaptic currents in each cell, which combined to produce a small net current. Stochastic fluctuations in these currents gave rise to irregular spiking activity (Figure 4.2.1a). These features

are characteristic of the balanced regime (Van Vreeswijk and Sompolinsky, 1998) observed in cortical networks during up states.

In the oscillatory state, the instantaneous firing probabilities of both principal and inhibitory cell populations fluctuated strongly at approximately 41 Hz while individual neurons fired irregularly at lower rates (Figure 4.2.2). Average Fano factors for neurons in the oscillating state were close to one (0.96 for a 100 ms bin). These sparsely synchronized dynamics are consistent *in vitro* studies that show irregular activity of individual units, but oscillatory activity at the network level (see literature review). Excitatory and inhibitory synaptic currents oscillated approximately in phase, again consistent with recent *in vivo* and *in vitro* measurements during gamma band network oscillations (Atallah and Scanziani, 2009; Oren et al., 2006).

We used one-dimensional circular variables as the stimuli encoded and transmitted by the sender and distractor networks. (We make this choice for simplicity of network design and clarity of explanation, although the gating mechanism described here can be extended to more complicated stimuli.) Variables were encoded as population codes in which each principal cell had a bell-shaped firing rate tuning curve with respect to stimulus orientation, such that they fired most strongly when the stimulus was aligned with their preferred orientation (Figure 4.3.1b). Population codes with such tuning curves occur widely in the brain, and the one-dimensional case we consider here is analogous to orientation-selective cells in V1 or head-direction cells in the postsubiculum. This tuning was implemented by imposing a spatial pattern on the external input exciting the principal cells. Each principal cell was assigned a preferred stimulus orientation and the external Poisson rate to each cell was determined by a cosine function of the difference between its preferred orientation and the stimulus orientation. The preferred orientation varied smoothly through 180° across the population of 8000 principal cells, so cells 1 and 8000 had similar orientation preference, giving the network a ring topology.

We verified that the activity of the principal cells during asynchronous network activity could be decoded to produce an accurate estimate of the stimulus value using a template-matching decoding method (Deneve et al., 1999). The average spatial pattern of firing rates as a function of stimulus angle was first estimated from a training set of network activity. This spatial pattern was then used as a template for decoding by finding the stimulus estimate that minimized the mean squared error between firing rates measured over a 50 ms test period and the template of firing rates as a function of stimulus angle.

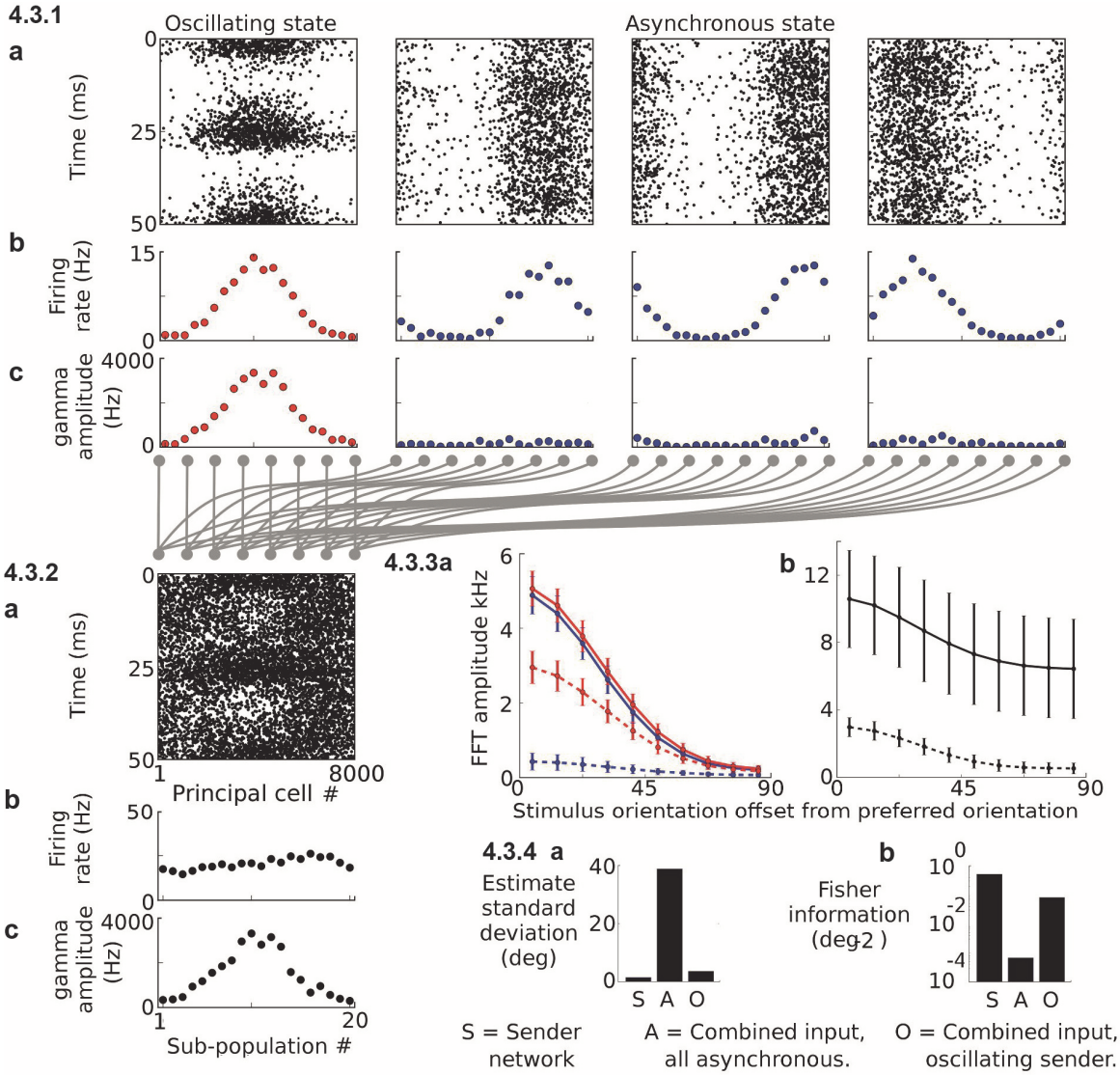

Figure 4.3 **Stimulus representation in network activity.** (**4.3.1**) Activity in one oscillating and three asynchronous sender networks during 50 ms: (**a**) spike raster, (**b**) average principal cell firing rate for 20 sub-populations, each of 400 neurons, **(c)** spatial pattern of gamma amplitude (population firing rate oscillation amplitude at 41 Hz) across the 20 sub-populations. (**4.3.2**) Postsynaptic input obtained by summing activity in the 4 sender networks. (**4.2.3**) Average 0 Hz amplitude (solid line) and gamma amplitude (dashed line) as function of stimulus orientation for (**a**) presynaptic activity in oscillating (red) and asynchronous (blue) networks and (**b**) summed postsynaptic input. Error bars show S.D. For the combined input, both gamma amplitude and firing rate (0 Hz amplitude) show stimulus tuning, but the gamma amplitude is far less variable due to the small contribution of distracting inputs. (**4.3.4**) Accuracy of stimulus representation as measured from the orientation estimate standard deviation (**a**) and Fisher information (**b**), for activity in the presynaptic network (P), and for the summed postsynaptic input when the sender network was in an asynchronous state (A) or an oscillatory state.

To quantify decoding accuracy we calculated the standard deviation of the stimulus estimate (standard deviation 1.40°), and the circular correlation coefficient between the true values of uniformly distributed stimuli and their estimates decoded from neural activity (correlation 0.998). When the network was switched to a sparsely synchronized state, the mean firing rates of individual principal cells showed a very similar dependence on stimulus orientation as in the asynchronous state (Figure 4.3.1b, 4.3.3a). Template matching decoding continued to produce a reliable estimate of the stimulus orientation from the average firing rates over a 50 ms period of network activity (estimate standard deviation 1.22°, correlation 0.998).

We asked whether the periodic temporal structure induced by the oscillation provided new coding possibilities. One possible coding variable is the phase of firing of individual cells relative to the network oscillation, as observed in hippocampal place cells during theta oscillations. Although an analogous form of phase coding has also been proposed to occur in gamma oscillating networks (Fries et al., 2007), we have not explored this further here. Instead, we asked if the spatial pattern of the amplitude of oscillations in the firing rate can itself encode information about the stimulus.

Because individual neurons fired irregularly with average rates well below the population oscillation frequency, the Fourier spectrum of spike patterns for individual neurons was dominated by Poisson-like noise. The spatial pattern of oscillation amplitude only became apparent when looking at the firing rate of populations of principal cells with similar stimulus preference. We therefore grouped them into 20 sub-populations of 400 adjacent cells. We then evaluated the frequency spectrum of the total firing rate of each sub-population using a short-time Fourier transform (STFT) with a 50 ms Hanning window (Figure 4.2.4). We used two measurements from the Fourier spectrum in further analysis: the amplitude at 0 Hz (which is simply the average firing rate of the population over the window) and the amplitude at the 41 Hz oscillation frequency, which we refer to as the gamma amplitude.

These two different frequency components (0 and 41 Hz) of the firing rate are effectively two separate channels, each of which carries information about the stimulus orientation. Because the network only generated large gamma amplitudes in the oscillating state, when the signal from an oscillating sender network was summed with signals from asynchronous distractor networks, the gamma amplitude of the combined signal was dominated by activity in the oscillating network. Can this allow accurate estimation of the stimulus represented in the oscillating sender with minimal contamination by the distractors?

4.3.2 Signal gating among convergent pathways

We considered a situation in which the sender network, and three distractor networks, converged onto a single receiver network, such that the postsynaptic input was simply the sum of the presynaptic activity patterns (Figure 4.3.2). When the sender network was in the same asynchronous state as the distractors, the orientation of the stimulus driving the sender network was ambiguous and could be estimated little better than chance from the combined spike input (estimate standard deviation 38.78°, correlation 0.171).

We asked whether changing the sender network to an oscillatory state increased the information available to the receiver. To do this we analyzed the spatial pattern of gamma amplitude for the postsynaptic input using the method described above for the presynaptic activity. As before, we divided the summed input from the sender and distractor networks into 20 sub-populations, each containing afferents with similar stimulus tuning (400 from each of the 4 input networks). Activity in each group of afferents was pooled to produce a firing rate signal. We analyzed this signal using the STFT to evaluate the 0 Hz and 41 Hz Fourier components for 50 ms sections of the combined input. While the 0 Hz amplitude was uninformative (Figure 4.3.2b), the gamma amplitude faithfully reproduced the pattern of activity in the oscillating sender network, almost as if the distracting inputs were not present (Figure 4.3.2c,4.3.3c). The stimulus driving the oscillating sender network could be accurately estimated from the gamma amplitude of the combined input (estimate standard deviation 3.53°, correlation 0.986). This improved estimation accuracy corresponded to >100 fold increase in the lower bound on the Fisher information available to the post synaptic network (presynaptic, 0.51 deg^{-2}; postsynaptic, asynchronous sender, 0.00066 deg^{-2}; postsynaptic, oscillating sender, 0.08 deg^{-2}; Figure 4.3.4).

4.3.3 Gating using a spiking network filter

The results above demonstrate that a population-level oscillation in the sender network greatly enhances the information available to the receiver about the stimulus it encodes. Can a biologically plausible neuronal network read out this information? A re-formulation of this problem is to ask whether a network of simulated neurons can reproduce the spatial activity pattern of its oscillating input in the firing rates of its output neurons, while ignoring the asynchronous component of the input it receives.

In designing such a network we took as our starting point the detailed balance model recently outlined by Vogels and Abbott (2009), in which an excitatory input is precisely balanced by feed-forward inhibition, such that changes in the firing rate of the input do not alter the activity of the target principal cells. We mapped the orientation-tuned excitatory inputs onto a population of 2000 principal cells, and a population of 2000 interneurons that formed a feed-forward layer, projecting

to the principal cells (Figure 4.4.1). Interneurons innervating a given principal cell received inputs from afferents with similar orientation tuning to those afferents innervating the principal cell directly (though the fine structure of the connectivity was random). This produced a pattern of feed-forward inhibitory input that balanced out the pattern of excitation in the target principal cells. Interneurons were also recurrently connected; this connectivity was local such that only interneurons receiving input from afferents with similar orientation preference made synaptic connections with one another.

When this receiver network was driven by a bell-shaped pattern of asynchronous Poisson spike input, the pattern of input firing rates was reproduced in the interneuron layer activity and the resulting feed-forward inhibition prevented spiking in the principal cell population (Figure 4.4.3).

To retain sensitivity to periodically modulated input patterns, we exploited a network resonance phenomenon that occurs in recurrently connected interneuron networks. Under conditions of tonic excitatory drive, interneuron networks can generate spontaneous oscillations (Brunel and Hakim, 1999) but these break down to an asynchronous state as the level of heterogeneity or external noise is increased (Brunel et al., 2006). We found that in the asynchronous state, but near to the transition to sparsely synchronized oscillation, the interneuron network acted like a damped oscillator, showing clear resonance behavior when driven by periodic input. To illustrate this resonance behavior we drove the input afferents with a sinusoidally modulated Poisson spike input, with a range of modulation frequencies from 0 – 55 Hz (Figure 4.4.2). The periodic modulation of the input firing rate evoked a periodic fluctuation of the firing rate of the feed-forward interneuron population. Resonance was observed both in the amplitude of the firing rate modulation, especially prominent between 25 and 40 Hz, and also in the phase of the interneuron firing rate modulation relative to the input firing rate modulation. The interneuron firing rate was in phase with the input at frequencies up to ~25 Hz but lagged behind the input at higher frequencies, with approximately 90° lag for 40 Hz input modulation. This resonance phenomenon was a network effect arising from the recurrent connectivity in the interneuron layer and was not a result of sub-threshold resonance in the individual interneurons (Fourcaud-Trocme et al., 2003).

The 90° phase lag between the input firing rate oscillation in the gamma band and the response of the feed-forward inhibitory population allowed the principal cells to fire in response to the oscillating input. The phase-delayed oscillations in the inhibitory firing rate disinhibited the principal cells at the phase when excitatory input was strongest. The ability to respond to spatially patterned oscillation was tested by driving the receiver network with a bell-shaped pattern of Poisson input, sinusoidally modulated at 40 Hz (Figure 4.4.4). This periodically modulated input activity pattern was reproduced in robust spiking activity in the principal cell layer.

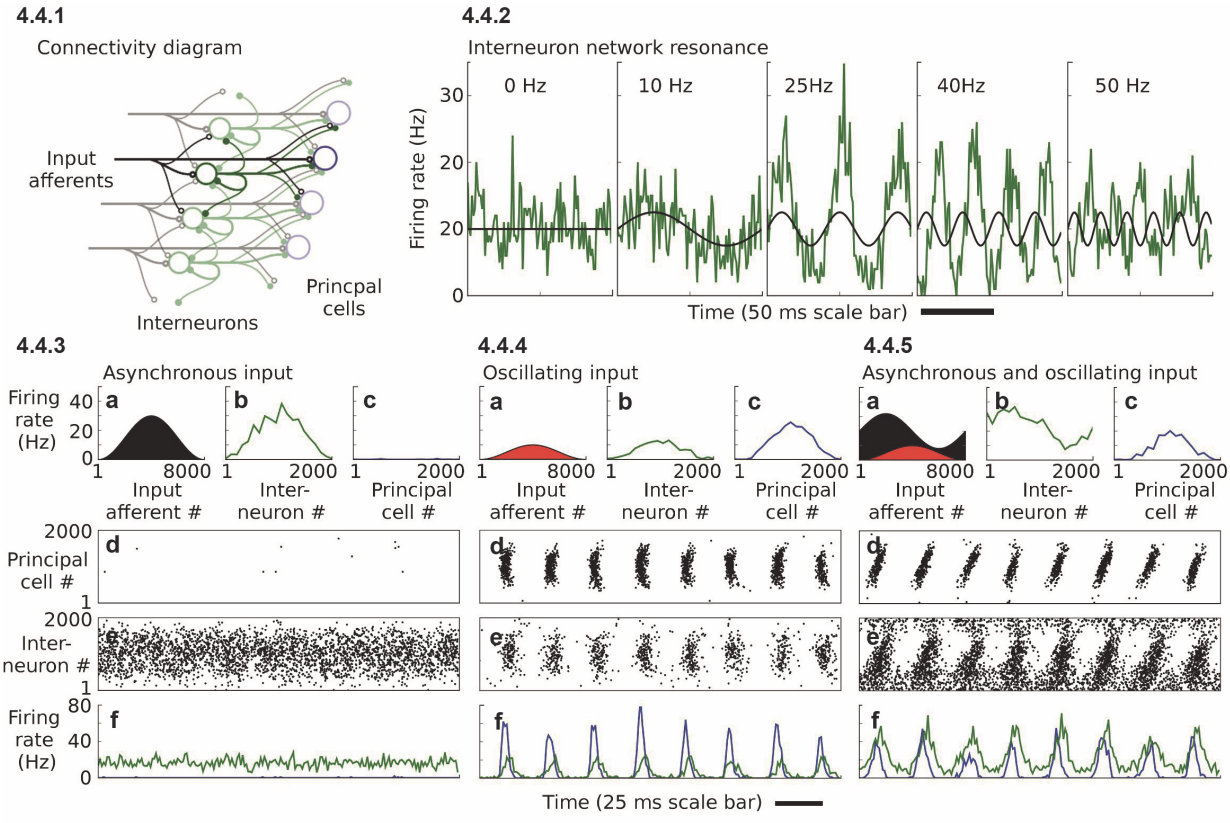

Figure 4.4 **Filter network.** (**4.4.1**) Diagram of filter network connectivity showing the input afferents (black), feed-forward interneuron layer (green) and principal cells (blue). (**4.4.2**) Resonance in filter network interneuron population activity. Panels show firing rate of interneuron population (green) driven by periodically modulated Poisson spike input (mean rate indicated in black) at a range of frequencies bracketing the network resonance frequency. (**4.4.3-5**) Filter network principal cells reproduce position of oscillating input activity, irrespective of spatial pattern of asynchronous input. Filter network activity driven by (**4.4.3**) asynchronous input, (**4.4.4**) gamma modulated input, (**4.4.5**) mixed gamma modulated and asynchronous input. (**a**) Spatial pattern of firing rates in afferent fibers (black - asynchronous Poisson input, Poisson input sinusoidally modulated at 40 Hz). (**b**) Spatial pattern of firing rate in interneuron layer. (**c**) Spatial pattern of firing rate in principal cell layer. (**d**) Spike raster for principal cells and (**e**) interneurons. (**f**) Firing rate of principal cell (blue) and interneuron (green) populations.

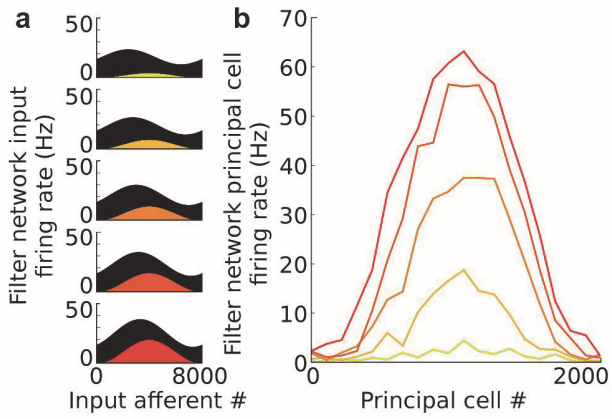

Figure 4.5 **Graded response of filtering network to the average firing rate of oscillating input.** The filtering network was driven with a Poisson spike input consisting of an asynchronous and an oscillating component (sinusoidally modulated at 40 Hz). The firing rate of the asynchronous component was held fixed while the average firing rate of the oscillating component was varied (average firing rate per input afferent indicated by color: dark blue - 2 Hz, light blue - 4 Hz, green - 6 Hz, yellow - 8 Hz, red - 10 Hz). (**a**) Spatial pattern of activity in the input afferents showing the asynchronous (black) and oscillating (colored) components. (**b**) Spatial pattern of firing rate of filter network principal cells averaged over 500ms.

For effective signal gating, the pattern of activity induced by an oscillating input should be minimally affected by converging inputs from other asynchronous networks. We tested this by driving the receiver network with the same bell-shaped pattern of periodically modulated input as in Figure 4.4.4, but with an additional bell-shaped asynchronous Poisson input with a 3-fold larger average firing rate and a peak position rotated in orientation space from the peak of the oscillating input (Figure 4.4.5). The spatial pattern of spiking activity in the receiver network was very similar to that induced in the absence of the asynchronous input, faithfully reproducing the location of the hump of oscillating input. The filter network output responded to a change in the average firing rate of the oscillating component of the input in a graded manner (Figure 4.5). To quantify the signal gating performance of the filtering network, we drove it with the combined input from one oscillating sender network and 3 asynchronous distractor networks. Spiking activity in the filter network output layer reproduced the pattern of activity of the oscillating input regardless of the spatial pattern of asynchronous input. The stimulus encoded in the oscillating input network could be accurately decoded from the spatial pattern of filter network principal cell firing rates using template matching on 50 ms sections of activity (estimate standard deviation 4.25°, correlation 0.978). Population firing rates in the filter network oscillated strongly but individual neurons fired highly irregularly (mean Fano factor 1.51 for 100 ms bin).

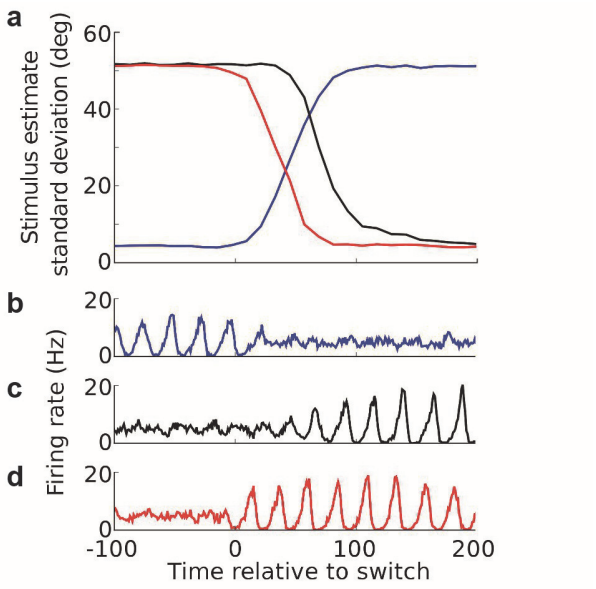

Figure 4.6 **Time-course of switching between input stimuli.** (**a**) Accuracy of stimulus estimate decoded from filter network output during switch between input networks. (**b-c**) Firing rate in input networks during switching. Blue traces - network switching from oscillating to asynchronous. Black traces - network switching from asynchronous to oscillating (note slow transition into oscillating state). Red traces – network rapidly switched from asynchronous to oscillating by giving interneuron population a brief kick at the time of transition.

4.3.4 Switching among input networks

Because the sender and distractor networks considered here had the same architecture, information about the stimulus represented in any one of the different input populations could be made available to the receiving network by switching which one was in an oscillatory state: one of the distractors could thus become the sender, and vice versa.

We tested how rapidly the filter network responded to this switching. After such a transition, it took ~ 150 ms (~6 oscillatory cycles) for the stimulus estimate decoded from the filter network to reach steady state accuracy (Figure 4.6a). We observed that when a presynaptic network was switched from asynchronous to oscillatory dynamics, the oscillation did not start suddenly but rather developed slowly over a number of cycles, limiting the speed of switching (Figure 4.6c).

However, by delivering a small kick to the network at the time of switching (a brief pulse of excitatory input to the interneurons) a strong oscillation could be induced immediately, reaching full amplitude on the first cycle after switching (Figure 4.6d). This reduced the time taken for the filter network output to reach steady state accuracy to 75 ms (~3 cycles, Figure 4.6a). The rapid response

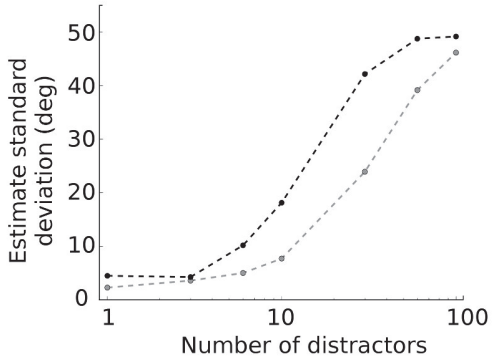

Figure 4.7 **Effect of the number of distractors.** Traces show standard deviation of stimulus estimate as function of the number of distracting inputs, for estimates decoded from the filter network output (black trace), or the combined spike input (gray trace).

of the filtering network could allow brief episodes of network oscillation lasting only a few cycles to transmit a pulse of information down a pathway whose default state was gated off.

We tested the how the gating performance varied depending on the number of distracting inputs (Figure 4.7). As the number of distracting inputs increased, decoding accuracy decreased both for decoding from the gamma amplitude of the combined input, and decoding from filter network firing rates. This occurred because although each individual distractor generates a small amount of noise in the gamma band, as the numbers of distractors increased, their combined contribution grew until it eventually drowned out the signal from the oscillating sender. As with the detailed balance gating mechanism (Vogels et al., 2009), high signal propagation performance requires that the number of active distracting inputs be restricted.

4.3.5 Multiplexing population codes in the frequency domain

The gating mechanism we have described works because only the oscillating sender network contributes strongly to the gamma band amplitude of the combined signal. For this reason, signal gating is severely compromised if distracting inputs also oscillate in the same frequency band (Figure 4.8). However, network oscillations occur in the brain over a wide range of frequencies, raising the possibility that multiple population codes originating from networks oscillating at different frequencies could be multiplexed into a single set of inputs. This could allow the receiving network to choose which of several different inputs to respond to, by choosing which frequency band to filter from the combined input. Just as frequency division multiplexing in electronic communication networks allows multiple independent signals to share the

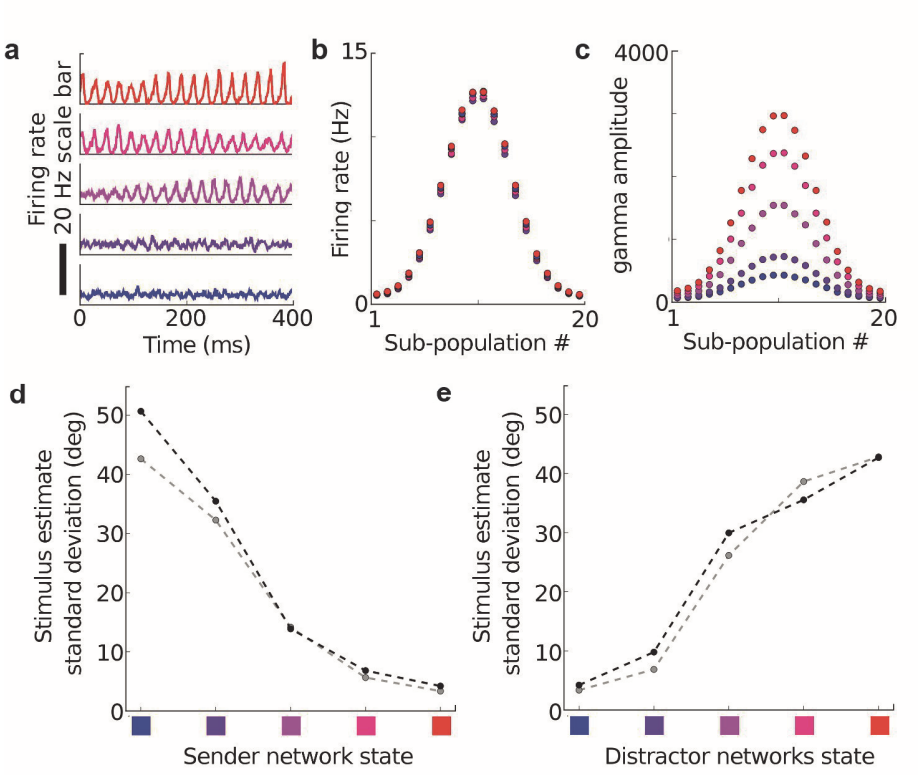

Figure 4.8 **Effect of presynaptic network state on gating performance.** (**a**) Example traces showing network firing rate for 5 different states ranging from asynchronous to strongly oscillating. (**b**) Spatial pattern of neuronal firing rates in the 5 states, color-coded as in (**a**). (**c**) Spatial pattern of gamma amplitude in the 5 states. (**d**) Effect of varying the state of the sender network on gating performance. Black trace shows standard deviation of stimulus estimate using filter network output, gray trace shows standard deviation of estimate from input to filter network. (**e**) Effect of varying state of distractor networks on gating performance

electromagnetic spectrum or optical fiber bandwidth, multiplexing may facilitate efficient use of white matter tracts in the brain.

To explore the possibility for multiplexing in our model, we replaced two of the asynchronous distracting networks with modified versions of the sender network, one of which oscillated at a high gamma frequency (~100 Hz) and the other in the beta frequency band (~16 Hz). The combined signal therefore contained an asynchronous, a low gamma, a high gamma and a beta frequency component, each of which encoded a different stimulus in its spatial pattern of activity (Figure 4.9). The spatial pattern of activity in each of the oscillating inputs could be accurately read out from the combined signal by evaluating the spatial pattern of firing rate oscillation amplitude at the appropriate frequency. The estimate standard deviations decoded from 125 ms sections of the

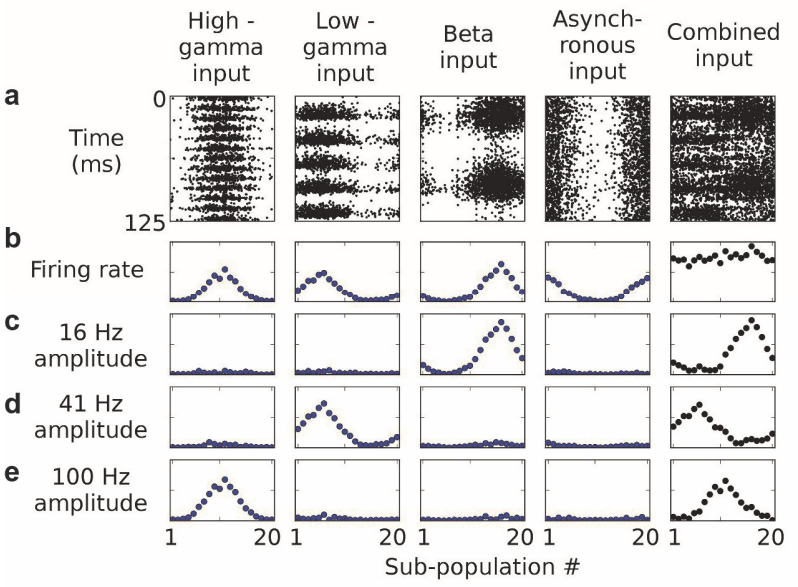

Figure 4.9 **Multiplexing multiple signals in the frequency domain.** Four input networks, one asynchronous, one oscillating in the high gamma band, one in the low gamma band and one in the beta band, converge to produce a combined pattern of input activity. Reading out the pattern of amplitude of the combined input at the appropriate frequency recovers the spatial pattern of activity in any one of the oscillating networks. (**a**) Spike rasters, (**b**) Spatial patterns of firing rate. (**c-e**) Spatial pattern of firing rate oscillation amplitude in beta (**c**), low gamma (**d**) and high gamma (**e**) frequency bands.

combined input activity for the beta frequency input was 1.93°; for the low gamma input 2.19°; and for the high gamma input 1.72°. (A longer window - 125 ms as opposed to 50 ms for Figure 4.3, was used both to capture the longer period of the beta frequency oscillation, and to reduce broadening of Fourier spectral peaks due to the time-frequency uncertainty principle.)

We drove the filter network with this combined input to test whether it could extract the low gamma input in the presence of distractors oscillating in other frequency bands. The stimulus encoded in the low gamma input network could be accurately decoded from the spatial pattern of filter network firing rates evaluated over 125 ms sections (estimate standard deviation 4.60°, correlation 0.976). The high correlation between the input stimulus and the estimate decoded from the filter network output shows that the filter network is able to perform the band-pass filtering needed to extract one of the 3 multiplexed signals. However the accuracy is lower than that achieved by decoding from the gamma amplitude directly, suggesting that the performance of the filter network could be improved.

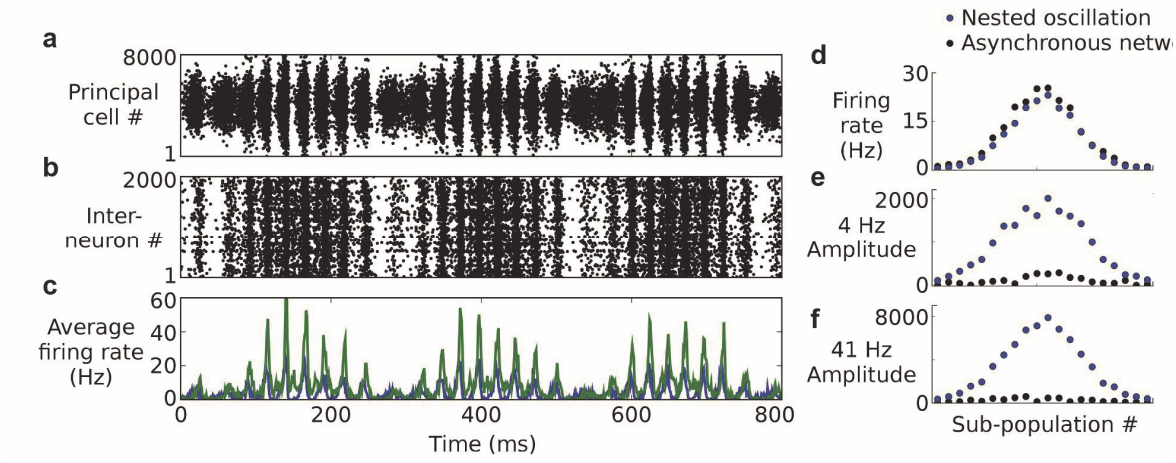

Figure 4.10 **Nested oscillations create amplitude patterns in multiple frequency bands.** (**a-c**) Network activity during nested oscillations, where a network oscillating at 40 Hz was modulated at 4 Hz. (**a**) Principal cell spike raster. (**b**) Interneuron spike raster. (**c**) Average firing rate in principal cell (blue) and interneuron (green) populations. (**d-f**) Spatial pattern of firing rate and firing rate oscillation amplitude in the network with nested oscillations (blue) and for comparison in an asynchronous network (black). (**d**) Neuronal firing rate evaluated over 3 cycles of 4 Hz oscillation (750 ms). (**e**) Firing rate oscillation amplitude at 4 Hz. (**f**) Firing rate oscillation amplitude at 41 Hz. Amplitudes were calculated for Hanning-windowed sections of activity lasting 3 cycles of the oscillation frequency being measured (75 ms at 41 Hz, 750 ms at 4 Hz).

Modulation of the amplitude of a high frequency oscillation by the phase of a low frequency oscillation has been observed in several brain regions (Roopun et al., 2008). We found that this arrangement reproduced the spatial pattern of firing rates in the spatial pattern of amplitude at both oscillation frequencies (Figure 4.10). This suggests a possible role for these dynamics in multiplexing a stimulus into two frequency bands simultaneously.

4.3.6 Time varying stimuli

We have hitherto only considered stationary stimuli. Can the encoding scheme and the filtering network function with time-varying stimuli? We tested this by summing the activity in one oscillating sender and 3 asynchronous distractor networks representing stimuli that varied independently over time (Figure 4.11). We analyzed the spatio-temporal pattern of gamma amplitude of the combined input using a 50 ms Hanning window as before, but moved the window

along the input activity in 25 ms steps. The spatio-temporal pattern of gamma amplitude reproduced the activity in the oscillating sender network and was decoded to produce an accurate estimate of the time varying stimulus driving the oscillating network (Figure 4.11f).

We drove the input afferents of the filtering network with this convergent spike activity (Figure 4.11g-j). This induced an oscillating bump of spiking activity in the principal cells of the filtering network that followed activity in the oscillating input network. The firing rates of the principal cells in the receiver network were decoded to produce an estimator that accurately tracked the orientation of the stimulus driving the oscillating sender network (Figure 4.11g). We thus conclude that, for stimuli that vary relatively slowly relative to the oscillation frequency, the mechanism described here is indeed able to route signals with high accuracy.

4.3.7 Alternative filter networks

In this section we illustrate two alternative filter networks which achieve the same functionality as the original using the same dynamical principles, but with different biological implementation. We do this to address a potentially unphysiological aspect of the parameters of the original network (see below) and to illustrate how a varietly of circuits can implement resonant feed-forward inhibition.

At the algorithmic level (Marr and Poggio, 1976), the filtering network encodes the amplitude of firing rate oscillation in its input afferents at a given frequency, into the firing rate of its output afferents. At the mechanistic level, asynchronous input is canceled by feed-forward inhibition, but oscillatory input induces large amplitude phase delayed oscillations in the inhibitory firing rate due to a strong resonance in the interneuron population at a lower frequency than that of the input oscillation. This disinhibits the principal cells at the phase when excitation is strong, allowing them to fire.

In the original filter network the low frequency resonance in the inhibitory population was generated by slow recurrent synapses among the interneurons. However, the inhibition received by principal cells must decay quickly to produce periods of dis-inhibition in response to oscillating inputs. This necessitated faster kinetics at the interneuron-principal cell synapses than at interneuron-interneuron synapses. This slower inhibition onto interneurons relative to excitatory cells is atypical of many interneuron populations (Jonas et al., 2004), prompting us to explore whether other biological mechanisms could produce the required resonance in the interneuron population.

Before discussing these alternative filtering networks, we note that late spiking interneurons of cortical layer 1 exhibit considerably slower kinetics at their recurrent synapses than at their synapses onto pyramidal cells (Chu et al., 2003). These interneurons are ideally located to control

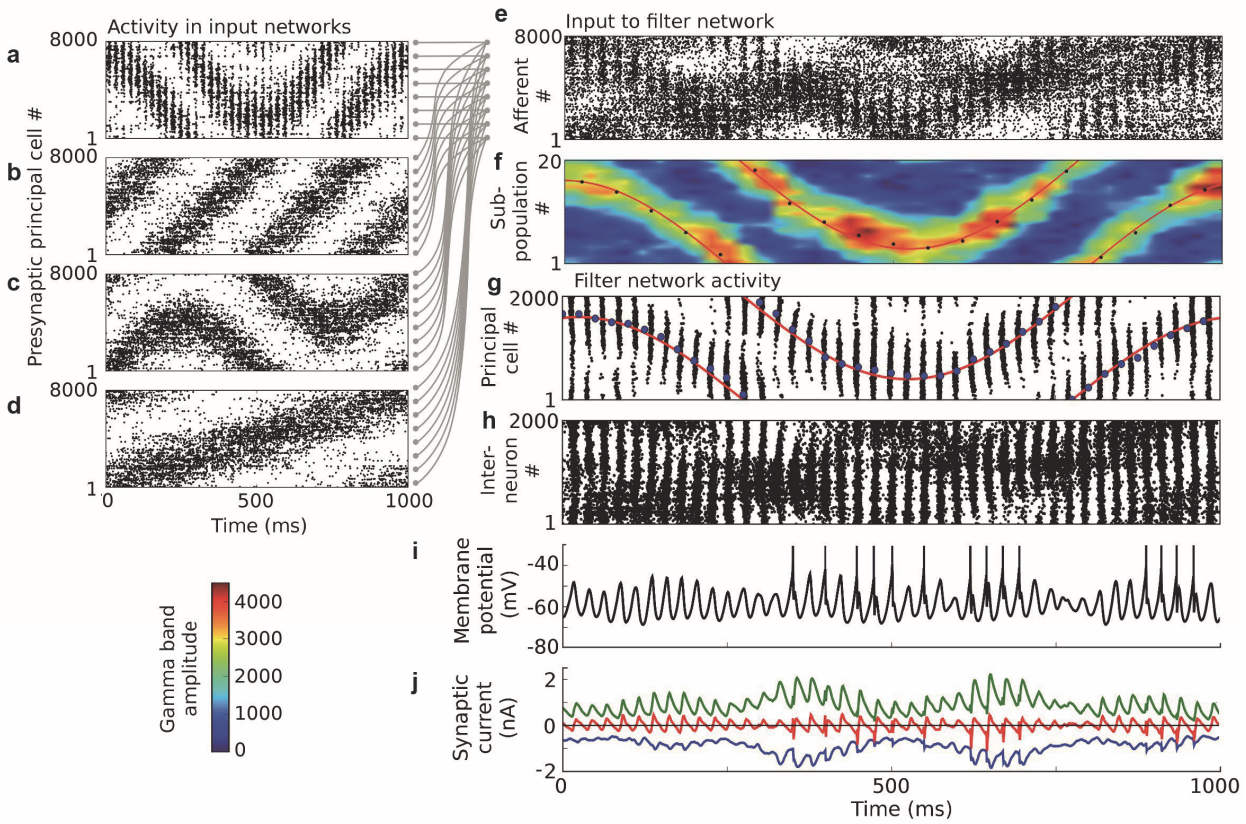

Figure 4.11 **Gating time-varying stimuli.** (**a-d**) Spike rasters of principal cells in 4 input networks, each encoding a different time-varying stimulus. Network generating raster (**a**) is in the oscillating state while the other three networks are in the asynchronous state. (**e-f**) Combined input obtained by summing activity in the input networks: (**e**) spike raster, (**f**) spatio-temporal pattern of gamma band amplitude, together with the stimulus driving oscillating network (red line) and decoded stimulus estimate (black dots). (**g-j**) Activity in filtering network when driven by convergent input: (**g**) principal cell spike raster (black), stimulus driving oscillating network (red), stimulus estimate decoded from pyramidal cell activity (blue), (**h**) interneuron spike raster, (**i**) membrane potential of sample principal cell, (**j**) synaptic currents in a sample principal cell (inhibitory - green, excitatory - blue, net current – red).

integration of activity in the long-range collaterals of layer 1. The slow synaptic kinetics of these interneurons suggests that if they are acting as a filtering network, the pass-band would be situated in the alpha or beta frequency range. The anatomical location and synaptic properties of these cells, in combination with *in vivo* data implicating low frequency oscillations in tasks involving long-

range interactions, make these cells a promising candidate implementation of the described filtering network.

In the first alternative version of the filtering network (Figure 4.12.3), low frequency resonance in the interneuron population was induced by a combination of spike after-hyperpolarisation and gap junction connections between interneurons. In this mechanism, the gap junctions promoted synchronization of the interneuron population at a frequency that was determined by the AHP time-course. The filtering performance of the network was very similar to that of the original filtering network (Figure 4.12.2, 4.12.3). We expect that resonance can be conferred on a neuronal population responses by other features contributing to intrinsic cellular dynamics such as sub-threshold voltage-gated conductances (Geisler et al., 2005). Gap junction coupling may promote the transfer of sub-threshold dynamics to population responses by homogenizing membrane potential trajectories across populations.

Although it is conceptually simple to have a particular filtering function implemented in a single interneuron population, it is possible that more than one interneuron type participates. In a second alternative implementation of the filtering network, the slow inhibitory synapses that generated resonance at the required frequency were expressed in a separate population of interneurons from those mediating fast feed-forward inhibition (Figure 4.12.4). The 'slow' population made inhibitory connections both recurrently and onto the 'fast' population. The 'fast' population made synapses recurrently and onto the principal cells. Recurrent connections in the 'slow' population induced resonance at a low frequency causing large amplitude, phase-shifted oscillations in its firing rate in response to oscillating input. These firing rate oscillations were imposed on the 'fast' interneurons by the synaptic connection between the two populations.

Though differing in their precise biological implementation, due to their common dynamical mechanism, these alternative filtering networks share characteristic, experimentally testable electrophysiological features. Specifically, spike output of the principal cells is associated with large amplitude oscillation in the excitatory and inhibitory synaptic current rather than being determined by the average excitatory synaptic input. Additionally, spiking activity is associated with a phase shift between oscillation in the excitatory and inhibitory synaptic currents received by the output cells of the filtering network.

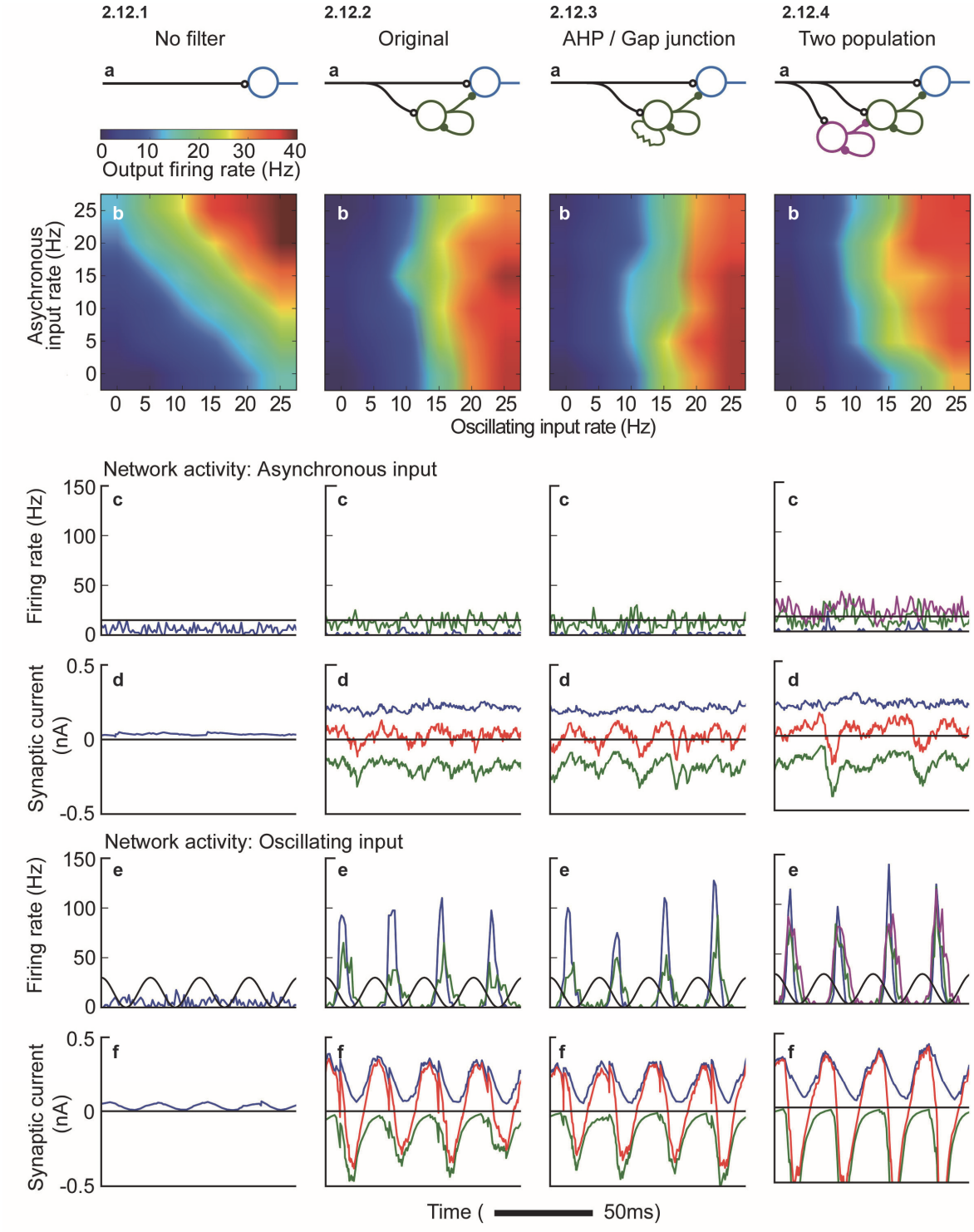

Figure 4.12 **Alternative filter network implementations.** Two alternative filter networks were designed (**4.12.3,4**), which perform the same function as the original filtering network with alternative biological implementation of the resonant feed-forward inhibition. These are compared with the original filtering network (**4.12.2**) and a pathway with no feed-forward filtering (**4.12.1**).

(**Figure 4.12 legend cont.**) For simplicity, we show results for a filtering network in which all input afferents have the same firing rate. (**a**) Filter network diagrams showing input afferents (black), interneurons (green, purple) and principal cells (blue). The input consisted of Poisson spiking activity in the input afferents with an asynchronous and an oscillating component. The firing rate of the oscillating component was sinusoidally modulated at 40 Hz. (**b**) To illustrate each network's ability to respond differentially to the asynchronous and oscillating inputs, the firing rate of the filter network principal cells was measured as the average firing rates of the asynchronous and oscillatory components of the input were systematically varied. For all three networks incorporating resonant feed forward inhibition (**4.12.2-4b**), the output firing rate responded strongly to increases in the firing rate of the oscillating input component (abscissa), while changes in the asynchronous input (ordinate) had little effect. In the pathway with no filtering (**4.12.1b**) the output rate responded strongly to changes in both components of the input. (**c**) Neuronal firing rates in response to asynchronous input (traces colored as in diagrams (**a**). (**d**) Synaptic current in a sample principal cell in response to asynchronous input (blue – excitatory current, green – inhibitory current, red – net current). (**e**) Neuronal firing rates in response to oscillating input. (**f**) Synaptic currents in a sample principal cell in response to oscillating input.

4.3.8 Filtering in the presence of feedback inhibition

The filter network hitherto described contains only principal cells and a feed-forward interneuron layer. We used this greatly simplified structure to illustrate the minimal circuitry needed to implement the filtering. However, real neural circuits are more complex; feedback inhibition is ubiquitous and many interneuron populations mediate both feed-forward and feedback inhibition. We tested whether filtering could continue to function in the presence of feedback inhibition.

We first tested whether filtering continued to function in the presence of an additional population of interneurons mediating feedback inhibition of the principal cell population. Filtering continued to function effectively in the presence of feedback inhibition (Figure 4.13). We then tested whether a feedback connection from the principal cells to the interneurons disrupted the filtering function. As long as the feedback connection was not too strong, filtering continued to function effectively (Figure 4.13.4, 4.13.5). As the strength of feedback connection was increased, a threshold was reached above which the principal cell interneuron loop started to oscillate spontaneously, even when driven by asynchronous input (Figure 4.13.6). This caused principal cells to fire strongly in response to asynchronous input and hence the filtering no longer functioned. This transition to spontaneous oscillation occurred when the feed-back synapses were approximately 1/3 the strength of the feed-forward synapses (each interneuron received an equal number of feed-forward and feed-back excitatory synapses).

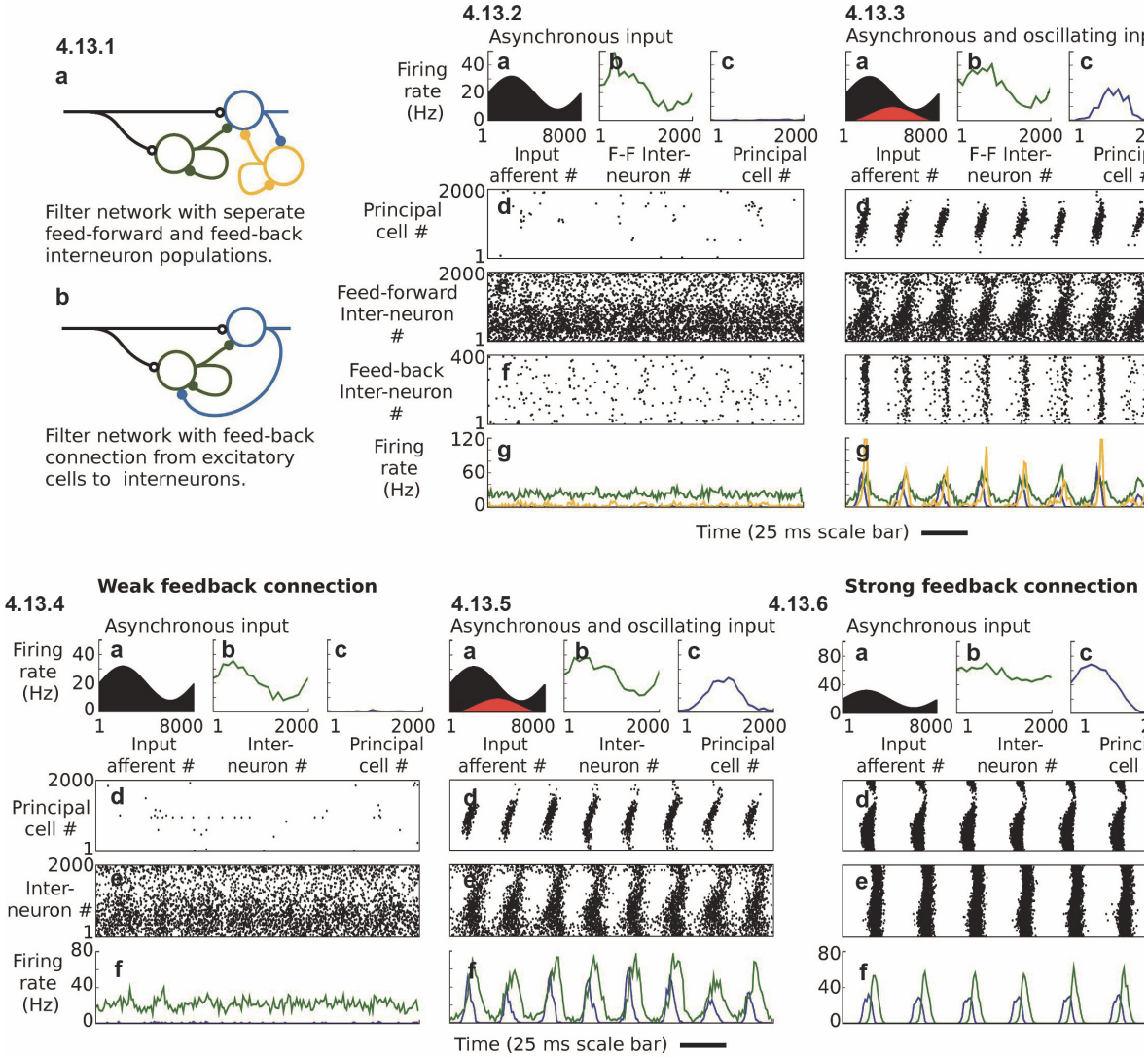

Figure 4.13 **Filtering in the presence of feedback inhibition.** Filter network with an additional population of feedback interneurons (**4.13.1a**), driven by (**4.13.2**) asynchronous input, (**4.13.3**) combined asynchronous and oscillating input. (**4.13.1b**) Filter network with connection from principal cells to interneurons. With a weak feedback connection, filtering continues to function effectively (**4.13.4-5**); above a threshold strength of feedback connection, the E-I loop starts to oscillate spontaneously when driven by asynchronous input (**4.13.6**). (**a**) Spatial pattern of firing rates in afferent fibers (black - asynchronous Poisson input, Poisson input sinusoidally modulated at 40 Hz). (**b**) Spatial pattern of firing rate in interneuron layer. (**c**) Spatial pattern of firing rate in principal cell layer. (**4.13.2-3d-f, 4.13.4-6d-e**) Spike rasters, cell type indicated by label. (**4.13.2-3g, 4.13.4-6f**) Firing rate of principal cell and interneuron populations, line color corresponds to color of populations in diagram.

4.4 Discussion

We have described a novel mechanism by which changes in the dynamical state of neural networks can turn on and off functional connectivity between anatomically connected regions. The mechanism exploits two principles: firstly, in a sparsely synchronized oscillating network, a spatial pattern of firing rates is reproduced as a spatial pattern of firing rate oscillation amplitude. This can be decoded like a conventional population code to recover the value of the encoded stimulus. Crucially, asynchronous networks or networks oscillating in different frequency bands contribute only very weakly to this amplitude pattern. Secondly, the pattern of oscillation amplitude at a given frequency can be read out (converted into a pattern of firing rates) by a feed-forward interneuron layer tuned to act as a band-pass filter. Importantly, and in contrast to an alternative proposal (Fries, 2005), there is no requirement for an external pacemaker to synchronize the sender and receiver networks in the scheme described here. It is sufficient for the sender network to oscillate within the pass-band for information to be selectively routed to the receiver. Of course, gating mechanisms with and without pace-making signals are not mutually exclusive and each may offer distinct advantages in different applications.

Although we have performed most of our simulations with gamma band oscillations, the gating mechanism is not restricted to a particular frequency. The principal determinants of the filter network's frequency selectivity are the resonance frequency of the feed forward interneuron population and the synaptic time-courses of excitatory and inhibitory input received by the principal cells. The former is itself strongly influenced by the time-courses of synapses and intrinsic conductances such as the afterhyperpolarization (AHP). These kinetics are highly heterogeneous across different types of interneurons, suggesting that different microcircuits may support temporal filtering operations over a wide frequency range. Gap junction coupling between interneurons of the same class may promote resonant network dynamics required for filtering (Bennett and Zukin, 2004; Hestrin and Galarreta, 2005). To illustrate filtering in a different frequency band, we implemented a version of the filtering network with synaptic kinetics based on the late spiking interneurons of layer 1 (Chu et al., 2003). Due to the slow time-course of these conductances, the pass band of this filtering network was tuned to a frequency of ~10 Hz (Figure 4.14).

Neuromodulatory inputs are an attractive candidate mechanism for controlling the dynamic state of networks involved in gating. Such inputs must have sufficient spatial and cellular selectivity to change the state of local networks, but do not need to be targeted differentially to individual cells within a population. This is a potential advantage over the detailed balance scheme (Vogels et al., 2009), which requires the control input to apply a pattern of gain modulation at the single neuron level unless each signal pathway has its own associated interneuron population.

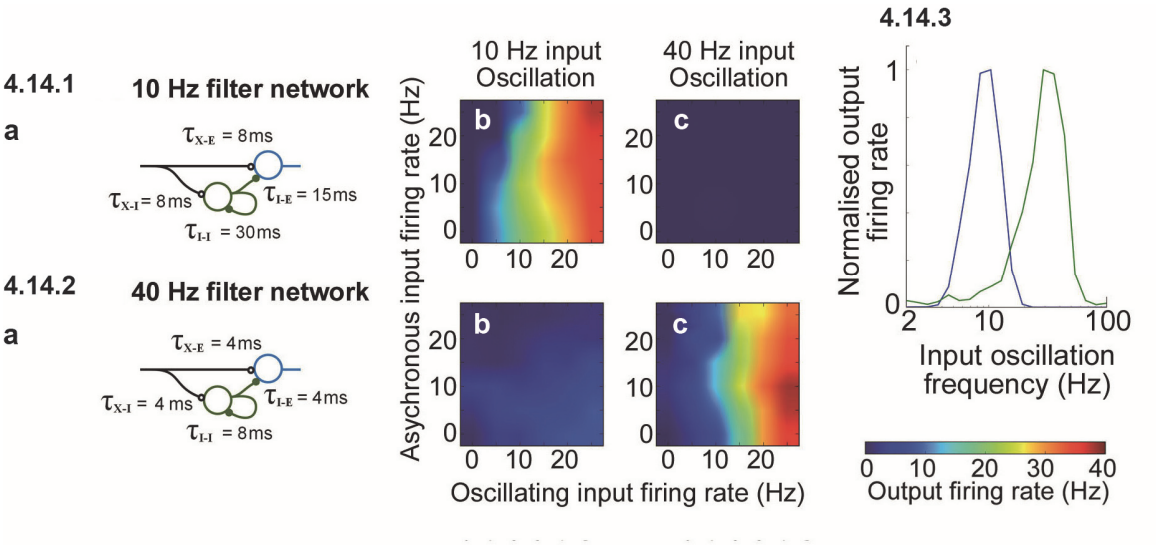

Figure 4.14 **Filtering in different frequency bands.** Filtering networks with pass-bands at different frequencies can be implemented by interneuron populations with different synaptic kinetics. (**4.14.1**) Filter network with passband at 10 Hz. (**4.14.2**) Filter network with passband at 40 Hz. (**a**)Diagram of filter networks showing the alpha function tau values for each synaptic connection. (b**)** Filtering performance when driven by input oscillating at 10 Hz. The filter network was driven by a Poisson input consisting of an asynchronous component and a component sinusoidally modulated at 10 Hz. The firing rate of the filter network principal cells is plotted as a function of the firing rate of the oscillating and asynchronous components of the input. (c**)** Filtering performance when driven by 40 Hz input oscillation. (**4.14.3**) Pass-bands of the two filter networks. The filter networks were driven by a sinusoidally modulated input (Average firing rate 30 Hz, modulation depth 0.5) whose modulation frequency was varied between 2 and 100 Hz (Blue – 10 Hz filter network, green 40 Hz filter network).

Several forms of cross frequency interaction including phase-amplitude coupling (nesting) and phase locking have been reported in network oscillations *in vivo*. Although we have identified one possible coding consequence of nesting (Figure 4.10), a full treatment of this subject is outside the scope of the current work (Palva and Palva, 2007; Roopun et al., 2008; Schroeder and Lakatos, 2009).

Our study builds on previous literature addressing both the flexible routing of neural signals and the possible role of network oscillations in gain modulation. Several authors have described models in which asynchronous signals are routed by interposing dedicated circuitry between sending and receiving regions (Anderson and Essen, 1987; Olshausen et al., 1993; Zylberberg et al., 2010).

Using oscillatory mechanisms to turn on and off direct inter-region connections could alleviate the need for this additional circuitry.

Prior studies have focused on how oscillatory mechanisms could reproduce effects of attention on V4 neuronal responses (Niebur et al., 1993; Zeitler et al., 2008; Mishra et al., 2006). Our focus was not to reproduce a particular experimental result but rather to build a network that performs the specific computational task of signal gating - turning on and off functional connectivity for a given fixed anatomical connectivity. Other studies have explored how the input-output relationship of neuronal networks can be modulated by oscillatory synchronization (Börgers et al., 2005, 2008; Masuda, 2009; Tiesinga et al., 2004). Our model demonstrates significant novel functionality by allowing selective and accurate gating of population-coded signals on the basis of their oscillatory modulation, even in the presence of multiple overlapping distracting inputs.

Although our model generates a very high correlation between true input stimulus values and their estimates decoded from the filter network, there is a reduction in accuracy compared with stimulus representation in the input populations. Due to the data processing inequality (Cover et al., 1991), the output of the filter network could at best contain as much information about the stimulus as the activity of the input network. However, information transmission through the convergent pathway does not come close to this upper bound, and substantial information about the stimulus is lost. A major factor contributing to this is that although distracting inputs are not oscillating, they produce noise in the gamma band due to their stochastic spiking which degrades the signal. Detailed balance (Vogels et al., 2009) also suffers from signal degradation due to the distracting inputs, because although gated-off signals are on average canceled by inhibition, stochastic spiking causes fluctuations which degrade the output. This is why the authors report that the number of active inputs must be limited for accurate signal propagation. In both mechanisms, even with a small number of active distracting inputs, the output signal is degraded compared to the input resulting in reduced accuracy for a given integration time. The data rate per neuron will therefore be reduced in pathways in which multiple distracting inputs are active and flexible signal routing is required.

The output of the filtering network we have described is itself oscillating and hence the signal gating mechanism is not recursive. In other words, the output of the filtering network would need to be desynchronized before it could be used as the input to another convergent pathway employing the same gating mechanism. Possible desynchronization mechanisms include neurons with sub-threshold bursting dynamics to sustain spiking over the phase when they are not receiving strong input, or low pass filtering provided either by slow synaptic conductances such as NMDA receptors or by intrinsic neuronal properties such as dendritic filtering.

A key signature of the described oscillatory gating mechanism is strong, coherent oscillation between sending and receiving regions during communication. Task-dependent increases in strength and inter-region coherence of network oscillations have been reported in numerous brain systems including the visual system during attentional processing (Fries et al., 2001; Siegel et al., 2008; Buschman and Miller, 2007), the hippocampus (Colgin et al., 2009) during memory tasks (Montgomery et al., 2007), between the amygdala and striatum during learning (Popescu et al., 2009), the frontal and parietal cortex during working memory (Dotson et al., 2009) and decision making (Pesaran et al., 2008), and within the motor system during movement tasks (Lee, 2003; Schoffelen et al., 2005). Especially consistent with our model are those studies that have shown strong task-dependent synchronization in a narrow frequency band between distinct brain regions (Popescu et al., 2009; Pesaran et al., 2008). In both these studies the oscillatory activity was limited to a sub-population of cells recorded in the relevant regions, and the oscillations were confined to short bursts. This dispersal of oscillatory activity suggests that without careful analysis the strength of oscillatory events may be underestimated due to spatial and temporal averaging.

Finally, the mechanism described here makes strong predictions for the intracellular currents during signal gating. If a network is gating 'on' a subset of its inputs using the mechanism we describe, the spike rate in principal cells will be strongly correlated with the amplitude of oscillatory fluctuation in its synaptic input. Additionally, spiking activity will be strongly correlated with a phase shift between periodic modulation of excitatory and inhibitory synaptic currents. These experimentally testable predictions are distinct from gating mechanisms such as detailed balance (Vogels et al., 2009) that do not rely on oscillatory synchronization.

Chapter 5: Accurate selective oscillatory communication requires orthogonal modulations.

5.1 Introduction

The 'communication through coherence' (CTC) hypothesis (Fries, 2005, 2009) is an influential proposal for how network oscillations may control the flow of signals between brain regions. CTC proposes that network oscillations impose periodic modulation of the gain of neurons, such that input arriving at some phases of the oscillation elicits more spikes that the same input arriving at another phase. Selective communication between brain regions is proposed to occur by synchronization of oscillations in sending and receiving regions. This selectively enhances the gain for signal flow between the synchronised regions by ensuring that spikes arrive during the phase when the receiving region is most excitable.

In this chapter we ask how accurately the CTC mechanism can in principle separate a target signal from distracting inputs on the basis of their oscillatory modulations. Unlike in the previous chapter, we look at the question purely from a coding perspective and do not consider network dynamics. This is because our aim is to demonstrate that some structures of oscillatory activity work much better than others for multiplexing population codes and hence for achieving selective communication. We argue this is an important and previously unexplored aspect of the coding possibilities provided by oscillations, which may help distinguish oscillatory phenomena that play a causal role in routing signal from those that are a consequence of other mechanisms. To investigate this we need models we can optimize, this means moving away from biophysical models to algorithmic descriptions.

As we discuss in the introduction, the basic operations that underpin selective communication by oscillations are multiplexing and demultiplexing. Where several different inputs to a network are differentiated by their oscillatory modulations, this is a form of multiplexing. Where a receiving region exploits this structure to selectively respond to a target input, this is demultiplexing. Although proponents of the CTC hypothesis do not discuss it in these terms, the proposal defines an operation for demultiplexing a combined spike input to selectively recover a target signal: apply gain modulation coherent with the oscillation of the target signal to neurons receiving a combined input.

In order for the target signal to be accurately recovered by the demultiplexing operation, it is crucial that changes in other components of the signal are ignored and do not affect the output; i.e. that the different components of the signal are as close as possible to orthogonal under the demultiplexing operation. This ensures that crosstalk between components is small. In electronic communication systems this is often achieved by separating components into separate time slots or frequency bands of a communication channel. The analogous schemes for network oscillations are respectively phase coding and separating oscillations into different frequency bands. As we will see later in this chapter, both these arrangement are efficient ways of multiplexing population codes.

An alternative arrangement described as 'non-communication through non-coherence' was proposed in the original CTC paper. Instead of separating signals in frequency or phase, multiple networks could oscillate incoherently in the same broad frequency band. In this arrangement, random variability in the phase relationship between networks prevents communication between them. The expected electrophysiological signatures of such an arrangement are clearly different from frequency division or phase coding. Specifically, incoherent oscillations in the same frequency band in anatomically connected regions are consistent with this scheme but not with frequency or phase coding. Additionally, changes in inter-region coherence alone without any change in frequency, amplitude or relative phase are a causal mechanism for changing signal flow under this mechanism only. These more relaxed constraints on the experimental evidence needed to argue for oscillatory signal routing have contributed to the widespread embrace of this hypothesis by experimentalists.

However, this arrangement does not satisfy the requirement that different components of a combined signal must be orthogonal to minimize crosstalk. As we show in this chapter this leads to a severe reduction in signal propagation accuracy compared with arrangements where signals are distinguished by frequency, amplitude or phase of oscillation. This makes unlikely the proposal that incoherent oscillations are widely used to decouple anatomically connected networks.

We also explore how the strength of oscillatory modulation affects the accuracy with which the CTC mechanism can selectively recover a target signal. As in the previous chapter we find that the oscillation of the target signal must be strong to achieve a high signal to noise ratio against stochastic spiking. Although this is unsurprising it has received little previous attention in the literature and we feel it is important in the context of the absence of evidence for strong oscillations in several systems where they have been proposed to play functional roles.

To investigate these questions we return to the convergent pathway paradigm used in the last chapter. To facilitate construction of different structures of oscillatory activity across different

inputs we replaced the biophysical models of input networks with statistical models of the spiking activity. We then developed an algorithmic model of the filtering performed by the receiving network which could be optimized to minimize the error of stimulus estimates decoded from the networks output. Using this optimized filtering we explored the signal propagation accuracy that could be achieved for different structures of oscillatory activity across the input networks.

5.2 Materials and Methods

As in the previous chapter the description of the model is shared between the current section, which provides equations and parameters, and the results section, where diagrams and description are provided to facilitate interpreting the results in the context of the models that generated them.

5.2 .1 Mathematical description of model

N input networks representing independent orientation variables θ^n (range 0-180˚), converged to a single output network. Each input network was represented as a population of 10,000 Poisson neurons with bell-shaped firing rate tuning curves $R_i(\theta - \theta_i) = R_0 \frac{2}{3}(1 + \cos(2(\theta - \theta_i)))^2$, where R_i is the firing rate of the ith neuron, θ_i is the neurons preferred orientation and R_0 is the average firing rate across the population. Except where stated otherwise the average firing rate per neuron was 5 Hz. Oscillations in the input networks were represented by periodic firing rate modulation $m^n(t)$. The modulation was a Von Mises function of the oscillation phase $\Phi^n(t)$ such that $m(\Phi^n(t)) = \frac{e^{k\cos(\Phi)}}{I_0(k)}$ where k is a concentration parameter that determines how tightly synchronized the activity is, and $I_0(k)$ is the modified Bessel function of order 0, which normalizes the modulation such that its average value over time is 1. Where we report synchronization strength, we use the following measure:

$$Synchronisation\ strength = 1 - circular\ variance\ \big(m(\Phi)\big) = \frac{I_1(k)}{I_0(k)}$$

Where $I_n(k)$ is the modified Bessel function of order n. This measure is 1 if all spikes occur at the same phase and 0 if the firing rate is equal at all phases (Figure 5.2b). Synchronization strength was 0.5 except where reported otherwise. To investigate the effect of separating inputs in frequency in Figure 5.5 we used a modulation that was a sinusoidal function of phase $m(\Phi) = 1 + \sin(\Phi)$. To model the irregularity of network oscillations we allowed the oscillation angular frequency $\omega(t)$ and concentration parameter $k(t)$ to fluctuate around their mean values ω_0 and k_0. These fluctuation were modeled as $(t) = \omega_0(1 + Z\varepsilon(t))$, $k(t) = k_0(1 + V\eta(t))$, where $\varepsilon(t)$, $\eta(t)$ were

low-pass filtered Gaussian white noise with amplitude 1 and a cut-off frequency of $\frac{\omega_0}{2}$. The variability of the frequency and amplitude respectively were therefore determined by Z and V, which were the standard deviation of fluctuations divided by the mean value of the frequency ω_0 or amplitude k_0. The amplitude variability parameter V was set to 0.1 for all simulations. The frequency variability parameter was set to 0.1 for narrowband oscillations (Figures 5.2, 5.5, 5.6, 5.7) and 0.3 for broadband oscillations (Figures 5.3, 5.4, 5.5, and incoherent distractors condition in Figures 5.7 and 5.8).

The spatiotemporal pattern of firing rates in one input network was:

$$R_i^n(\theta^n, t) = R_i(\theta^n - \theta_i)m^n(t)$$

The combined input spike rates I to the receiving network are a sum of activity in all input networks:

$$I_i(t) = \sum_n R_i(\theta^n - \theta_i)m^n(t)$$

The combined spike input S is:

$$s_i(t) \sim Poisson(I_i(t))$$

The receiving network consisted of a layer of 8 units, each of which received spike input from neurons with similar orientation preference in each input network. We divided the range of orientation preference from 0˚ to 180˚ into 8 bands of equal width, and neurons in each input network with orientation preference in a given band projected to the same unit in the receiving network. The receiving network separated target from distracting input by applying a multiplicative gain modulation $g(t)$ to the combined input, coherent with the firing rate modulation of the target. We describe below how the gain modulation was optimized to best filter the target from distracting inputs. The output $O_j(\mathrm{t})$ of unit j in the receiving network was:

$$O_j(t) = g(t)s_j(t)$$

where $S_j(t)$ was the combined spike input received by the unit. $O_j(\mathrm{t})$ was integrated over time T to produce a spatial pattern of activity P:

$$P_j(t) = \int_{t-T}^{t} O_j(t')dt'$$

An estimate $\hat{\theta}$ of the stimulus encoded in the target input network was decoded from the integrated activity using a locally optimal linear estimator (LOLE).

$$\hat{\theta}(t) = \sum_j w_j P_j\,(t) + b$$

where w_j are the weights for each unit of the receiving network and b is a constant.

$$\hat{\theta}(t) = \sum_j w_j \int_{t-T}^{t} g(t')s_j(t')\mathrm{d}t' + b$$

The simulations were performed in discrete time with a resolution of 1 ms, such that the integral over time was computed as a sum over time bins:

$$\hat{\theta} = \sum_j w_j \sum_t g_t\, s_{tj} + b$$

where S_{tj} is the spike count received by unit j in time bin t.

5.2.2 Optimizing the receiving network

For Figures 5.2-5.6, the gain modulation $g(t)$ was a linearly filtered version of the modulation of the target input $m(t)$. For this model we optimized the receiving network by using gradient descent to find the frequency response of the filter (the gain and phase shift as a function of frequency) which optimized decoding accuracy with respect to the variance of the stimulus estimates.

We used Plancherel's theorem to express $\hat{\theta}$ in terms of the discrete Fourier transforms G_k and S_k of the gain modulation g_t and spike input s_t (S^* indicates the complex conjugate).

$$\hat{\theta} = \sum_j w_j \sum_{t=0}^{N-1} g_t\, s_{tj} + b = \frac{1}{N}\sum_j w_j \sum_{k=0}^{N-1} G_k S_{kj}^* + b$$

As the gain modulation and spike input are both real valued, the imaginary parts of $\sum_{k=0}^{N-1} G_k S_{kj}^*$ at positive and negative frequencies cancel and only the real parts contribute to the sum.

$$\hat{\theta} = \frac{1}{N}\sum_j w_j \sum_{k=0}^{N-1} real\left(G_k S_{kj}^*\right) + b$$

Also, $real\left(G_k S_{kj}^*\right) = real\left(G_{(N-k)} S_{(N-k)j}^*\right)$ so the second half of the sum is redundant:

$$\hat{\theta} = \frac{1}{N}\sum_j w_j \sum_{k=0}^{N/2} c_k real\left(G_k S_{kj}^*\right) + b$$

where $c_k = 1$ for $\mathrm{k} = 0, \mathrm{N}/2$, $c_k = 2$ for $\mathrm{k} \neq 0, \mathrm{N}/2$.

We expressed the Fourier transform of the gain modulation G_k as the product of the frequency response of the filter F_k and the Fourier transform M_k of the of the target inputs firing rate modulation. The frequency response is a complex valued function of frequency where $\mathrm{abs}(f_k)$ is the gain of the filter at frequency k and $\arg(f_k)$ is the phase shift.

$$G_k = M_k F_k$$

We can then express the stimulus estimate as:

$$\hat{\theta} = \frac{1}{N}\sum_j w_j \sum_{k=0}^{N/2} c_k real\left(M_k F_k S_{kj}^*\right) + b$$

$$\hat{\theta} = \frac{1}{N}\sum_j w_j \sum_{k=0}^{N/2} c_k \, abs\left(M_k S_{kj}^*\right) \; (real(F_k)\cos(\arg(M_k S_{kj}^*)) - imag(F_k)\sin(\arg(M_k S_{kj}^*))) + b$$

We define $Q_{kj}^{real} = c_k \, abs\left(M_k S_{kj}^*\right)\cos(\arg(M_k S_{kj}^*))$

$Q_{kj}^{imag} = -c_k \, abs\left(M_k S_{kj}^*\right)\sin(\arg(M_k S_{kj}^*))$

$$\hat{\theta} = \frac{1}{N}\sum_j w_j \sum_{k=0}^{N/2} Q_{kj}^{real} \, real(f_k) + Q_{kj}^{imag} imag(f_k) + b$$

This can be written in vector notation as:

$$\hat{\theta} = \boldsymbol{w}\,\boldsymbol{Q}^{\boldsymbol{real}}\boldsymbol{f}_{\boldsymbol{real}} + \boldsymbol{w}\boldsymbol{Q}^{\boldsymbol{imag}}\boldsymbol{f}_{\boldsymbol{imag}} + b$$

Where $\boldsymbol{w}$ is a row vector whose components are the weights of the LOLE, $\boldsymbol{Q}^{\boldsymbol{real}}$ and $\boldsymbol{Q}^{\boldsymbol{imag}}$ are matrices whose components are Q_{kj}^{real} and Q_{kj}^{imag}, and $\boldsymbol{f}_{\boldsymbol{real}}$ and $\boldsymbol{f}_{\boldsymbol{imag}}$ are column vectors whose components are respectively the real and imaginary parts of the filter frequency response $real(f_k)$ and $imag(f_k)$. To further simplify the expression we concatenate the vectors $\boldsymbol{f}_{\boldsymbol{real}}$ and $\boldsymbol{f}_{\boldsymbol{imag}}$ to make a single vector $\boldsymbol{f}$ containing both the real and imaginary parts of the filter frequency response and concatenate the matrices $\boldsymbol{Q}^{\boldsymbol{real}}$ and $\boldsymbol{Q}^{\boldsymbol{imag}}$ to make a single matrix $\boldsymbol{Q}$. We can now express the decoded stimulus estimate as:

$$\hat{\theta} = \boldsymbol{w}\,\boldsymbol{Q}\boldsymbol{f} + b$$

To use gradient descent to find the optimal LOLE weights and filter frequency response we define a cost function and calculate the gradient with respect to it. We define the cost function as the squared error between the true stimulus value and the decoded estimate, averaged over a training set of data:

$$E = \frac{1}{N}\sum_i (\hat{\theta}_i - \theta_i)^2 = \frac{1}{N}\sum_i (\boldsymbol{w}\boldsymbol{Q}_{\boldsymbol{i}}\boldsymbol{f} + b - \theta_i)^2$$

$$\frac{dE}{db} = \frac{2}{N}\sum_i (\boldsymbol{w}\boldsymbol{Q}_{\boldsymbol{i}}\boldsymbol{f} + b - \theta_i) = 0$$

$$b = <\theta>_{tr} - <\boldsymbol{w}\boldsymbol{Q}\boldsymbol{f}>_{tr}$$

Where $<>_{tr}$ indicates the average over the training set.

$$E = \frac{1}{N}\sum_i (\boldsymbol{w}(\boldsymbol{Q_i} - < \boldsymbol{Q} >_{tr})\boldsymbol{f} - (\theta_i - < \theta >_{tr}))^2$$

$$\frac{dE}{d\boldsymbol{W}} = \frac{2}{N}\sum_i (\boldsymbol{w}(\boldsymbol{Q_i} - < \boldsymbol{Q} >_{tr})\boldsymbol{f} - (\theta_i - < \theta >_{tr})\,(\boldsymbol{Q_i} - < \boldsymbol{Q} >_{tr})\boldsymbol{f}$$

$$\frac{dE}{d\boldsymbol{f}} = \frac{2}{N}\sum_i (\boldsymbol{w}(\boldsymbol{Q_i} - < \boldsymbol{Q} >_{tr})\boldsymbol{f} - (\theta_i - < \theta >_{tr})\,\boldsymbol{w}(\boldsymbol{Q_i} - < \boldsymbol{Q} >_{tr})$$

5.2.3 Simulations and analysis

The following procedure was performed to evaluate the decoding accuracy for each set of input parameters. All simulations were performed in MATLAB. A training set and a test set of input activity were generated, each consisting of 5000 samples of 100 ms each. In each set, half of the samples had target stimulus orientation θ_1 and the other half θ_2. The separation $\delta\theta = \theta_1 - \theta_2$ was chosen iteratively such that 75-80% of samples were correctly classified from the decoded stimulus estimates. The orientation of stimuli encoded by the distracting input networks were uniformly randomly distributed. To reduce spectral leakage due to finite integration times, we applied a Hanning window to the spike activity in each sample. The weight vectors for the LOLE and the frequency response of the filter were optimized using a two-stage gradient descent procedure. Firstly we used gradient descent to find the filter frequency response $\boldsymbol{f}$ that minimized the mean squared error between the output of the units comprising the receiving network and the firing rate each unit received from neurons in the target input network. This gradient descent stage was initialized with all components of the filter frequency response set to zero. We then performed gradient descent simultaneously on the LOLE weights $\boldsymbol{w}$ and the filter frequency response $\boldsymbol{f}$ to minimize the mean squared error of target stimulus estimates, using the gradients calculated above. This second stage of the gradient descent was initialized with the filter frequency response found in the first gradient descent and with the weights of the LOLE set to zero. We used this two-stage procedure because it converged much more rapidly than initializing the simultaneous gradient descent for $\boldsymbol{w}$ & $\boldsymbol{f}$ with random weights. To prevent over-fitting we evaluated the mean squared error for the test set and halted gradient descent when this started to rise. We evaluated the mean and variance of the stimulus estimates for both orientations on the test set:

$$\left\{\langle\hat{\theta}_i\rangle, \sigma_i^2\right\}_{i=1,2}$$

The lower bound on the Fisher information was given by:

$$I = \frac{\left(\left(\langle\hat{o}_1\rangle - \langle\hat{o}_2\rangle\right)/\delta o\right)^2}{\frac{1}{2}(\sigma_1^2 + \sigma_2^2)}$$

An alternative approach to evaluating $\boldsymbol{w}$ and $\boldsymbol{f}$ would have been to try and solve the equations $\frac{dE}{d\boldsymbol{W}} = 0$ and $\frac{dE}{d\boldsymbol{f}} = 0$ directly for the training set of data. However, in previous work utilizing LOLEs, gradient decent was employed to find the weights even though solving for them analytically would have been trivial (Seriès et al., 2004; Beck et al., 2008). Our understanding is that this is because using gradient decent offers a principled way of avoiding over-fitting to the training set, by monitoring the estimator error over the test set (J. Beck, personal communication).

For Figure 5.7 we allowed the gain modulation to be an arbitrary function of the modulation of the target input. To do this we generated training and test sets as described above, but instead of generating a different modulation of the target input network for each sample, we used the same modulation of the target input network while generating different modulations for the distractors. Instead of optimizing the filter parameters $\boldsymbol{f}$ that transformed the modulation of the target input into the gain modulation, we directly fitted the gain modulation g_t using gradient descent. To do the gradient descent we rewrite the equation for the stimulus estimate in vector form:

$$\hat{\theta} = \sum_j w_j \sum_t g_t \, s_{tj} + b \;\; = \boldsymbol{w}\boldsymbol{S}\boldsymbol{g} + b$$

Where $\boldsymbol{w}$ is a row vector with components w_j, $\boldsymbol{S}$ is a matrix with components s_{tj} and $\boldsymbol{g}$ is a column vector with components g_t. As this has identical form as $\hat{\theta} = \boldsymbol{w}\boldsymbol{Q}\boldsymbol{f} + b$, we can use the gradient descent procedure described above to find the gain modulation $\boldsymbol{g}$ that minimizes the mean squared error of target stimulus estimates. Decoding accuracy varies somewhat depending on the precise waveform of the modulation of the target, so we repeated the procedure 100 times using different instances of the gain modulations of the target input and report the mean and standard deviation of the decoding accuracy over these different modulations.

5.3 Results

5.3.1 Model

We considered a model consisting of a behaviourally relevant 'target' input network converging together with several distracting input networks onto a single receiving network (Figure 5.1). To selectively gate 'on' one input, the gain of units in the receiving network was modulated coherently

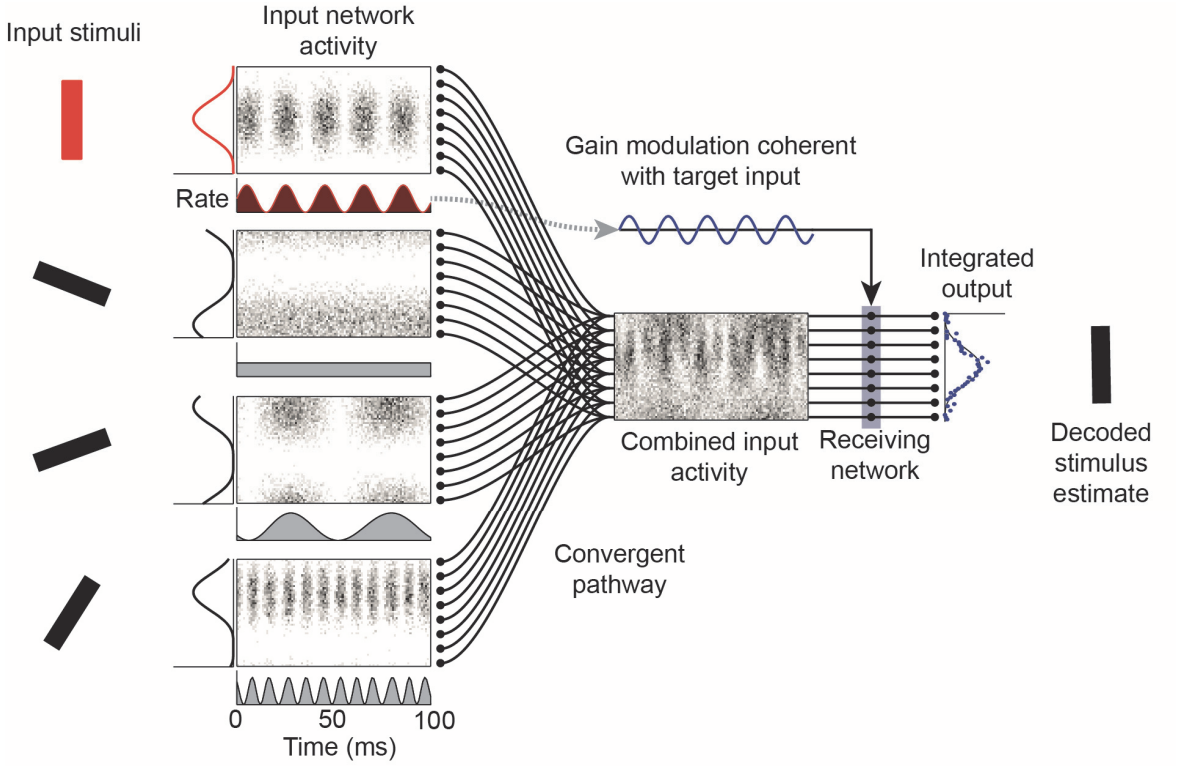

Figure 5.1 **Model diagram.** Independent orientation stimuli are represented in separate input networks as population codes with bell shaped firing rate tuning curves. Input networks converge to provide a combined input to the receiving network, which applies gain modulation coherent with the firing rate modulation of the target input. The output of the receiving network is integrated over time to produce a spatial pattern of activity which is decoded to produce an estimate of the target stimulus.

with the firing rate oscillation of the target input. The output of this layer was integrated over time and decoded to produce an estimate of the stimulus encoded in the target network.

5.3.2 Input networks

Each input network modeled a cortical hypercolumn of 10,000 neurons, which represented an orientation variable using a population code. The average firing rates of individual neurons were given by bell-shaped tuning curves with respect to the stimulus orientation. Spike generation was a Poisson process whose rate could be modulated to simulate a network oscillation. This modulation was modelled as a Von Mises function of the phase of the oscillation, characterized by a modulation strength and frequency. As network oscillations *in vivo* are irregular in frequency and amplitude, we allowed the instantaneous strength and frequency to fluctuate around their mean values. These

fluctuations were modelled as low-pass filtered Gaussian white noise. The resulting activity was consistent with *in vivo* data showing irregular spiking of single units during sparsely synchronized oscillatory activity.

5.3.3 Receiving network

We required a model of the receiving network that could be optimized to generate the temporal pattern of gain modulation that best separated target from distracting inputs. If the receiving network was not optimized, the results would be uninformative about the performance of the CTC scheme in general and would only shed light on its specific implementation. Optimizing a biophysical model of the network was intractable, so instead we developed an algorithmic description that could be optimized with respect to the variance of target stimulus estimates decoded from the network output.

The receiving network consisted of a layer of units whose input gain was modulated as a function of time. Each unit represented a population of cells innervated by neurons with similar orientation preferences in each input network and whose output was an analogue firing rate signal. We allowed the gain to take both positive and negative values (corresponding to net excitatory and inhibitory output respectively) such that spikes arriving during periods of negative gain contribute negatively to the integrated output of the network. Physiologically, gain modulation could be generated by a local interneuron circuitry modulating the distribution of membrane potentials, degree of shunting inhibition (Mitchell and Silver, 2003) or level of synaptic noise (Chance et al., 2002) received by the projection neurons of the unit. We have previously demonstrated a biophysical network model with an average gain of zero for asynchronous input and a strong response to input oscillating at a specific frequency.

Coherence between networks *in vivo* could occur through entrainment to an external pace-making signal or through their direct interaction. We do not explicitly consider the mechanisms underlying coherence between the target input and receiving networks, but instead model the entrainment and subsequent gain modulation as a filtering process, such that the gain is a filtered version of the firing rate modulation of the target input. Optimizing the gating mechanism then becomes a problem of finding the filter that transforms the firing rate modulation of the target into the gain modulation that best separates the target from distracting inputs. This problem is closely analogous to that of matched filtering in the engineering literature in which a target signal of known waveform must be detected against a background of noise.

We initially considered gain modulations that were linearly filtered versions of the firing rate modulation of the target input. We could rapidly optimize this model to training data, allowing us

to explore the parameter space of input activity patterns. We then verified that our key results obtained for this linear model held when we allowed the gain to be an arbitrary function of the modulation of the target input.

5.3.4 Decoding and Optimization

The output of the receiving network was integrated over 100 ms to give a spatial pattern of activity. This was then decoded to produce an estimate of the target stimulus. We report the lower bound on the Fisher information given by the reciprocal of the mean squared error of the stimulus estimates. Locally optimal linear estimators (LOLEs) were used for decoding. The principle reason for using linear decoders was that they were sufficiently simple that we could work out a way of optimizing the temporal filtering with respect to the mean squared error of decoded stimulus estimates (see Materials and Methods). For stimuli encoded by bell shaped tuning curves, a given linear estimator will only perform well over a narrow range of stimulus angles, and hence we were forced to use a discrimination task in which only two similar angles were presented, rather than an estimation task in which any angle could be presented. We could alternatively have used a simple non-local estimator such as population vector or template matching, which would have permitted an estimation task. However, our understanding is that these methods perform less well than LOLEs where noise is non-independent. Maximum likelihood decoding would have been preferable but we did not see any way to optimise the temporal filtering using this decoding approach.

Under many noise distributions LOLEs perform close to optimally, as indicated by the minimal difference in performance when compared with more sophisticated non-linear methods (Seriès et al., 2004; Beck et al., 2008). These decoders are, moreover, biologically plausible as their performance corresponds to that of denoising by networks implementing line attractor dynamics (Deneve et al., 1999; Latham et al., 2003).

5.3.5 Asynchronous distractors

We first considered the task of separating an oscillating target input from distracting inputs whose firing rates were not modulated (‘asynchronous’ distractors). The gain modulation that optimally recovered the target signal was near-sinusoidal, in phase with the oscillation in the target input (Figure 5.2a). The oscillating target input contributed strongly to the integrated output because periods of high firing rate occurred concurrently with large positive gain, while firing rates were low during periods of negative gain. Because the average gain was zero, asynchronous distractors only contributed to the integrated output as a result of stochastic fluctuations in their spiking activity.

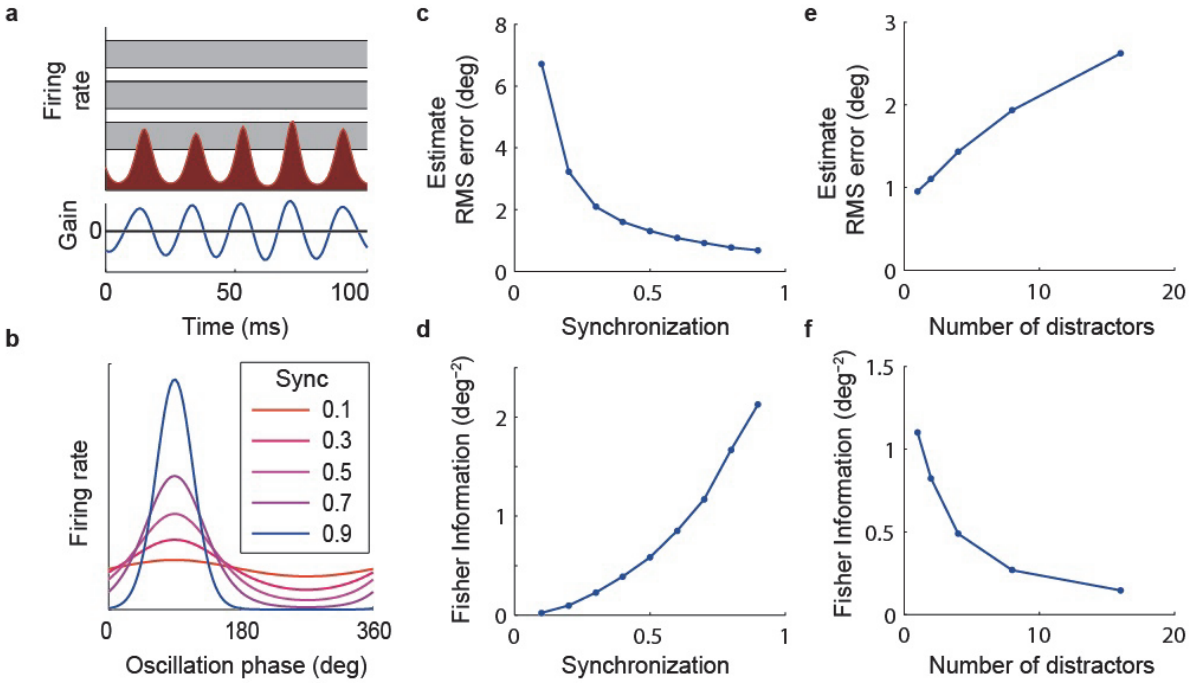

Figure 5.2 **Asynchronous distractors: effects of oscillation strength and number of distractors. a**) Top: Example firing rate modulation of the target (red) and distracting inputs (gray) over the 100 ms integration time. Bottom: Gain modulation (blue) produced by the optimized receiving network. **b**) Firing rate as a function of oscillation phase for synchronization strengths from 0.1-0.9. **c**) Estimate root mean squared error and (**d**) Fisher information as a function of the synchronization strength of the target input for stimulus estimates decoded from receiving network output integrated over 100ms. (**e**,**f**) Effect of number of distracting inputs on decoding accuracy.

Decoding accuracy was strongly dependent on the strength of oscillatory modulation of the target input (Figure 5.2c,d). Accuracy was high for strongly modulated input, dropping steeply as the oscillation strength decreased. We quantified the synchronization strength using a measure that ranged between 0 (for asynchronous activity) and 1 (if all spikes occur at the same phase – see Materials and Methods, Figure 5.2b). Over the range of modulation strengths from 0.1 to 0.9, Fisher information increased by a factor of 95.7, with the majority of this increase occurring in the range from weak to moderate synchronization (Fisher information increased 26-fold when synchronization strength increased from 0.1 to 0.5, and 3.65-fold as it increased from 0.5 to 0.9). Weak modulation resulted in poor decoding accuracy because the signal read out by the receiving network was small relative to noise from stochastic spiking. Increasing the number of active

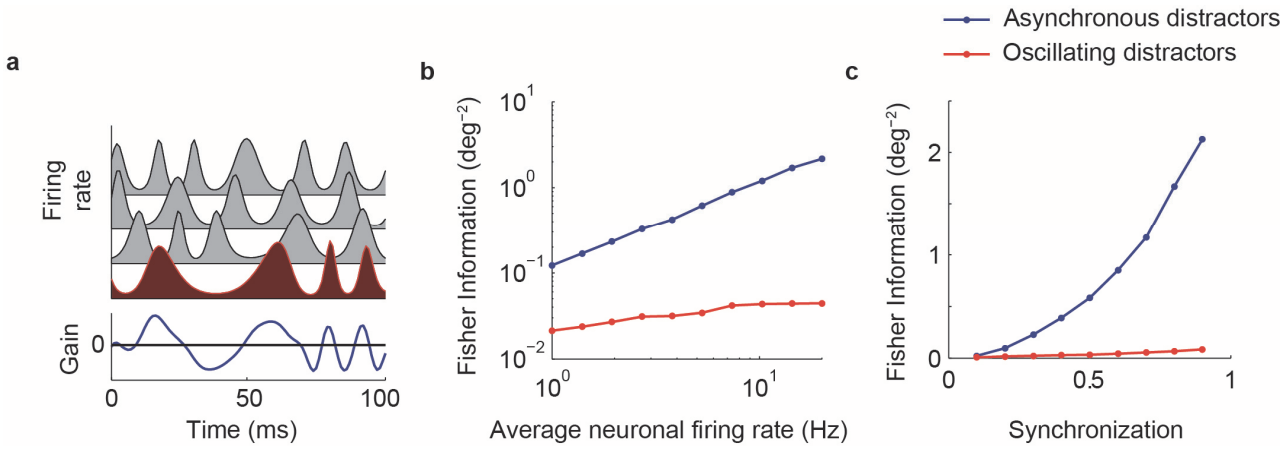

Figure 5.3 **Distractors oscillating incoherently in the same frequency band severely degrade stimulus estimate.** Distractors oscillating incoherently in the same frequency band as the target input. **a**) Example input firing rate modulations and receiving network gain modulation. **b**,**c**) Comparison of Fisher information for asynchronous and incoherently oscillating distracting inputs as function of firing rate (**b**) and synchronization strength (**c**) of input networks.

asynchronous inputs decreased the accuracy of stimulus estimates (Figure 5.2e,f) because fluctuations in the spiking activity of each distracting input contributed noise to the output of the receiving network.

5.3.6 'Non-communication through non-coherence?

We next evaluated the proposal that changes in the inter-region coherence of oscillatory activity (as distinct from changes in frequency or amplitude, or changes in a consistent phase relationship) play a causal role in modulating functional connectivity (Fries, 2005; Schoffelen et al., 2005; Womelsdorf et al., 2007). Under this 'non-communication through non-coherence (Fries, 2005)' scheme the absence of a reliable phase relationship between sending and receiving regions prevents information transmission. In our convergent pathway paradigm it corresponds to target and distracting inputs oscillating with irregular broad-band oscillations in the same frequency band. How effectively can input gain modulation distinguish the target signal from distractors in this condition?

It is possible to generate a pattern of gain modulation which is strongly driven by the target input but has an average gain of zero for incoherent distracting inputs. Just as for asynchronous

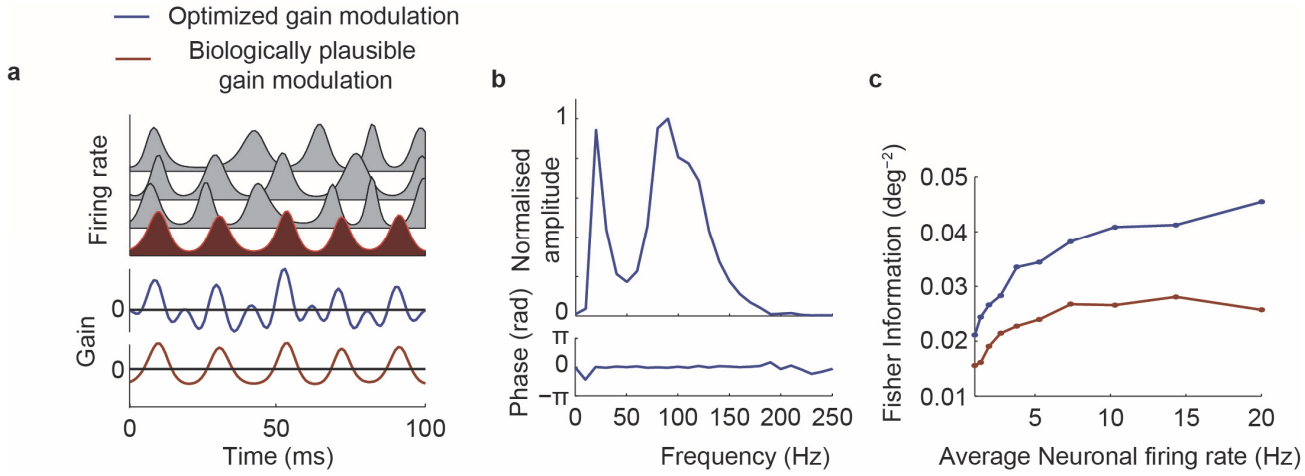

Figure 5.4 **Comparison of optimized and biologically plausible gain modulations.** **a**) Example input firing rate modulations and gain modulations. Blue trace is the gain modulation generated by the optimized receiving network, brown trace is a gain modulation that oscillates around zero with the same waveform as the firing rate modulation of the target. **b**) Frequency response of the filter that transforms the firing rate modulation of the target input into the optimized gain modulation. **c**) Comparison of Fisher information for receiving networks using optimized and alternative gain modulations.

distractors, this can be achieved by a gain modulation which oscillates around zero, in phase with the target input. Given sufficient integration time the target stimulus can be decoded with arbitrary accuracy from the integrated output. However, the gain for distracting inputs is highly variable from cycle to cycle as they drift in and out of phase with the target. This source of noise is quite distinct from that due to stochastic spiking of individual neurons. We refer to it as 'overlap' noise as it occurs because of random variability in the overlap between firing rate and gain modulations. This additional variability will increase the integration time required to reach a given decoding accuracy when compared with asynchronous distracting inputs. How severely does this additional noise degrade the signal?

Fisher information was greatly reduced when distracting inputs oscillated incoherently compared with the situation where distracting inputs were asynchronous (Figure 5.3b,c). The precise ratio of Fisher information between the two conditions depended on the population firing rate of the input networks.

When distractors were asynchronous, information increased linearly with the firing rate of the input networks. However, with incoherently oscillating distractors, information increased sublinearly with firing rate (Figure 5.3b). For average firing rates of 1 Hz per neuron, the Fisher information was 5.7 times higher when distractors fired asynchronously than when they oscillated incoherently, and this ratio increased to 27.8 when the average firing rate was 10 Hz. This dependence on firing rate can be understood by considering the two sources of noise that degrade the stimulus estimate. Noise due to stochastic spiking of individual neurons occurs for both asynchronous and oscillating distractors, and becomes smaller relative to the signal as the firing rates of the input networks increase. Overlap noise, on the other hand, occurs only for oscillating distractors and increases in proportion to the signal size with increasing input firing rates. With incoherently oscillating distractors, this second source of noise becomes dominant as the mean firing rate increases and causes the signal to noise ratio to saturate.

At very low population firing rates, noise in the output of the receiving network was dominated by stochastic spiking of individual neurons. In this regime decoding accuracy was comparable for asynchronous and incoherently oscillating distractors. In section 5.3.8 we evaluate the firing rate threshold above which overlap noise dominates. Above this threshold 'non-communication through non-coherence' results in severe signal degradation compared with schemes in which distracting inputs are asynchronous or separated from the target in frequency or phase (see below). This threshold is proportional to the oscillation frequency but for physiological frequencies it is low relative to firing rates relevant for coding in cortex.

Increasing the synchronization of oscillations in the input networks improved decoding accuracy (Figure 5.3c), but across all oscillation strengths accuracy was much higher when distractors were asynchronous.

Gain modulations generated by the receiving network were often a very different shape from the firing rate modulation of the target (Figures 5.3a, 5.4a, 5.7b). This was because the optimized filter that transformed the firing rate modulation of the target input into the gain modulation strongly emphasized the high and low frequency components of the target modulation (Figure 5.4b). Such gain modulation is arguably biologically implausible so we also evaluated the performance of a receiving network that applied a gain modulation that oscillated around 0 with the same waveform as the firing rate modulation of the target input (Figure 5.4a). This considerably reduced decoding accuracy, resulting in ~40 % lower Fisher information than the optimized receiving network (Figure 5.4c).

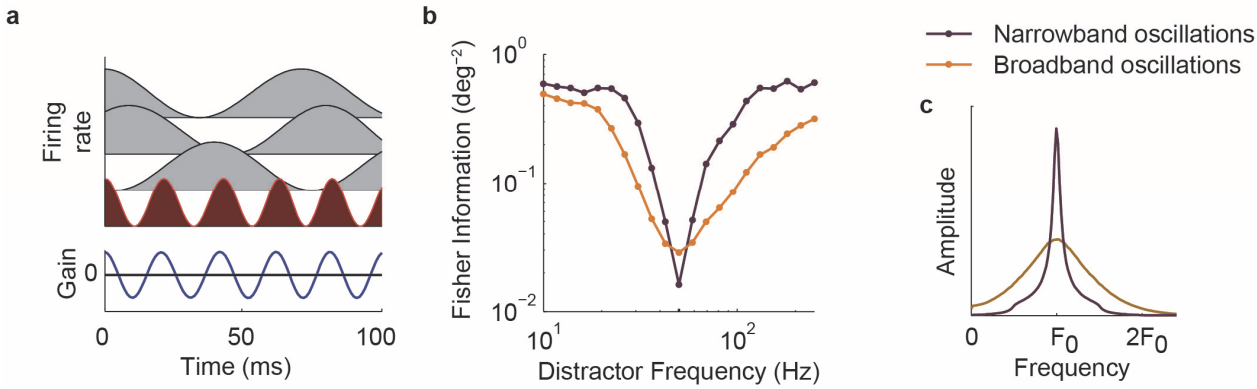

Figure 5.5 **Separation of target from distracting inputs in frequency.** **a**) Example input firing rate modulations and gain modulation. **b**) Fisher information as function of oscillation frequency of distractor networks for narrow (purple) and broadband (orange) oscillations. **c**) Amplitude spectrum of oscillatory modulations for narrow and broadband oscillations (F_0 is oscillation centre frequency).

5.3.7 Frequency separation

We tested whether separating distracting inputs from the target in frequency improved performance (Figure 5.5). For these simulations we used sinusoidal firing rate modulation as a function of oscillation phase rather than the Von Mises modulation used in the rest of this study, in order to avoid harmonics that broaden the frequency band occupied by the modulation. As in other simulations the oscillation frequency fluctuated, allowing us to compare the effects of frequency separation for narrow- and wide-band oscillations.

Decoding accuracy increased as the modulation frequency of the distracting inputs was moved to either higher or lower frequencies than that of the target input (Figure 5.5b). When distracting inputs were sufficiently separated in frequency from the target, decoding accuracy was comparable to that for asynchronous distracting inputs. Highly irregular oscillations occupied a wider frequency band (Figure 5.5c) and hence the target and distractor inputs had to be more broadly separated in frequency to avoid interference (Figure 5.5b).

Separation in frequency works because sinusoids of different frequency are orthogonal under the overlap integral operation that separates target from distracting inputs. Distracting inputs that are well separated from the target in frequency therefore only contribute noise due to stochastic spiking and not due to fluctuations in the overlap of their firing rate modulation with the gain modulation.

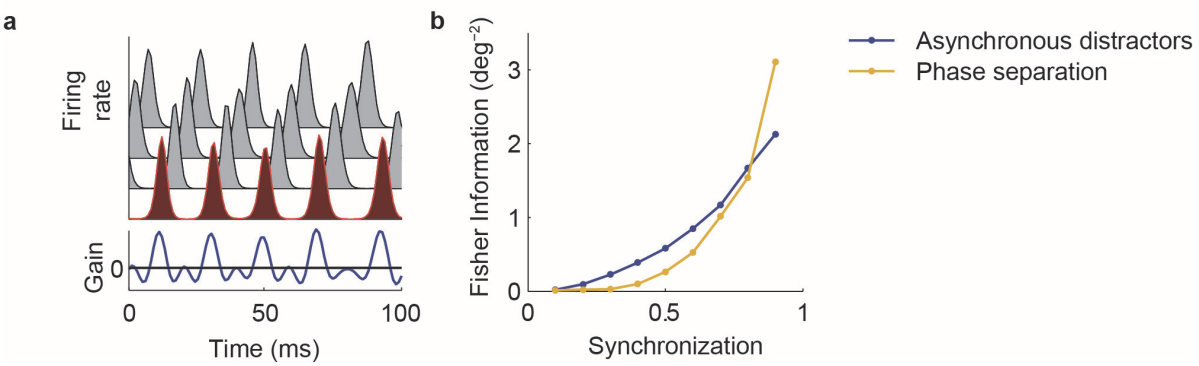

Figure 5.6 **Phase coding.** Example input firing rate modulations and gain modulation. Comparison of Fisher information as function of synchronization strength for asynchronous distractors (blue) and distractors coherent with target input but equally spaced in phase (yellow).

5.3.8 Phase coding

Phase coding, in which assemblies of neurons fire at different phases relative to a global oscillation, has been reported in several neural systems (O'Keefe and Recce, 1993; Friedrich et al., 2004), most notably in the hippocampus where place cells representing past, present and future locations fire at progressively later phases with respect to the theta oscillation.

We evaluated how accurately gain modulation could separate a target input from distractors oscillating coherently with it, evenly separated in phase (Figure 5.6a). For strongly synchronized activity, decoding was very accurate, with better performance than for asynchronous distractors. This was because the absolute value of the gain modulation was small except at the phase where the target but not distracting inputs were firing strongly. This reduced noise due to stochastic spiking of distracting inputs.

Performance dropped rapidly as modulation strength was decreased, such that for weakly and moderately synchronized inputs decoding accuracy was worse than for asynchronous distractors (Figure 5.6b). Unsurprisingly, increasing the separation in phase between the peak firing of target and distractors reduced how tightly synchronized they needed to be to reach a given decoding accuracy (data not shown).

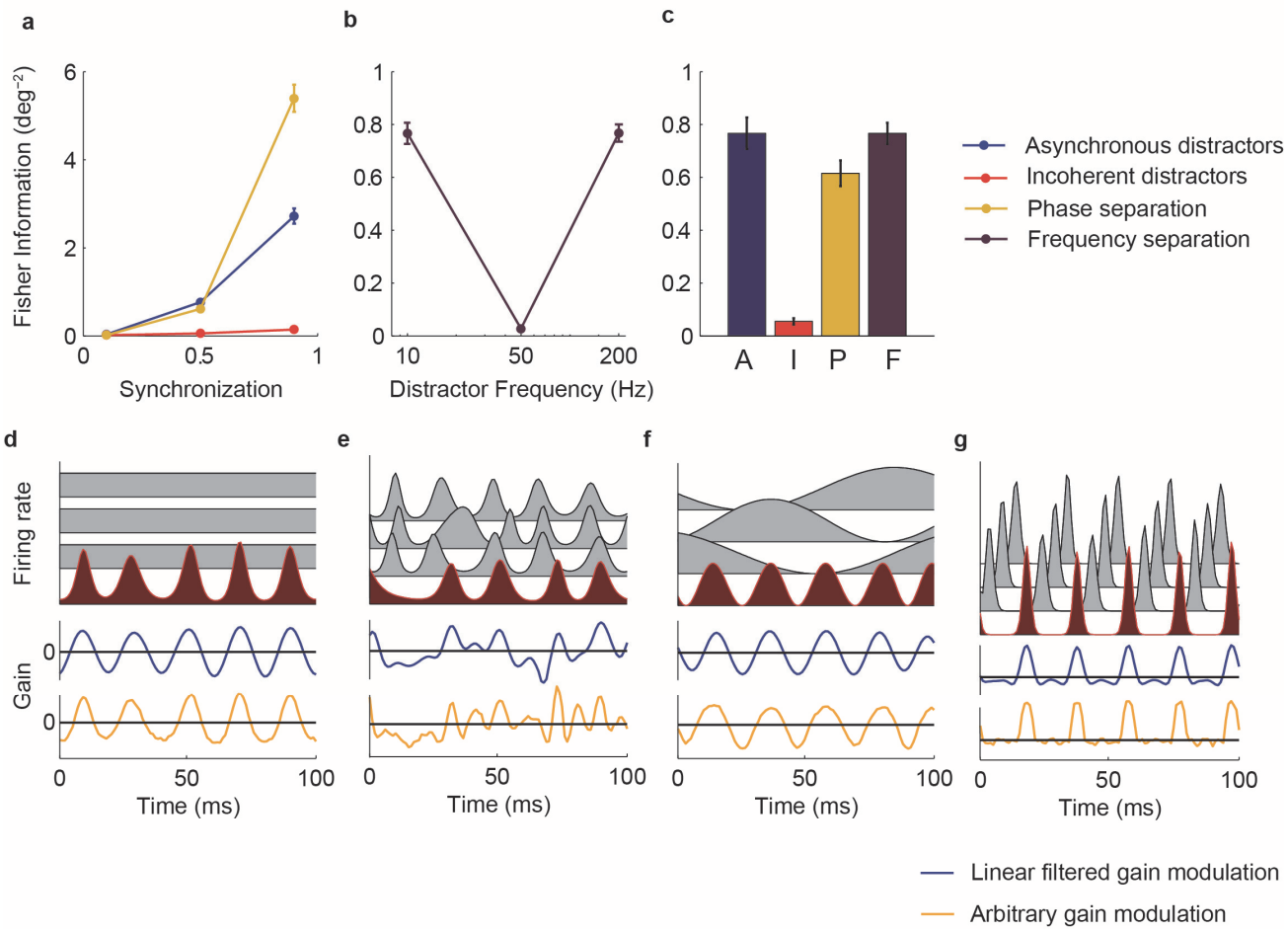

Figure 5.7 **Filtering with arbitrary gain modulations. a,** Effect of synchronization strength on decoding accuracy for asynchronous distractors (blue), distractors oscillating incoherently in the same frequency band as the target (red) and distractors oscillating coherently with the target but equally space in phase (yellow). **b**, Effect of distractor frequency on decoding accuracy. **c**, Comparison of decoding accuracy for different distractor conditions (indicated by color as above) for synchronization strength of 0.5 and average neuronal firing rate of 5 Hz. **d-g**) Example input firing rate modulations, gain modulation generated by optimized linear filter (blue), and gain modulation found to optimize decoding accuracy for specific example of target firing rate modulation (yellow). **d**) Asynchronous distractors, **e**) incoherently oscillating distractors in same frequency band as target, **f**) Frequency separation, **g**) Phase separation.

5.3.9 Arbitrary gain modulations

So far we have presented results for receiving networks which applied a gain modulation that was a linearly filtered version of the firing rate modulation of the target input. We tested whether the comparatively poor performance obtained with incoherently oscillating distractors was an artifact of this assumption. To do this we evaluated decoding accuracy for receiving networks where the gain modulation was allowed to be an arbitrary function of the target firing rate modulation. To find the optimal gain modulation, we took a single instance of the target firing rate modulation over the integration window and used gradient descent to find the pattern of gain modulation that maximized decoding accuracy for this particular target input waveform (see Materials and Methods). Only the modulation of the target input was frozen; distracting input modulations varied as before for each sample in the training and test set. We repeated this for 100 individual instances of the target firing rate modulation, each of which was different because of random variation in its frequency, amplitude and phase.

The shape of gain modulations found by this approach was similar to that found by optimized linear filtering of the target firing rate modulation (Figure 5.7 d-g). For asynchronous distractors (Figure 5.7 d) and those well separated from the target signal in frequency (Figure 5.7 f), gain modulations were close to sinusoidal with a mean value of zero. For distracting inputs oscillating incoherently in the same frequency band as the target, the optimized gain modulation again strongly emphasized frequency components above and below the central frequency of the target firing rate modulation (Figure 5.7e).

5.3.10 Low firing rates

The above results show that when distracting inputs oscillate incoherently in the same frequency band as the target signal they severely degrade the accuracy with which the target stimulus can be recovered. This occurs because of random variation in the overlap between the distractor firing rate modulations and gain modulation in the receiving region. This overlap noise can be minimized by structured oscillatory activity in which distracting inputs are asynchronous or separated from the target in phase or frequency. The relative advantage of such structured activity increases with the population firing rate of the input networks because, as firing rate is increased, noise due to stochastic spiking of individual neurons becomes smaller relative to the signal size while the relative size of overlap noise is unchanged. Is there a population firing rate threshold below which structured oscillatory activity offers little advantage? We show here that such a firing rate threshold exists but argue that is low relative to firing rates relevant to coding in cortex.

Defining a firing rate threshold for a population code is complicated as the code is itself a distribution of firing rates over neurons. To provide a number that is straightforward to interpret we

considered a local region of receiving network for which all afferents have the same stimulus tuning, such that each input is characterized by an average firing rate R^n and modulation $m^n(t)$. The spiking activity due to input network N is:

$$s^n(t) \sim Poisson(R^n m^n(t))$$

The total spike input is:

$$S(t) = \sum_n s^n(t)$$

The output of the receiving network is:

$$O(\mathrm{t}) = g(t)S(t)$$

Where $g(t)$ is the gain modulation of the receiving network. The integrated output of the receiving network is:

$$P(t) = \int_{t-T}^{t} O(t')\, dt'$$

Our approach to determining the firing rate threshold at which overlap noise becomes dominant was to compare the noise due to an asynchronous distracting input with that due to an incoherently oscillating distracting input (both with the same average firing rate). This will depend on their firing rates, on the gain modulation, and on the firing rate modulation of the incoherently oscillating input. As in Figure 5.3, we assume that the target input and the oscillating distracting input have broadband oscillations with the same central frequency and same synchronization strength.

We considered two different gain modulations: that found in Figure 5.3 to maximize decoding accuracy for incoherently oscillating distractors (but which is physiologically implausible as it is often a multimodal function of oscillation phase), and the biologically plausible gain modulation used in Figure 5.4 which oscillated about zero with the same waveform as the firing rate modulation of the target input. For networks in which the average value of the gain modulation over time is zero, either an asynchronous or an incoherently oscillating distracting input contributes on average zero to the integrated output, irrespective of their average firing rate. However, for any given time window the contribution will not be exactly zero because of stochastic spiking of individual neurons and variability in the overlap between the firing rate modulation of the distracting input and gain modulation in the receiving network.

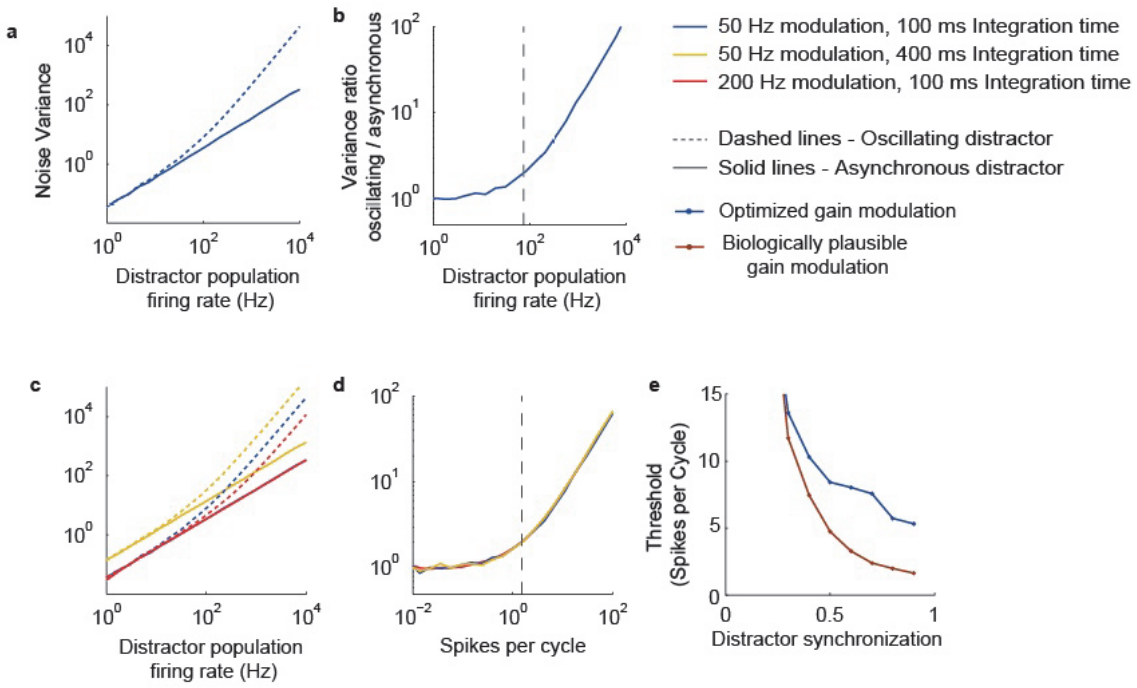

Figure 5.8 **Evaluating the low firing rate threshold.** Variance of noise in integrated output of receiving network due to an asynchronous (solid line) and an oscillating (dotted line) distracting input as function of distracting inputs firing rate. **b**) ratio of the noise variances plotted in (**a**), vertical line indicates firing rate threshold at which ratio is two. **c**,**d**) As for (**a**,**b**) but for different integration times and modulation frequencies indicated by line colour (see key). **e**) Firing rate threshold plotted as function of the synchronization strength of the oscillating distracting input for optimized and biologically plausible gain modulation.

Across an ensemble of time windows there will be a distribution centred on a mean of zero. The variance of this distribution is a measure of the noise contributed by the distracting input:

$$Distractor\ noise\ variance = var\left(\int_{t-T}^{t} g(t')s^n(t')dt'\right)$$

We evaluated the noise variance as a function of average population firing rate for the asynchronous and incoherently oscillating distracting inputs (Figure 5.8a). For the asynchronous distracting input noise variance increased linearly with average firing rate as expected for Poisson noise. However, for the distracting input oscillating incoherently in the same frequency band as the target signal, the relationship between firing rate and variance was different at low and high firing rates. At low firing rates the noise variance was identical to that due to an asynchronous distractor and increased approximately linearly with firing rate (Figure 3.8a). At higher firing rates the noise variance for

the oscillating distractor increased with the square of the firing rate, rapidly becoming much larger than that due to the asynchronous distractor. In the high firing rate regime the dominant source of noise is random variability in the overlap between firing rate modulation of the input and gain modulation in the receiving region.

We defined a threshold that distinguished these regimes as the population firing rate at which the noise due to the oscillating distractor was two-fold larger than that due to the asynchronous distractor (Figure 5.8b). This threshold was invariant with respect to changes in the integration time, as noise variance for both asynchronous and oscillating distractors scaled proportionately (Figure 5.8c). The firing rate threshold increased linearly with the oscillation frequency because at higher frequencies the overlap between gain modulation and firing rate modulation was averaged over more oscillation cycles (Figure 5.8c). By expressing the firing rate threshold in units of spikes per cycle rather than Hz, the threshold remained invariant to changes in the oscillation frequency (Figure 5.8d).

The threshold population firing rate varied with the synchronization strength of the inputs (Figure 5.8e). This is because with weak modulations overlap noise is smaller relative to stochastic spiking of individual neurons. However, where target and distracting input have comparable modulation strength, this reflects a worsening of the signal to noise ratio due to stochastic spiking rather than an improvement in the signal to noise ratio due to overlap variability. As shown above, for a given firing rate weak oscillations give much worse decoding accuracy (Figure 5.3c).

For moderately to strongly oscillating distracting inputs, the threshold population firing rate was in the range 5-10 spikes per cycle for a receiving network using the optimized gain modulation. For the receiving network with a biologically plausible gain modulation the threshold firing rate was in the range 1.5-5 spikes per cycle.

A threshold firing rate of 5 spikes per cycle corresponds to 200-400 Hz for gamma oscillations, and proportionally less for lower oscillation frequencies. As this threshold applies to a population firing rate, both the firing rates of individual neurons and the population size determine which regime the system is in. Although average firing rates in cortex are thought to be low (< 1Hz (Lennie, 2003), mean rates in sensory cortex during behavioral tasks are considerable higher (5-10 Hz (O'Connor et al., 2010; Vijayan et al., 2010) with cells that are strongly driven by a particular stimulus firing at rates up to 100 Hz. A population consisting of just a few tens of active neurons would therefore be in the high firing rate regime where 'non-communication through non-coherence' performs poorly relative to schemes using more structured oscillations.

The relevant population size is that of a functionally defined groups of afferents that share the same oscillatory modulation and target a single functional region of a receiving network, i.e. a region where cells have similar tuning properties and gain modulations. In regions of cortex where tuning to stimulus features is spatially mapped across the cortical surface, it is reasonable to take the size of such a functional group as the number of neurons in a small area of cortex over which tuning properties vary only modestly. Taking as an example macaque V1, where orientation tuning typically varies over the full range of 180º in 0.5 – 1mm (Mountcastle, 1997; Horton and Adams, 2005) and where neuronal density is ~10^5 per mm^2 of cortical surface (Collins et al., 2010), a population of 1000-10000 neurons might reasonably be assumed to share similar orientation tuning and receptive field location. Taking only principal neurons in a single layer would still leave populations that were firmly in the high firing rate regime even for average neuronal firing rates of 1 Hz and gamma oscillation frequencies. Defining functional groups by similar tuning for multiple stimulus dimensions such as spatial frequency, colour and orientation might in principle reduce their size sufficiently to make a case for the low firing rate regime. Whether this is an appropriate definition would depend on the details of the circuitry and the function the CTC mechanism was hypothesised to subserve in a given neural system.

5.4 Discussion

This study provides a quantitative assessment of the proposal that selective communication can be achieved by coherence between firing rate modulation in a sending region and gain modulation in a receiving region (Fries, 2005). Our results demonstrate that this is a viable mechanism for gating functional connectivity, allowing flexible routing of population-coded information. However, they show a strong and previously unrecognized dependence of the accuracy of information transmission on the structure and strength of oscillatory activity across a set of inputs.

Our findings question the proposal that incoherent oscillations functionally decouple anatomically connected regions. While random variation in the phase between a firing rate modulation and a gain modulation can reduce the average gain for an input to arbitrarily low levels, this is achieved at the cost of large fluctuations in gain from cycle to cycle. Unless firing rates are very low or population sizes relevant for coding are very small, these fluctuations are the dominant source of noise in the recovered signal and severely limit the accuracy with which information can be propagated. These random fluctuations can be greatly reduced if distracting inputs are asynchronous, or separated from the target input in frequency or phase. These more structured arrangements for multiplexing population codes support flexible modulation of functional connectivity with much less degradation of the target signal.

What is the functional significance of incoherent oscillatory activity in anatomically connected regions? It is possible that 'non-communication through non-coherence' is used in pathways where flexibility is crucial and low information rates can be tolerated. It is also possible that seemingly random variability in phase relationships actually represents deterministic moment-to-moment changes in a highly structured pattern of oscillations. Alternatively, if oscillations in one or both regions are weak and produce only shallow modulation of firing rates or gains, the effect of changes in relative phase on functional connectivity will be negligible. Task-dependent changes in coherence would in this case be a consequence rather than a cause of changes in signal flow.

The strength of oscillatory modulation of the target signal also has a strong effect on the signal to noise ratio. Weak oscillations result in poor signal to noise ratio because the firing rate modulation read out by the receiving network is small relative to noise from stochastic spiking of individual neurons. This conclusion is likely to generalize beyond CTC to other mechanisms in which the principal carrier of information is non-zero frequency components of the firing rate generated by oscillatory network activity. It is certainly the case for the gating mechanism described in the previous chapter in which frequency selective filtering networks read out information encoded in firing rate oscillation amplitude patterns.

Estimating the modulation depth of sparsely synchronized oscillatory activity is technically challenging. Individual neurons fire irregularly at rates potentially well below the oscillation frequency, such that the spike pattern of a single neuron provides little information about the population firing rate modulation. A common approach to estimating modulation strength is to look at the distribution of spikes relative to the phase of a band pass filtered local field potential (LFP) oscillation. This method can underestimate modulation strength if the LFP signal is corrupted by noise, for example from neurons not participating in the oscillation, if the analysis combines activity from periods with and without strong oscillation, or includes neurons not participating in the oscillation. Despite these technical difficulties measured spike phase histograms show a wide range of modulation strengths across different oscillations, from very strong modulations during hippocampal theta oscillations (Klausberger et al., 2003), and oscillations in the olfactory system of zebrafish (Friedrich et al., 2004) and locusts (Perez-Orive et al., 2002), to apparently weaker modulation during gamma oscillations in the hippocampus (Tukker et al., 2007; Colgin et al., 2009) and entorhinal cortex (Colgin et al., 2009). Our results suggest that where oscillations are genuinely weak, mechanisms exploiting them for selective routing of signals would recover only a tiny fraction of the information represented in the sending population.

The modelling work in this chapter made the simplifying assumptions that inputs sum linearly and that gain modulation multiplicatively scales the combined input. Though these are a reasonable set

of assumptions for an initial investigation of this question, both assumptions are likely to be violated to a greater or lesser extent in real neural networks. Clearly patterns of multiplicative modulation that accurately separate linearly summed inputs will no longer work effectively if input summation is highly sub- or super-linear. Likewise, non-multiplicative modulations of the network input-output function will behave differently as demultiplexing operations. It may be possible to compensate for non-linear input summation by modifying the gain-modulation operation, or vice versa. Exploring these possibilities in future work would be a valuable extension to our results.

We cannot completely rule out the possibility that a network implementing a more complex demultiplexing operation could more accurately separate signals oscillating incoherently in the same frequency band. If we wish to retain the basic mechanism of coherence between firing rate and gain modulation, an obvious extension is to consider a class of models in which the instantaneous input-output relationship of the receiving network is a non-linear function of the input, and the gain modulation acts by changing the shape of this nonlinearity. We have explored the performance of several models in this class, including those with threshold-linear, power law and threshold-power law nonlinearities (data not shown). In these experiments the gain modulation could vary both a linear input gain and the threshold and/or exponent of the non-linearity. These extensions to the model did not, however, result in any improvement in performance over the linear gain modulation outlined above. Although we cannot claim to have exhaustively explored all possible models in this class, we think it unlikely that any approach based on coherence between firing rate and gain modulations can efficiently separate signals oscillating incoherently in the same frequency band.

Throughout this work we have discussed gain modulation that acts on the input-output relationship for the activity of a population of neurons. Oscillatory activity can also modulate the gain of synaptic plasticity (Pavlides et al., 1988; Huerta and Lisman, 1993). This could be used to selectively potentiate or depress inputs depending on their oscillatory modulations. As our results are due to signal to noise considerations they are equally applicable to identifying which structures of activity permit accurate selective plasticity of a subset of inputs by oscillatory modulation of the gain for plasticity.

To summarize, selective communication can be achieved by coherence between gain and firing rate modulations. However, to achieve a high signal to noise ratio the oscillatory modulation of the target signal must be strong, and distracting inputs must be distinguished from the target by frequency, phase or amplitude of oscillation. Failure to satisfy these constraints greatly reduces the accuracy of information transmission. Where oscillatory activity plays a causal role in modulating functional connectivity we expect it to be organized to maximize the accuracy of communication.

Chapter 6: Waves or ripples? Estimating the strength of network oscillations from spike-field and spike-spike coherence spectrums.

6.1 Introduction

Though it is common to talk about asynchronous and oscillating network states as discrete, for real networks it is more accurate to consider a continuum of states from asynchronous, through resonant, weakly and strongly oscillating. This absence of a clear demarcation occurs because of the type of bifurcation that leads to oscillating network states and the presence of noise and finite size effects.

Transitions between asynchronous and sparsely synchronised network states occur through supercritical Hopf bifurcations in which a stable fixed point changes into an unstable fixed point surrounded by a small amplitude limit cycle. In idealised noise-free, infinite size systems there is still a clear distinction between the asynchronous and oscillating state even though oscillating states near the state transition have small amplitude. This distinction becomes blurred by the presence of noise and finite size effects. The instantaneous firing rate in any finite size network must fluctuate due to the discreet nature of spikes. These fluctuations act like a source of noise in the recurrent synaptic drive. In biological networks these fluctuations are supplemented by additional sources of noise such as stochastic transmitter release and thermal fluctuations in channel opening. The upshot of this is that the total activity in the asynchronous state is not constant but instead can be thought of as a stochastic process. If the parameters of the network are smoothly varied to move the network between an 'asynchronous' and oscillating state, there is no sharp transition in the autocorrelation function or power spectrum of the total activity, but rather a smooth change between states.

The implication of these dynamics for interpreting *in vivo* data is that statistically significant peaks in spectral measures of network activity in no way provide evidence for strong network oscillations. This fact is perhaps underappreciated in the experimental literature, where papers arguing for the functional significance of oscillatory phenomenon rarely comment on the strength of the observed periodic fluctuations. This may in part be due to researchers implicitly making an incorrect analogy between the asynchronous to oscillating state transition and that between quiescence and spiking in single neurons, where just super-threshold currents produce large amplitude spikes.

Our results from the previous two chapters indicate that the strength of network oscillations has a profound effect on the efficiency with which they can be used for controlling the gain of functional

interactions. In the oscillatory routing mechanisms we have studied, information is encoded by spatial patterns of oscillatory modulations of the firing rate. The signal to noise ratio is determined by the size of these modulations relative to stochastic spiking of individual neurons. Where network oscillations are weak this leads to poor communication accuracy. This is likely to be true for any multiplexing schemes which use oscillations, and as we argue in the introduction, multiplexing is implicit in many hypotheses about the function of network oscillations. Evaluating the strength of network oscillations in behaving animals will therefore likely prove important in evaluating whether they are indeed functionally significant in a given system. This would be trivial if we could measure the spiking activity of all neurons in a local region, but is challenging using experimentally available data as we can only observe the spiking of a handful of neurons and indirect measures such as the LFP.

In this short results chapter we presents two small pieces of work we have found useful for thinking about oscillatory fluctuations in *in vivo* data. The first is simply an illustration of the smooth transition between asynchronous and oscillating states in the presence of noise, using the Wilson-Cowan equations as a model system. The second is an exploration of how synchronisation strength and neuronal firing rates affect spike-field and spike-spike coherence spectrums. These measures are widely used to assess neuronal synchronisation but they are difficult to interpret; is a peak of 0.1 in a spike-field coherence spectrum indicative of a strong or weak oscillation? We consider the coherence spectrums that are expected for networks in which slowly varying spatial patterns of firing rates are multiplicatively modulated by faster oscillatory activity. This multiplicative modulation model is a reasonable description of the activity in our simulated networks in Chapter 4 and is the explicit form used in Chapter 5. Making a very crude assumption about the LFP, we can write analytical approximations for the coherence spectra which indicate a simple relationship between coherence, firing rate, sampling frequency and the spectrum of the oscillatory modulation.

6.2 Materials and Methods

6.2.1 Models and simulations

Two models were used to generate data for the analyses in this chapter; the Wilson-Cowan model used in Chapter 3 to simulate slice rephasing, and the periodically modulated Poisson model of network activity used in Chapter 5.

The Wilson-Cowan model was used for figures 6.1 and 6.2. The model was identical to that used in Chapter 3 apart from the removal of the transient input pulse and changes to the population time

constants τ_e, τ_i and the standard deviation σ of the noise. The time constants were adjusted such that their mean was always 2 ms and their ratio $r = \tau_e/\tau_i$ was varied across simulations to move the model between the asynchronous and oscillatory state. For a given ratio r the time constants were given by:

$$\tau_e = 2r/(1+r) \qquad\qquad \tau_i = 2/(1+r)$$

For figures 6.1.1a,b a range of 5 ratios was chosen which spanned the transition between asynchronous and oscillatory activity. To choose this range we calculated the value of r at which the network transitioned between asynchronous and oscillating states. A necessary condition (Latham et al., 2000) for the stability of the asynchronous state can be written:

$$\frac{\tau_e}{\tau_i} > \frac{\Phi_{E,E} - 1}{1 - \Phi_{I,I}}$$

Where $\Phi_{L,M}$ is the partial derivative $\frac{\partial \Phi_L}{\partial M}$ of the sigmoidal activation function for population L evaluated at the equilibrium point. For our model parameters this gives the condition $\frac{\tau_e}{\tau_i} > 0.4919$ for the stability of the asynchronous state.

The following parameter values were used for simulations to generate figures:

Figure 6.1.1ai σ = 0, r = 2 Figure 4.1.1bi = 0.2, r =2

Figure 6.1.1aii σ = 0, r = 0.6 Figure 4.1.1bii = 0.2, r = 0.6

Figure6.1.1aiii = 0, r = 0.5 Figure 4.1.1biii σ = 0.2, r = 0.5

Figure6.1.1aiv σ = 0, r = 0.45 Figure 4.1.1biv σ = 0.2, r = 0.45

Figure6.1.1av σ = 0, r = 0.25 Figure 4.1.1bv σ = 0.2, r = 0.25

For figure 6.2a σ = 0 and r was varied from 0.6 to 0.12 in steps of 0.03.

For figure 6.2b σ = 0.2 and r was varied from 2 to 0.1 in steps of 0.1.

Covariance functions and spectra were evaluated from 200 seconds of simulated network activity; downsampled to time resolution of 1 ms. Activity was normalized such that the average firing rate was 1 before evaluating these measures.

Modulations used in figures 6.4 – 6.4 were generated by the periodically modulated Poisson model used in Chapter 5. Briefly, the firing rate modulation was a Von Mises function of the oscillation phase. Frequency and modulation strength fluctuated as low pass filtered Gaussian white noise. For all figures the central oscillation frequency was 50 Hz, the frequency variability parameter Z= 0.2 and the amplitude variability parameter $V = 0.1$. Modulation strength was varied across figures as indicated in the figure legends. Coherence spectra were evaluated from 10000 seconds of activity with a time resolution of 1 ms.

6.2.3 Spectral analysis

Spectrums in figures 6.1c and 6.2 and coherence spectrums in figures 6.3-6 were evaluated using multi-taper methods for smoothing in the frequency domain. Multi-taper methods work by multiplying the signal by multiple different tapers before calculating the Fourier transform. The Fourier transform for a single taper is given by:

$$x_k(f) = \sum_{t=1}^{n} w_k(t)x(t)e^{-2\pi ift}$$

Where $w_k(t)$ are K orthogonal tapers. We used 7 Slepian functions as tapers as these are an optimal family of orthogonal tapers. Spectra and cross-spectra are calculated by averaging across tapers:

$$S_x(f) = \frac{1}{k}\sum_{1}^{K}|x_k(f)|^2$$

$$S_{xy}(f) = \frac{1}{k}\sum_{1}^{K}x_k(f)x_k(f)^{\dagger}$$

In figures 6.1 and 6.2 activity was divided into non overlapping 500 ms sections and zero padded to 512 samples before Fourier transforms. For figures 6.3 – 6.4 activity was divided into non overlapping 250 ms sections and zero padded to 256 samples.

6.3 Results

6.3.1 Transition between asynchronous and oscillating states in the noise-free and noisy Wilson-Cowan model

The Wilson-Cowan model from Chapter 3 was used to illustrate how noise changes the abrupt transition between the asynchronous and oscillating states in noise free systems into a smooth transition. The only parameter that was varied to move the system across the state transition was the ratio τ_e/τ_i of the time constants of the excitatory and inhibitory populations. This ratio was varied while holding the mean of the two values constant to minimise changes in the oscillation or resonance frequency. As the ratio is reduced the asynchronous state loses stability to an oscillating state.

In figure 6.1.1 we illustrate the state of the network for 5 different values of the τ_e/τ_i ratio, spanning a range from far inside the asynchronous state (i), to a strongly oscillating state (v). The third state (iii) was very close to the state transition but just on the asynchronous side. We show an example 500 ms section of the activity of the excitatory population (Figure 6.1.1-2a), the covariance function of the excitatory population activity (Figure 6.1.1-2b), and the power spectrum of this activity (Figure 6.1.1-2c). To give a more complete picture than is provided by just these 5 states, we use surface plots in figure 6.2 to illustrate the evolution of the activity power spectrum across the state transition. Multi-taper methods were used for frequency smoothing in all spectral analyses in this chapter (see methods).

For the noise-free model (Figure 6.1.1) the activity exhibited a sharp transition between the asynchronous and oscillating state. In the asynchronous state (i-iii) the activity is constant in time (a), the covariance function is zero for all lags (b), and the power spectrum is zero for all frequencies (c). In the oscillating state (iv-v) the activity has periodic fluctuations (a), which cause a periodic covariance function (b) and a peaked power spectrum (c). As the system moves further from the state transition the modulation depth increases (v) and harmonics become visible in the power spectrum (c.v).

Adding noise to the system changed the transition between asynchronous and oscillatory activity (Figure 6.1.2). When the ratio τ_e/τ_i was high (i) fluctuations induced by noise were aperiodic (a), as evidenced by the absence of periodicity in the covariance function (b) or a peak in the power spectrum (c). As the ratio was reduced noise induced fluctuations became more periodic (a.ii) and a clear peak emerged in the power spectrum (c.ii). Further reduction of the ratio increased the size

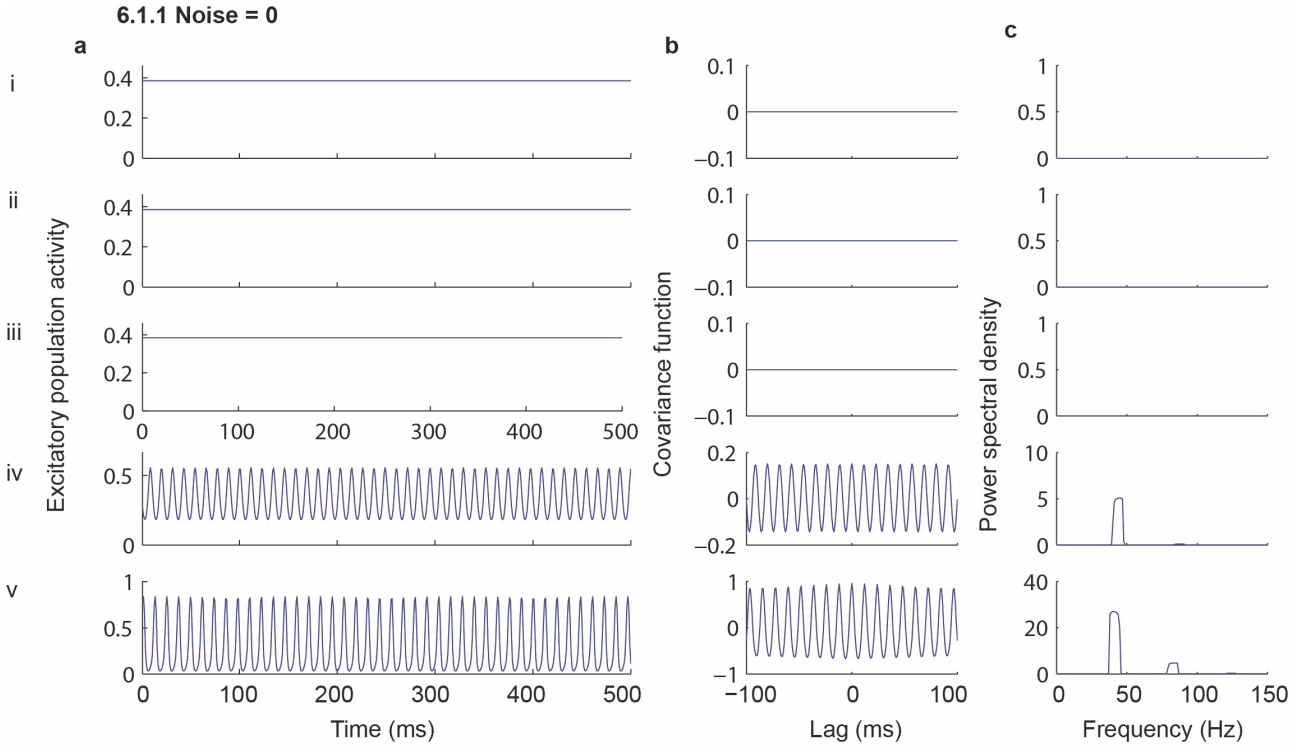
6.1.1 Noise = 0
a
b
c
i
ii
iii
iv
v
Excitatory population activity
Covariance function
Power spectral density
Time (ms)
Lag (ms)
Frequency (Hz)

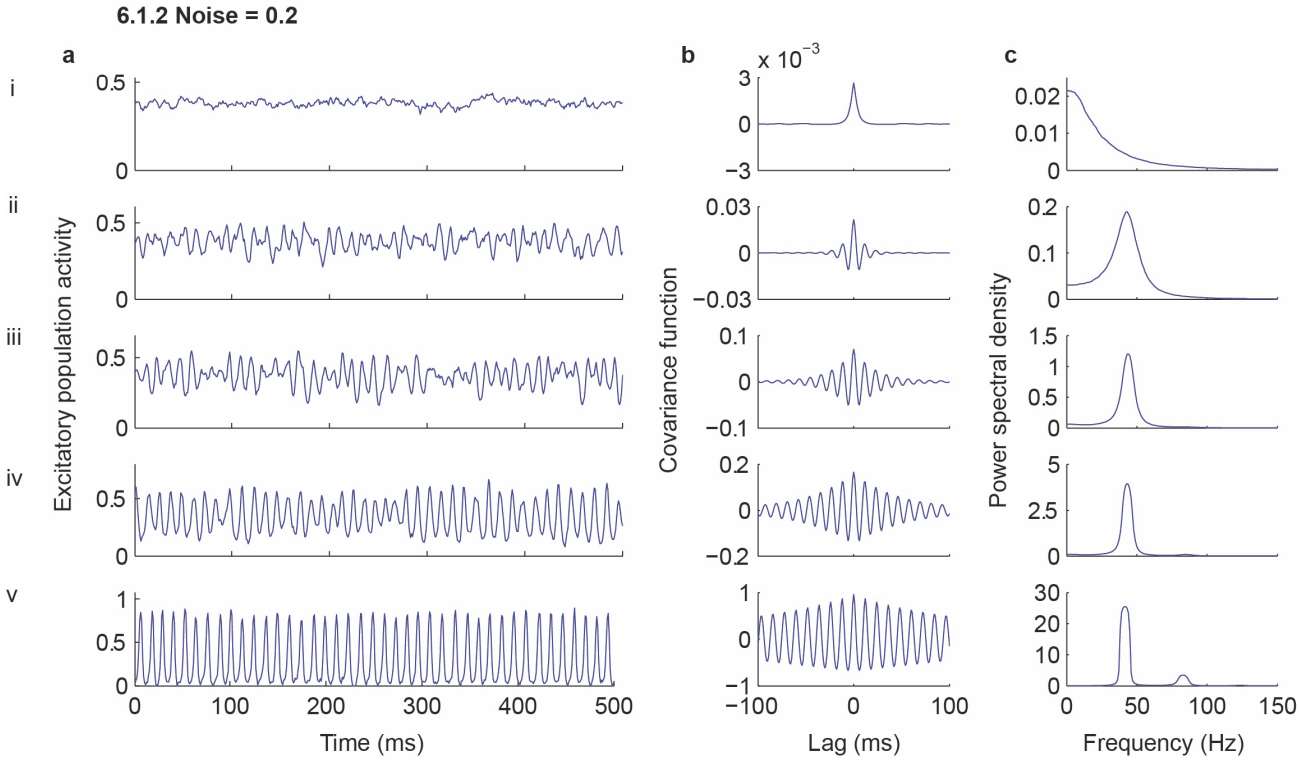
6.1.2 Noise = 0.2
a
b
c
x 10^-3
i
ii
iii
iv
v
Excitatory population activity
Covariance function
Power spectral density
Time (ms)
Lag (ms)
Frequency (Hz)

Figure 6.1 (Preceding page) **Transition between asynchronous and oscillating states in noise-free and noisy Wilson-Cowan model.** Transition between asynchronous and oscillating state for the Wilson-Cowan model with noise = 0 (**6.1.1**) and with noise = 0.2 (**6.1.2**). Rows **i** to **v** show network activity with the following values of the ratio τ_e/τ_i : **i**: 2, **ii**: 0.6, **iii**: 0.5, **iv**: 0.45, **v**: 0.25. **a**) Example of 500 ms of activity of the excitatory population. **b**) Covariance function of the activity of the excitatory population. **c**) Spectrum of the activity of the excitatory population.

and regularity of the periodic activity fluctuations (a.ii-v), increased the size and sharpness of the spectral peak (c.ii-v) and the power of harmonics of the oscillation frequency (c.v). The smooth nature of this transition is illustrated by the surface plot in figure 6.2.b and is in marked contrast to the sharp transition in the absence of noise (figure 6.2.

The two key points illustrated by these figures are that there is a continuum of states between asynchronous and strongly oscillating, and that strongly peaked power spectra emerge when fluctuation are still shallow relative to the mean activity. A similar gradual transition between asynchronous activity and strong oscillation is shown for the spiking network models used in Chapter 4 in figure 4.8.

6.3.2 Relating coherence measurements to the strength of network oscillations

The above results illustrate that the presence of a peak in spectral measures of network activity does not necessarily imply a strong oscillation. Given the likely importance of oscillation strength, we would like to be able to infer the strength of network oscillations from spectral measures. Here we focus on spike-field and spike-spike coherence spectra which are widely used measures of local circuit and inter-region oscillatory synchronisation. Coherence is a frequency domain measure defined as:

$$C_{xy} = \frac{S_{xy}(\omega)}{\sqrt{S_x(\omega)S_y(\omega)}}$$

Where $S_x(\omega)$, $S_y(\omega)$ are the autospectral density of signals x and y and $S_{xy}(\omega)$ is their cross spectral density. Some authors define the coherence as the square of the above quantity but we use the above definition as it is frequently used in the experimental literature.

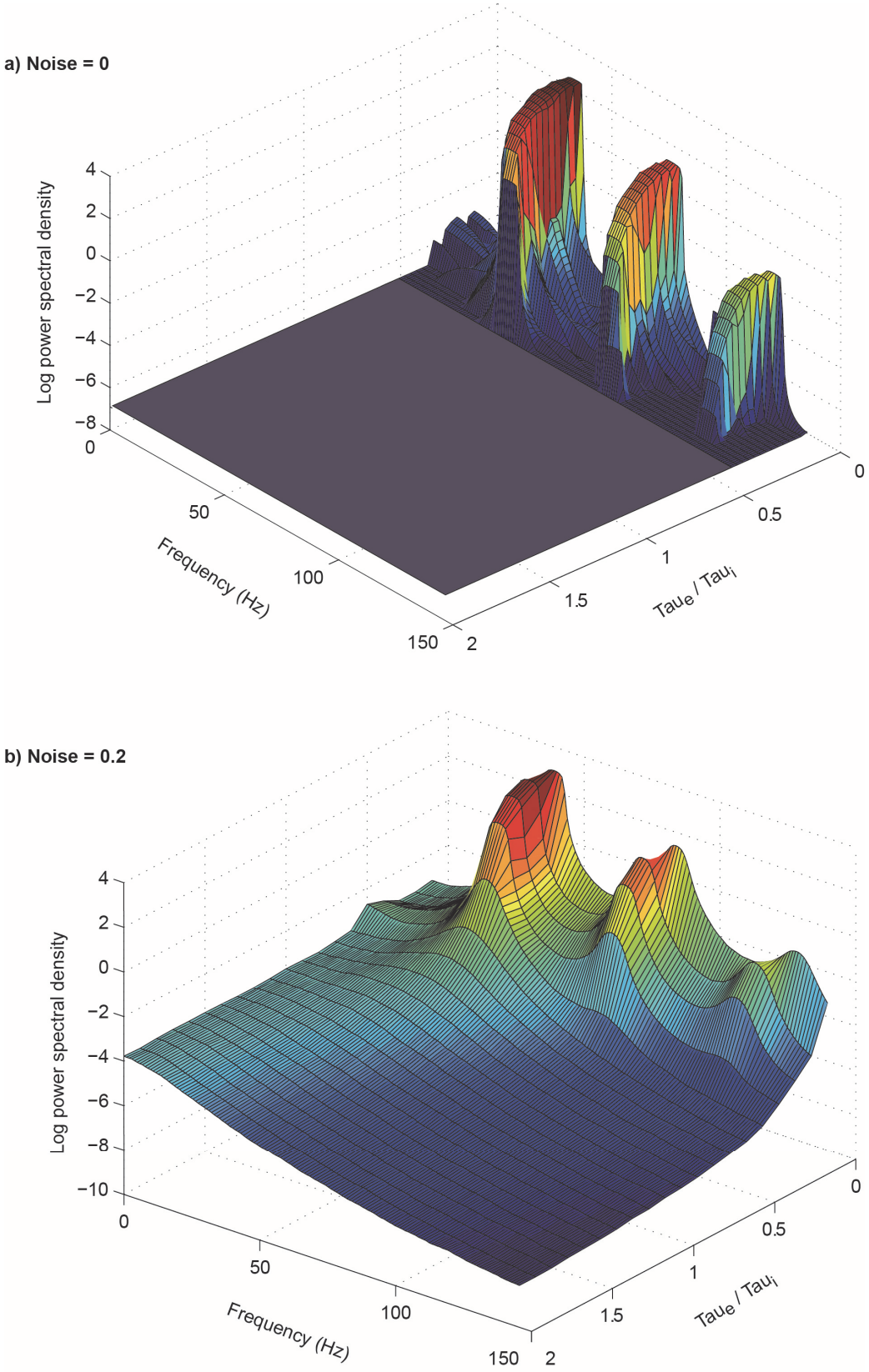

Figure 6.2 **Activity power spectra across state transition.** Power spectra as a function of τ_e/τ_i ratio for the noise free (**a**) and noisy (**b**) Wilson – Cowan model.

Coherence measures the phase consistency and amplitude covariation of two signals as a function of frequency. Coherence spectra takes values between one and zero with a value of one indicating that fluctuations of a given frequency are identical up to a constant phase shift, while a value of zero indicates the fluctuations are uncorrelated.

Here we explore the expected spike-spike and spike-field coherence spectra for networks where oscillatory activity can be modelled as a homogeneous multiplicative modulation of firing rates and spiking is a Poisson process. The model for activity of individual neurons is:

$$S_i = Poisson(R_i(t)M(t))$$

Where S_i is the spike activity of unit i, $M(t)$ is a multiplicative oscillatory modulation applied to all units, and $R_i(t)$ is a spatial pattern of firing rates. $R_i(t)$ varies on a much slower timescale than $M(t)$ and we initially consider networks where R_i does not vary.

This model is of interest for several reasons. Firstly, the model is a reasonable description of the oscillatory activity we observed in Chapter 4 generated by randomly connected networks with oscillatory dynamics driven by spatially patterned Poisson spike input. Secondly, the multiplicative modulation model is a reasonable approximation to make about network activity in a local network *in vivo* in the absence of experimental evidence suggesting differential modulation of distinct sub-populations. Thirdly, multiplicative modulation can work as an effective multiplexing scheme for population codes as demonstrated in the previous two chapters.

We initially consider a model in which the spatial pattern of firing rates is stationary.

$$S_i = Poisson(R_i M(t))$$

To make any statements about the spike-field coherence we need a model of the LFP. We assume that the LFP can be modelled as a linearly filtered version of the modulation $M(t)$. This is clearly a very crude approximation but is not completely unreasonable. The LFP is thought to primarily reflect fluctuations in the synaptic input to neurons in a region of a couple of hundred micron radius around the electrode. Fluctuations which are correlated across neurons summate to make a much greater contribution than uncorrelated fluctuations such that the common fluctuations driving the modulation can be expected to contribute strongly to the LFP unless the modulation is very shallow. The contribution of synaptic currents to the LFP is thought to be low pass filtered due to both dendritic filtering effects (Lindén et al., 2010b) and potentially due to the extra cellular medium (Bédard et al., 2010b).

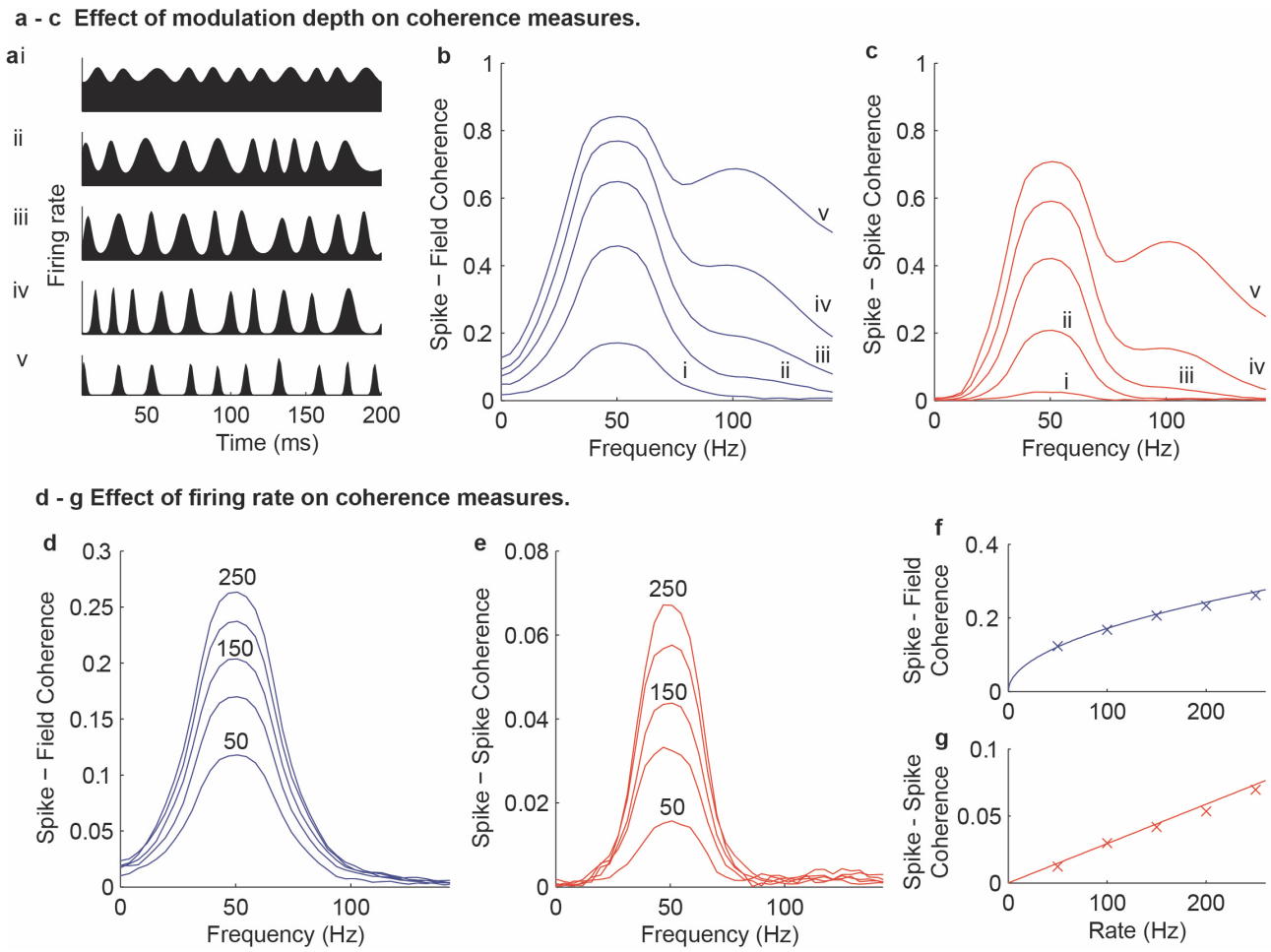

Figure 6.3 **Effect of modulation depth and firing rate on coherence measures. a)** Firing rate modulations ranging from modulation strength 0.1 (i) to 0.9 (v) in steps of 0.2. **b)** Spike-field coherence spectrums for 100 Hz firing rate. Labels (i-v) on traces correspond to modulation depths in (a). **c)** Spike-spike coherence spectrums. **d)** Spike-field coherence spectrums for modulation strength of 0.1 at a range of firing rates from 50 Hz to 250 Hz in 50 Hz intervals. Labels on traces indicate firing rate in Hz. **e)** Spike-spike coherence spectrums. **f,g)** Coherence plotted as a function of firing rate. Crosses indicate measured coherence values, lines indicate approximated coherence values.

However, as long as these filtering effects are linear they do not change the coherence spectra as they scale both the spike-field cross spectrum and the field autospectrum by the same amount. We can therefore ignore these filtering effects when considering coherence spectra and model the LFP as simply the modulation $M(t)$.

For the modulations we use the statistical description used in Chapter 5, in which the modulation is a Von Mises function of phase, and both the angular frequency and modulation strength fluctuate as low pass filtered Gaussian noise. Figure 6.3a shows example modulations of 5 strengths ranging from 0.1 to 0.9 using the strength measure from Chapter 5 where 0 is asynchronous activity and 1 has all spikes occurring at the same phase. We evaluated the spike-field (Figure 6.3b) and spike-spike (Figure 6.3c) coherence spectra as a function of modulation strength for multi-unit activity with total firing rates of 100 Hz per spike train. As expected both coherence measures show a clear peak at the oscillation frequency, the size of which increases monotonically with modulation depth. For any given modulation depth spike-field coherence was higher than spike-spike coherence. For highly synchronised oscillations additional coherence peaks occur at the harmonics of the oscillation frequency.

It is frequently stated in the experimental literature that coherence measures are independent of spike rate. It is unclear where this belief came from as it is very clearly not true under reasonable assumptions about the network activity and LFP. In figure 6.3d-g we show coherence spectra for a network with a fixed modulation depth of 0.1 for a range of firing rates of the spike trains used to calculate the coherence measures. The height of the peak of both coherence spectra increases monotonically with firing rate, with a faster increase for spike field compared with spike-spike coherence. The reason for this is that as firing rates increase the waveform of the spike trains becomes more and more similar to the waveform of the modulation. This dependence on firing rate makes it impossible to make inferences about the strength of oscillatory modulation in a network unless average firing rates are reported alongside coherence spectra. This dependence also suggests that reports of task dependent changes in coherence should be treated with caution unless steps are taken to compensate for the dependence.

6.3.3 The Relationship between firing rate, modulation strength and coherence spectra

What is the functional form relating firing rate, modulation strength and coherence spectra for this model? To answer this question we turn to a recent paper by Zeitler et al (2006) which analytically evaluated the coherence spectra for a very similar model to ours. The Zeitler model consists of Poisson neurons with firing rate:

$$x_i(t) = \lambda + N_c\sigma\eta_0(t) + (1 - N_c)\sigma\eta_i(t)$$

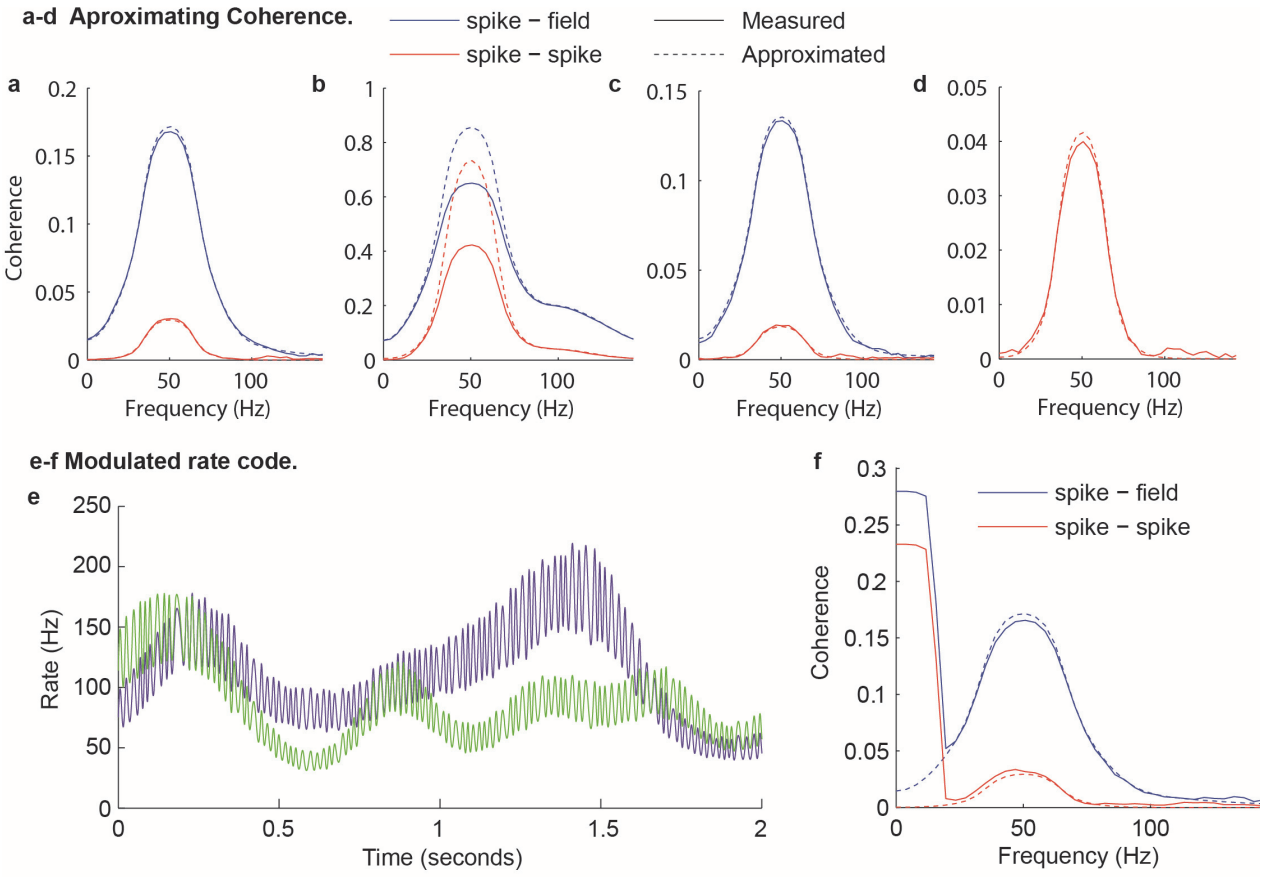

Figure 6.4 **Approximating coherence spectrums.** **6.4** Real (solid lines) and approximated (dash lines) coherence spectrums for (**a)** modulation strength 0.1, firing rate 100 Hz, (**b**) modulation strength 0.5, firing rate 100Hz, (**c**) modulation strength 0.025, firing rate 1000 Hz, (**d**) Spike-spike coherence between two units with rates 100 Hz and 200 Hz, modulation depth 0.1. **e)** Firing rate for two units (average firing rates 100 Hz) with partially correlated low frequency rate variation modulated by high frequency oscillation with modulation depth 0.1. **f)** Coherence spectrums (solid lines), and approximated coherence spectrums based only on oscillatory modulation and average rate.

Where $x_i(t)$ is instantaneous firing rate of unit i, λ is average firing rate (common to all units), N_c is fraction of firing rate variability that is common to all units, σ is total variance of the firing rate modulation (common to all units), $\eta_0(t)$ is Gaussian coloured noise with zero mean and variance (representing Network Oscillation), $\eta_i(t)$ is Gaussian white noise, zero mean, variance 1 (representing non-common input).

They model the LFP as the common input:

$$LFP(t) = \eta_0(t)$$

For this model they analytically derive the following approximate expression for the coherence spectra.

Single unit spike-field coherence $C_{SF} \approx \frac{\Delta t \sigma N_c}{\sqrt{\Delta t \lambda}} \sqrt{\rho(\omega)}$

Spike-Spike coherence for two single units: $C_{SS} \approx \frac{(\Delta t \sigma N_c)^2}{\Delta t \lambda} \rho(\omega)$

Where Δt is the time resolution at which the spike trains are sampled, $\rho(\omega)$ is the autospectrum of $\eta_0(t)$. The approximations are accurate in the limit $\Delta t \lambda \ll 1$ (due to binomial approximation of spike train, i.e. not more than one spike in each bin) and $(\Delta t \sigma)^2 \ll \Delta t \lambda$ due to an approximation to simplify the expression.

The derivation does not rely on the Gaussian nature of the fluctuations and hence our multiplicative modulation model and the Zeitler model can be transformed into each other by the following change of variables if we assume for now that all units in our model share the same average firing rate R.

$$N_c = 1, \qquad \lambda = R\,, \qquad \sigma\eta_0(t) = R(M(t) - 1)$$

This gives the following expressions for the spike-field and spike-spike coherence in our model:

Spike-field coherence: $C_{SF} \approx \sqrt{R \Delta t \mu(\omega)}$

Spike-spike Coherence: $C_{SF} \approx \Delta t R \mu(\omega)$

Where $\mu(\omega)$ is the autospectrum of the modulation $M(t)$. The limits provided by Zeitler et al suggest that these approximations are valid in the limit $\Delta t\, Rvar(M(t)) \ll 1$ and $\Delta t R \ll 1$ (but see below). As all neurons have the same modulation in this model, the results are valid for single or multi-units as long as they have total firing rate R.

Figure 6.4a shows the correspondence between measured and approximated coherence measures for a firing rate of 100 Hz and modulation strength of 0.1. The approximations provide an excellent match to the measured spectra. The correspondence between the measured and approximated spectra broke down for high coherence values (figure 6.4b). The conditions based on those

provided by Zietler et al did not correctly predict which spectra were accurately described by the approximation. Spectra were accurately predicted for firing rates that were much too high to satisfy $\Delta tR \ll 1$ (Figure 6.4c) and the approximation broke down for parameters which satisfied $\Delta t\ R\ var(M(t)) \ll 1$ (Figure 6.4b, $\Delta t\ R\ var(M(t)) = 0.054$). In practice, spectra were accurately predicted in regions where spike field coherence was less than ~0.2 and spike-spike coherence less than ~0.04.

Can we relax the assumption that the two spike trains used to asses spike-spike coherence have the same firing rate? The structure of the problem suggests the form:

$$C_{SF} \approx \Delta t\sqrt{R_1 R_2}\mu(\omega)$$

Where R_1 and R_2 are the average firing rates of the two spike trains. This accurately modelled the spike-spike coherence between pairs spike trains where the spike-spike coherence was less than ~0.04 (Figure 6.4d) .

We explored what happened when the spatial pattern of firing rates was no longer fixed but instead was allowed to vary on a timescale that was much slower than the modulation frequency. The low frequency variability of the rate of each spike train was modelled as:

$$R_i(t) = 2\ \Phi(0.5\ \mu_0(t) + \mu_i(t))$$

Where μ(t) were low pass filtered Gaussian noise with a cut-off frequency of 5 Hz and a variance of 1, and Φ was a sigmoidal function $\Phi(a) = \frac{1}{1+e^{-a}}$.

This produced partially correlated slowly varying firing rates which were modulated by a common high frequency oscillation. Figure 6.4e shows an example 2 second section of the firing rates generated by this model.

The LFP was modelled as the component of rate fluctuations that were correlated across units:

$$LFP(t) = \Phi(0.5\ \mu_0(t))M(t)$$

We evaluated the spike-spike and spike field coherence spectra for this model and compared them with the approximation based only on the modulation, which ignores the low frequency variation in rates and LFPs (Figure 6.4f). Unsurprisingly the spectra showed a large peak at low frequencies due to the common low frequency fluctuations, in addition to the high frequency peak due to the modulations. This shape of spectrum is strikingly similar to that observed in V4 during visual

stimulation (Fries et al., 2008). The approximation based only on the high frequency modulation continued to accurately model the spectra for frequency ranges where the low frequency rate variation did not contribute significant power.

6.4 Discussion

The work in this chapter focuses on some basic points that need to be taken into account when interpreting evidence of oscillatory activity in *in vivo* data. We initially looked at the dynamics of the transition between asynchronous and oscillatory activity and illustrated how in the presence of noise there is no clear demarcation between asynchronous and oscillatory states. There is rather a continuum of states of increasing periodicity in which the activity spectrum becomes strongly peaked while the fluctuations are still shallow relative to the average firing rate.

The effect of noise on non-linear dynamical systems has been studied extensively in other contexts (reviewed in Lindner, 2004), and our finding that noise blurs the distinction between stationary and oscillating states is not novel. In a neuroscience context a similar phenomenon occurs in the dynamics of single neurons at the bifurcation to spiking; in deterministic neuron models a clear demarcation exists between quiescent and spiking states as the input current is increased through the rheobase, while in the presence of noise this transition is blurred (Hansel and van Vreeswijk, 2002; Lindner et al., 2003). To our knowledge such effects have not been described at the network level, and while they are unsurprising from a dynamical systems perspective they may well be relevant to interpreting periodic signals observed *in vivo*. Network level resonance effects near the boundaries between asynchronous and oscillating states have recently been characterised analytically for rate and integrate and fire models driven by sinusoidal inputs (Ledoux and Brunel, 2011).

The other results in this chapter look at what can be inferred about the strength of oscillatory modulations from coherence measures. The strong dependence of coherence on rate precludes meaningful quantitative inference about or comparisons of network state if the firing rate of the spike trains is not reported or compensated for. Though this point is apparent from a close reading of the work of Zeitler et al (2008), the relationship between coherence and rate is obscured by the mathematical form of the model they use and is not emphasized in their discussion. The point has certainly not been widely appreciated in the experimental community where it is still frequently stated that coherence does not depend on rate and where coherence spectra are rarely accompanied by sufficient information about firing rates. Since the work detailed in this chapter was carried out, a paper has been published which identifies and characterises analytically the dependence of coherence on firing rate for various stochastic models of spike trains similar to those considered in

this chapter (Lepage et al., 2011). The dependence of coherence on firing rate identified in this chapter occurs through a different mechanism from a previously recognised dependence on firing rate of spike count correlation between cells receiving common input (de La Rocha et al., 2007). The latter occurs due to the transformation of input fluctuations by a nonlinear neuronal input-output relation, while the former is due to the effect of rate on the relative magnitude of fluctuations due to Poisson spike generation and those due to oscillatory modulation of the Poisson process intensity.

If we know the firing rate of spike trains and are willing to make some assumptions about the structure of oscillatory activity and LFP, we can use coherence spectra to make inferences about the spectrum of network activity. The accuracy of inferences based on the spike-field coherence will depend on how closely the LFP resembles a linearly filtered version of the local circuit activity. The forward model that links activity to LFP remains only partially understood (see literature review). Deviation of the LFP from this linear model will reduce spike-field coherence values. Using spike-spike coherence measures removes concerns about the LFP forward model but at the expense of requiring very large amounts of data to obtain accurate spectra.

For either type of coherence spectra, the accuracy of inferences about the network state based on the relationships we report in this chapter will depend on the extent to which activity in the frequency band of interest can be described as a common multiplicative temporal modulation of spatial patterns of firing rates. Activity could deviate strongly from this assumption for several reasons. Rate coding of signals with power in the frequency band of interest would cause non-periodic independent variability of firing rates. However, if oscillations are being used as a mechanism for multiplexing we expect the signal carried by changing patterns of firing rates to be at considerably lower frequency than the oscillatory modulation.

Even where signal variability does not contain power in the relevant frequency band, the oscillatory modulation could deviate from homogenous multiplicative modulation in several ways. Though multiplicative modulation appears to be a reasonable model in randomly connected networks based on visual inspection of the simulations presented in Chapter 4, we have neither quantified how much of the variability is captured by this description nor tested how dependent this is on network parameters. Real networks are of course not randomly connected and this brings with it the possibility of much richer patterns of oscillatory activity such as multiple distinct sub-populations exhibiting different modulations. More complex structures of oscillatory activity would cause coherence measurements to underestimate the strength of oscillatory modulations where coherence is measured between neurons participating in different oscillations.

What the simple models considered in this chapter can do is indicate approximately what strength of oscillatory activity experimental data provides evidence for, in the absence of evidence of oscillatory structures more sophisticated than uniform modulation of network firing rates.

Chapter 7. Discussion

The work described in this thesis has aimed to help understand the dynamics and possible functional significance of task dependent changes in large scale oscillatory activity in mammalian brains. The hypothesis I have developed is that such activity implements a specific low level operation; multiplexing population codes to permit selective control of gain in divergent and convergent anatomical pathways. This is an incremental step in a line of research which previously developed many of the ideas central to the hypothesis. Oscillations have long been proposed to play a role in controlling signal flow (Crick and Koch, 1990; Salinas and Sejnowski, 2001; Varela et al. 2001), and the potential they offer for communication that is more selective than the underlying anatomical connectivity has been previously recognised (Fries 2005). The major conceptual difference between the above hypothesis and previous work is the emphasis we place on multiplexing. This is the ability of oscillatory dynamics to create multiple, orthogonal information channels in a single firing rate signal. Multiplexing is both necessary if oscillations are to be utilised for selective communication, and is what provides potential advantages over more straightforward asynchronous gain control mechanisms. This emphasis was not present from the start of this project but instead emerged through investigating the practicalities of neural codes that permitted selective gain control using oscillations and considering why these mechanisms might confer advantages to organisms.

Perhaps more important than this conceptual emphasis are the practical steps taken towards understanding the dynamics underlying *in vivo* data, and to develop a quantitative framework outlining how biologically plausible network dynamics and coding strategies can achieve selective gain control. In this discussion I will first summarise my ideas concerning why and how the brain may use network oscillations to control the gain of anatomical pathways. I will then outline the null hypothesis, describing briefly how the experimental phenomena that suggest the existence of these mechanisms could arise in a system in which oscillations do not play a functional role. It is useful to explicitly explain how task dependent changes to oscillatory activity could occur as epiphenomena in order to facilitate interpretation of data and the design of experiments to evaluate the hypothesis. Finally, I identify experimental tests that could help to distinguish these two possibilities.

7.1 Why use network oscillations as a gain control mechanism?

There are two components to the question of why oscillatory gain control mechanisms may be valuable to organisms. The first is why mechanisms for controlling the gain of pathways are useful for brain function? The second is what advantages do oscillatory mechanisms offer over other more straightforward approaches to gate information flow?

Gain control is a basic operation with great computational power (Salinas and Thier, 2000; Salinas and Sejnowski, 2001b). This power stems from the fundamental role that the connection structure or weight matrix of a network plays in determining activity. Changing the gain of a pathway is trivially equivalent to changing the weight matrix, while increasing the input gain of an individual neuron is equivalent to increasing the strength of all the synapses received by that cell. Hence, controlling the gain of pathways or neurons can effectively remap the connection structure of a network. The weight matrix profoundly affects internally generated activity patterns and the response of a network to external inputs, such that networks of simple units with appropriately structured connectivity can implement a wide range of complex computational functions. Consequently, by changing the connection structure, the function performed by a network may be transformed. As discussed in the introduction, context dependent behavioural flexibility likely requires dynamically reshaping many aspects of the function of networks throughout the brain. Gain control allows the dynamic reshaping of network structure and hence provides a powerful mechanism to modulate the computational functions performed by networks.

There are several mechanisms including shunting inhibition and background synaptic input which can modulate the gain of neurons (Chance et al., 2002; Mitchell and Silver, 2003; Rothman et al., 2009), and simple circuits can be constructed which selectively control signal flow without resorting to oscillatory dynamics (Anderson and Essen, 1987; Vogels and Abbott, 2009). There is therefore a question of whether oscillatory mechanisms confer any distinct advantage compared with more straightforward asynchronous mechanisms. The unique functionality which I argue oscillations provide in this context is the ability to multiplex multiple signals into the time or frequency domain of a single firing rate signal. As we demonstrated in Chapters 4 and 5, this can allow appropriately designed filtering networks to selectively read out components of a combined signal in a convergent pathway, and hence to selectively control the gain of signals by varying either the oscillatory modulations of the inputs or the filtering performed by the receiving network. Although we did not explicitly model divergent pathways, it is clear that if different postsynaptic targets have distinct filtering properties, changes in modulation of the signal can differentially affect their gain. Such selectivity does not permit any fundamentally new computational operations. For example, if multiplexing is used to send independently controllable signals to two targets in a

divergent pathway, the same functionality could be implemented without multiplexing using two separate anatomical pathways. However, multiplexing can permit a given level of functionality to be implemented with a greatly reduced amount of physical connectivity. Given the considerable metabolic expense of nervous tissue and spiking activity (Attwell and Laughlin, 2001; Lennie, 2003), this could have significant advantages for organisms.

7.2 Multiplexing and demultiplexing population codes with oscillations and filtering networks

To outline the framework developed for selective gain control in divergent and convergent pathways I first focus on the coding strategy used to represent information, then on how operations to generate and work with these codes may be implemented by biological networks.

7.2.1 Periodically modulated population codes.

The description outlined here for how information can be multiplexed and demultiplexed by networks with oscillatory dynamics goes considerably beyond previous work on the topic in the degree of quantitative detail concerning the coding used to represent information, i.e. which aspects of the network activity are signal and which are noise. Even if the central hypothesis outlined above is broadly correct in some systems, the quantitative picture proposed here will inevitably be a great simplification and perhaps wide of the mark. Nonetheless, if oscillations do play a role in controlling signal flow, there is a pressing need to develop quantitative models of how information is represented in this mechanism. These are required both to determine whether qualitative proposals in fact work efficiently, and to evaluate whether *in vivo* data are consistent with the hypothesis.

The coding strategy, which I describe as periodically modulated population codes (PMPCs), consists of conventional population rate codes which vary on a slow time-scale as the encoded information changes, periodically modulated in an approximately multiplicative manner by oscillatory dynamics on a faster time-scale. The computationally attractive feature of multiplicative modulations is that they are extremely well suited for multiplexing. The multiplexing schemes used in AM radio, and in time division and code division multiplexing of digital signals, can all be expressed as a slowly varying signal multiplicatively modulated by a rapidly varying carrier. For spatial firing rate codes in populations of neurons, multiplicative modulation reproduces the spatial pattern of firing rates into a spatial pattern of oscillatory firing rate modulation. These patterns can

be read out by evaluating the amplitude of firing rate oscillation at the network frequency (Chapter 4), or by multiplicative gain modulation coherent with the oscillation (Chapter 5). Neither of these readout mechanisms would recover the spatial firing rate code if the oscillatory modulation was additive, as in this case the amplitude would be constant across the network and both readouts would recover a flat spatial pattern. The power of these alternative readout mechanisms is that they recover the information encoding spatial pattern of activity but are orthogonal to the average firing rate, other frequencies of modulation, and potentially input at other phases (for readout by appropriately structured gain modulation). Therefore, different readouts can access independent information channels within one firing rate signal. Population codes can be selectively transmitted into these channels by engaging the appropriate multiplicative modulation, and different channels within a combined signal can be accessed by engaging the appropriate readout circuitry.

These codes are closer to conventional rate codes than they are to proposals such as synfire chains (Abeles, 1991; Bienenstock, 1995) or polychronization (Izhikevich, 2006) that rely on precise temporal sequences of spikes across neurons. However, unlike conventional rate codes where only the average firing rate over some integration time carries information, in the PMPC framework periodic modulations of the firing rate provide additional information channels. The use of firing rates rather than precise spike times is attractive from a network dynamics perspective as the rate modulations generated by sparsely synchronised dynamics are robust against noise. There are compelling experimental (London et al., 2010) and theoretical (Van Vreeswijk and Sompolinsky, 1998; Banerjee et al., 2008) arguments to suggest that the micro-structure of activity in the asynchronous balanced state of cortical networks is chaotic, which indicate that macroscopic measures of the activity such as rate are better suited as coding variables. I am not aware of studies explicitly addressing whether the microstructure of spike timing in sparsely synchronised states is chaotic but the random walk like behaviour of the sub-threshold membrane potential in these states suggests that it is (Brunel and Wang, 2003; Brunel and Hakim, 2008).

PMPCs are restricted to encoding signals that vary slowly relative to the oscillation frequency. This is because the readout mechanisms obtain at most one sample of the encoded signal per cycle of the oscillation. This is also true for phase coding schemes which use the time of spikes relative to an ongoing oscillation as the coding variable. If the encoded signal is a continuous time series, the Nyquist sampling theory indicates that to avoid aliasing it must not contain frequencies higher than half the oscillation frequency (Nyquist, 1928; Shannon, 1949). In practice a larger separation of time-scales may be necessary as signals that vary this rapidly might interact strongly with the oscillatory or resonant dynamics of the sending and filtering networks.

The requirement that the encoded signal varies on a slower timescale than the modulation suggests an organising principle for division of labour among frequency bands, with low frequency oscillations used for encoding signals which have a naturally slow timescale of variation. This is consistent with the use of low frequency oscillations in the hippocampus as a substrate for encoding slowly varying spatial information (O'Keefe and Recce, 1993; Skaggs et al., 1996). These considerations question recent proposals which suggest that the phase of firing relative to very slow oscillations plays a role in encoding rapidly varying sensory stimuli (Montemurro et al., 2008; Kayser et al., 2009).

7.3 Implementation and dynamics

I now focus on how biological networks can implement the operations required to use these codes for selective gain control in convergent and divergent pathways. There are three components to this; generation of multiplicative modulations, implementation of readout mechanisms, and varying modulations or readouts to flexibly control signal flow.

7.3.1 Generating multiplicative modulations

The activity generated by the network simulations in Chapter 4 is to visual inspection similar to that generated explicitly by the multiplicative modulation model in Chapter 5. This correspondence indicates that at least for some network structures and parameter ranges, sparsely synchronised dynamics can generate approximately multiplicative modulation of spatial firing rate patterns. This is a non trivial result as other forms of modulation can be imagined such as additive oscillatory fluctuations in the firing rate. An important question is the extent to which this is a general feature of such dynamics or a special case for those particular networks. Two features of the networks considered in Chapter 4 were supportive of this activity. The first is that connectivity in the excitatory-inhibitory loop was random, which ensured that the all excitatory cells received similar oscillating inhibitory drive. Real networks are obviously not randomly structured. This could permit considerably more complex structures of oscillatory activity which may be more computationally powerful but could invalidate the PMPC model. However, while the brain's large scale connection structure is clearly non-random, the fine structure of connectivity is likely stochastic in many networks. Additionally, it may be that random connectivity in a given excitatory-inhibitory loop is sufficient to generate multiplicative modulation even where excitatory-excitatory connectivity, or that involving other interneuron populations, is structured. It may therefore be useful to think about structured spatial envelopes of modulation (modulation fields) within which modulation can be described by multiplicative modulation. Note that while a pattern of oscillatory activity may be spatially structured in the sense that only a given population of

neurons participate, those neurons may not be segregated in physical space. The individual input networks used in Chapters 4 and 5 are very crude example of such modulation fields in the larger structured network of a convergent pathway. Indeed, spatially selective changes in large scale structures of oscillatory activity are necessary if oscillations are to be used to selectively control the gain of interactions.

A second feature of the networks considered in Chapter 4 which promoted multiplicative modulation was that, although the spatial pattern of firing rates changed with the stimuli, the average network firing rates remained constant. Increases in excitatory drive can increase the strength of sparsely synchronised oscillatory activity (Brunel and Hakim, 1999; Brunel and Wang, 2003; Mazzoni et al., 2008) and hence where the total firing rate of a network varies the strength of oscillatory modulation may itself be a function of average firing rate. However, this does not invalidate the PMPC model as long as the modulation is approximately multiplicative in its effect on the spatial pattern of activity across the range of modulation strengths, and the average firing rates change on a slower time-scale than the oscillatory modulation. Total input firing rate would then be one of the factors that cause the modulation structure to change in order to generate the required connection structure for the task in hand.

7.3.2 Readout algorithms and their biological implementation

Information encoded into spatial patterns of firing rate modulation may be read out directly into activity in a post synaptic network, or by plasticity mechanism into changes in the strength of synaptic connections. We have primarily focused on the former case though the latter may be equally important, particularly in the hippocampus which shows prominent theta oscillations and plays a critical role in long term memory storage.

We have identified two operations that can selectively read out inputs with particular modulations while ignoring other components of the signal. The first of these is evaluating the spatial pattern of firing rate oscillation amplitude. This can selectively read out inputs with a particular oscillation frequency while ignoring asynchronous inputs or those oscillating with other frequencies. We demonstrated in Chapter 4 that simple feed forward inhibitory networks can implement this readout operation, converting spatial patterns of firing rate oscillation amplitude into spatial patterns of firing rate. The network performed this conversion in two steps. Firstly, the input spike signal was effectively bandpass filtered as it was converted into a synaptic current received by the output cells. The high-pass component of this filtering occurred due to feed-forward inhibition, which cancelled low frequency variation of the firing rate but did not cancel modulation at the oscillation frequency due to a resonance induced phase shift of the inhibitory activity relative to the input. The low pass component of the filtering was due to synaptic timecourses. This bandpass filtered synaptic current

was then rectified by the spike threshold to produce a spike output whose average firing rate was proportional to the amplitude of input firing rate oscillation.

The second readout mechanism we considered was a quantitative model of the qualitative 'communication through coherence' hypothesis (Fries, 2005). This hypothesis proposed that selective communication between two networks could be achieved by coherence between firing rate modulation in a sending region and gain modulation in a receiving region. We demonstrated that, for multiplicative firing rate modulations in the sending region and multiplicative gain modulations in the receiving region, this mechanism can selectively recover the spatial pattern of activity encoded into a specific firing rate modulation. In principle this readout approach is more powerful than reading out amplitude patterns as it can cope with phase-coded inputs and can separate a target signal from other inputs oscillating incoherently in the same frequency band. However, we argue that the great increase in noise that results from allowing multiple inputs to oscillate incoherently in the same frequency band makes this an unattractive way of utilising oscillations of selective communication compared with schemes based on orthogonal modulations.

We have not explicitly addressed how the required patterns of gain modulation can be generated by biological networks. Several mechanisms including shunting inhibition (Mitchell and Silver, 2003) and synaptic noise (Chance et al., 2002) can generate multiplicative gain modulation at the level of individual neurons. Utilising these mechanisms to implement the filtering would require interneuron circuitry that could phase lock to the target signal and hence generate the required periodic gain modulation. If the target signal is the only component oscillating in a given frequency band, the gain modulation circuitry could entrain directly to the combined input as the modulation of the target can be recovered simply by filtering at the appropriate frequency. This would require circuitry with tight bandpass properties similar to the networks considered in Chapter 4 such that it could ignore fluctuations in the input at other frequencies. In the case of phase coded signals, a reference signal is required such that the readout circuitry knows which phase it should be listening to.

Readout by coherent gain modulation is the most plausible mechanism for converting PMPCs into patterns of synaptic plasticity. The gain of synaptic plasticity can be directly modulated by oscillatory activity (Pavlides et al., 1988; Huerta and Lisman, 1993). Alternatively, the combination of periodic post-synaptic activity with spike timing dependent plasticity (Dan and Poo, 2004) will produce periodically modulated gain for plasticity. This may play a role in converting phase coded sequences of sequentially visited locations into patterns of synaptic strengths in the hippocampus (Skaggs et al., 1996; Sato and Yamaguchi, 2003).

In our modelling work we have only considered readout mechanisms that selectively recover one component of a combined signal identified by a specific oscillation modulation, while ignoring other components. However, in many cases it may be that an analogue reweighting of different components of the input is required rather than an all or nothing selection of single components. From an algorithmic perspective this flexible reweighting operation could be implemented by a linear combination of demultiplexing operations tuned to different components of the signal. For example, if two different components of a phase coded signal can be selectively read out by two different patterns of gain modulation, a linear combination of these gain modulations will generate a linear combination of the two signal components. Flexible reweighting of the different input components can then be achieved by varying the weights in the linear combination. An alternative approach to reweighting would be to hold the demultiplexing operation constant and change the modulation of the different signal components. In the phase coding example this would correspond to shifting the phases of different components of the input activity relative to the gain modulation in the receiving network. Intuitively it seems that this approach may result in a worse signal to noise ratio than the former as the reduction in gain is achieved by throwing away some of the signal rather than rescaling the whole. It may however be more straight forward to implement. The second approach would not work well in the case of inputs separated in frequency due to beating between inputs with similar but non-identical frequencies.

A further question is whether our conclusion that ´non-communication through non-coherence´ performs poorly relative to other multiplexing schemes applies also to the task of subtly reweighting multiple inputs. Reweighting could be achieved using a linear combination of a constant positive gain and a set of oscillatory gain modulations coherent with different input components. If the weights of the oscillatory gain modulation are small relative to the constant gain, the noise due to overlap variation will clearly be reduced; however the contribution of each input will only be modestly reweighted. If on the other hand we require substantial reweighting, this will be achieved at the cost of substantial overlap noise. A similar situation will arise if reweighting is achieved by varying the coherence of different inputs with a single oscillatory gain modulation in the receiving network. If deviations from coherence are small there will be little overlap noise but also little reweighting. These arguments suggest that while the absolute noise level may be less for a situation where ´non-communication through non-coherence´ is used to subtly reweight inputs, the magnitude of the noise relative to the reweighting achieved is likely to be largely invariant. In sensitive systems where a modest reweighting of different inputs has functionally important consequences it seems likely that even small amounts of additional noise will be undesirable.

7.3.3 Varying pathway gain

Flexibly and selectively controlling the gain of pathways with oscillations requires mechanisms for varying either the modulation of a network's outputs or the filtering performed by networks on their inputs. Modulations can be characterised by their frequency, phase and amplitude (or equivalent strength parameter for non-sinusoidal modulations) and any of these features could in principle be varied to control the effect on post-synaptic populations.

Perhaps the simplest mechanism for changing pathway gain is controlling the strength of oscillatory modulation. Switching networks between asynchronous and oscillating states can be achieved by many mechanisms that could be implemented by neuromodulatory or control inputs. These include changes in synaptic coupling strengths, average firing rates, noise levels or intrinsic neuronal parameters. Such changes could be used to switch signals on and off but are perhaps less well suited to implementing graduated changes in synchronisation strength. This is because, for the spiking networks and noisy rate models simulated in this thesis, states that were near the transition between asynchrony and oscillation had large random variation in amplitude under the influence of noise, which would be undesirable if amplitude is a coding variable. Although the average amplitude grew smoothly as the state transition was crossed, the amplitude appeared much more variable for weak oscillations than for asynchronous or strongly oscillating states. A possible way of producing graduated changes in amplitude without large amplitude variability would be to smoothly vary the coupling to a coding population from a strongly oscillating inhibitory network, for example by varying its firing rate.

The experimental signature of gain control mechanisms based on changes in oscillation amplitude would be task dependent changes in the strength of oscillatory modulation of local circuits, which have reported in a wide variety of experiments (Fries et al., 2001; Lee et al., 2005; Jones and Wilson, 2005b; Pesaran et al., 2008; van der Meer and Redish, 2009). These are most convincing in studies where there is both a large change in modulation of strength and a strong modulation at some point in the task (Lee et al., 2005; Pesaran et al., 2008).

Varying the frequency of modulation could be implemented either by engaging distinct inter-neuronal circuits with different oscillation frequencies, or through varying the frequency of a single oscillating circuit. In circuits with spike to spike dynamics this is very straightforward as oscillation frequency increases monotonically with excitatory drive (e.g Vida et al., 2006). In sparsely synchronised networks the oscillation frequency is determined by synaptic filtering, by the relative influence of excitatory-inhibitory and inhibitory-inhibitory loops, and by sub-threshold membrane dynamics (Brunel and Wang, 2003; Geisler et al., 2005). While synaptic kinetics are presumably fairly hard wired, the other determinants could be modulated by control inputs. Several studies

have demonstrated distinct oscillations frequencies at different times in a single region, suggesting multiple independently controlled oscillation generating circuits (Fries et al., 2008; Colgin et al., 2009; van der Meer and Redish, 2009; Tort et al., 2010). Analogue control of the frequency of a single oscillation generating circuit is suggested by variation in hippocampal theta frequency with speed of motion (Slawinska and Kasicki, 1998) and the novelty of the environment (Jeewajee et al., 2008).

Phase coding is a highly efficient form of multiplexing because it minimises noise due to distracting signals. Implementing such a mechanism requires the ability to control the relative phase of spiking in different populations, both to generate the coding and to implement the readout. Phase coding is well documented in the hippocampus where spike phase precesses as animals move through the place field of each cell (O'Keefe and Recce, 1993; Skaggs et al., 1996), indicating that neural circuits are able to control relative spiking phase of different neural groups. A variety of mechanisms, discussed in the literature review, have been proposed to generate this activity. Our results from Chapter 3 suggest an alternative mechanism for flexibly controlling the relative phase of coupled oscillating networks. We demonstrated that changing the relative strength of an external input to excitatory and inhibitory populations of an oscillating network can translate the phase response curve. The phase response curve determines the phase at which an oscillator will entrain to periodic inputs and the relative phase at which coupled oscillators will synchronise. Therefore, by controlling the relative coupling of inter-network connections onto excitatory and inhibitory populations, the relative phase of coupled networks can be varied. Such mechanisms could be used both to generate phase coded signals and to control the phase of readout circuitry relative to an oscillation.

7.4 The null hypothesis

Although task dependent changes in oscillatory phenomena may be a signature of the mechanisms outlined above, they could also occur as an epiphenomenon of other functional changes in network activity ('the exhaust fumes of computation' according to one sceptic). As discussed in Chapter 6, the presence of statistically significant peaks in the spectrum of network activity may only indicate shallow ripples on essentially asynchronous activity. Recurrently connected networks have a strong tendency to oscillate and synchronisation is promoted by features such as strong coupling that may be desirable for computation, or that are biophysically unavoidable such as delayed inhibition. Therefore, it is reasonable to ask what we would expect spectral measures of network activity to look like in a brain that used asynchronous rate codes in balanced networks. It is not implausible that activity would show weak periodic fluctuations, leading to statistically significant peaks in

spectral measures of network activity when evaluated with powerful statistical methods such as multi-taper smoothing.

If there is any tendency for periodic fluctuations, task dependent changes in both local circuit and inter-region synchronisation are expected. Changes in firing rates are the most straightforward potential cause of changes in spectral measures of local circuit synchronisation. For example, if the balanced 'asynchronous' state generates weak gamma frequency fluctuations, changes from quiescent to activated states will produce a large increase in gamma power in MEG or EEG signals. Smaller changes in firing rates in the balanced state may also produce changes in the amplitude of fluctuations by moving the system along the axis between asynchronous and strongly oscillating states, even if the fluctuations at all times remain shallow relative to the mean firing rate. Frequency specific changes in inter-region coherence could occur in weakly periodic networks as a result of the changes in coupling strength between networks. The effective coupling between networks will vary with the firing rate of the projection neurons that connect them, and might also occur as a result mechanisms such as that proposed by Vogels and Abbott (2009) for flexibly routing asynchronous rate coded signals.

7.5 Experimental tests to evaluate the hypothesis

Here we suggest directions for additional experiments and analyses, motivated by the work in this thesis, which could help distinguish between structures of oscillatory activity that play a causal role in controlling signal flow and those that are functionally irrelevant ripples.

Current *in vivo* data provides abundant evidence for statistically significant periodic fluctuations in network activity but in most cases provides only a limited quantitative picture of the strength and structure of modulations across local populations. The strength of oscillatory activity is important for the plausibility of the hypothesis as weak oscillations result in poor signal to noise ratios for codes exploiting modulations to carry signal. A further critical question is whether sub-populations of excitatory neurons in local circuits selectively participate in oscillations or whether the oscillation is essentially homogeneous across the local network. Many reports show that only a fraction of neurons within a region have statistically significant modulation or coherence (e.g, Tukker et al., 2007; Pesaran et al., 2008; Colgin et al., 2009). However, this could occur if oscillations are weak but homogeneous and only a fraction of the neurons reach significance in the data. A further complication is that patterns of oscillatory activity are likely to be highly non-stationary in freely behaving animals, though this can be reduced using carefully controlled behavioural tasks.

Developing a more detailed quantitative picture of these potentially complex structures of oscillatory activity is essential to evaluating whether activity is consistent with a role for oscillations in controlling signal flow. Limitations on the numbers of neurons that can be simultaneously recorded mean that only a tiny fraction of the neurons in a local network can be simultaneously recorded and hence population activity must be inferred from partial data. One approach would be to make explicit quantitative models of the structure of activity which can be fitted to or compared statistically with experimental data. Such models could either be statistical descriptions of network activity or dynamical models. These would provide a means of testing whether a given data set indicates homogeneous or spatially structured activity within a local population. To do this the distribution of measures of modulation strength across the population should be evaluated for simple models in which activity is homogeneous, such as the multiplicative modulations of Chapter 5 or randomly connected dynamical models. A statistically significant disparity between the expected distribution under homogeneous oscillations and that observed in *in vivo* data would provide evidence for structured oscillatory activity. In the absence of such evidence it should be possible to quantify the range oscillation strengths that are consistent with the data. Where oscillatory activity is spatially patterned within a local network the increased complexity will make it harder to accurately quantify the structure of activity and parallel recordings of large numbers of neurons may be necessary. Identifying structure in such large data sets, such as sub-populations of neurons with similar oscillatory modulation, is itself a challenging problem. Automated clustering methods exist for identifying spike trains with similar temporal structure (Fellous et al., 2004; Slonim et al., 2005; Humphries, 2011). Alternatively, the distribution across the population of quantities of interest such as the strength or preferred phase of spike-field phase locking may be used to identify structure in the data. Parallel recordings of large numbers of neurons would also be well suited to identifying the relationship between spatial patterns of firing rate and firing rate modulation, which could identify whether *in vivo* oscillations produce approximately multiplicative firing rate modulations.

Complementary to testing whether *in vivo* activity is consistent with the hypothesis are experimental tests of whether neurons or networks implement the filtering mechanisms needed to exploit information encoded into patterns of firing rate modulation. The filtering mechanism explored in Chapter 5 utilises periodic gain modulation to selectively readout target signals. The strength of *in vivo* gain modulation during oscillations could be directly tested using intracellular current injections. However, performing the required intracellular recordings in behaving animals would be challenging and in anaesthetised animals the network states may be very different from when the network is engaged in a task. A recent study used a more indirect method to measure gain modulation by oscillation phase in the motor system of behaving humans (van Elswijk et al., 2010).

Transcranial magnetic stimulation (TMS) pulses were delivered to motor cortex and the evoked muscle responses were measured as an electromyogram (EMG). The phase of beta frequency oscillatory activity in spinal motor networks at the time of TMS modulated the gain of the EMG response in an approximately multiplicative manner, though the modulations were small.

Optogenetic methods offer the possibility of directly measuring the filtering properties of networks by driving temporally structured activity in large populations of neurons. These were used to demonstrate resonance at gamma frequency in the LFP response evoked in a cortical network by periodic stimulation of local circuit interneurons (Cardin et al., 2009). Similar methods could be used to test for the existence of frequency selective filtering networks similar to those described in Chapter 4. That network utilised resonant but not oscillatory circuitry and hence did not spontaneously generate periodic gain modulations. The filtering properties would therefore only become apparent when the network is driven by modulated inputs. The experimental signature would be a strong dependence of principal cell firing rates on the modulation frequency of the input. While resonant LFP responses would be consistent with such networks they do not provide direct evidence as the LFP is extremely sensitive to correlation of activity and hence the amplitude could increase purely due to increased synchronisation without any change in average firing rates.

Optogenetic fMRI (Lee et al., 2010) offers a potentially powerful and complementary tool for identifying such filtering properties. This method uses functional magnetic resonance imaging to evaluate the effect of optogenetic stimulation on neural activity. fMRI measures changes in blood oxygen level and hence metabolic activity, and is thought to correlate closely with synaptic activity rather than spiking in a given region (Logothetis et al., 2001). However, unlike with the LFP, changes in the correlation of synaptic activity are not expected to affect the BOLD signal if the total rate of synaptic events is unchanged. As long as the input firing rate is approximately constant while its modulation frequency is varied, changes in the BOLD signal should therefore reflect post synaptic rate changes (and hence changes in the amount of local circuit synaptic activity). Additionally, fMRI measures activity simultaneously across the whole brain and hence can test all pathways originating from a single population in parallel. This could potentially identify a key prediction of the hypothesis; that different projection targets of a single population of neurons have different filtering properties.

An alternative approach to testing the functional significance of oscillations is to manipulate oscillatory activity during the execution a task and evaluate the effect of these manipulations on behaviour. Decrease in the power of hippocampal theta oscillations due to administration of canabinoids was shown to correlate with behavioural impairment on a hippocampal dependent memory task (Robbe et al., 2006). Importantly, while the oscillatory patterning of activity was

disrupted, average firing rates were not affected by the pharmacological manipulation. In a conceptually similar experiment, Stopfer et al (1997) demonstrated that selectively disrupting oscillatory activity in the honeybee olfactory system impaired odour discrimination.

This approach is a powerful way of demonstrating that oscillations play functional role in a given system but do not speak directly to the hypothesis that this function involves control of gain between networks. Manipulation of oscillations in spatial attention tasks may permit more direct tests of the hypothesis in this context. In spatial attention tasks the presence of nearby distracting stimuli can degrade (Bouma, 1970; Levi, 2008; Pelli, 2008) or bias (Wenderoth and Johnstone, 1988; Westhhmer, 1990) discriminations about a target stimulus, and these effects can be precisely quantified with psychophysical methods. Oscillatory modulations at gamma frequency have been proposed to play a role in differential processing of attended and unattended visual stimuli by controlling the flow of signals between visual cortical networks (Womelsdorf and Fries, 2006). If this is the case then manipulating oscillatory activity in early visual cortical networks representing individual stimuli should affect the perceptual interaction between attended and non attended stimuli. This manipulation could be achieved using optogenetic stimulation, or a more simple approach may be to flicker the stimuli. Flicker induces phase locked periodic activity in early visual cortex at frequencies up to ~ 90 Hz (Rager and Singer, 1998; Herrmann, 2001) and is perceptually subliminal at gamma frequencies. Our results from Chapter 3 suggest that sparsely synchronised oscillations in excitatory-inhibitory networks can be readily entrained by periodic inputs near their natural frequency.

If oscillatory modulation at a specific frequency contributes to selective processing of a target stimulus then perceptual interference between target and distracting stimuli should be increased by inducing oscillations in networks representing distracting stimuli that are coherent with those in the network representing the target. The simplest way to do this would be to drive networks representing both stimuli with a periodic input at the frequency at which oscillations occur in the target network in the absence of stimulation. However, any manipulation used to drive oscillation may have side effects on the activity such as changes in average firing rate which would compromise the comparison of a manipulation-off with a manipulation-on condition. For this reason a better approach would be to contrast the effects of driving in-phase with anti-phase modulations in networks representing target and distracting stimuli. This would profoundly change the spatio-temporal structure of modulation received by any upstream region receiving input from both networks. If the perceptual discrimination was unaffected by this relative phase manipulation when the induced modulations were of comparable strength to those occurring in the unperturbed system, this would offer compelling evidence that naturally occurring modulations were not

functionally important in this system. If the phase manipulation produced changes in psychophysical performance, the nature of these changes should provide insight into how the modulation structure of input activity affects input integration in that system.

7.6 Final thoughts

We have explored how oscillatory network dynamics offer rich possibilities for layering multiple information channels into firing rate signals. By modulating the dynamical state of local circuits, control inputs may determine which of these channels a network receives input from or transmits signal to, thereby remapping the brains effective connectivity structure and so changing the function of circuits in response to task demands. We have shown that these principles can be used to control the flow of information between networks, using coding strategies that extend population rate coding into the frequency domain, and dynamics that are resilient to noise and exhibit the irregular micro-structure of activity characteristic of *in vivo* recording.

There is abundant circumstantial evidence suggesting that changes in structures of oscillatory activity play important roles in brain function. The rapid pace of development of new tools for measuring and manipulating activity in large populations of neurons, offers exciting possibilities to directly test predictions of the hypothesis that oscillations control signal flow in neural circuits. By outlining a quantitative framework for how these mechanisms may function, I hope this work helps to bridge the gap between *in vivo* data and qualitative proposals about its function.

Notations and Abbreviations

Brain Regions

CA1	Hippocampal Subfield
CA3	Hippocampal Subfield
DMS	Dorsomedial striatum
IT	Inferotemporal cortex
LA	Lateral Amygdala
PMd	dorsal premotor cortex
PRR	Parietal reach region
V1	striate visual cortex
V2	extrastriate visual cortex subfield
V4	extrastriate visual cortex subfield

Experimental Methods

LFP	Local Field Potential
EEG	Electroencephalography
MEG	Magnetoencephalography
TMS	Transcranial magnetic stimulation
EMG	Electromyography

Other

CS+	Conditioned stimulus
EPSP	Excitatory post synaptic potential
$GABA_b$	gamma-aminobutyric acid receptor subtype

NMDA	N-Methyl-D-aspartic acid
PMPC	Periodically modulated population codes

Oscillation frequency bands

Slow	<1 Hz
Delta	1 - 4 Hz
Theta	4 - 8 Hz
Alpha	8 – 15 Hz
Beta	15 – 30 Hz
Gamma	30 – 80 Hz

Bibliography

Abeles, M. (1991). Corticonics: neural circuits of the cerebral cortex (Cambridge University Press).

Abeles, M. (2009). Synfire chains. Scholarpedia *4*, 1441.

Abouzeid, A., and Ermentrout, B. (2009). Type-II phase resetting curve is optimal for stochastic synchrony. Phys. Rev. E *80*, 011911.

Acsady, L., Kamondi, A., Sik, A., Freund, T., and Buzsáki, G. (1998). GABAergic Cells Are the Major Postsynaptic Targets of Mossy Fibers in the Rat Hippocampus. J. Neurosci. *18*, 3386–3403.

Adhikari, A., Topiwala, M.A., and Gordon, J.A. (2010). Synchronized activity between the ventral hippocampus and the medial prefrontal cortex during anxiety. Neuron *65*, 257–269.

Adrian, E.D., and Matthews, B.H.C. (1934). The interpretation of potential waves in the cortex. The Journal of Physiology *81*, 440.

Akam, T., and Kullmann, D. (2010). Oscillations and Filtering Networks Support Flexible Routing of Information. Neuron *67*, 308–320.

Albright, T.D. (1984). Direction and orientation selectivity of neurons in visual area MT of the macaque. Journal of Neurophysiology *52*, 1106.

Amit, D.J., and Brunel, N. (1997). Model of global spontaneous activity and local structured activity during delay periods in the cerebral cortex. Cerebral Cortex *7*, 237–252.

Anderson, C.H., and Essen, D.C.V. (1987). Shifter circuits: a computational strategy for dynamic aspects of visual processing. Proceedings of the National Academy of Sciences *84*, 6297–6301.

Anderson, J.R., Bothell, D., Byrne, M.D., Douglass, S., Lebiere, C., and Qin, Y. (2004). An integrated theory of the mind. Psychological Review *111*, 1036–1060.

Arabzadeh, E., Panzeri, S., and Diamond, M.E. (2006). Deciphering the spike train of a sensory neuron: counts and temporal patterns in the rat whisker pathway. The Journal of Neuroscience *26*, 9216.

Atallah, B.V., and Scanziani, M. (2009). Instantaneous Modulation of Gamma Oscillation Frequency by Balancing Excitation with Inhibition. Neuron *62*, 566–577.

Attwell, D., and Laughlin, S.B. (2001). An energy budget for signaling in the grey matter of the brain. Journal of Cerebral Blood Flow & Metabolism *21*, 1133–1145.

Averbeck, B.B., Latham, P.E., and Pouget, A. (2006). Neural correlations, population coding and computation. Nature Reviews Neuroscience *7*, 358.

Aviel, Y., Mehring, C., Abeles, M., and Horn, D. (2003). On embedding synfire chains in a balanced network. Neural Computation *15*, 1321–1340.

Azouz, R., and Gray, C.M. (2000). Dynamic spike threshold reveals a mechanism for synaptic coincidence detection in cortical neurons in vivo. Proceedings of the National Academy of Sciences of the United States of America *97*, 8110.

Baddeley, R., Abbott, L.F., Booth, M.C., Sengpiel, F., Freeman, T., Wakeman, E.A., and Rolls, E.T. (1997). Responses of neurons in primary and inferior temporal visual cortices to natural scenes. Proceedings of the Royal Society B: Biological Sciences *264*, 1775.

Bair, W., and Koch, C. (1996). Temporal precision of spike trains in extrastriate cortex of the behaving macaque monkey. Neural Computation *8*, 1185–1202.

Bair, W., Koch, C., Newsome, W., and Britten, K. (1994). Power spectrum analysis of bursting cells in area MT in the behaving monkey. Journal of Neuroscience *14*, 2870.

Baker, S.N., Kilner, J.M., Pinches, E.M., and Lemon, R.N. (1999). The role of synchrony and oscillations in the motor output. Experimental Brain Research *128*, 109–117.

Banerjee, A., Seriès, P., and Pouget, A. (2008). Dynamical constraints on using precise spike timing to compute in recurrent cortical networks. Neural Comput *20*, 974–993.

Battaglia, D., Brunel, N., and Hansel, D. (2007). Temporal decorrelation of collective oscillations in neural networks with local inhibition and long-range excitation. Phys.Rev.Lett. *99*, 238106.

Bauer, M., Oostenveld, R., Peeters, M., and Fries, P. (2006). Tactile spatial attention enhances gamma-band activity in somatosensory cortex and reduces low-frequency activity in parieto-occipital areas. J.Neurosci. *26*, 490–501.

Beck, J.M., Ma, W.J., Kiani, R., Hanks, T., Churchland, A.K., Roitman, J., Shadlen, M.N., Latham, P.E., and Pouget, A. (2008). Probabilistic Population Codes for Bayesian Decision Making. Neuron *60*, 1142–1152.

Bédard, C., and Destexhe, A. (2009). Macroscopic models of local field potentials and the apparent1/ f noise in brain activity. Biophysical Journal *96*, 2589–2603.

Bedard, C., Kr\öger, H., and Destexhe, A. (2006). Model of low-pass filtering of local field potentials in brain tissue. Physical Review E *73*, 051911.

Bédard, C., Rodrigues, S., Roy, N., Contreras, D., and Destexhe, A. (2010a). Evidence for frequency-dependent extracellular impedance from the transfer function between extracellular and intracellular potentials. Journal of Computational Neuroscience 1–15.

Bédard, C., Rodrigues, S., Roy, N., Contreras, D., and Destexhe, A. (2010b). Evidence for frequency-dependent extracellular impedance from the transfer function between extracellular and intracellular potentials. J Comput Neurosci *29*, 389–403.

Belitski, A., Gretton, A., Magri, C., Murayama, Y., Montemurro, M.A., Logothetis, N.K., and Panzeri, S. (2008). Low-frequency local field potentials and spikes in primary visual cortex convey independent visual information. Journal of Neuroscience *28*, 5696.

Benchenane, K., Peyrache, A., Khamassi, M., Tierney, P.L., Gioanni, Y., Battaglia, F.P., and Wiener, S.I. (2010). Coherent theta oscillations and reorganization of spike timing in the hippocampal-prefrontal network upon learning. Neuron *66*, 921–936.

Bennett, M.V.L., and Zukin, R.S. (2004). Electrical coupling and neuronal synchronization in the Mammalian brain. Neuron *41*, 495–511.

Benson, D.M., Blitzer, R.D., and Landau, E.M. (1988). An analysis of the depolarization produced in guinea-pig hippocampus by cholinergic receptor stimulation. The Journal of Physiology *404*, 479–496.

Berger, H. (1929). Uber das Elektrenkephalogramm des Menschen. Arch.Psychiatrie Nerv. *87*, 527–570.

Berman, R., and Colby, C. (2009). Attention and active vision. Vision Res *49*, 1233–1248.

Bichot, N.P., Rossi, A.F., and Desimone, R. (2005). Parallel and Serial Neural Mechanisms for Visual Search in Macaque Area V4. Science *308*, 529–534.

Bienenstock, E. (1995). A model of neocortex. Network: Computation in Neural Systems *6*, 179–224.

Bishop, G. (1932). Cyclic changes in excitability of the optic pathway of the rabbit. American Journal of Physiology–Legacy Content *103*, 213.

Bissiere, S., Zelikowsky, M., Ponnusamy, R., Jacobs, N.S., Blair, H.T., and Fanselow, M.S. (2011). Electrical synapses control hippocampal contributions to fear learning and memory. Science *331*, 87.

Bollimunta, A., Chen, Y., Schroeder, C.E., and Ding, M. (2008). Neuronal Mechanisms of Cortical Alpha Oscillations in Awake-Behaving Macaques. The Journal of Neuroscience *28*, 9976–9988.

Borgers, C., Epstein, S., and Kopell, N.J. (2005). Background gamma rhythmicity and attention in cortical local circuits: A computational study. Proceedings of the National Academy of Sciences of the United States of America *102*, 7002–7007.

Borgers, C., Epstein, S., and Kopell, N.J. (2008). Gamma oscillations mediate stimulus competition and attentional selection in a cortical network model. Proc. Natl. Acad. Sci. U.S.A *105*, 18023–18028.

Bouma, H. (1970). Interaction effects in parafoveal letter recognition. Nature *226*, 177–178.

Bragin, A., Jando, G., Nadasdy, Z., Hetke, J., Wise, K., and Buzsaki, G. (1995). Gamma (40-100 Hz) oscillation in the hippocampus of the behaving rat. J.Neurosci. *15*, 47–60.

Broadbent, D.E. (1958). Perception and communication. (Oxford University Press).

Brody, C.D. (1999). Correlations without synchrony. Neural Computation *11*, 1537–1551.

Brunel, N. (2000). Dynamics of sparsely connected networks of excitatory and inhibitory spiking neurons. J.Comput.Neurosci. *8*, 183–208.

Brunel, N., and Hakim, V. (1999). Fast global oscillations in networks of integrate-and-fire neurons with low firing rates. Neural Comput. *11*, 1621–1671.

Brunel, N., and Hakim, V. (2008). Sparsely synchronized neuronal oscillations. Chaos. *18*, 015113.

Brunel, N., and Hansel, D. (2006). How noise affects the synchronization properties of recurrent networks of inhibitory neurons. Neural Comput. *18*, 1066–1110.

Brunel, N., and Wang, X.J. (2003). What determines the frequency of fast network oscillations with irregular neural discharges? I. Synaptic dynamics and excitation-inhibition balance. J.Neurophysiol. *90*, 415–430.

Buehlmann, A., and Deco, G. (2008). The Neuronal Basis of Attention: Rate versus Synchronization Modulation. J. Neurosci. *28*, 7679–7686.

Burgess, N., Barry, C., and O'Keefe, J. (2007). An oscillatory interference model of grid cell firing. Hippocampus *17*, 801–812.

Busch, N.A., Dubois, J., and VanRullen, R. (2009). The phase of ongoing EEG oscillations predicts visual perception. The Journal of Neuroscience *29*, 7869.

Buzsáki, G. (2002). Theta oscillations in the hippocampus. Neuron *33*, 325–340.

Buzsaki, G., and Draguhn, A. (2004). Neuronal oscillations in cortical networks. Science *304*, 1926–1929.

Campbell, S., and DeLiang Wang (1996). Synchronization and desynchronization in a network of locally coupled Wilson-Cowan oscillators. Neural Networks, IEEE Transactions On *7*, 541–554.

Cantero, J.L., Atienza, M., Stickgold, R., Kahana, M.J., Madsen, J.R., and Kocsis, B. (2003). Sleep-Dependent Θ Oscillations in the Human Hippocampus and Neocortex. The Journal of Neuroscience *23*, 10897–10903.

Carandini, M., Demb, J.B., Mante, V., Tolhurst, D.J., Dan, Y., Olshausen, B.A., Gallant, J.L., and Rust, N.C. (2005). Do we know what the early visual system does? Journal of Neuroscience *25*, 10577.

Carandini, M., Heeger, D.J., and Movshon, J.A. (1997). Linearity and normalization in simple cells of the macaque primary visual cortex. The Journal of Neuroscience *17*, 8621.

Cardin, J.A., Carlén, M., Meletis, K., Knoblich, U., Zhang, F., Deisseroth, K., Tsai, L.-H., and Moore, C.I. (2009). Driving fast-spiking cells induces gamma rhythm and controls sensory responses. Nature *459*, 663–667.

Castelo-Branco, M., Neuenschwander, S., and Singer, W. (1998). Synchronization of Visual Responses between the Cortex, Lateral Geniculate Nucleus, and Retina in the Anesthetized Cat. The Journal of Neuroscience *18*, 6395–6410.

Chalk, M., Herrero, J.L., Gieselmann, M.A., Delicato, L.S., Gotthardt, S., and Thiele, A. (2010). Attention Reduces Stimulus-Driven Gamma Frequency Oscillations and Spike Field Coherence in V1. Neuron *66*, 114–125.

Chance, F.S., Abbott, L.F., and Reyes, A.D. (2002). Gain Modulation from Background Synaptic Input. Neuron *35*, 773–782.

Chu, Z., Galarreta, M., and Hestrin, S. (2003). Synaptic interactions of late-spiking neocortical neurons in layer 1. Journal of Neuroscience *23*, 96.

Cole, A.E., and Nicoll, R.A. (1984). Characterization of a slow cholinergic post-synaptic potential recorded in vitro from rat hippocampal pyramidal cells. The Journal of Physiology *352*, 173–188.

Colgin, L.L., Denninger, T., Fyhn, M., Hafting, T., Bonnevie, T., Jensen, O., Moser, M.B., and Moser, E.I. (2009). Frequency of gamma oscillations routes flow of information in the hippocampus. Nature *462*, 353–357.

Collins, C.E., Airey, D.C., Young, N.A., Leitch, D.B., and Kaas, J.H. (2010). Neuron densities vary across and within cortical areas in primates. Proceedings of the National Academy of Sciences *107*, 15927–15932.

Contreras, D., Timofeev, I., and Steriade, M. (1996). Mechanisms of long-lasting hyperpolarizations underlying slow sleep oscillations in cat corticothalamic networks. The Journal of Physiology *494*, 251.

Coombes, S. (2010). Large-scale neural dynamics: Simple and complex. NeuroImage *52*, 731–739.

Courtemanche, R., and Lamarre, Y. (2005). Local Field Potential Oscillations in Primate Cerebellar Cortex: Synchronization With Cerebral Cortex During Active and Passive Expectancy. Journal of Neurophysiology *93*, 2039–2052.

Courtemanche, R., Fujii, N., and Graybiel, A.M. (2003). Synchronous, Focally Modulated β-Band Oscillations Characterize Local Field Potential Activity in the Striatum of Awake Behaving Monkeys. The Journal of Neuroscience *23*, 11741–11752.

Courtemanche, R., Pellerin, J.-P., and Lamarre, Y. (2002). Local Field Potential Oscillations in Primate Cerebellar Cortex: Modulation During Active and Passive Expectancy. Journal of Neurophysiology *88*, 771–782.

Cover, T.M., Thomas, J.A., Wiley, J., and others (1991). Elements of information theory (Wiley Online Library).

Crick, F., and Koch, C. (1990). Some reflections on visual awareness. In Cold Spring Harb Symp Quant Biol, pp. 953–962.

Crunelli, V., and Hughes, S.W. (2010). The slow (<1 Hz) rhythm of non-REM sleep: a dialogue between three cardinal oscillators. Nat Neurosci *13*, 9–17.

Csicsvari, J., Jamieson, B., Wise, K.D., and Buzsaki, G. (2003). Mechanisms of gamma oscillations in the hippocampus of the behaving rat. Neuron *37*, 311–322.

Czurko, A., Huxter, J., Li, Y., Hangya, B., and Muller, R.U. (2011). Theta Phase Classification of Interneurons in the Hippocampal Formation of Freely Moving Rats. J. Neurosci. *31*, 2938–2947.

Dan, Y., and Poo, M.-ming (2004). Spike Timing-Dependent Plasticity of Neural Circuits. Neuron *44*, 23–30.

Darvas, F., Pantazis, D., Kucukaltun-Yildirim, E., and Leahy, R.M. (2004). Mapping human brain function with MEG and EEG: methods and validation. Neuroimage *23*, S289–S299.

Dayan, P., and Abbott, L.F. (2001). Theoretical neuroscience: Computational and mathematical modeling of neural systems.

Dayan, P., and Solomon, J.A. (2010). Selective Bayes: Attentional load and crowding. Vision Research.

Dayan, P., Kakade, S., and Montague, P.R. (2000). Learning and selective attention. Nature Neuroscience *3*, 1218–1223.

Debener, S., Herrmann, C.S., Kranczioch, C., Gembris, D., and Engel, A.K. (2003). Top-down attentional processing enhances auditory evoked gamma band activity. Neuroreport *14*, 683.

deCharms, R.C., and Zador, A. (2000). Neural Representation and the Cortical Code. Annu. Rev. Neurosci. *23*, 613–647.

Deco, G., Jirsa, V.K., Robinson, P.A., Breakspear, M., and Friston, K. (2008). The dynamic brain: from spiking neurons to neural masses and cortical fields. PLoS Computational Biology *4*, e1000092.

DeCoteau, W.E., Thorn, C., Gibson, D.J., Courtemanche, R., Mitra, P., Kubota, Y., and Graybiel, A.M. (2007). Learning-related coordination of striatal and hippocampal theta rhythms during acquisition of a procedural maze task. Proceedings of the National Academy of Sciences *104*, 5644–5649.

Deneve, S., Latham, P.E., and Pouget, A. (1999). Reading population codes: a neural implementation of ideal observers. Nat. Neurosci *2*, 740–745.

Deneve, S., Latham, P.E., and Pouget, A. (2001). Efficient computation and cue integration with noisy population codes. Nat Neurosci *4*, 826–831.

Von Der Malsburg, C. (1981). The correlation theory of brain function.

Desimone, R. (1998). Visual attention mediated by biased competition in extrastriate visual cortex. Philosophical Transactions of the Royal Society of London. Series B: Biological Sciences *353*, 1245.

Desimone, R., and Duncan, J. (1995). Neural mechanisms of selective visual attention. Annual Review of Neuroscience *18*, 193–222.

Destexhe, A., Hughes, S.W., Rudolph, M., and Crunelli, V. (2007). Are corticothalamic up states fragments of wakefulness? TRENDS in Neurosciences *30*, 334–342.

Destexhe, A., Rudolph, M., and Pare, D. (2003). The high-conductance state of neocortical neurons in vivo. Nat Rev Neurosci *4*, 739–751.

Diesmann, M., Gewaltig, M.O., and Aertsen, A. (1999). Stable propagation of synchronous spiking in cortical neural networks. Nature *402*, 529–533.

Van Dijk, H., Nieuwenhuis, I.L.., and Jensen, O. (2010). Left temporal alpha band activity increases during working memory retention of pitches. European Journal of Neuroscience *31*, 1701–1707.

Dong, Y., Mihalas, S., Qiu, F., von der Heydt, R., and Niebur, E. (2008). Synchrony and the binding problem in macaque visual cortex. Journal of Vision *8*,.

Donoghue, J.P., Sanes, J.N., Hatsopoulos, N.G., and Gaál, G. (1998). Neural discharge and local field potential oscillations in primate motor cortex during voluntary movements. J. Neurophysiol *79*, 159–173.

Driver, J. (2001). A selective review of selective attention research from the past century. British Journal of Psychology *92*, 53–78.

Duncan, J. (1980). The locus of interference in the perception of simultaneous stimuli. Psychological Review *87*, 272–300.

Eckhorn, R., Bauer, R., Jordan, W., Brosch, M., Kruse, W., Munk, M., and Reitboeck, H.J. (1988). Coherent oscillations: A mechanism of feature linking in the visual cortex? Biological Cybernetics *60*, 121–130.

van Ede, F., de Lange, F., Jensen, O., and Maris, E. (2011). Orienting Attention to an Upcoming Tactile Event Involves a Spatially and Temporally Specific Modulation of Sensorimotor Alpha- and Beta-Band Oscillations. The Journal of Neuroscience *31*, 2016–2024.

Ekstrom, A.D., Caplan, J.B., Ho, E., Shattuck, K., Fried, I., and Kahana, M.J. (2005). Human hippocampal theta activity during virtual navigation. Hippocampus *15*, 881–889.

Ekstrom, L.B., Roelfsema, P.R., Arsenault, J.T., Bonmassar, G., and Vanduffel, W. (2008). Bottom-Up Dependent Gating of Frontal Signals in Early Visual Cortex. Science *321*, 414–417.

Elhilali, M., Fritz, J.B., Klein, D.J., Simon, J.Z., and Shamma, S.A. (2004). Dynamics of Precise Spike Timing in Primary Auditory Cortex. The Journal of Neuroscience *24*, 1159–1172.

van Elswijk, G., Maij, F., Schoffelen, J.M., Overeem, S., Stegeman, D.F., and Fries, P. (2010). Corticospinal Beta-Band Synchronization Entails Rhythmic Gain Modulation. Journal of Neuroscience *30*, 4481.

Ermentrout, B. (1996). Type I membranes, phase resetting curves, and synchrony. Neural Comput. *8*, 979–1001.

Ermentrout, G.B., and Kopell, N. (1984). Frequency Plateaus in a Chain of Weakly Coupled Oscillators, I. SIAM J. Math. Anal. *15*, 215.

Fellous, J.M., Tiesinga, P.H.., Thomas, P.J., and Sejnowski, T.J. (2004). Discovering spike patterns in neuronal responses. The Journal of Neuroscience *24*, 2989.

Fisahn, A., Pike, F.G., Buhl, E.H., and Paulsen, O. (1998). Cholinergic induction of network oscillations at 40 Hz in the hippocampus in vitro. Nature *394*, 186–189.

Fisher, N.I., and Lee, A.K. (1983). A correlation coefficient for circular data. Biometrika *70*, 327–332.

Fourcaud-Trocme, N., Hansel, D., van Vreeswijk, C., and Brunel, N. (2003). How Spike Generation Mechanisms Determine the Neuronal Response to Fluctuating Inputs. J. Neurosci. *23*, 11628–11640.

Freeman, W. (2007). Hilbert transform for brain waves. Scholarpedia *2*, 1338.

Freeman, W.J., Rogers, L.J., Holmes, M.D., and Silbergeld, D.L. (2000). Spatial spectral analysis of human electrocorticograms including the alpha and gamma bands. Journal of Neuroscience Methods *95*, 111–121.

Friedman-Hill, S., Maldonado, P.E., and Gray, C.M. (2000). Dynamics of striate cortical activity in the alert macaque: I. Incidence and stimulus-dependence of gamma-band neuronal oscillations. Cerebral Cortex *10*, 1105.

Friedrich, R.W., Habermann, C.J., and Laurent, G. (2004). Multiplexing using synchrony in the zebrafish olfactory bulb. Nature Neuroscience *7*, 862–871.

Fries, P. (2005). A mechanism for cognitive dynamics: neuronal communication through neuronal coherence. Trends Cogn Sci. *9*, 474–480.

Fries, P. (2009). Neuronal Gamma-Band Synchronization as a Fundamental Process in Cortical Computation. Annu. Rev. Neurosci. *32*, 209–224.

Fries, P., Nikolić, D., and Singer, W. (2007). The gamma cycle. Trends in Neurosciences *30*, 309–316.

Fries, P., Reynolds, J.H., Rorie, A.E., and Desimone, R. (2001). Modulation of oscillatory neuronal synchronization by selective visual attention. Science *291*, 1560–1563.

Fries, P., Roelfsema, P.R., Engel, A.K., K\önig, P., and Singer, W. (1997). Synchronization of oscillatory responses in visual cortex correlates with perception in interocular rivalry. Proceedings of the National Academy of Sciences of the United States of America *94*, 12699.

Fries, P., Womelsdorf, T., Oostenveld, R., and Desimone, R. (2008). The Effects of Visual Stimulation and Selective Visual Attention on Rhythmic Neuronal Synchronization in Macaque Area V4. J. Neurosci. *28*, 4823–4835.

Fuster, J.M., and Alexander, G.E. (1971). Neuron activity related to short-term memory. Science *173*, 652.

Geisler, C., Brunel, N., and Wang, X.J. (2005). Contributions of intrinsic membrane dynamics to fast network oscillations with irregular neuronal discharges. J.Neurophysiol. *94*, 4344–4361.

Geisler, C., Robbe, D., Zugaro, M., SIROTA, A., and Buzsáki, G. (2007). Hippocampal place cell assemblies are speed-controlled oscillators. Proceedings of the National Academy of Sciences *104*, 8149–8154.

Georgopoulos, A.P., Kalaska, J.F., Caminiti, R., and Massey, J.T. (1982). On the relations between the direction of two-dimensional arm movements and cell discharge in primate motor cortex. The Journal of Neuroscience *2*, 1527.

Gewaltig, M.-O., and Diesmann, M. (2007). NEST (Neural Simulation Tool). Scholarpedia *2*, 1430.

Gieselmann, M.A., and Thiele, A. (2008). Comparison of spatial integration and surround suppression characteristics in spiking activity and the local field potential in macaque V1. European Journal of Neuroscience *28*, 447–459.

Goldman-Rakic, P.S. (1995). Cellular basis of working memory. Neuron *14*, 477–485.

Golomb, D., and Rinzel, J. (1994). Clustering in globally coupled inhibitory neurons. Physica D: Nonlinear Phenomena *72*, 259–282.

Goodman, D.F.M., and Brette, R. (2009). The Brian simulator. Front. Neurosci. *3*, 192–197.

Goutagny, R., Jackson, J., and Williams, S. (2009). Self-generated theta oscillations in the hippocampus. Nature Neuroscience *12*, 1491–1493.

Gray, C.M. (1999). The Temporal Correlation Hypothesis Review of Visual Feature Integration: Still Alive and Well. Neuron *24*, 31–47.

Gray, C.M., and Singer, W. (1989). Stimulus-specific neuronal oscillations in orientation columns of cat visual cortex. Proceedings of the National Academy of Sciences of the United States of America *86*, 1698.

Gray, C.M., König, P., Engel, A.K., and Singer, W. (1989). Oscillatory responses in cat visual cortex exhibit inter-columnar synchronization which reflects global stimulus properties. Nature *338*, 334–337.

Gregoriou, G.G., Gotts, S.J., Zhou, H., and Desimone, R. (2009). High-Frequency, Long-Range Coupling Between Prefrontal and Visual Cortex During Attention. Science *324*, 1207–1210.

Groenewegen, H.J., der Zee, E.V.-V., te Kortschot, A., and Witter, M.P. (1987). Organization of the projections from the subiculum to the ventral striatum in the rat. A study using anterograde transport of Phaseolus vulgaris leucoagglutinin. Neuroscience *23*, 103–120.

Gross, J., Kujala, J., Hämäläinen, M., Timmermann, L., Schnitzler, A., and Salmelin, R. (2001). Dynamic imaging of coherent sources: Studying neural interactions in the human brain. Proceedings of the National Academy of Sciences *98*, 694–699.

Gross, J., Schmitz, F., Schnitzler, I., Kessler, K., Shapiro, K., Hommel, B., and Schnitzler, A. (2004). Modulation of long-range neural synchrony reflects temporal limitations of visual attention in humans. Proc Natl Acad Sci U S A *101*, 13050–13055.

Gruber, T., Müller, M.M., Keil, A., and Elbert, T. (1999). Selective visual-spatial attention alters induced gamma band responses in the human EEG. Clinical Neurophysiology *110*, 2074–2085.

Hafting, T., Fyhn, M., Bonnevie, T., Moser, M.-B., and Moser, E.I. (2008). Hippocampus-independent phase precession in entorhinal grid cells. Nature *453*, 1248–1252.

Haider, B., Duque, A., Hasenstaub, A.R., and McCormick, D.A. (2006). Neocortical Network Activity In Vivo Is Generated through a Dynamic Balance of Excitation and Inhibition. J. Neurosci. *26*, 4535–4545.

Hajos, N., Palhalmi, J., Mann, E.O., Nemeth, B., Paulsen, O., and Freund, T.F. (2004). Spike timing of distinct types of GABAergic interneuron during hippocampal gamma oscillations in vitro. J.Neurosci. *24*, 9127–9137.

Hansel, D., and van Vreeswijk, C. (2002). How Noise Contributes to Contrast Invariance of Orientation Tuning in Cat Visual Cortex. The Journal of Neuroscience *22*, 5118–5128.

Hansel, D., Mato, G., and Meunier, C. (1995). Synchrony in excitatory neural networks. Neural Comput. *7*, 307–337.

Harris, K.D., Henze, D.A., Hirase, H., Leinekugel, X., Dragoi, G., Czurko, A., and Buzsáki, G. (2002). Spike train dynamics predicts theta-related phase precession in hippocampal pyramidal cells. Nature *417*, 738–741.

Harvey, C.D., Collman, F., Dombeck, D.A., and Tank, D.W. (2009). Intracellular dynamics of hippocampal place cells during virtual navigation. Nature *461*, 941–946.

Hasenstaub, A., Shu, Y., Haider, B., Kraushaar, U., Duque, A., and McCormick, D.A. (2005). Inhibitory Postsynaptic Potentials Carry Synchronized Frequency Information in Active Cortical Networks. Neuron *47*, 423–435.

Häusser, M., Spruston, N., and Stuart, G.J. (2000). Diversity and Dynamics of Dendritic Signaling. Science *290*, 739–744.

Heil, P., and Irvine, D.R.F. (1997). First-Spike Timing of Auditory-Nerve Fibers and Comparison With Auditory Cortex. Journal of Neurophysiology *78*, 2438–2454.

Henrie, J.A., and Shapley, R. (2005). LFP power spectra in V1 cortex: the graded effect of stimulus contrast. J.Neurophysiol. *94*, 479–490.

Henry, G.H., Dreher, B., and Bishop, P.O. (1974). Orientation specificity of cells in cat striate cortex. Journal of Neurophysiology *37*, 1394.

Henze, D.A., Wittner, L., and Buzsáki, G. (2002). Single granule cells reliably discharge targets in the hippocampal CA3 network in vivo. Nat Neurosci *5*, 790–795.

Herrmann, C.S. (2001). Human EEG responses to 1–100 Hz flicker: resonance phenomena in visual cortex and their potential correlation to cognitive phenomena. Experimental Brain Research *137*, 346–353.

Hestrin, S., and Galarreta, M. (2005). Electrical synapses define networks of neocortical GABAergic neurons. Trends in Neurosciences *28*, 304–309.

Hipp, J.F., Engel, A.K., and Siegel, M. (2011). Oscillatory Synchronization in Large-Scale Cortical Networks Predicts Perception. Neuron *69*, 387–396.

Holt, G.R., and Koch, C. (1999). Electrical interactions via the extracellular potential near cell bodies. Journal of Computational Neuroscience *6*, 169–184.

Hô, N., and Destexhe, A. (2000). Synaptic Background Activity Enhances the Responsiveness of Neocortical Pyramidal Neurons. Journal of Neurophysiology *84*, 1488–1496.

Horton, J.C., and Adams, D.L. (2005). The cortical column: a structure without a function. Philosophical Transactions of the Royal Society B: Biological Sciences *360*, 837–862.

Hubel, D.H., and Wiesel, T.N. (1962). Receptive fields, binocular interaction and functional architecture in the cat's visual cortex. The Journal of Physiology *160*, 106.

Huerta, P.T., and Lisman, J.E. (1993). Heightened synaptic plasticity of hippocampal CA1 neurons during a cholinergically induced rhythmic state. Nature.

Hughes, S.W., and Crunelli, V. (2005). Thalamic Mechanisms of EEG Alpha Rhythms and Their Pathological Implications. The Neuroscientist *11*, 357–372.

Humphries, M.D. (2011). Spike-Train Communities: Finding Groups of Similar Spike Trains. J. Neurosci. *31*, 2321–2336.

Huxter, J., Burgess, N., and O'Keefe, J. (2003). Independent rate and temporal coding in hippocampal pyramidal cells. Nature *425*, 828–832.

Huxter, J.R., Senior, T.J., Allen, K., and Csicsvari, J. (2008). Theta phase-specific codes for two-dimensional position, trajectory and heading in the hippocampus. Nat Neurosci *11*, 587–594.

Hyman, J.M., Zilli, E.A., Paley, A.M., and Hasselmo, M.E. (2005). Medial prefrontal cortex cells show dynamic modulation with the hippocampal theta rhythm dependent on behavior. Hippocampus *15*, 739–749.

Izhikevich, E.M. (2006). Polychronization: computation with spikes. Neural Comput. *18*, 245–282.

Izhikevich, E.M. (2007). Synchronization. In Dynamical Systems in Neuroscience: The Geometry of Excitability and Bursting, (The MIT press), pp. 443–505.

Jarvis, M.R., and Mitra, P.P. (2011). Sampling Properties of the Spectrum and Coherency of Sequences of Action Potentials. Neural Computation *13*, 717–749.

Jeewajee, A., Lever, C., Burton, S., O'Keefe, J., and Burgess, N. (2008). Environmental novelty is signaled by reduction of the hippocampal theta frequency. Hippocampus *18*, 340–348.

Jensen, O. (2001). Information transfer between rhythmically coupled networks: reading the hippocampal phase code. Neural Computation *13*, 2743–2761.

Jensen, O., Gelfand, J., Kounios, J., and Lisman, J.E. (2002). Oscillations in the alpha band (9–12 Hz) increase with memory load during retention in a short-term memory task. Cerebral Cortex *12*, 877.

Jensen, O., Kaiser, J., and Lachaux, J.P. (2007). Human gamma-frequency oscillations associated with attention and memory. Trends in Neurosciences *30*, 317–324.

Jonas, P., Bischofberger, J., Fricker, D., and Miles, R. (2004). Interneuron Diversity series: Fast in, fast out - temporal and spatial signal processing in hippocampal interneurons. Trends in Neurosciences *27*, 30–40.

Jones, M.W., and Wilson, M.A. (2005a). Phase precession of medial prefrontal cortical activity relative to the hippocampal theta rhythm. Hippocampus *15*, 867–873.

Jones, M.W., and Wilson, M.A. (2005b). Theta Rhythms Coordinate Hippocampal–Prefrontal Interactions in a Spatial Memory Task. PLoS Biol *3*, e402.

Jones, S.R., Kerr, C.E., Wan, Q., Pritchett, D.L., H\äm\äl\äinen, M., and Moore, C.I. (2010). Cued spatial attention drives functionally relevant modulation of the mu rhythm in primary somatosensory cortex. The Journal of Neuroscience *30*, 13760.

Jutras, M.J., Fries, P., and Buffalo, E.A. (2009). Gamma-band synchronization in the macaque hippocampus and memory formation. The Journal of Neuroscience *29*, 12521.

Kahana, M.J. (2006). The Cognitive Correlates of Human Brain Oscillations. The Journal of Neuroscience *26*, 1669–1672.

Kahana, M.J., Sekuler, R., Caplan, J.B., Kirschen, M., and Madsen, J.R. (1999). Human theta oscillations exhibit task dependence during virtual maze navigation. Nature *399*, 781–784.

Katzner, S., Nauhaus, I., Benucci, A., Bonin, V., Ringach, D.L., and Carandini, M. (2009). Local Origin of Field Potentials in Visual Cortex. Neuron *61*, 35–41.

Kawaguchi, Y. (1997). Selective Cholinergic Modulation of Cortical GABAergic Cell Subtypes. Journal of Neurophysiology *78*, 1743–1747.

Kayser, C., Logothetis, N.K., and Panzeri, S. (2010). Millisecond encoding precision of auditory cortex neurons. Proceedings of the National Academy of Sciences *107*, 16976–16981.

Kayser, C., Montemurro, M.A., Logothetis, N.K., and Panzeri, S. (2009). Spike-Phase Coding Boosts and Stabilizes Information Carried by Spatial and Temporal Spike Patterns. *61*, 597–608.

Klausberger, T., Magill, P.J., Márton, L.F., Roberts, J.D.., Cobden, P.M., Buzsáki, G., and Somogyi, P. (2003). Brain-state-and cell-type-specific firing of hippocampal interneurons in vivo. Nature *421*, 844–848.

Klimesch, W. (1996). Memory processes, brain oscillations and EEG synchronization. International Journal of Psychophysiology *24*, 61–100.

Klimesch, W., Doppelmayr, M., Schwaiger, J., Auinger, P., and Winkler, T. (1999). Paradoxical alpha synchronization in a memory task. Cognitive Brain Research *7*, 493–501.

Klimesch, W., Sauseng, P., and Hanslmayr, S. (2007). EEG alpha oscillations: the inhibition-timing hypothesis. Brain Research Reviews *53*, 63–88.

Knutson, B., Delgado, M.R., and Phillips, P.E.. (2008). Representation of Subjective Valuein the Striatum. In Neuroeconomics: Decision Making and the Brain, (Elsevier), pp. 389–406.

König, P., and Schillen, T.B. (1991). Stimulus-Dependent Assembly Formation of Oscillatory Responses: I. Synchronization. Neural Computation *3*, 155–166.

König, P., Engel, A.K., and Singer, W. (1996). Integrator or coincidence detector? The role of the cortical neuron revisited. Trends Neurosci. *19*, 130–137.

Kopell, N., Ermentrout, G.B., Whittington, M.A., and Traub, R.D. (2000). Gamma rhythms and beta rhythms have different synchronization properties. Proc. Natl. Acad. Sci. U.S.A *97*, 1867–1872.

de La Rocha, J., Doiron, B., Eric Shea-Brown, K.J., and Reyes, A. (2007). Correlation between neural spike trains increases with firing rate. Nature *448*, 802–806.

Lakatos, P., Shah, A.S., Knuth, K.H., Ulbert, I., Karmos, G., and Schroeder, C.E. (2005). An Oscillatory Hierarchy Controlling Neuronal Excitability and Stimulus Processing in the Auditory Cortex. Journal of Neurophysiology *94*, 1904–1911.

Lamme, V.A.F., and Spekreijse, H. (1998). Neuronal synchrony does not represent texture segregation. Nature *396*, 362–366.

Latham, P.E., Deneve, S., and Pouget, A. (2003). Optimal computation with attractor networks. Journal of Physiology *97*, 683–694.

Latham, P.E., Richmond, B.J., Nelson, P.G., and Nirenberg, S. (2000). Intrinsic Dynamics in Neuronal Networks. I. Theory. J Neurophysiol *83*, 808–827.

LeBeau, F.E.N., Traub, R.D., Monyer, H., Whittington, M.A., and Buhl, E.H. (2003). The role of electrical signaling via gap junctions in the generation of fast network oscillations. Brain Research Bulletin *62*, 3–13.

Ledoux, E., and Brunel, N. (2011). Dynamics of Networks of Excitatory and Inhibitory Neurons in Response to Time-Dependent Inputs. Front Comput Neurosci.

LeDoux, J.E. (2000). Emotion circuits in the brain. Annu. Rev. Neurosci *23*, 155–184.

Lee, H., Simpson, G.V., Logothetis, N.K., and Rainer, G. (2005). Phase Locking of Single Neuron Activity to Theta Oscillations during Working Memory in Monkey Extrastriate Visual Cortex. Neuron *45*, 147–156.

Lee, J.H., Durand, R., Gradinaru, V., Zhang, F., Goshen, I., Kim, D.S., Fenno, L.E., Ramakrishnan, C., and Deisseroth, K. (2010). Global and local fMRI signals driven by neurons defined optogenetically by type and wiring. Nature *465*, 788–792.

Leiberg, S., Lutzenberger, W., and Kaiser, J. (2006). Effects of memory load on cortical oscillatory activity during auditory pattern working memory. Brain Research *1120*, 131–140.

Lengyel, M., Szatmáry, Z., and Érdi, P. (2003). Dynamically detuned oscillations account for the coupled rate and temporal code of place cell firing. Hippocampus *13*, 700–714.

Lennie, P. (2003). The Cost of Cortical Computation. Current Biology *13*, 493–497.

Lepage, K.Q., Kramer, M.A., and Eden, U.T. (2011). The Dependence of Spike Field Coherence on Expected Intensity. Neural Computation 1–33.

Levi, D.M. (2008). Crowding–an essential bottleneck for object recognition: A mini-review. Vision Research *48*, 635–654.

Lima, B., Singer, W., Chen, N.-H., and Neuenschwander, S. (2010). Synchronization Dynamics in Response to Plaid Stimuli in Monkey V1. Cerebral Cortex *20*, 1556–1573.

Lindén, H., Pettersen, K.H., and Einevoll, G.T. (2010a). Intrinsic dendritic filtering gives low-pass power spectra of local field potentials. Journal of Computational Neuroscience 1–22.

Lindén, H., Pettersen, K.H., and Einevoll, G.T. (2010b). Intrinsic dendritic filtering gives low-pass power spectra of local field potentials. J Comput Neurosci *29*, 423–444.

Lindner, B. (2004). Effects of noise in excitable systems. Physics Reports *392*, 321–424.

Lindner, B., Longtin, A., and Bulsara, A. (2003). Analytic Expressions for Rate and CV of a Type I Neuron Driven by White Gaussian Noise. Neural Computation *15*, 1761–1788.

Logothetis, N.K., Pauls, J., Augath, M., Trinath, T., and Oeltermann, A. (2001). Neurophysiological investigation of the basis of the fMRI signal. Nature *412*, 150–157.

London, M., Roth, A., Beeren, L., Häusser, M., and Latham, P.E. (2010). Sensitivity to perturbations in vivo implies high noise and suggests rate coding in cortex. Nature *466*, 123–127.

Lorincz, M.L., Kékesi, K.A., Juhász, G., Crunelli, V., and Hughes, S.W. (2009). Temporal Framing of Thalamic Relay-Mode Firing by Phasic Inhibition during the Alpha Rhythm. Neuron *63*, 683–696.

Losonczy, A., Zemelman, B.V., Vaziri, A., and Magee, J.C. (2010). Network mechanisms of theta related neuronal activity in hippocampal CA1 pyramidal neurons. Nat Neurosci *13*, 967–972.

Lubenov, E.V., and Siapas, A.G. (2009). Hippocampal theta oscillations are travelling waves. Nature *459*, 534–539.

Luck, S.J., Chelazzi, L., Hillyard, S.A., and Desimone, R. (1997). Neural mechanisms of spatial selective attention in areas V1, V2, and V4 of macaque visual cortex. Journal of Neurophysiology *77*, 24.

MacKay, W.A. (1997). Synchronized neuronal oscillations and their role in motor processes. Trends in Cognitive Sciences *1*, 176–183.

Mackintosh, N.J. (1975). A theory of attention: Variations in the associability of stimuli with reinforcement. Psychological Review *82*, 276.

Mann, E.O., Kohl, M.M., and Paulsen, O. (2009). Distinct Roles of GABAA and GABAB Receptors in Balancing and Terminating Persistent Cortical Activity. The Journal of Neuroscience *29*, 7513–7518.

Mann, E.O., Suckling, J.M., Hajos, N., Greenfield, S.A., and Paulsen, O. (2005). Perisomatic feedback inhibition underlies cholinergically induced fast network oscillations in the rat hippocampus in vitro. Neuron *45*, 105–117.

Markram, H. (2006). The blue brain project. Nature Reviews Neuroscience *7*, 153–160.

Marr, D., and Poggio, T. (1976). From understanding computation to understanding neural circuitry. AIM-357.

Masuda, N. (2009). Selective Population Rate Coding: A Possible Computational Role of Gamma Oscillations in Selective Attention. Neural Computation 1–28.

Mathewson, K.E., Gratton, G., Fabiani, M., Beck, D.M., and Ro, T. (2009). To see or not to see: prestimulus α phase predicts visual awareness. The Journal of Neuroscience *29*, 2725.

Maurer, A.P., Cowen, S.L., Burke, S.N., Barnes, C.A., and McNaughton, B.L. (2006). Phase Precession in Hippocampal Interneurons Showing Strong Functional Coupling to Individual Pyramidal Cells. The Journal of Neuroscience *26*, 13485–13492.

Ma, W.J., Beck, J.M., Latham, P.E., and Pouget, A. (2006). Bayesian inference with probabilistic population codes. Nat Neurosci *9*, 1432–1438.

Mazzoni, A., Panzeri, S., Logothetis, N.K., and Brunel, N. (2008). Encoding of Naturalistic Stimuli by Local Field Potential Spectra in Networks of Excitatory and Inhibitory Neurons. PLoS Comput Biol *4*,.

McAdams, C.J., and Maunsell, J.H.R. (1999). Effects of Attention on Orientation-Tuning Functions of Single Neurons in Macaque Cortical Area V4. The Journal of Neuroscience *19*, 431–441.

McGeorge, A.J., and Faull, R.L.M. (1989). The organization of the projection from the cerebral cortex to the striatum in the rat. Neuroscience *29*, 503–537.

Meador, K.J., Thompson, J.L., Loring, D.W., Murro, A.M., King, D.W., Gallagher, B.B., Lee, G.P., Smith, J.R., and Flanigin, H.F. (1991). Behavioral state-specific changes in human hippocampal theta activity. Neurology *41*, 869.

van der Meer, M.A.A., and Redish, A.D. (2009). Low and High Gamma Oscillations in Rat Ventral Striatum have Distinct Relationships to Behavior, Reward, and Spiking Activity on a Learned Spatial Decision Task. Front Integr Neurosci *3*,.

van der Meer, M.A.A., and Redish, A.D. (2011). Theta Phase Precession in Rat Ventral Striatum Links Place and Reward Information. J. Neurosci. *31*, 2843–2854.

Mehring, C., Hehl, U., Kubo, M., Diesmann, M., and Aertsen, A. (2003). Activity dynamics and propagation of synchronous spiking in locally connected random networks. Biological Cybernetics *88*, 395–408.

Mehta, M.R., Lee, A.K., and Wilson, M.A. (2002). Role of experience and oscillations in transforming a rate code into a temporal code. Nature *417*, 741–746.

Milner, P.M. (1974). A model for visual shape recognition. Psychological Review *81*, 521.

Mishra, J., Fellous, J.-M., and Sejnowski, T.J. (2006). Selective attention through phase relationship of excitatory and inhibitory input synchrony in a model cortical neuron. Neural Netw *19*, 1329–1346.

Mitchell, S.J., and Silver, R.A. (2003). Shunting inhibition modulates neuronal gain during synaptic excitation. Neuron *38*, 433–445.

Mo, J., Schroeder, C.E., and Ding, M. (2011). Attentional Modulation of Alpha Oscillations in Macaque Inferotemporal Cortex. The Journal of Neuroscience *31*, 878–882.

Montemurro, M.A., Rasch, M.J., Murayama, Y., Logothetis, N.K., and Panzeri, S. (2008). Phase-of-firing coding of natural visual stimuli in primary visual cortex. Current Biology *18*, 375–380.

Moore, T., and Armstrong, K.M. (2003). Selective gating of visual signals by microstimulation of frontal cortex. Nature *421*, 370–373.

Moran, and Desimone, R. (1985). Selective attention gates visual processing in the extrastriate cortex. Science *229*, 782–784.

Mori, M., Abegg, M.H., Gahwiler, B.H., and Gerber, U. (2004). A frequency-dependent switch from inhibition to excitation in a hippocampal unitary circuit. Nature *431*, 453–456.

Motter, B.C. (1993). Focal attention produces spatially selective processing in visual cortical areas V1, V2, and V4 in the presence of competing stimuli. Journal of Neurophysiology *70*, 909.

Mountcastle, V.B. (1997). The columnar organization of the neocortex. Brain *120*, 701–722.

Muller, R. (1996). A quarter of a century of place cells. Neuron *17*, 813–822.

Murthy, V.N., and Fetz, E.E. (1992). Coherent 25- to 35-Hz oscillations in the sensorimotor cortex of awake behaving monkeys. Proceedings of the National Academy of Sciences *89*, 5670–5674.

Nadasdy, Z. (2009). Information Encoding and Reconstruction from the Phase of Action Potentials. Front Syst Neurosci *3*,.

Nadasdy, Z. (2010). Binding by asynchrony: the neuronal phase code. Front Neurosci *4*,.

Narayanan, R.T., Seidenbecher, T., Kluge, C., Bergado, J., Stork, O., and Pape, H. (2007). Dissociated theta phase synchronization in amygdalo- hippocampal circuits during various stages of fear memory. European Journal of Neuroscience *25*, 1823–1831.

Nicholson, C., and Freeman, J.A. (1975). Theory of current source-density analysis and determination of conductivity tensor for anuran cerebellum. Journal of Neurophysiology *38*, 356.

Niebur, E., Koch, C., and Rosin, C. (1993). An oscillation-based model for the neuronal basis of attention. Vision Research-oxford- *33*, 2789–2789.

Nir, Y., Mukamel, R., Dinstein, I., Privman, E., Harel, M., Fisch, L., Gelbard-Sagiv, H., Kipervasser, S., Andelman, F., Neufeld, M.Y., et al. (2008). Interhemispheric correlations of slow spontaneous neuronal fluctuations revealed in human sensory cortex. Nat Neurosci *11*, 1100–1108.

Nyquist, H. (1928). Certain topics in telegraph transmission theory. American Institute of Electrical Engineers, Transactions of The *47*, 617–644.

O'Connor, D.H., Peron, S.P., Huber, D., and Svoboda, K. (2010). Neural Activity in Barrel Cortex Underlying Vibrissa-Based Object Localization in Mice. Neuron *67*, 1048–1061.

O'Keefe, J. (1976). Place units in the hippocampus of the freely moving rat. Experimental Neurology *51*, 78–109.

O'Keefe, J., and Burgess, N. (1996). Geometric determinants of the place fields of hippocampal neurons. Nature *381*, 425–428.

O'Keefe, J., and Burgess, N. (2005). Dual phase and rate coding in hippocampal place cells: Theoretical significance and relationship to entorhinal grid cells. Hippocampus *15*, 853–866.

O'Keefe, J., and Dostrovsky, J. (1971). The hippocampus as a spatial map: Preliminary evidence from unit activity in the freely-moving rat. Brain Research.

O'Keefe, J., and Recce, M.L. (1993). Phase relationship between hippocampal place units and the EEG theta rhythm. Hippocampus *3*, 317–330.

Olshausen, B., Anderson, C., and Van Essen, D. (1993). A neurobiological model of visual attention and invariant pattern recognition based on dynamic routing of information. J. Neurosci. *13*, 4700–4719.

Oren, I., Mann, E.O., Paulsen, O., and Hajos, N. (2006). Synaptic currents in anatomically identified CA3 neurons during hippocampal gamma oscillations in vitro. J.Neurosci. *26*, 9923–9934.

Palva, S., and Palva, J.M. (2007). New vistas for [alpha]-frequency band oscillations. Trends in Neurosciences *30*, 150–158.

Panzeri, S., and Schultz, S.R. (2001). A Unified Approach to the Study of Temporal, Correlational, and Rate Coding. Neural Computation *13*, 1311–1349.

Panzeri, S., Brunel, N., Logothetis, N.K., and Kayser, C. (2010). Sensory neural codes using multiplexed temporal scales. Trends in Neurosciences *33*, 111–120.

Pape, H., Narayanan, R.T., Smid, J., Stork, O., and Seidenbecher, T. (2005). Theta activity in neurons and networks of the amygdala related to long-term fear memory. Hippocampus *15*, 874–880.

Paré, D., and Collins, D.R. (2000). Neuronal Correlates of Fear in the Lateral Amygdala: Multiple Extracellular Recordings in Conscious Cats. The Journal of Neuroscience *20*, 2701–2710.

Paré, D., Shink, E., Gaudreau, H., Destexhe, A., and Lang, E.J. (1998). Impact of spontaneous synaptic activity on the resting properties of cat neocortical pyramidal neurons in vivo. Journal of Neurophysiology *79*, 1450.

Pavlides, C., Greenstein, Y.J., Grudman, M., and Winson, J. (1988). Long-term potentiation in the dentate gyrus is induced preferentially on the positive phase of theta-rhythm. Brain Research *439*, 383–387.

Pelli, D.G. (2008). Crowding: a cortical constraint on object recognition. Current Opinion in Neurobiology *18*, 445–451.

Penttonen, M., Kamondi, A., Acsady, L., and Buzsaki, G. (1998). Gamma frequency oscillation in the hippocampus of the rat: intracellular analysis in vivo. Eur.J.Neurosci. *10*, 718–728.

Perez-Orive, J., Mazor, O., Turner, G.C., Cassenaer, S., Wilson, R.I., and Laurent, G. (2002). Oscillations and sparsening of odor representations in the mushroom body. Science *297*, 359.

Perkel, D.H., Gerstein, G.L., and Moore, G.P. (1967a). Neuronal Spike Trains and Stochastic Point Processes:: I. The Single Spike Train. Biophysical Journal *7*, 391–418.

Perkel, D.H., Gerstein, G.L., and Moore, G.P. (1967b). Neuronal Spike Trains and Stochastic Point Processes:: II. Simultaneous Spike Trains. Biophysical Journal *7*, 419–440.

Pesaran, B., Nelson, M.J., and Andersen, R.A. (2006). Dorsal premotor neurons encode the relative position of the hand, eye, and goal during reach planning. Neuron *51*, 125–134.

Pesaran, B., Nelson, M.J., and Andersen, R.A. (2008). Free choice activates a decision circuit between frontal and parietal cortex. Nature *453*, 406–409.

Pesaran, B., Pezaris, J.S., Sahani, M., Mitra, P.P., and Andersen, R.A. (2002). Temporal structure in neuronal activity during working memory in macaque parietal cortex. Nat.Neurosci. *5*, 805–811.

Pettersen, K.H., Hagen, E., and Einevoll, G.T. (2008). Estimation of population firing rates and current source densities from laminar electrode recordings. Journal of Computational Neuroscience *24*, 291–313.

Pfurtscheller, G. (2003). Induced oscillations in the alpha band: functional meaning. Epilepsia *44*, 2–8.

Pfurtscheller, G., and Lopes da Silva, F.H. (1999). Event-related EEG/MEG synchronization and desynchronization: basic principles. Clinical Neurophysiology *110*, 1842–1857.

Platt, M.L., and Glimcher, P.W. (1999). Neural correlates of decision variables in parietal cortex. Nature *400*, 233–238.

Popescu, A.T., Popa, D., and Pare, D. (2009). Coherent gamma oscillations couple the amygdala and striatum during learning. Nat Neurosci *12*, 801–807.

Quach, M., Brunel, N., and d' Alché-Buc, F. (2007). Estimating parameters and hidden variables in non-linear state-space models based on ODEs for biological networks inference. Bioinformatics *23*, 3209.

Rager, G., and Singer, W. (1998). The response of cat visual cortex to flicker stimuli of variable frequency. European Journal of Neuroscience *10*, 1856–1877.

Raghavachari, S., Kahana, M.J., Rizzuto, D.S., Caplan, J.B., Kirschen, M.P., Bourgeois, B., Madsen, J.R., and Lisman, J.E. (2001). Gating of Human Theta Oscillations by a Working Memory Task. The Journal of Neuroscience *21*, 3175–3183.

Raghavachari, S., Lisman, J.E., Tully, M., Madsen, J.R., Bromfield, E.B., and Kahana, M.J. (2006). Theta oscillations in human cortex during a working-memory task: evidence for local generators. Journal of Neurophysiology *95*, 1630.

Ray, S., and Maunsell, J.H.R. (2010). Differences in Gamma Frequencies across Visual Cortex Restrict Their Possible Use in Computation. Neuron *67*, 885–896.

Reich, D.S., Victor, J.D., Knight, B.W., Ozaki, T., and Kaplan, E. (1997). Response Variability and Timing Precision of Neuronal Spike Trains In Vivo. Journal of Neurophysiology *77*, 2836–2841.

Reimer, J., and Hatsopoulos, N.G. (2010). Periodicity and Evoked Responses in Motor Cortex. The Journal of Neuroscience *30*, 11506.

Remme, M.W.H., Lengyel, M., and Gutkin, B.S. (2010). Democracy-Independence Trade-Off in Oscillating Dendrites and Its Implications for Grid Cells. Neuron *66*, 429–437.

Reynolds, J.H., Chelazzi, L., and Desimone, R. (1999). Competitive mechanisms subserve attention in macaque areas V2 and V4. The Journal of Neuroscience *19*, 1736.

Reynolds, J.H., Pasternak, T., and Desimone, R. (2000). Attention increases sensitivity of V4 neurons. Neuron *26*, 703–714.

Richmond, B.J., Optican, L.M., Podell, M., and Spitzer, H. (1987). Temporal encoding of two-dimensional patterns by single units in primate inferior temporal cortex. I. Response characteristics. Journal of Neurophysiology *57*, 132.

Riehle, A., Grün, S., Diesmann, M., and Aertsen, A. (1997). Spike Synchronization and Rate Modulation Differentially Involved in Motor Cortical Function. Science *278*, 1950–1953.

Rieke, F., Warland, D., De Ruyter van Steveninck, R., and Bialek, W. (1999). Spikes: exploring the neural code.

Rihs, T.A., Michel, C.M., and Thut, G. (2007). Mechanisms of selective inhibition in visual spatial attention are indexed by ?-band EEG synchronization. Eur J Neurosci *25*, 603–610.

Rinzel, J., and Ermentrout, G.B. (1998). Analysis of neural excitability and oscillations. Methods in Neuronal Modeling *2*, 251–292.

Robbe, D., Montgomery, S.M., Thome, A., Rueda-Orozco, P.E., McNaughton, B.L., and Buzsáki, G. (2006). Cannabinoids reveal importance of spike timing coordination in hippocampal function. Nat Neurosci *9*, 1526–1533.

Roelfsema, P.R., Lamme, V.A.F., and Spekreijse, H. (2004). Synchrony and covariation of firing rates in the primary visual cortex during contour grouping. Nat Neurosci *7*, 982–991.

Roopun, A.K., Kramer, M.A., Carracedo, L.M., Kaiser, M., Davies, C.H., Traub, R.D., Kopell, N.J., and Whittington, M.A. (2008). Temporal interactions between cortical rhythms. Frontiers in Neuroscience *2*, 145.

Rothman, J.S., Cathala, L., Steuber, V., and Silver, R.A. (2009). Synaptic depression enables neuronal gain control. Nature *457*, 1015–1018.

Roudi, Y., and Latham, P.E. (2007). A balanced memory network. PLoS Computational Biology *3*,.

Rubino, D., Robbins, K.A., and Hatsopoulos, N.G. (2006). Propagating waves mediate information transfer in the motor cortex. Nature Neuroscience *9*, 1549–1557.

Rudolph, M., and Destexhe, A. (2003). A Fast-Conducting, Stochastic Integrative Mode for Neocortical Neurons InVivo. Journal of Neuroscience *23*, 2466.

Rutishauser, U., Ross, I.B., Mamelak, A.N., and Schuman, E.M. (2010). Human memory strength is predicted by theta-frequency phase-locking of single neurons. Nature *464*, 903–907.

Saalmann, Y.B., Pigarev, I.N., and Vidyasagar, T.R. (2007). Neural mechanisms of visual attention: how top-down feedback highlights relevant locations. Science *316*, 1612.

Salinas, E., and Sejnowski, T.J. (2001a). Correlated neuronal activity and the flow of neural information. Nat Rev Neurosci *2*, 539–550.

Salinas, E., and Sejnowski, T.J. (2001b). Gain modulation in the central nervous system: where behavior, neurophysiology, and computation meet. Neuroscientist *7*, 430–440.

Salinas, E., and Thier, P. (2000). Gain modulation: a major computational principle of the central nervous system. Neuron *27*, 15–21.

Samejima, K., Ueda, Y., Doya, K., and Kimura, M. (2005). Representation of Action-Specific Reward Values in the Striatum. Science *310*, 1337–1340.

Sanchez-Vives, M.V., and McCormick, D.A. (2000). Cellular and network mechanisms of rhythmic recurrent activity in neocortex. Nat Neurosci *3*, 1027–1034.

Sanes, J.N., and Donoghue, J.P. (1993). Oscillations in local field potentials of the primate motor cortex during voluntary movement. Proceedings of the National Academy of Sciences *90*, 4470–4474.

Sato, N., and Yamaguchi, Y. (2003). Memory Encoding by Theta Phase Precession in the Hippocampal Network. Neural Computation *15*, 2379–2397.

Sauseng, P., Klimesch, W., Stadler, W., Schabus, M., Doppelmayr, M., Hanslmayr, S., Gruber, W.R., and Birbaumer, N. (2005). A shift of visual spatial attention is selectively associated with human EEG alpha activity. European Journal of Neuroscience *22*, 2917–2926.

Scanziani, M., Gahwiler, B.H., and Thompson, S.M. (1995). Presynaptic inhibition of excitatory synaptic transmission by muscarinic and metabotropic glutamate receptor activation in the hippocampus: are Ca2+ channels involved? Neuropharmacology *34*, 1549–1557.

Scheeringa, R., Mazaheri, A., Bojak, I., Norris, D.G., and Kleinschmidt, A. (2011). Modulation of Visually Evoked Cortical fMRI Responses by Phase of Ongoing Occipital Alpha Oscillations. The Journal of Neuroscience *31*, 3813–3820.

Schnitzler, A., and Gross, J. (2005). Normal and pathological oscillatory communication in the brain. Nat Rev Neurosci *6*, 285–296.

Schoffelen, J.M., Oostenveld, R., and Fries, P. (2005). Neuronal coherence as a mechanism of effective corticospinal interaction. Science's STKE *308*, 111.

Schroeder, C.E., and Lakatos, P. (2009). Low-frequency neuronal oscillations as instruments of sensory selection. Trends in Neurosciences *32*, 9–18.

Schultz, W., Dayan, P., and Montague, P.R. (1997). A Neural Substrate of Prediction and Reward. Science *275*, 1593–1599.

Schwartz, O., and Simoncelli, E.P. (2001). Natural signal statistics and sensory gain control. Nature Neuroscience *4*, 819–825.

Schwartz, O., Hsu, A., and Dayan, P. (2007). Space and time in visual context. Nat Rev Neurosci *8*, 522–535.

Seidenbecher, T., Laxmi, T.R., Stork, O., and Pape, H.-C. (2003). Amygdalar and Hippocampal Theta Rhythm Synchronization During Fear Memory Retrieval. Science *301*, 846–850.

Sejnowski, T.J., and Paulsen, O. (2006). Network oscillations: emerging computational principles. Journal of Neuroscience *26*, 1673.

Seriès, P., Latham, P.E., and Pouget, A. (2004). Tuning curve sharpening for orientation selectivity: coding efficiency and the impact of correlations. Nature Neuroscience *7*, 1129–1135.

Shadlen, M.N., and Newsome, W.T. (1994). Noise, neural codes and cortical organization. Current Opinion in Neurobiology *4*, 569–579.

Shadlen, M.N., and Newsome, W.T. (1998). The variable discharge of cortical neurons: implications for connectivity, computation, and information coding. The Journal of Neuroscience *18*, 3870.

Shadlen, M.N., and Newsome, W.T. (2001). Neural Basis of a Perceptual Decision in the Parietal Cortex (Area LIP) of the Rhesus Monkey. Journal of Neurophysiology *86*, 1916–1936.

Shannon, C.E. (1949). Communication in the presence of noise. Proceedings of the IRE *37*, 10–21.

Shu, Y., Hasenstaub, A., and McCormick, D.A. (2003). Turning on and off recurrent balanced cortical activity. Nature *423*, 288–293.

Siapas, A.G., Lubenov, E.V., and Wilson, M.A. (2005). Prefrontal phase locking to hippocampal theta oscillations. Neuron *46*, 141–151.

Siegel, M., Donner, T.H., Oostenveld, R., Fries, P., and Engel, A.K. (2008). Neuronal synchronization along the dorsal visual pathway reflects the focus of spatial attention. Neuron *60*, 709–719.

Singer, W. (1999). Neuronal synchrony: a versatile code for the definition of relations? Neuron *24*, 49–25.

Sitz, A., Schwarz, U., Kurths, J., and Voss, H.U. (2002). Estimation of parameters and unobserved components for nonlinear systems from noisy time series. Physical Review E *66*, 16210.

Skaggs, W.E., McNaughton, B.L., Wilson, M.A., and Barnes, C.A. (1996). Theta phase precession in hippocampal neuronal populations and the compression of temporal sequences. Hippocampus *6*, 149–172.

Slawinska, U., and Kasicki, S. (1998). The frequency of rat's hippocampal theta rhythm is related to the speed of locomotion. Brain Research *796*, 327–331.

Slonim, N., Atwal, G.S., Tkačik, G., and Bialek, W. (2005). Information-based clustering. Proceedings of the National Academy of Sciences of the United States of America *102*, 18297–18302.

Smeal, R.M., Ermentrout, G.B., and White, J.A. (2010). Phase-response curves and synchronized neural networks. Philosophical Transactions of the Royal Society B: Biological Sciences *365*, 2407–2422.

Softky, W. (1994). Sub-millisecond coincidence detection in active dendritic trees. Neuroscience *58*, 13–41.

Softky, W., and Koch, C. (1993). The highly irregular firing of cortical cells is inconsistent with temporal integration of random EPSPs. J. Neurosci. *13*, 334–350.

Steriade, M., McCormick, D., and Sejnowski, T. (1993). Thalamocortical oscillations in the sleeping and aroused brain. Science *262*, 679–685.

Steriade, M., Timofeev, I., and Grenier, F. (2001). Natural waking and sleep states: a view from inside neocortical neurons. Journal of Neurophysiology *85*, 1969.

Stevens, C.F., and Zador, A.M. (1998). Input synchrony and the irregular firing of cortical neurons. Nature Neuroscience *1*, 210–217.

Stevenson, I.H., and Kording, K.P. (2011). How advances in neural recording affect data analysis. Nat Neurosci *14*, 139–142.

Stopfer, M., Bhagavan, S., Smith, B.H., and Laurent, G. (1997). Impaired odour discrimination on desynchronization of odour-encoding neural assemblies. Nature *390*, 70–73.

Tabuchi, E.T., Mulder, A.B., and Wiener, S.I. (2000). Position and behavioral modulation of synchronization of hippocampal and accumbens neuronal discharges in freely moving rats. Hippocampus *10*, 717–728.

Taylor, K., Mandon, S., Freiwald, W.A., and Kreiter, A.K. (2005). Coherent Oscillatory Activity in Monkey Area V4 Predicts Successful Allocation of Attention. Cereb. Cortex *15*, 1424–1437.

Tesche, C.D., and Karhu, J. (2000). Theta oscillations index human hippocampal activation during a working memory task. Proceedings of the National Academy of Sciences *97*, 919–924.

Thiele, A., and Stoner, G. (2003). Neuronal synchrony does not correlate with motion coherence in cortical area MT. Nature *421*, 366–370.

Thut, G., Nietzel, A., Brandt, S.A., and Pascual-Leone, A. (2006). Alpha-Band electroencephalographic activity over occipital cortex indexes visuospatial attention bias and predicts visual target detection. The Journal of Neuroscience *26*, 9494.

Tiesinga, P.H.E., and Sejnowski, T.J. (2004). Rapid Temporal Modulation of Synchrony by Competition in Cortical Interneuron Networks. Neural Computation *16*, 251–275.

Tiitinen, H., May, P., and Näätänen, R. (1997). The transient 40-Hz response, mismatch negativity, and attentional processes in humans. Progress in Neuro-Psychopharmacology and Biological Psychiatry *21*, 751–771.

Tiitinen, H., Sinkkonen, J., Reinikainen, K., Alho, K., Lavikainen, J., and Näätänen, R. (1993). Selective attention enhances the auditory 40-Hz transient response in humans. Nature *364*, 59–60.

Tolhurst, D.J., Movshon, J.A., and Dean, A.F. (1983). The statistical reliability of signals in single neurons in cat and monkey visual cortex. Vision Research *23*, 775–785.

Tort, A.B.L., Fontanini, A., Kramer, M.A., Jones-Lush, L.M., Kopell, N.J., and Katz, D.B. (2010). Cortical Networks Produce Three Distinct 7–12 Hz Rhythms during Single Sensory Responses in the Awake Rat. The Journal of Neuroscience *30*, 4315–4324.

Traub, R.D., Whittington, M.A., Stanford, I.M., and Jefferys, J.G. (1996). A mechanism for generation of long-range synchronous fast oscillations in the cortex. Nature *383*, 621–624.

Treisman, A.M. (1969). Strategies and models of selective attention. Psychological Review *76*, 282.

Tsodyks, M.V., and Sejnowski, T. (1995). Rapid state switching in balanced cortical network models. Network: Computation in Neural Systems *6*, 111–124.

Tsodyks, M.V., Skaggs, W.E., Sejnowski, T.J., and McNaughton, B.L. (1996). Population dynamics and theta rhythm phase precession of hippocampal place cell firing: a spiking neuron model. Hippocampus *6*, 271–280.

Tukker, J.J., Fuentealba, P., Hartwich, K., Somogyi, P., and Klausberger, T. (2007). Cell type-specific tuning of hippocampal interneuron firing during gamma oscillations in vivo. J.Neurosci. *27*, 8184–8189.

Uhlhaas, P.J., Pipa, G., Lima, B., Melloni, L., Neuenschwander, S., Nikolić, D., and Singer, W. (2009). Neural Synchrony in Cortical Networks: History, Concept and Current Status. Front Integr Neurosci. *3*, 17.

Vanderwolf, C.. (1969). Hippocampal electrical activity and voluntary movement in the rat. Electroencephalography and Clinical Neurophysiology *26*, 407–418.

VanRullen, R., Reddy, L., and Koch, C. (2006). The Continuous Wagon Wheel Illusion Is Associated with Changes in Electroencephalogram Power at ~13 Hz. The Journal of Neuroscience *26*, 502–507.

Varela, F., Lachaux, J.P., Rodríguez, E., and Martinerie, J. (2001). The brainweb: phase synchronization and large-scale integration. Nat.Rev.Neurosci. *2*, 229–239.

Van Veen, B.D., Van Drongelen, W., Yuchtman, M., and Suzuki, A. (1997). Localization of brain electrical activity via linearly constrained minimum variance spatial filtering. Biomedical Engineering, IEEE Transactions On *44*, 867–880.

Victor, J.D., and Purpura, K.P. (1996). Nature and precision of temporal coding in visual cortex: a metric-space analysis. Journal of Neurophysiology *76*, 1310.

Vida, I., Bartos, M., and Jonas, P. (2006). Shunting inhibition improves robustness of gamma oscillations in hippocampal interneuron networks by homogenizing firing rates. Neuron *49*, 107–117.

Vidal, J.R., Chaumon, M., O'Regan, J.K., and Tallon-Baudry, C. (2006). Visual grouping and the focusing of attention induce gamma-band oscillations at different frequencies in human magnetoencephalogram signals. Journal of Cognitive Neuroscience *18*, 1850–1862.

Vijayan, S., Hale, G.J., Moore, C.I., Brown, E.N., and Wilson, M. (2010). Activity in the barrel cortex during active behavior and sleep. J. Neurophysiol *103*, 2074–2084.

Vogels, T.P., and Abbott, L.F. (2009). Gating multiple signals through detailed balance of excitation and inhibition in spiking networks. Nat Neurosci *12*, 483–491.

Van Vreeswijk, C., Abbott, L.F., and Ermentrout, G.B. (1994). When inhibition not excitation synchronizes neural firing. J.Comput.Neurosci. *1*, 313–321.

Van Vreeswijk, C., and Sompolinsky, H. (1998). Chaotic balanced state in a model of cortical circuits. Neural Computation *10*, 1321–1371.

Van Vreeswijk, V.C., and Sompolinsky, H. (1996). Chaos in neuronal networks with balanced excitatory and inhibitory activity. Science *274*, 1724–1726.

Wan, E.A., and Van Der Merwe, R. (2000). The unscented Kalman filter for nonlinear estimation. In Adaptive Systems for Signal Processing, Communications, and Control Symposium 2000. AS-SPCC. The IEEE 2000, pp. 153–158.

Wang, X.J., and Buzsaki, G. (1996). Gamma oscillation by synaptic inhibition in a hippocampal interneuronal network model. J.Neurosci. *16*, 6402–6413.

Wehr, M., and Laurent, G. (1996). Odour encoding by temporal sequences of firing in oscillating neural assemblies. Nature *384*, 162–166.

Wehr, M., and Zador, A.M. (2003). Balanced inhibition underlies tuning and sharpens spike timing in auditory cortex. Nature *426*, 442–446.

Wenderoth, P., and Johnstone, S. (1988). The different mechanisms of the direct and indirect tilt illusions. Vision Research *28*, 301–312.

Westhhmer, G. (1990). Simultaneous orientation contrast for lines in the human fovea. Vision Research *30*, 1913–1921.

Whittington, M.A., Stanford, I.M., Colling, S.B., Jefferys, J.G., and Traub, R.D. (1997a). Spatiotemporal patterns of gamma frequency oscillations tetanically induced in the rat hippocampal slice. J.Physiol *502 (Pt 3)*, 591–607.

Whittington, M.A., Traub, R.D., and Jefferys, J.G. (1995). Synchronized oscillations in interneuron networks driven by metabotropic glutamate receptor activation. Nature *373*, 612–615.

Whittington, M.A., Traub, R.D., Faulkner, H.J., Stanford, I.M., and Jefferys, J.G. (1997b). Recurrent excitatory postsynaptic potentials induced by synchronized fast cortical oscillations. Proc.Natl.Acad.Sci.U.S.A *94*, 12198–12203.

Wilson, H.R., and Cowan, J.D. (1972). Excitatory and inhibitory interactions in localized populations of model neurons. Biophys.J. *12*, 1–24.

Winfree A. (2000). The Geometry of Biological Time. 2nd ed. (Springer - Verlag).

Witham, C.L., Wang, M., and Baker, S.N. (2007). Cells in somatosensory areas show synchrony with beta oscillations in monkey motor cortex. European Journal of Neuroscience *26*, 2677–2686.

Wolfe, J.M. (1998). Visual search. Attention *1*, 13–73.

Womelsdorf, T., and Fries, P. (2006). Neuronal coherence during selective attentional processing and sensory–motor integration. Journal of Physiology-Paris *100*, 182–193.

Womelsdorf, T., and Fries, P. (2007). The role of neuronal synchronization in selective attention. Current Opinion in Neurobiology *17*, 154–160.

Womelsdorf, T., Fries, P., Mitra, P.P., and Desimone, R. (2006). Gamma-band synchronization in visual cortex predicts speed of change detection. Nature *439*, 733–736.

Womelsdorf, T., Schoffelen, J.M., Oostenveld, R., Singer, W., Desimone, R., Engel, A.K., and Fries, P. (2007). Modulation of neuronal interactions through neuronal synchronization. Science *316*, 1609–1612.

Worden, M.S., Foxe, J.J., Wang, N., and Simpson, G.V. (2000). Anticipatory biasing of visuospatial attention indexed by retinotopically specific alpha-band electroencephalography increases over occipital cortex. Journal of Neuroscience *20*, RC63.

Wróbel, A., Ghazaryan, A., Bekisz, M., Bogdan, W., and Kamiński, J. (2007). Two Streams of Attention-Dependent β Activity in the Striate Recipient Zone of Cat's Lateral Posterior–Pulvinar Complex. The Journal of Neuroscience *27*, 2230.

Xing, D., Yeh, C.I., and Shapley, R.M. (2009). Spatial spread of the local field potential and its laminar variation in visual cortex. The Journal of Neuroscience *29*, 11540.

Ylinen, A., Soltész, I., Bragin, A., Penttonen, M., Sik, A., and Buzsáki, G. (1995). Intracellular correlates of hippocampal theta rhythm in identified pyramidal cells, granule cells, and basket cells. Hippocampus *5*, 78–90.

Yu, A.J., and Dayan, P. (2005). Uncertainty, Neuromodulation, and Attention. Neuron *46*, 681–692.

Yu, A.J., Dayan, P., and Cohen, J.D. (2009). Dynamics of attentional selection under conflict: Toward a rational Bayesian account. Journal of Experimental Psychology: Human Perception & Performance *35*, 700–717.

Zeitler, M., Fries, P., and Gielen, S. (2006). Assessing Neuronal Coherence with Single-Unit, Multi-Unit, and Local Field Potentials. Neural Computation *18*, 2256–2281.

Zeitler, M., Fries, P., and Gielen, S. (2008). Biased competition through variations in amplitude of ?-oscillations. Journal of Computational Neuroscience *25*, 89–107.

Zelinsky, G.J. (2005). Specifying the components of attention in a visual search task. Neurobiology of Attention 395–400.

Zylberberg, A., Fernández Slezak, D., Roelfsema, P.R., Dehaene, S., and Sigman, M. (2010). The Brain's Router: A Cortical Network Model of Serial Processing in the Primate Brain. PLoS Comput Biol *6*, e1000765.